

**SCALE-MODEL INVESTIGATION OF HIGHWAY TRAFFIC NOISE
BARRIERS**

By

Todd Busch

B. A. Sc. (Mechanical Engineering) University of British Columbia, 1994

A THESIS SUBMITTED IN PARTIAL FULFILLMENT OF
THE REQUIREMENTS FOR THE DEGREE OF
MASTER OF APPLIED SCIENCE

in

THE FACULTY OF GRADUATE STUDIES
MECHANICAL ENGINEERING

THE UNIVERSITY OF BRITISH COLUMBIA

March 3, 1997

© Todd Busch, 1997

In presenting this thesis in partial fulfilment of the requirements for an advanced degree at the University of British Columbia, I agree that the Library shall make it freely available for reference and study. I further agree that permission for extensive copying of this thesis for scholarly purposes may be granted by the head of my department or by his or her representatives. It is understood that copying or publication of this thesis for financial gain shall not be allowed without my written permission.

Mechanical Engineering
The University of British Columbia
2075 Wesbrook Place
Vancouver, Canada
V6T 1Z1

Date:

April 3, 1997

Abstract

Barriers, such as walls, earth berms, and earth-berm/wall combinations, are used to control highway noise. Factors that affect noise attenuation include profile, height, location, and surface composition. A literature review was conducted on the topics of outdoor sound propagation, ground impedance, noise barriers, and acoustical scale modelling. The noise attenuation provided by vertical walls, earth berms, and earth berms crested by a vertical wall — for a line source of vehicular traffic — has received little attention. Using an ultrasonic air-jet source, scale-model materials were selected by measuring their Excess Attenuations, at scales of 1:20, 25, 31.5, 40, and 50. A new method was employed to select materials: the residuals between measurements and theoretical, best-fit curves were calculated for each cell of a 2-D array whose axes were scale factor versus effective flow resistivity. An optimal scale of 1:31.5 was selected, in conjunction with specifying three model materials to simulate berms and soft ground (expanded polystyrene), vertical walls (dense polystyrene), and roadways (varnished particle board). Berms, typically 4 m in height, were tested with slopes of 1.5, 2 and 3:1; for each of these slopes, five crest profiles were tested: wedge, flat-top (widths of 1 m and 2 m), and round-top (radii of 1 m and 2 m). For berms crested by a vertical wall, the relative heights of berm and wall were either 1m/3m, 2m/2m, or 3m/1m; for each height combination, berm slopes of 1.5, 2, and 3:1 were tested. The surface composition of berms were altered using dense polystyrene, and felt. Weighted Insertion Losses (*ILAs*) for a line source were obtained by applying A-weighted, traffic-noise spectra, before integrating the 80–2500 Hz full-scale, third-octave bands. Contrary to current highway practice — where a “soft-top correction” of +3 dBA is often applied to earth berms — walls out-performed berms by 1–2 dBA. For berms, shallower slopes degraded third-octave *ILs* in the 250 Hz band, but had little effect on a berm’s *ILA*. For berms crested by a vertical wall, shallower slopes increased *ILAs*.

Table of Contents

Abstract	ii
List of Tables	vi
List of Figures	vii
Nomenclature	xii
Acknowledgement	xvi
1 Introduction	1
2 Literature Review	15
2.1 Outdoor Sound Propagation	15
2.1.1 Atmospheric Phenomenon	16
2.1.2 Excess Attenuation of Ground Surfaces	19
2.2 Ground Surface Impedance	23
2.3 Noise Barriers	34
2.4 Acoustical Scale Modelling	41
2.5 Human Response to Traffic Noise	48
3 Theoretical Considerations	49
3.1 Excess Attenuation: Prediction	49
3.2 Principles of Acoustical Scale Modelling	54
3.2.1 Air-Absorption Coefficient Calculation	57
3.2.2 Scale-Model Noise Sources	58

3.2.3	Method for Determining Optimal Scale-Model Materials and Scale Factor	58
4	Field Tests	61
4.1	Traffic-Noise Spectra	61
4.2	Field-Test Geometries: Earth Berms	63
4.3	Excess Attenuation of Ground	64
4.4	Barrier Insertion Loss	66
5	Experiment	68
5.1	Experimental Introduction	68
5.2	Test Equipment	68
5.3	Air-Jet Source Design	73
5.4	Air-Jet-Source Testing	74
5.4.1	Variation of Noise Spectrum with Air-Line Pressure	75
5.4.2	Variation of Noise Spectrum with Source Rotation	77
5.4.3	Variation of Noise Spectrum with Distance	78
5.4.4	Variation of Noise Spectrum with Source and Microphone Inclination Angle	79
5.5	Anechoic-Chamber Testing	83
5.6	Scale-Model Material Testing	87
5.6.1	Measurement of Excess Attenuation	87
5.6.2	Effective Flow Resistivity of Scale-Model Materials	89
5.6.3	Selecting Scale-Model Materials	103
5.7	Insertion-Loss Experiments	105
5.7.1	Point-Source Insertion-Loss Tests	107
5.7.2	Line-Source Insertion-Loss Tests	108
5.7.3	Barrier Configurations for Line-Source Insertion-Loss Tests	111
5.7.4	Insertion-Loss Test-Result Reporting	114
5.8	Experimental Conclusion	115

6	Scale-Model Results: Line-Source Third-Octave Insertion Losses	116
6.1	Introduction to Results	116
6.2	Optimum Surface Impedance	117
6.2.1	Variable Wall Thickness	117
6.2.2	Variable Berm Slope	117
6.2.3	Variable Berm Top Width	121
6.2.4	Variable Berm Top Radius	121
6.2.5	Variable Flat-Top-Berm/Wall Height	125
6.2.6	Variable Flat-Top-Berm/Wall Slope	127
6.2.7	Variable Barrier Height	127
6.3	Alternative Surface Impedances	130
6.3.1	Variable Berm Surface Impedance	130
6.3.2	Variable Berm Slope	131
6.3.3	Variable Flat-Top-Berm Surface Impedance with/without a Wall	131
6.3.4	Variable Berm-Crest-Wall Height	134
6.4	Conclusion to Results	134
7	Applications	137
7.1	Introduction to Applications	137
7.2	Scale-Model Results: Point-Source Total <i>IL</i> and Total <i>ILA</i>	138
7.3	Scale-Model Results: Line-Source Total <i>IL</i> and Total <i>ILA</i>	139
7.3.1	Comparison to Field Tests	147
7.4	Discussion of Total <i>IL</i> and Total <i>ILA</i> Results	148
7.5	Conclusion to Applications	152
8	Conclusion	154
	Bibliography	157

List of Tables

2.1	Values of effective flow resistivity for outdoor ground surfaces	25
4.1	Location of outdoor test co-ordinates relative to the road-shoulder datum: The microphone was 1.5 m higher. (A) Highway shoulder at berm base; (B) Crest of berm; (C) Receiver-side base of berm; (D) Receiver-side of berm at a typical front-yard distance.	63
5.1	Average standard deviations based on three and (best two of three) tests of <i>EA</i> for each scale factor and test material.	89
5.2	Bins integrated together to produce third-octaves of a given centre frequency at full-scale: scale-model tests extended from 0–100 kHz in four-hundred bins of 250 Hz bandwidths, at a scale of 1:31.5.	115
7.1	Unweighted Total Insertion Losses versus Distance	138
7.2	Weighted Total Insertion Losses versus Distance	139
7.3	Total <i>ILs/ILAs</i> of Scale-Model Barriers: Walls and Earth Berms	140
7.4	Total <i>ILs/ILAs</i> of Scale-Model Barriers: Berms with Crest Walls	142
7.5	Total <i>ILs/ILAs</i> of Scale-Model Barriers: Alternative Surface <i>Z</i>	144
7.6	Range of Scale-Model Barrier Total <i>ILs/ILAs</i>	145

List of Figures

1.1	Some existing noise-barrier cross-sections and/or theoretically-studied shapes. . .	4
1.2	Attenuation of sound pressure with distance due to air absorption.	7
1.3	Sound propagation over open ground.	10
1.4	Sound propagation over a barrier.	12
1.5	Sound propagation from a highway cut.	13
3.1	Air absorption in dB/m at full-scale frequencies for both full-scale calculations and 31.5:1 model-scale calculations translated to full scale.	55
3.2	Surface impedance at two scale factors ($n = 1$ and 31.5) and three effective flow resistivities (75, 300, 20000 c.g.s. Rayls/cm).	59
3.3	Predicted <i>EAs</i> for effective flow resistivities of 75, 300, 600, 20000 and Inf c.g.s. Rayls/cm.	60
4.1	Measured unweighted and A-weighted third-octave traffic-noise spectra.	62
4.2	Measured <i>EAs</i> in third-octaves for three test geometries with traffic-noise at three outdoor test locations.	65
4.3	Measured <i>ILs</i> in third-octaves for three test geometries with traffic-noise for three outdoor test locations.	67
5.1	Plan view of the anechoic chamber, air-jet-source apparatus and test platform. .	69
5.2	Photograph of Stanford Research Systems SR-770 and air-line.	70
5.3	Photograph taken outside of the anechoic chamber.	71
5.4	Photograph taken inside of the anechoic chamber.	72
5.5	Air-jet source: assembly drawing where (1) is the outer housing, (2) is an o-ring of size no.15 and (3) is the core-piece.	74

5.6	Source-pressure study: variation of air-jet-source spectra with air-line pressure.	76
5.7	Source-pressure study: measured variation of total sound-pressure level generated by the air-jet source with air-line pressure.	77
5.8	Source-pressure study: the accumulation of variance with frequency for thirteen air-line pressures.	78
5.9	Source-pressure study: the average standard deviation, from 0–100 kHz, at thirteen air-line pressures.	79
5.10	Source-rotation study: standard deviation from thirty-six tests over the frequency range of 0–100 kHz.	80
5.11	Source sound-power-level study: (x) uncorrected L_p data; (o) L_p corrected for air absorption and microphone response.	81
5.12	Source sound-power-level study: best-fit sound-power levels.	81
5.13	Source-inclination study: a 3-D plot of sound pressure 1 m from the air-jet source over angles from 0° to 90°	82
5.14	Source-inclination study: total source output over the 0° to 90° interval.	82
5.15	Source-inclination study: the frequency dependency of sound-pressure levels averaged over ten inclination-angle measurements.	83
5.16	Anechoic-chamber study: low- and high-frequency performance.	84
5.17	Anechoic-chamber study: near-wall and room-centre comparison.	85
5.18	Anechoic-chamber study: near-wall reflection-induced error.	86
5.19	Aluminum — array of effective flow resistivity versus scale factor.	92
5.20	Measured EA of aluminum compared to theoretical best-fit curves.	92
5.21	Cloth (one layer) — array of effective flow resistivity versus scale factor.	93
5.22	Measured EA of cloth (one layer) compared to theoretical best-fit curves.	93
5.23	Cloth (two layer) — array of effective flow resistivity versus scale factor.	94
5.24	Measured EA of cloth (two layers) compared to theoretical best-fit curves.	94
5.25	Felt — array of effective flow resistivity versus scale factor.	95

5.26	Measured <i>EA</i> of felt compared to theoretical best-fit curves.	95
5.27	Expanded Polystyrene — array of effective flow resistivity versus scale factor. . .	97
5.28	Measured <i>EA</i> of expanded polystyrene compared to theoretical best-fit curves. . .	97
5.29	Dense Polystyrene — array of effective flow resistivity versus scale factor.	98
5.30	Measured <i>EA</i> of dense polystyrene compared to theoretical best-fit curves.	98
5.31	Rough Masonite — array of effective flow resistivity versus scale factor.	99
5.32	Measured <i>EA</i> of rough masonite compared to theoretical best-fit curves.	99
5.33	Smooth Masonite — array of effective flow resistivity versus scale factor.	101
5.34	Measured <i>EA</i> of smooth masonite compared to theoretical best-fit curves.	101
5.35	Varnished Particle Board — array of effective flow resistivity versus scale factor.	102
5.36	Measured <i>EA</i> of varnished particle board compared to theoretical best-fit curves.	102
5.37	Profile view of the highway configuration.	106
5.38	Profile view of the point-source test configurations.	108
5.39	Plan view of the line-source test configuration.	109
5.40	Picture of a scale-model earth berm of 3 m height, 2:1 sloped, 2 m top width, with a crest wall of 1 m height.	111
5.41	Profile view of barrier configurations.	113
6.1	Measured third-octave <i>ILs</i> for 4 m high walls with full-scale thicknesses of 5, 10 and 15 cm.	118
6.2	Measured third-octave <i>ILs</i> for wedge-shaped grass berms of 4 m height, and with 1.5, 2 and 3:1 slopes.	118
6.3	Measured third-octave <i>ILs</i> for flat-topped grass berms of 4 m height, with a 1 m wide flat-top, and with 1.5, 2 and 3:1 slopes.	119
6.4	Measured third-octave <i>ILs</i> for flat-topped grass berms of 4 m height, with a 2 m wide flat-top, and with 1.5, 2 and 3:1 slopes.	119
6.5	Measured third-octave <i>ILs</i> for round-topped grass berms of 4 m height, with a 1 m radius round-top, and with 1.5, 2 and 3:1 slopes.	120

6.6	Measured third-octave <i>ILs</i> for round-topped grass berms of 4 m height, with a 2 m radius round-top, and with 1.5, 2 and 3:1 slopes.	120
6.7	Measured third-octave <i>ILs</i> for grass berms of 4 m height with a fixed slope of 1.5:1, and with top widths of 0, 1 and 2 m.	122
6.8	Measured third-octave <i>ILs</i> for grass berms of 4 m height with a fixed slope of 2:1, and with top widths of 0, 1 and 2 m.	122
6.9	Measured third-octave <i>ILs</i> for grass berms of 4 m height with a fixed slope of 3:1, and with top widths of 0, 1 and 2 m.	123
6.10	Measured third-octave <i>ILs</i> for grass berms of 4 m height with a fixed slope of 1.5:1, and with top radii of 0, 1 and 2 m.	123
6.11	Measured third-octave <i>ILs</i> for grass berms of 4 m height with a fixed slope of 2:1, and with top radii of 0, 1 and 2 m.	124
6.12	Measured third-octave <i>ILs</i> for grass berms of 4 m height with a fixed slope of 3:1, and with top radii of 0, 1 and 2 m.	124
6.13	Measured third-octave <i>ILs</i> for flat-topped grass berms of 1.5:1 slope, with 2 m top width, and with 1/3, 2/2 and 3/1 m berm/wall heights.	125
6.14	Measured third-octave <i>ILs</i> for flat-topped grass berms of 2:1 slope, with 2 m top width, and with 1/3, 2/2 and 3/1 m berm/wall heights.	126
6.15	Measured third-octave <i>ILs</i> for flat-topped grass berms of 3:1 slope, with 2 m top width, and with 1/3, 2/2 and 3/1 m berm/wall heights.	126
6.16	Measured third-octave <i>ILs</i> for flat-topped grass berms of 2 m height, with 2 m top width, and with slopes of 1.5:1, 2:1 and 3:1, topped by a 2 m high crest wall.	128
6.17	Measured third-octave <i>ILs</i> for flat-topped grass berms of 3 m height, with 2 m top width, and with slopes of 1.5:1, 2:1 and 3:1, topped by a 1 m high crest wall.	128
6.18	Measured third-octave <i>ILs</i> for flat-topped grass berms of both 3 m and 4 m heights, with 2 m top width, and with a fixed slope of 3:1; also considered is a 3 m berms with a 1 m crest wall.	129

6.19	Measured third-octave <i>ILs</i> for wedge-shaped berms of 4 m height, with 1.5:1 slope, covered by dense polystyrene, expanded polystyrene and felt.	129
6.20	Measured third-octave <i>ILs</i> for wedge-shaped berms of 4 m height, with 2:1 slope, covered by dense polystyrene, expanded polystyrene and felt.	130
6.21	Measured third-octave <i>ILs</i> for wedge-shaped berms of 4 m height, with 3:1 slope, covered by dense polystyrene, expanded polystyrene and felt.	131
6.22	Measured third-octave <i>ILs</i> for wedge-shaped berms of 4 m height, covered by dense polystyrene, and with 1.5, 2 and 3:1 slopes.	132
6.23	Measured third-octave <i>ILs</i> for wedge-shaped berms of 4 m height, covered by felt, and with 1.5, 2 and 3:1 slopes.	132
6.24	Measured third-octave <i>ILs</i> for flat-topped berms of 2 m top width, 3 m height, a fixed 3:1 berm slope, and with surfaces of dense polystyrene, expanded polystyrene and felt.	133
6.25	Measured third-octave <i>ILs</i> for flat-topped berms of 2 m top width, 3 m height, a fixed 3:1 berm slope, topped by a 1 m high crest wall, and with surfaces of dense polystyrene, expanded polystyrene and felt.	133
6.26	Measured third-octave <i>ILs</i> for flat-topped berms of 2 m top width, 3 m height, fixed 3:1 slope, a berm surface of dense polystyrene, and topped with or without a 1 m crest wall.	135
6.27	Measured third-octave <i>ILs</i> for flat-topped berms of 2 m top width, 3 m height, fixed 3:1 slope, a berm surface of expanded polystyrene, and topped with or without a 1 m crest wall.	136
6.28	Measured third-octave <i>ILs</i> for flat-topped berms of 2 m top width, 3 m height, fixed 3:1 slope, a berm surface of felt, and topped with or without a 1 m crest wall.	136

Nomenclature

ABL	Acoustic boundary Layer.
A_1, B_1, C_1, D_1	Intermediate quantities for erfc calculation.
D	Divergence coefficient (incoherent point source 20, incoherent line source 10).
EA	Excess Attenuation of ground surface, in dB.
$EA_{measured}^{n,\sigma}(f_i)$	Measured Excess Attenuation at a reduced scale, in dB.
$EA_{predicted}^{n,\sigma}(f_i)$	Predicted Excess Attenuation at a reduced scale for a given flow resistivity, in dB.
E_h	Error bound for erfc calculation.
EP	Expanded polystyrene surface material.
F	Felt surface material.
$F^{n,\sigma}(\vec{f})$	Least-squares residuals averaged over a range of frequencies, in dB.
$F(w)$	Spherical correction (or loss) factor.
H	Barrier height (including separate heights for berms and their crest walls), in m.
H_{yx}	Real part of the complementary error function.
IL	Insertion Loss of barrier, in dB.
ILA	A-weighted traffic-noise Insertion Loss of barrier, in dBA.
K	Berm slope in the ratio run:rise.
K	Shape factor.
K_{yx}	Imaginary part of the complementary error function.
L_{eq}	Time-averaged sound-pressure level, in Pa.
$L_{eq,A}$	A-weighted time-averaged sound-pressure level, in Pa.
L_p	Sound-pressure level, in dB.
$L_{p,barrier}$	Sound-pressure level with a barrier on a surface, in Pa.
$L_{p,free-field}$	Sound-pressure level in a free field, in Pa.

$L_{p,surface}$	Sound-pressure level over a surface, in Pa.
L_w	Sound-power level, in dB.
P	Polystyrene surface material.
P_2, Q_2	Intermediate quantities for <i>erfc</i> calculation.
Q	Spherical-wave reflection coefficient.
R	Surface resistance of ground, in $\text{kg/m}^2 \text{ s}$ (Rayls).
R_p	Plane-wave reflection coefficient.
STD	Standard deviation of Total IL/ILA , in dB.
T	Thickness of a wall, in m.
T	Temperature, in degrees Kelvin.
T_o	Reference temperature of 273.15 K.
W	Sound power, in Watts.
W	Width of the flat top of a berm, in m.
X	Surface reactance of ground, in Rayls.
Z	Impedance, in Rayls.
Z_c	Characteristic surface impedance of ground, in Rayls.
Z_n	Normal-incidence surface impedance of ground, in Rayls.
b_1	Index denoting lower-most frequency bin.
b_2	Index denoting upper-most frequency bin.
d	Horizontal distance, in m.
d_2	Horizontal distance to roadside measurement position, in m.
d_A	Horizontal distance to roadside reference position, in m.
<i>erfc</i>	Complementary Error Function.
f	Frequency, in Hz.
$f(w)$	Modified form of the <i>erfc</i> .
h	Vertical source or receiver height above a surface, in m.
h	New constant for establishing the error bound of the <i>erfc</i> .

h_1, h_2	Source or receiver height above a surface, in m.
h_{1+2}	Combined vertical source or receiver height above a surface, in m.
k	Wavenumber, in 1/m.
l	Characteristic length, in m.
m_1	Index denoting lower-most frequency bin for an octave band.
m_2	Index denoting upper-most frequency bin for an octave band.
n	Scale factor.
n'	Grain-shape factor.
p	Acoustic pressure, in Pa.
p_o	standard reference acoustic pressure, 2×10^{-5} Pa.
r	Radial distance between sound source and receiver, in m.
r_1	Radial distance between sound source and receiver, in m.
r_2	Radial distance between image sound source and receiver, in m.
s_f	Pore-shape factor.
t	Time, in seconds.
w	Numerical distance.
x, y	Defined as the real and imaginary parts of the numerical distance.
x, y, z	Cartesian co-ordinates, in m.
z_o	Reference height of impedance plane, in m.
ΔIL	Range of Total IL observed due to single-parameter changes, in dB.
ΔILA	Range of Total ILA observed due to single-parameter changes, in dB.
$\Delta L_{p,air}$	Change in sound-pressure level due to air absorption, in dB.
$\Delta L_{p,div}$	Geometric divergence, in dB/dd.
$\Delta L_{p,microphone}$	Change in sound-pressure level due to microphone response, in dB.
Ω	Porosity.
Φ	Velocity potential of a sound field.
$\Phi_{free-field}$	Velocity potential of a free-field.

α	Air absorption coefficient, in Np/m.
α_{cr}	Classical air-absorption coefficient, in Np/m.
α_e	Exponent describing exponential decreases in porosity with depth.
$\alpha_{vib,N}$	Nitrogen's vibrational-relaxational air-absorption coefficient, in Np/m.
$\alpha_{vib,O}$	Oxygen's vibrational-relaxational air-absorption coefficient, in Np/m.
β	Air absorption, in dB/m.
β	Normalized admittance.
β_{ABL}	Normalized acoustic-boundary-layer admittance.
γ	Propagation constant of air, in Np/m.
λ	Sound wavelength, in m.
ψ	Grazing angle of reflected sound, in degrees.
ϕ	Impedance phase, in degrees.
ρ	Density, in kg/m ³ .
σ	Flow resistivity, in c.g.s. Rayls/cm.
σ_e	Effective flow resistivity, in c.g.s. Rayls/cm.
'	Superscript denotes model-scale tests.

Acknowledgement

First, I extend my gratitude to my advisor, Dr. Murray Hodgson, for his contributions to the development of this project, and tutelage in bring the work to a satisfactory conclusion. Second, to Mr. Clair Wakefield, whose experience and perspective — as an acoustical consultant working with highway noise control — proved to be extremely valuable, and thanks also to his associates Richard Kwan and Barry for their field-testing efforts. See their publication: Report 92-M69-1, "Guidelines for the use of Earth Berms to Control Highway Noise", prepared by them for the B.C. Ministry of Transportation and Highways, using the results of this work. Third, to Mr. Michael Kent, as director of the British Columbia Ministry of Transportation and Highways — Highway Environment Branch, for his energy in securing the funding that made the entire endeavor possible. Fourth, to Dr. Josef Novak of the Slovak Academy of Sciences, for his co-operation in providing me with a schematic of the air-jet source that was adapted for scale-model testing. As well, to Mr. Dean Leonard for his co-operation in allowing me the use of hot-wiring equipment and project space for constructing the noise barriers. Also, thank you to Dr. Gilles Daigle and Dr. Michael Stinson of the National Research Council, and Dr. Ken Fyfe of the University of Alberta for their informed advice at various points in time during the project. Finally, to all of my friends and family, for their support throughout this endeavour.

Chapter 1

Introduction

Road traffic is the most prolific source of man-made noise in the world. Acceptable limits on noise levels are the subject of research, since it is known that excessive traffic noise reduces people's quality of life by disrupting their ability to communicate, relax and sleep. Informed decisions to implement noise mitigation measures require both a knowledge of the health effects of noise and of the expenditure associated with differing amounts of noise abatement. Recent B.C. Ministry of Transportation and Highways guidelines endeavour to entrench noise mitigation as part of the planning phase of future road constructions [1]. To this end, the research project reported here was undertaken with its support. Highway noise control is increasingly being achieved by designing and constructing highway noise barriers. The objective was to determine how changes to noise-barrier geometry and composition affect the barrier's noise attenuation. Noise barriers, such as walls, earth berms and earth berms crested by a wall, are the predominant means of achieving significant reductions in highway noise levels. Barrier height, footprint, cross-section and surface properties all affect its noise attenuation. Common barrier materials include concrete, earth, wood, metal and plastic. For aesthetic reasons, the heights of barriers adjacent to provincial highways are restricted [1] to 3 m, but earth berms (with or without a crest wall) have no stipulated height limit. As well, it was commonly assumed [2] that the attenuation produced by an earth berm, via a soft-top correction of 3 dBA, was greater than by a wall of the same height — the validity of this assumption needed to be explored.

Traffic-noise levels depend on the type, number, speed and acceleration of vehicles on a roadway. Noise is generated by the power train, exhaust, tires and aerodynamic forces. Averaging the noise power from all these sources, with respect to the height and sound power

of each distinct noise source, allows for the assignment of an effective source height for the noise from a vehicle. This process can be extended to the traffic flow over a highway, with the effective source height being strongly influenced by the noise from the elevated exhausts found on trucks. At lower speeds power-train noise is dominant, but for vehicles travelling at highway speeds tires are the most prevalent noise source. For the purposes of this thesis, an effective source height of 0.5 m was assumed. At sufficiently high traffic densities and receiver distances it is reasonable to describe the traffic noise as an incoherent line source. In recent decades, significant advances have been made in reducing noise levels from vehicles. Despite this, increasing volumes of traffic flow have largely offset these gains so that overall noise levels in urban areas have not decreased appreciably, and may have increased slightly.

To design noise barriers properly it is necessary to understand how sound propagates outdoors, and what environmental factors are of significance. Atmospheric phenomena such as geometric divergence, air absorption, temperature or wind gradients, and turbulence, can have significant effects on the measured sound-pressure level, L_p . Noise can propagate directly from a source to a receiver through the air, by reflection from a surface such as pavement, or by bending (diffracting) around the edges of intervening obstacles such as vegetation, hills, buildings and noise barriers. Sound doesn't necessarily travel in a straight line through the air; in fact, it is unusual for it to do so. More commonly, sound follows a curved trajectory due to variations in temperature or wind speed above a ground surface. Such curving of sound paths (called refraction) can substantially reduce noise levels at a receiver or can cause the levels to increase. Air turbulence can introduce small changes to the path travelled by sound waves (called turbulent scattering). For sound that originates from a coherent source but which has travelled by multiple paths to reach a reception point, turbulence disrupts the coherence between the separate paths. The turbulence in the air is often described in terms of the scale of turbulence (a characteristic dimension for atmospheric vortices). Upon reflection from the ground, sound energy in the reflected wave is reduced — the reduction of sound levels due to ground absorption and interference is often referred to as the 'ground effect'. The acoustical

properties of pavement and ground can be altered, by making the surface more porous to the flow of air, in order to reduce the amount of sound reaching a receiver.

A preferred method of controlling noise is to introduce an obstacle — a noise barrier — between the source and receiver; this attenuates noise by interrupting the direct path, so that sound must be diffracted to reach a receiver. Such noise barriers generally block the line-of-sight, and must allow negligible amounts of noise to be transmitted through them. Vegetation is sometimes used, but its benefits in reducing average noise levels, in terms of space efficiency, are less than those of commonly used noise barriers; however, root structures can act to reduce sound levels by making the ground acoustically softer. It is crucial to realize that the effectiveness of a barrier is controlled by the extent to which sound waves diffract at its crest or edges, travelling into receiver areas that are out of the line of sight. Wave diffraction is the principle mechanism which defeats the sound attenuating benefits of noise barriers (e.g. walls, berms and vegetation). Diffraction is influenced by the acoustical properties of the barrier surface, particularly at its crest. The presence of acoustically-softer material at the crest of a noise barrier will increase its effectiveness.

A variety of noise-barrier configurations are in use; walls and earth berms are the most commonly employed noise barriers. The relative advantages of each are evaluated in this work. Noise attenuation is a function of the barrier's transmission-loss characteristics and the diffraction that occurs along its edges (horizontal, vertical or otherwise). Noise reductions are related to the barrier's type, profile, height, surface material and location. As seen in Fig. 1.1, the cross-sectional profile of a barrier can be any of a large number of shapes — notably walls, earth berms and earth berms crested by a wall. Pure walls (of concrete, wood, metal or plastic) can be vertical or inclined, and top profiles can be added. Earth berms can be formed, and walls can be built atop earth berms. Capital costs per running metre for barrier construction include the costs of labour, materials and rights-of-way; walls are generally more costly to build. Berms are generally landscaped to take advantage of their aesthetic appeal; long-term maintenance costs must be factored into the barrier selection process. The ground area required for

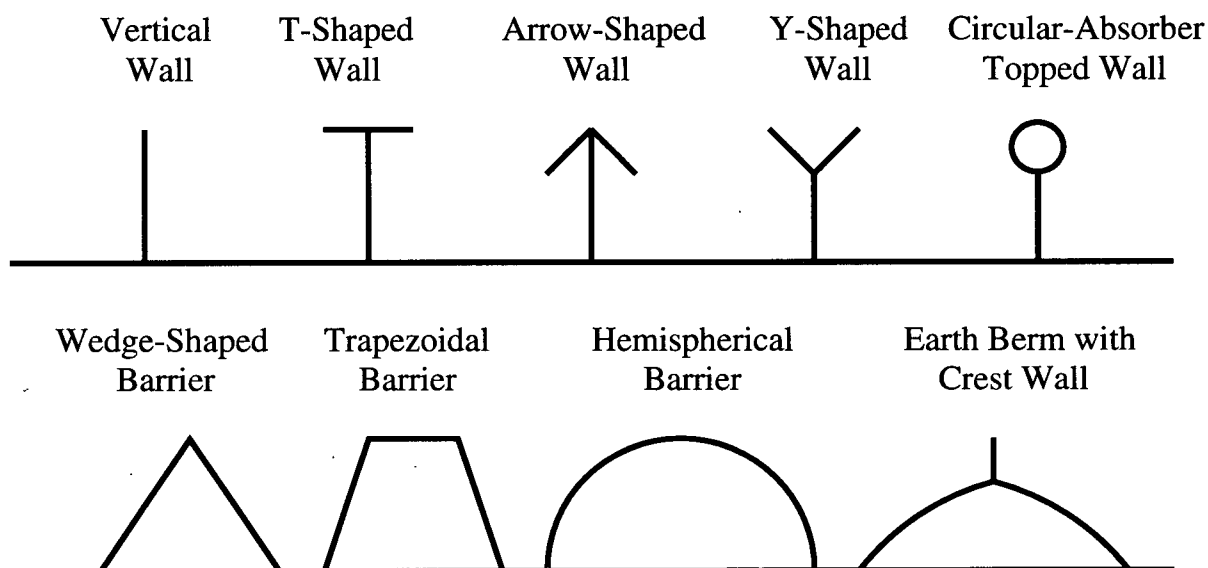


Figure 1.1: Some existing noise-barrier cross-sections and/or theoretically-studied shapes.

the barrier is a concern, and this may be limited by the available space or the related costs of rights-of-way. A berm may be created using excess material from highway construction, thereby eliminating removal expenses. Earth berms, with or without crest walls, are of particular relevance to British Columbians, due to the prevalence of topsoil to be found in areas of highway construction. Another factor, relevant in British Columbia, is the aforementioned restriction on the height of wall-type noise barriers; earth berms and earth berms with walls have no height limit. Thus, it was of particular interest to study berm/wall combinations.

Noise barriers can be studied by conducting full-scale tests, using computer models or by building scale models which have acoustical properties that are analogous their full-scale counterparts. The cost and effort of building full-scale models can be prohibitive. Furthermore, it is difficult to isolate parameters for study in an outdoor environment where testing is influenced by difficult to control factors, such as traffic flows and environmental conditions. Computer modelling is hindered in application by a lack of understanding of the ground effect and of diffraction phenomena in the presence of complicated topographies. Among other things, theories which have received widespread application ignore sound-wave interference (destructive or

constructive), by assuming incoherent addition of sound waves at a receiver. More sophisticated predictive techniques have little flexibility for altering the topography of terrain surrounding a noise barrier. For these reasons, acoustical scale modelling remains a cost-effective technique for studying the performance of noise barriers. Scale-model tests can, of course, be compared to full-scale outdoor tests, as well as to predictive theories. In the work reported here, an acoustical scale-modelling facility was developed to study the interplay of changes in noise-barrier profile and surface composition.

A major advantage of scale models is that important physical phenomenon such as diffraction are inherently reproduced, and environmental conditions can be more tightly controlled. A scale model is built at some reduced scale factor n , that determines the scale model's dimensions. The wavelengths of sound waves must be reduced by the same factor n , to maintain wavelength to dimension ratios. This is accomplished by employing sound that is increased in frequency by the same scale factor. Operating at these higher ultrasonic frequencies, it becomes necessary to employ materials in the scale model that differ from their counterparts, i.e. grass and pavement, in the outdoor world. It is necessary to find analogues to these materials that have the same acoustical properties at the higher test frequencies. An improved process of selecting appropriate scale-model materials is a feature of this thesis.

Some of the terminology to be used in the thesis will now be discussed. The properties of air are described in terms of fundamental factors like speed-of-sound, density and absorption. The speed-of-sound c in m/s — the rate at which a wave disturbance travels — is calculated using Eq. (1.1), where T is the temperature in degrees Kelvin, and T_o is the reference temperature 273.15 K:

$$c = 343.23 \left(\frac{T}{T_o} \right)^{0.5} \quad (1.1)$$

The characteristic impedance of air Eq. (1.2) is a commonly used quantity that is derived from the fluid density ρ in kg/m³, and the speed-of-sound:

$$Z_c = \rho c \quad (1.2)$$

It is of particular significance when studying the reflection of sound at an interface between air

and some other medium (fluid, solid or a combination of the two). The propagation constant γ in m^{-1} of air Eq. (1.3) is another commonly used quantity involving the wavenumber $k = 2\pi f/c$, and the air-absorption coefficient α (in units of nepers per metre, such that one neper will reduce the acoustic pressure by a factor of $1/e$ over a 1 m distance):

$$\gamma = k + j \alpha \quad (1.3)$$

If the air absorption is assumed to be zero the propagation constant takes on the value of the wavenumber. When a sound wave travels from source to receiver without generating other waves by reflection or diffraction, it is said to be in a free-field. In such a medium the sound waves' pressure amplitudes decrease at a rate which is proportional to both the increasing surface area of the wavefront (referred to as geometrical divergence) and the attenuation of pressure due to air absorption. The rate at which sound energy decreases with increasing distance is dependent upon the type of source in question — planar, cylindrical, or as a point. The relative humidity, temperature and atmospheric pressure affect the air absorption.

For spherical waves generated by a point source, acoustic pressure, p , decreases with distance r as $1/r$, and the sound-pressure level, L_p , defined as $L_p = 10 \log_{10}(p^2/p_o^2)$ where $p_o = 2 \times 10^{-5}$ Pa, decreases due to spherical-wavefront divergence at $\Delta L_{p,div} = 6$ dB per doubling of distance (dB/dd). For cylindrical wavefronts — from a line source — the rate of decrease is $\Delta L_{p,div} = 3$ dB/dd. Air absorption typically reduces sound pressure p at a rate that is exponential with distance and depends on the air-absorption coefficient. Eq. (1.4) is the expression used to predict the decrease of sound-pressure levels with air-absorption coefficient.

$$\Delta L_{p,air} = -20 \log_{10}(\exp(-\alpha \Delta r)) = -8.69 \alpha \Delta r \quad (1.4)$$

Fig. 1.2 shows the exponential reduction of sound-pressure amplitude with distance. Attenuation can be expressed in terms of decibels of attenuation per metre (dB/m):

$$\beta = 20 \log_{10}(\exp(1)) \alpha \quad (1.5)$$

Refractive phenomena are controlled by the effective-sound-speed profile above a ground surface. The effective sound speed is the sum of the wind speed and the temperature-dependent

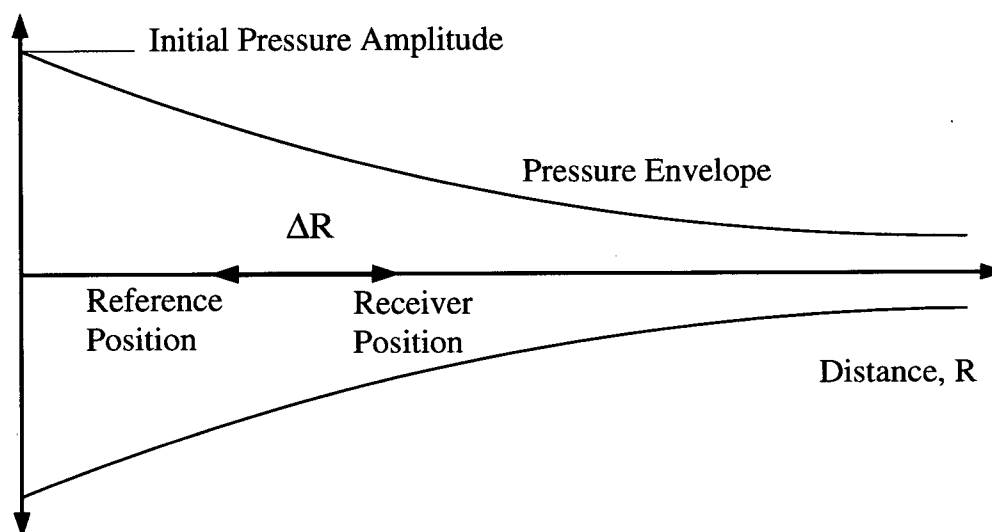


Figure 1.2: Attenuation of sound pressure with distance due to air absorption.

thermodynamic sound speed. Since wind and temperature can vary with height above the ground, so will the effective sound speed. The speed of sound increases with increasing temperature. Temperature variations are induced by the daily cycle of heating and cooling of air and ground by solar radiation; as well, wind convection can change the air temperature. When temperatures decrease with height, a temperature lapse condition exists — usually during daytime hours when the ground is warmer than the air above it. Due to the cycle of solar heating, there will be a time during morning when a temperature-inversion condition becomes a neutral one, and then goes to a temperature-lapse condition; during the early evening the transition is the reverse. Temperature inversions typically exist from evening to morning, during which time the sound levels perceived at ground level often increase, due to downward refraction. Cloud cover and precipitation tend to oppose the formation of a temperature gradient, resulting in temperature profiles tending to the neutral case. Wind speeds, of any given direction, typically increase with height above the ground; wind speeds generally peak in the afternoon, and are lowest at night. A positive-vector wind blows in the same direction in which sound

propagates; a negative-vector wind opposes the sound's direction of propagation; neutral conditions exist when there is no wind, or when the propagation is perpendicular to the wind vector. For an effective sound speed decreasing with height, sound will refract upwards, while it refracts downwards for an effective sound speed which increases with height. An effective-sound-speed profile that varies linearly with height will produce a circular path of refraction with a known radius of curvature. Shadow-zone attenuations can be created at a distance from a source whenever upwardly-refracting profile exists (upwind or temperature-lapse conditions) in the receivers direction. No ray-traced path will exist for direct and reflected wavefronts, and sound-pressure levels can be attenuated by 25 to 30 dB. A downwardly-refracting profile (downwind or temperature-inversion conditions) propagation leads to downward refraction. When sound rays reflect multiple times from the ground, new source-receiver paths can be created, thus changing the sound-pressure level.

The introduction of a ground plane generates complicated interference fields above the surface. The acoustic properties of plane surfaces are described by their surface impedance, Z . It describes the absorption of sound by the ground, as well as the time-lag-induced phase change that occurs when sound reflects from the ground. It is a complex-valued number written as in Eq. (1.6), in which the resistance R dictates the attenuation upon reflection, and the reactance X determines the phase change: The surface impedance can also be expressed in terms of its magnitude $|Z|$ and phase ϕ :

$$Z = R + j X = |Z| \phi \quad (1.6)$$

For a perfectly-reflective material the resistance goes to infinity and the reactance goes to zero. The impedance of any real surface has a finite magnitude and non-zero phase angle; there will be some attenuation and some time-lag imparted to reflected waves — implying a spring-like reactance which is mathematically analogous to a capacitor or spring. For an implied time dependency of $\exp(-j\omega t)$, a spring-like reactance is described by positive values of X ; R is always a non-negative number. For outdoor ground surfaces the surface impedance can vary widely. Surface impedance generally varies with grazing angle ψ (see Fig. 1.3) and

frequency, but the local-reaction ground-surface approximation allows for a normal-incidence surface impedance Z_n which does not vary with grazing angle. A ground surface is locally-reacting when: its refractive index is much larger than that of air, so that sound waves in the ground refract away from the surface; or the ground is highly-acoustically absorptive, so sound is absorbed quickly. The implication being that the vibrations of any two points on the ground surface are effectively uncoupled from one another. Thus, measurements of a surface's reflection coefficient R_p (see Eq. (3.8) on page 51) — for any given angle-of-incidence and frequency — should produce the same inference for Z_n . This would not be the case if the ground were an extended-reaction surface for which waves impacting at one point can transiently change the impedance at other points across the surface.

The ground surface impedance can be predicted accurately over a range of frequencies using the Delany & Bazley [3] model, which reduces the problem to one involving a single parameter — the specific flow resistivity per unit thickness, σ in c.g.s Rayls/cm — a measure of a material's resistance to air flow:

$$\frac{Z}{\rho c} = 1 + A \left(\frac{f}{\sigma}\right)^a + j B \left(\frac{f}{\sigma}\right)^b \quad (1.7)$$

in which $A = 9.08$, $a = -0.75$, $B = 11.9$ and $b = -0.73$ (Note that 1 c.g.s. Rayls/cm = 1000 Pa s/m²). The Delany & Bazley model has been used as a single-parameter descriptor of ground surfaces such as snow, soil, sand, gravel and asphalt — without changing any of the four constants just defined. Higher flow resistivities indicate larger impedance magnitudes and smaller phase shifts. More accurate specification of the frequency dependence of the surface impedance of a ground material requires even broader understanding of the contributions of microstructure. Other parameters to consider are: porosity — the volume fraction of interconnected air channels; shape-factor — the cross-section of air channels; and tortuosity — the deviation of air channels from linearity. Ground which is permeated with water has a reduced porosity, resulting in higher flow resistivities; these can vary with the height above the water table and the weather conditions. Vegetation typically has more of an effect on sound propagation due to the below-ground action of roots, which make the soil more porous and reduce the soil's flow

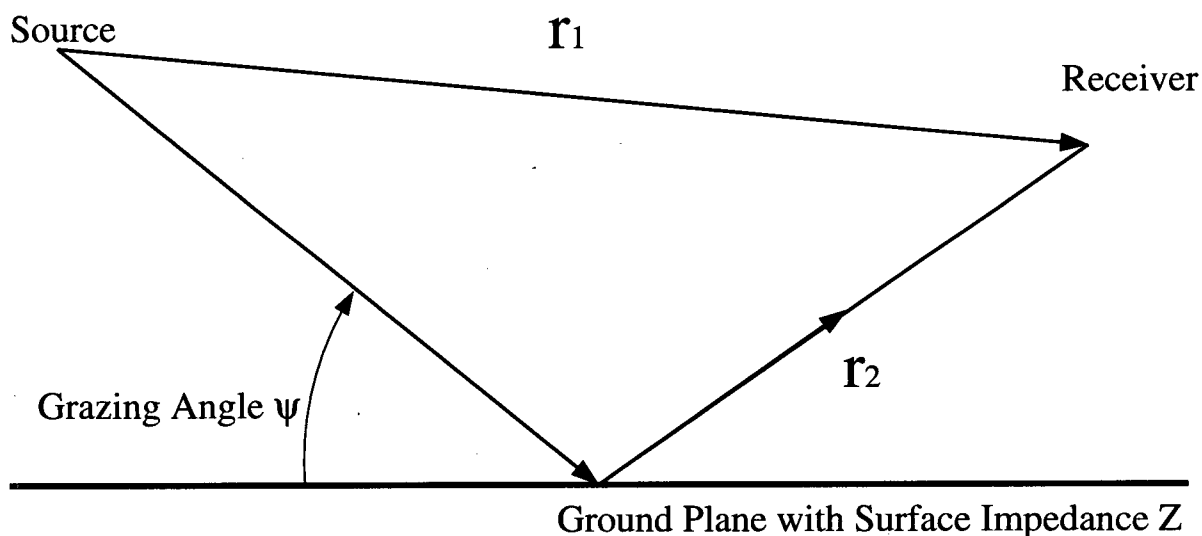


Figure 1.3: Sound propagation over open ground: ray-traced paths for direct r_1 and reflected r_2 components of the sound field over a surface.

resistivity.

Let us consider outdoor sound propagation in more detail. The simplest geometry that can exist between a traffic-noise source and receiver is depicted in Fig. 1.3. The ground is infinite in extent, the source and receiver are located above it as points in space, and the air is both homogeneous (no wind or temperature gradients) and motionless (no turbulence). Interference between the direct and reflected sound-propagation paths occurs due to the path-length difference between them and the phase lag introduced at the surface — in the absence of turbulence the sound waves are perfectly coherent. The resulting sound pressure will be a minimum at the receiver when the phase difference between the direct and reflected sound waves is equal to 180° ; this depends upon the frequency, test geometry and surface impedance. The concept of Excess Attenuation (EA) is used to isolate the contribution of a ground surface to changes in a sound field when that surface is introduced:

$$EA = L_{p,surface} - L_{p,free-field} + L_{p,div} + L_{p,air} \quad (1.8)$$

In this expression, sound-pressure levels for a given source-receiver position in a free-field

($L_{p,free-field}$) are subtracted from those in the presence of a surface ($L_{p,surface}$). Additionally, corrections are made to remove the effects of geometric divergence ($L_{p,div}$) and air absorption ($L_{p,air}$). A positive value of EA denotes an increase in sound-pressure level relative to free-field levels due to constructive interference, while negative values denote decreases due to destructive interference. Reflected waves travel further than direct waves, and they are also attenuated and phase shifted due to a finite surface impedance, so perfect cancellation between direct and reflected sound is impossible. In a general sense, the term ‘ground effect’ refers to surface-induced sound attenuation; more particularly, it refers to the first-attenuation minimum that occurs in the EA .

The EA can be both measured and predicted (see Eq. (3.4) on page 51), so measured values can be compared to predicted values in order to infer the surface impedance. By adjusting the flow-resistivity parameter of the Delany & Bazley impedance model, it is possible to find best-fit values of flow resistivity that give least-squares correlations over a wide frequency range. The best-fit flow resistivity for a given surface is called the effective flow resistivity σ_e . Another consideration is whether the ground reacts locally or extensively when sound waves reflect from a point on the surface.

Noise-barrier attenuation is quantified by comparing sound-pressure levels before and after a barrier is put in place. We define the the Insertion Loss (IL) as follows:

$$IL = L_{p,surface} - L_{p,barrier} \quad (1.9)$$

The term $L_{p,surface}$ is the received sound-pressure level over open ground with no barrier, while $L_{p,barrier}$ is that with a barrier placed on the ground. Due to sound-wave interference effects, the IL varies with frequency, source/receiver geometry and ground-surface impedance. The type of noise source is also important, since the IL of a barrier in the presence of a point source (e.g. loudspeaker, pistol, automobile) will differ from that of a line source (continuous line of vehicles). A positive IL indicates that attenuation has occurred, while a negative value implies an amplification of noise levels due to the addition of a barrier. Fig. 1.4 depicts the additional paths of reflection that are created by erecting a noise barrier, assumed infinitely

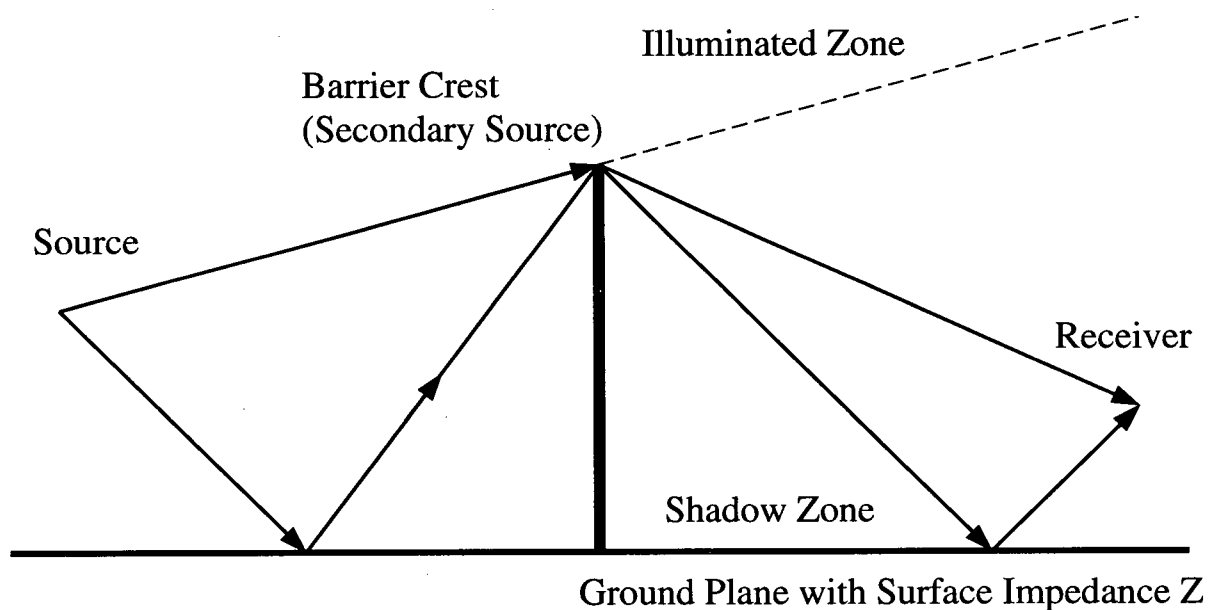


Figure 1.4: Sound propagation over a barrier: diffracted sound from a number of direct and reflected paths. Direct sound can travel directly to the receiver if barrier is lower.

long, which blocks the line-of-sight between a source and receiver. The IL can be predicted theoretically, measured outdoors at a barrier site, or measured in a scale-model environment. The benefits of changing a barrier's cross-sectional profile, height, width and surface impedance can be quantified using the IL . In particular, comparisons can be made between different classes of barrier, such as walls, earth berms, and earth berms/wall combinations.

In the absence of transmission through the noise barrier, atmospheric refraction and turbulent scattering, diffraction (the process by which sound waves travel around the edges of objects in a fashion which cannot be defined using ray acoustics) is the only means by which sound can reach a screened receiver position. Sound waves tend to have wavelengths that are comparable to the linear dimensions of a barrier. The amount of sound that is diffracted around an edge tends to decrease as frequencies increase. To isolate the effects of diffraction, the IL of a barrier can be assessed without any ground surface being present by comparing free-field levels to tests made with a barrier. The crest of the noise barrier acts as a secondary source by diffracting sound from the source side into the screened space behind a noise barrier. The

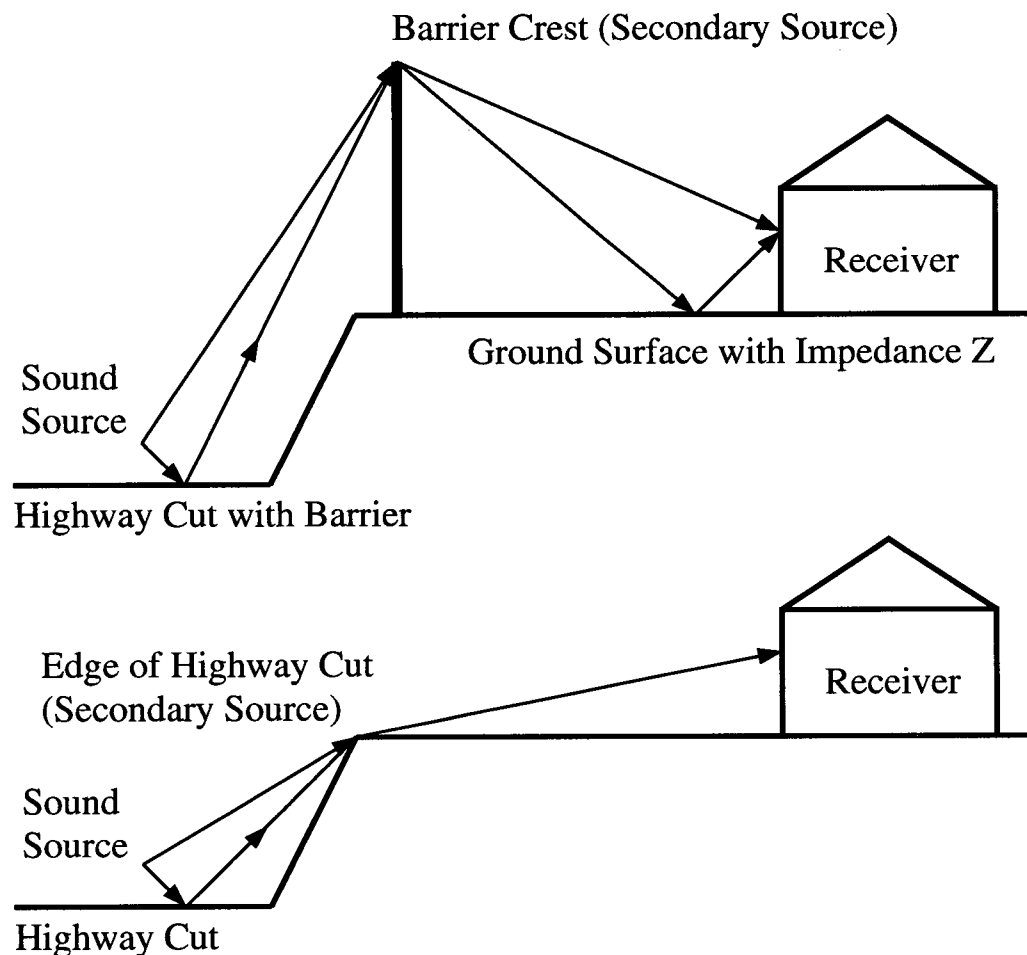


Figure 1.5: Sound propagation from a highway cut: in this case diffracted sound emanates from a secondary source at the crest of the roadside barrier.

barrier creates line-of-sight regions called illuminated zones, and screened regions called shadow zones (see Fig. 1.4). Direct sound can enter the illuminated zone, but only diffracted sound from the crest enters the shadow zone. Since the sound-pressure levels over open ground may result from interference between direct and reflected waves, the interposition of a barrier can reduce this effect and increase sound levels (negative IL). This is true at least for cases where the barrier is only high enough to block the reflected path, leaving the direct path open. A more complicated situation involving a highway cut is depicted in Fig. 1.5. In this configuration

noise levels at a near-highway receiver will typically be reduced; however, as receiver distance increases the noise levels may actually increase due to the elevation above the ground of the secondary source at the barrier crest.

Design and construction of the scale model required consideration of test-room requirements, air absorption at ultrasonic frequencies, ultrasonic noise sources, scale factors, model materials, and noise-barrier construction. An anechoic chamber was available for use as a test chamber; the properties of this room at ultrasonic frequencies had to be studied to see if reflections were problematic. An algorithm for predicting ultrasonic air absorption was programmed based on the published literature. A steady-state air-jet source design was selected, modified, and constructed. Previous approaches to the selection of scale-model materials were examined and a novel approach to material selection was successfully pursued. An algorithm was programmed for prediction of the *EA* of ground surfaces; this computer program was used to select the scale-model materials which were the best analogues of full-scale ground surfaces. Scale-model materials were used which had effective flow resistivities that adequately matched the applicable, effective values for outdoor ground surfaces. Highly cost-effective techniques for constructing scale-model noise barriers were developed.

The organization of the thesis is as follows. Chapter 2 reviews the literature in five topic areas: outdoor sound propagation; acoustical properties of ground surfaces; noise barriers; acoustical scale modelling; and human perception of traffic noise. Chapter 3 elaborates on the theory relevant to the project. Chapter 4 presents field tests performed to determine the traffic-noise spectra, and the *IL* of full-scale berms. Chapter 5 discusses the design and construction of the scale model, including noise-source development, material selection and choice of test equipment. Chapter 6 discusses the third-octave results of the *IL* testing of scale-model noise barriers. Chapter 7 applies these results to the real world by discussing the total *ILs*, with and without an accounting of the influence of both traffic-noise spectra and characteristics of human perception. Chapter 8 concludes the thesis by summarizing the most pertinent results of the work, and makes recommendations regarding future research.

Chapter 2

Literature Review

A literature review was undertaken on the subjects of outdoor sound propagation, ground surface impedance, noise-barrier performance, acoustical scale modelling of traffic noise and human perception of traffic noise.

2.1 Outdoor Sound Propagation

Delany [4] reviewed the historical development of understanding of outdoor sound propagation and its underlying physical mechanisms — divergence, absorption, reflection, refraction and diffraction; it is among the most comprehensive works of its kind. Minor atmospheric phenomena, such as fog and precipitation, affect sound propagation by changing the humidity, uniformity of temperature with height, and ground conditions. Piercy, Embleton and Sutherland [5], Embleton [6], and Embleton [7] summarized research performed by themselves and others, aimed at improved prediction of noise propagation outdoors, and studying community noise problems using theoretical models of coherent sound fields. Such prediction methods are inherently more sensitive, but are potentially very accurate. Piercy and Embleton [8] discussed the differences between standard methods used to infer the sound power of vehicular noise sources. They assessed the affect on measurements of variations in test geometry, ground surface impedance, instantaneous temperature, near-surface temperature gradients, and turbulence. Anderson and Kurze [9] reviewed international standards for predicting the A-weighted L_p ($L_{p,A}$) for common outdoor situations. At distances of up to 500 m, best-case and worst-case errors — depending on the location — were ± 5 dB and ± 15 –20 dB, respectively.

2.1.1 Atmospheric Phenomenon

Wayson and Bowlby [10] provided an excellent discussion of the statistical significance of various atmospheric effects influencing traffic noise; using regression analysis and hypothesis testing, the authors were unable to prove their null hypothesis — that traffic-noise levels are not affected by atmospheric phenomena at distances of 38.1 m. Measured variables were the average wind speed perpendicular to the roadway, vertical temperature-lapse rate, and Richardson number. Standard deviations were calculated for wind speeds parallel, perpendicular and vertical with respect to the roadway. Errors due to turbulence and changes in traffic-noise levels were minimized by averaging the sound-pressure levels over 10 s intervals. Using this information they produced empirical equations for calculating the attenuation of sound due to either positive- or negative-vector wind.

Geometrical Divergence — Maekawa [11] studied geometrical divergence for an incoherent point source and a finite-length incoherent line source. For a finite-length line source, at distances up to 1/10 the length of the line source, the decay is near 3 dB/dd. In this case the decay is line-source (3 dB/dd) dominated in the near-field, but experiences a transition to a point source at a distance related to the finite length of the line source. Beyond a distance equal to the length of the line source, the decay approaches the point-source rate of 6 dB/dd. Rathe [12] noted that the rate of decay of L_p with distance from an infinite number of incoherent point sources, spaced at equal and finite intervals, is dominated in proximity to an incoherent point source by the spherical-divergence decay rate of 6 dB/dd. There is a transition to a line-source decay rate of 3 dB/dd, at a distance from the infinite line of sources that is related to their finite spacing. Real traffic-noise sources can display the characteristics of both line and point sources.

Air Absorption — Wilson and Thomson [13] studied air-absorption fluctuations due to changes in temperature and humidity outdoors, examining how different time-averaging scales

affected measured fluctuations. Data, from which air-absorption coefficients were to be calculated, were averaged over half-hour periods for a total test duration of 1 year. The effect of averaging data over progressively-longer time scales was assessed in terms of changes in the calculated air absorption. Diurnal (daily) averaging produced up to 200% error, seasonal averaging 20–50% error, and annual means gave 20–50% error. They recommended meteorological data be averaged over time scales shorter than a day, and compiling a statistical distribution of calculated air absorptions from this short-term information. Winter air was quite dry and absorption varied dramatically with time due to the more pronounced winter-time dependency on humidity — temperature was less important. Summer air absorption peaks during the day and varies predominantly with temperature variations — humidity is fairly stable. ANSI [14] can be used to calculate air-absorption coefficients; for an accuracy of $\pm 10\%$, the standard applies to frequencies of 50–10000 Hz, temperatures from 0–40° C, relative humidities of 10–100%, and sea-level atmospheric pressures. A generalized-theoretical version of the ANSI standard is presented in [15] with corrections in [16] — the authors claim $\pm 5\%$ accuracy, for relative humidities from 0–100%, and frequencies from 50 Hz to 10 MHz.

Refraction: Wind Profiles and Temperature Gradients — Wiener and Keast [17] established that temperature and wind variations are the most significant atmospheric inhomogeneities. A comparison was made of test results over 9000 ft of flat ground comprised of grass and 1 ft high blueberry bushes — upwind and downwind results are discussed in terms of the expected distance and confining angle of the refractive-shadow zone. The radius of curvature is inversely proportional to the gradient of the effective sound speed; a 1° C per 100 m gradient corresponds to a 56 km radius of curvature. Embleton, Thiessen and Piercy [18] found that increases in sound-pressure level, due to propagation in a temperature inversion or downwind, were limited to 2.2 dB over perfectly reflective ground, and 0.5 dB over grass. They pointed out that this increase occurs due to an increase in the number of ray paths which can pass through a receiver's position — sound could be reflected several times from the ground surface before reaching the receiver. Although these are somewhat meager values, the authors also noted that

the additional paths of reflection can seriously degrade the 40 dB of EA that can occur due to destructive interference from a single ground reflection. The same paper presented a simple equation to predict the change in sound speed with height, as a function of the speed of sound at the ground surface, the height above the surface, and the linear rate of change of sound speed with height. A linear 1° F per 100 ft gradient will refract a ray circularly downward to a position 12,000 ft away, while reaching an apex of 180 ft. Piercy and Embleton [8] discussed the effects of a thermal boundary layer close to the ground, in which the generation of thermal plumes is related to wind variations, and the plumes in turn have an affect on turbulent eddies above the surface. Thermal-boundary-layer thickness tends to increase with decreases in wind speed. In this near-ground region, temperature fluctuations of 5° C were observed that lasted for several seconds in a steady wind, and these fluctuations were strongly correlated with changes in vehicle pass-by noise. The upward refraction of sound rays can be called an acoustic mirage which, when due to temperature, is analogous to the mirages seen at a distance on a hot day on a highway — in this case the temperature gradient above the asphalt is refracting light from the sky upwards away from the surface. Sound is affected similarly but the resulting radius of curvature for sound is some 1,700 times proportionately more sensitive to the temperature gradient. For a 15 m distance, attenuations due to the strong temperature lapse in the thermal-boundary layer were not observed at 1.0 m, but reached 10 dB at a height of 0.5 m — it was proposed that this could affect tire-noise testing. Rasmussen [19] concluded that a linear sound-speed profile can represent the combined effects of atmospheric sound-speed profiles and turbulence. However, the use of a more realistic effective-sound-speed profile (e.g. a logarithmic one) may require a more accurate representation of the effects of turbulence.

Turbulence — It was concluded [17] that turbulent sound-pressure level fluctuations at night were: 10–20 dB below daytime levels; greatest near the transition into a shadow zone; and that they increased with distance from the source. Chessell [20] studied the time differences between the arrival times of explosive sounds amongst an array of microphones at 4.3 km and 9.3 km distance from the source; data were acquired at midnight, sunrise, midday, and sunset.

The author concluded that turbulent fluctuations in the acoustic refraction index are greatest around midday, lesser at sunrise or sunset, and minimal at midnight. For the thirty explosive firings studied, the standard deviations of effective sound speed ranged from 0.5–1.2 m/s. The scale of turbulence was also studied, in the sense that atmospheric eddies can be assigned a characteristic dimension; vortices travel with the wind and the velocity of rotation will add to or subtract from the average wind speed. Daigle, Piercy and Embleton [21] studied the coherence between direct and reflected sound waves in the presence of turbulence. For a given test geometry, the standard deviations of measurements are typically greatest at frequencies where destructive interference occurs, due to the disruption of coherence amongst sound waves travelling along different paths. Their efforts were aimed at producing a method which could adequately predict the *EA* to be found at interference minima when turbulence was present. The net decrease of the magnitude of the sound in a spherically diverging shell tends to reach a limit; however, the effects of increasing turbulence upon the observed phase of a propagating wave are virtually unlimited.

2.1.2 Excess Attenuation of Ground Surfaces

Measurement of Excess Attenuation

Parkin and Scholes published in [22] and [23] the results of extensive measurements of *EA* derived from a year-long testing program — a database that is still being used by some researchers. Sound-pressure levels were recorded concurrently with environmental variables such as temperature and vector wind. Analysis of the *EAs* established the significance of ground effects, and atmospheric phenomena. They concluded that constructive and destructive interference were significant, as was refraction due to both wind profiles and temperature gradients. Parkin and Scholes [24] assessed the effect of source height, along with a more refined assessment of the effects of ground, temperature and vector wind. Moreland [25] conducted tests using an array of co-linear point sources radiating third-octave noise in the 500 Hz band, to discern changes in a sound field above a reflective surface, resulting from variations in the source's directivity.

It was found that sources with pronounced directivity can display less variation of L_p with distance over a reflective surface than does an omnidirectional point source; also, changes in the directional-source's orientation produced variations in L_p of up to 12 dB.

Prediction of Excess Attenuation

Homogeneous Atmosphere and Flat Semi-Infinite Ground — The first attempt to analytically predict the sound field over a plane boundary of finite impedance, by developing approximate velocity-potential solutions to the Helmholtz equation, can be found in Rudnick [26]. Lawhead and Rudnick [27] and [28], and Ingård [29] developed their approximate solutions using the complementary-error function. The papers brought theory and observation closer into line by starting with the assumption that the point source generates spherical wavefronts. A comparison of such approaches was made by Delany and Bazley [3]. Daigle, Embleton and Piercy [30] offered some important warnings to heed, particularly in regard to derivations based on [29]. Attenborough, Hayek and Lawther [31] claimed to have developed an exact solution for the two-media case (e.g. air and soil) of an extended-reaction surface. Their generalized model was simplified, by assuming that the ground's density and propagation constant are much larger than that of air, so as to make comparisons with previously published results. They demonstrated that, for a near-grazing angle of incidence, the extended-reaction solutions derived by [26], [27] and [28] are reduced forms of their solution. While deriving such solutions, it is often assumed that the ground surface is a local-reaction surface, as opposed to an extended-reaction surface, and the the grazing angle is small. They suggested that the assumption of a local-reaction model for grassland surfaces is invalid [32]. Rasmussen [33] derived asymptotic approximations for the extended-reaction model of [31]; the resulting expressions are claimed to be accurate up to 200 m — a distance beyond which atmospheric disruptions render the theory unusable in any event.

Wenzel [34], studied asymptotically the sound field near a soft and a hard boundary. It was hypothesized that a surface wave could exist over a soft boundary; it would diverge cylindrically

out from the source, and decay exponentially with height. Donato [35] discussed the relevance of the nature of the ground-surface impedance to the theoretical existence of a surface wave — the surface impedance must possess a stiffness-type reactance like that of a mechanical spring or electrical capacitor. Piercy, Embleton and Olson [36] conducted tests over a flat grassland surface, at distances from 1–1000 ft; the authors concluded that ground impedance dictates the EA , and that shadow-zone attenuations were limited by surface-wave sound energy. The impedance of the ground surface played a role in determining whether or not a surface wave exists. Thomasson [37], with his integral solution to the Helmholtz equation for a local-reaction surface, made amendments to the approach taken in [29], and confirmed that the predicted sound field over a finite-impedance boundary can be split into two terms — one of which has the form of a surface wave. However, it was argued that such a division of the sound field is not necessarily a reflection of physical reality. Rather, it is due to the selection of contours along which one chooses to integrate — a different integration contour can produce the same total field without a distinct surface-wave term. Scale-model experiments were conducted by Thomasson [38], and the results support the existence of a surface wave. A more concise version of the author's version of the solution [37] is given in Thomasson [39]. Thomasson [40] studied the relative dominance of direct, reflected, and surface waves by examining the relationships between source/receiver geometry, and the surface admittance (the inverse of the surface impedance) — it was shown that, in theory, the magnitude of the reactance of the surface impedance must exceed the resistance of the surface impedance, if a surface wave is to exist. Since reactances for ground surfaces tend to increase as frequency decreases, this implies amplified low-frequency EAs . Daigle, Stinson and Havelock [41] observed from scale-model tests using over a finite-impedance surface that the components of a spherical and surface wave can separate from each other. They hypothesized that, since a surface wave and spherical wave can satisfy the Helmholtz equation separately, they could exist independent of each other physically.

Computation of the spherical-loss factor can be performed to the desired degree of accuracy

by employing the method found in Matta and Reichel [42]. This procedure was first employed in this context by Chien and Soroka [43] (corrections to [43] are found in Chien and Soroka [44]). Pirinchievara [45] utilized this procedure, but typographical errors appear in the text. Stinson [46] clarified the relationship between the assumption of a spring-like or mass-like ground surface, the phase of the complex-valued numerical distance, and the spherical-loss factor; valid ranges for the phase of these expressions are clearly presented. A series approximation for calculating the spherical-loss factor is also discussed. Nobile and Hayek [47] developed expressions for a local-reaction boundary that allow the source/receiver distance to be arbitrarily small; the need to assume that the receiver is a half-dozen or so wavelengths from the source is avoided by employing a recursive formula that allows for calculations to any desired degree of accuracy.

Homogeneous Atmosphere and Non-Flat Semi-Infinite Ground — Howe [48] developed a theoretical model to account for a series of randomly-spaced hemispherical protrusions. Surface roughness mimics the effects of softer surface impedances, and promotes surface-wave generation, with the observable effect being to move the onset of the shadow zone further away from the source. More complicated surface topographies are left to the subsequent discussion on noise barriers.

Non-Homogeneous Atmosphere and Flat Semi-Infinite Ground — Atmospheric phenomena such as absorption, refraction, and turbulence can vary with both height and range. Li [49] developed a velocity-potential solution for a vertically-stratified, quiescent (non-turbulent) atmosphere over an extended-reaction surface. If the air is considered to be a homogeneous medium, the equations reduce to the form of those found in [31]. L'Espérance *et al.* [50] developed a heuristic model which accounts for a number of compromising factors: air absorption; atmospheric refraction (and transient fluctuations thereof); turbulence; and shadow zones created by upwind propagation. Attenborough *et al.* [51] reviewed extensively the computational approaches to sound-field prediction over a plane ground surface. The numerical approaches considered include parabolic equations (PE), fast-field prediction (FFP), and ray-tracing using

Gaussian beam theory. Furthermore, a set of analytically-defined test cases were developed, which are intended to be used as performance benchmarks for computer-coded prediction algorithms. By comparison, it was concluded that the PE and FFP methods agreed computationally within numerical accuracy for a number of test conditions, as well as agreeing with the available analytical solutions.

Non-Homogeneous Atmosphere and Non-Flat Semi-Infinite Ground — At this time, this area of inquiry has not been explored extensively in the academic literature; although this topic leads into material on noise barriers and the potentially-compromising effects of atmospheric phenomena on barrier *IL*.

2.2 Ground Surface Impedance

Delany & Bazley [3] developed power-law relations that predict the normalized characteristic impedances and propagation coefficients of rigidly-framed fibrous materials from the ratio of frequency divided by flow resistivity. The power-law equations are valid for $10 \leq f/\sigma \leq 1000$.

Piercy, Embleton, and Sutherland [5] observed that grass surfaces behave like porous, local-reaction media — the impedance's magnitude is related to the presence of a porous surface layer with holes that are small enough to offer resistance to air flow. Both the length of grass and inclement weather had a small effect on impedance. Also, snow or tilled soil was found to have a much lower impedance at lower frequencies; asphalt would have a much higher, though still finite, impedance.

Chessel [32] applied the Delany & Bazley model to study the impedance of soil surfaces to describe a porous local-reaction impedance boundary. By making comparisons between measurement and theory, he found that a grass-covered surface was best described by $\sigma = 300$ c.g.s. Rays/cm, and that soils can be treated as local-reaction boundaries. The ratio f/σ was extrapolated down to $0.5 \text{ cm}^3/\text{g}$ with good results. When applied to a grass surface, an effective flow resistivity of 300 corresponds to a lower bound on frequency of about 2500 Hz. As such,

studies of ground surfaces where the ground effect typically comes into play — below 500 Hz — are extrapolating the Delany & Bazley model outside of its valid range.

Attenborough [52] considered the relative usefulness of generating power-law relationships that employ either the non-dimensional parameter $\rho f/\sigma$ or the dimensional parameter f . A table of coefficients (A, B, C, D), uniquely varied for each ground surface, was presented based on the expressions $R/\rho c = 1 + Af^B$ and $X/\rho c = 1 + Cf^D$. The validity of these different approaches was not explored further in this paper. When the source and receiver are on the ground, a surface wave can exist mathematically when $X > R$; the necessary ratio of X to R increases with grazing angle. The author further explored the significance of ground cover on the A-weighted levels generated by a line source.

Attenborough, Hayek and Lawther [31] evaluated the characteristics which have been assigned to ground surfaces: local or extended reaction, layered media or a constant or graded porosity, and uniform or discontinuous impedance.

Embleton, Piercy and Daigle [53] coined the term 'effective flow resistivity', σ_e , to describe the value of flow resistivity that generated a best fit between measured and predicted EA spectra. They recognized that several material parameters other than flow resistivity may influence the effective flow resistivity, with the precise effect being dependent on the material in question. Table 2.1 summarizes the effective flow resistivity of eleven classes of ground material in terms of c.g.s. Rayls/cm. Acoustically-hard surfaces produce very little phase change upon reflection; interference phenomena were observed for frequencies for which the direct and reflected sounds were different by multiples of a half-wavelength. Low-frequency EAs can increase due to two phenomena: the acoustic impedance of ground increases with decreasing frequency; and surface waves are increasingly generated with decreasing frequency. Sound propagating in the ground can be attenuated by about 30 dB per wavelength, implying that assumptions of local reaction are justifiable. For very large effective flow resistivities the most significant effect of changing the value of σ is to change the attenuation at interference minima. When the source and receiver are placed on the ground, tests over a series of distances

Table 2.1: Values of effective flow resistivity for outdoor ground surfaces

dry snow, new fallen 0.1 m over about 0.4 m older snow	15-30
sugar snow	25-50
in forest, pine or hemlock	20-80
grass: rough pasture, airport, public buildings, etc.	150-300
roadside dirt, ill-defined, small rocks up to 0.1 m mesh	300-800
sandy silt, hard packed by vehicles	800-2500
clean limestone chips, thick layer (0.01-0.025 m mesh)	1500-4000
old dirt roadway, fine stones (0.05 m mesh) interstices filled	2000-4000
earth, exposed and rain packed	4000-8000
quarry dust, fine, very-hard packed by vehicles	5000-20000
asphalt, sealed by dust and use	30000

can be used to determine the flow resistivity, since the cutoff frequency for a surface wave is the frequency for which $X = R$. The spectrum shape varies rapidly enough as a function of effective flow resistivity that measured spectra can be used to determine the effective flow resistivity for a ground surface. These grazing-incidence tests provided reasonable accuracy. There is an upper limit for the surface impedance of a surface due to the thermal-conduction and viscous boundary layers at the surface. As predicted from the expression of Konstantinov [54], $|Z/\rho c| = 57200 f^{-0.5}$, for an atmospheric pressure of 1 atm, the limit in c.g.s Rayls/cm ranges from 3×10^5 at 100 Hz to 1×10^6 at 10 kHz.

Attenborough [55] examined the surface-impedance measurements of previous researchers by attempting to curve fit three different ground-impedance models to the data. The Delany & Bazley single-parameter model was compared to a pair of two-parameter models — one assuming a porosity Ω which decreased exponentially with depth at an effective rate α_e , the other assuming an effective layer depth on a rigid backing. A four-parameter model, using porosity, flow resistivity σ , grain-shape factor n' , and pore-shape factor s_f , is the basis for deriving the two-parameter models. First, assuming low-frequencies and high-flow-resistivities, an approximation is derived from the four-parameter model; only a single parameter (effective flow resistivity) is to be adjusted when fitting impedance versus frequency data. The characteristic

impedance of a ground surface in air is calculated from: $Z_c = 0.218 (\sigma_e/f)^{1/2}(1+i)$. From this approximation another model, valid up to several kHz, was developed to allow for exponential decreases in porosity with depth. The porosity-based model was derived assuming that flow resistivities are high: $Z_c = 0.218 (\sigma_e/f)^{1/2} + j[(\sigma_e/f)^{1/2} + 9.74 (\alpha_e/f)]$. The two parameters can be calculated from $\sigma_e = s_f^2 \sigma/\Omega$ and $\alpha_e = n' \alpha/\Omega$. This model was used further, in conjunction with the assumption of a layer that is small compared to the wavelength, to derive a two-parameter model for grounds that act as thin, hard-backed porous layers. The mathematical transformations for dealing with layered structures are also discussed. The impedance for the latter two-parameter models was thought to be adequately defined by measurements made at a single frequency at which the least-squares error among tests was minimized.

Attenborough [56] further studied his four-parameter theory for rigid-framed granular media — for example, isotropic and homogeneous air-filled soils and sands. The ground effect was shown to become important below 500 Hz and to be the dominant influence on near-grazing propagation at frequencies below 250 Hz. “Tolerable” agreement was found for predictions of impedance versus frequency for grass-covered ground, bare ground, and a layered forest floor when measured values of flow resistivity and porosity were used, along with estimated values of grain-shape factor and pore-shape factor. For sandy soils, it was noted that Delany & Bazley overestimates the frequency dependence of the real part of the impedance and all values of the imaginary part of the impedance. For layered forest soils Delany & Bazley is in error, since the real part of the impedance tends to be either a near-constant value or to display non-monotonic behaviour. The two-parameter models of [55] were rederived. The layer model is valid for frequency ranges for which the ground effect dominates near-grazing sound propagation. The normalized resistive part is more-or-less independent of frequency, with reactive parts that increase strongly with decreasing frequency. It was concluded that the reactive part of a thin, hard-backed layer will vary with layer depth, independent of the effective flow resistivity; increasing layer depth increases resistance while decreasing reactance. Measurements of the sound field over a ground surface allow for non-invasive assessments of a

ground surface's physical parameters.

Martens *et al.* [57] made *in situ* measurements of the normal specific surface impedance of forest soils, grass-covered soils and bare sandy soils. Physical parameters such as — porosity, water, air and solid content, soil texture, and flow resistivity — were measured. All measured ground surfaces were classified acoustically with regard to their impedance, plane-wave reflection coefficient and effective flow resistivity. For grass-covered and forest soils, the real part of the impedance was almost frequency independent, while the imaginary part varied strongly with frequency. The Delany & Bazley model was originally derived assuming homogeneous materials with porosities near unity; neither of these assumptions is valid for soils, particularly the assumption of high porosity. Direct measurement of flow resistivity was not a reliable means of predicting acoustical parameters when using the Delany & Bazley model — particularly for forest floors. Acoustically derived effective flow resistivities were invariably smaller than directly-measured values. The soil structure and the related acoustical properties of soil were strongly influenced by vegetation; vegetation created a layered soil structure. Litter layers on the surface were largely acoustically transparent, and the removal of a humus layer had little effect. For grass-covered floors only the root layer appeared to be important acoustically. Bare sandy soil can be assumed to be homogeneous and unlayered, so Delany & Bazley was more successful. Water was significant in its reduction of soil porosity.

Attenborough [58] considered the interaction of sound with ground and explored how the ground-effect dip in an *EA* spectrum varies with the acoustical properties of porous ground surfaces. *EA* minima occurred at progressively lower frequencies as either the boundary becomes softer (primarily) or the path-length difference between direct or reflected paths becomes greater (secondarily). Four types of surface modelling of rigidly-framed, porous media were described: homogenous, variable porosity (exponentially decreasing with depth), hard-backed layer, and multiple layers. Mathematical analyses which account for the elasticity of the soil reveal that a surface acoustic wave can exist, as can an air-coupled Rayleigh wave which travels below and parallel to the surface. For grounds with flow resistivities on the order of 300 c.g.s. Rayls/cm,

sound propagates through the pores at a speed that is much lower than in a free-field; thus, the index of refraction is very high and the ground can be treated as locally reacting. Complete modelling should account for the elasticity of the soil grains. For grounds for which the first few centimetres of soil display strong variations in acoustical properties or flow resistance, knowledge is required of the propagation constant within the ground and of the acoustical near-surface structure. The impedance for a hard-backed layer may be deduced from $Z = Z_c \coth(-jk_b d)$, where k_b is the propagation constant, and d is the thickness, of the layer. Thin, hard-backed layers are most theoretically likely to create surface waves, but field tests have yet to produce experimental evidence that they exist over such a surface. Surfaces such as forest floors and snow typically have effective flow resistivities near to or below 50 c.g.s. Rayls/cm; as such, they are assumed to be locally reacting. However, if they are layered the influence of external reaction may be modelled by assuming local reaction and adjusting the effective flow resistivity. Apparent changes in the effective flow resistivity could arise due to a change in the ground character, surface roughness, and/or environment.

Berengier, Hamet and Bar [59] studied porous asphalt, developed a theoretical model to predict its acoustical behaviour, and made comparisons between predictions and measurements. The advantages included reductions in external and internal vehicle noise levels, vehicle vibration, water splash and spray, improved skid resistance at high speeds, and temporary water storage during high-rainfall periods. The paper includes an excellent presentation of the assumptions and equations used to derive the material parameters for the relative air volume (porosity $0 < \Omega < 1$), flow resistance to motion (specific air-flow resistance R_s), inertial modifications (shape factor $K > 1$), and layer thickness. The effects of single-parameter changes are evaluated in terms of plots of absorption coefficient versus frequency. Peaks are observed among the absorption spectra, which can display shifts in their frequency location and amplitude. The significance of these peaks is related to the noise-generating mechanisms of tires. Tire noise arises from the tire's vibrational field and air-resonances in the tire/ground air-gap. Vibrations occur due to tire strains from rolling deformation, tire-tread impacts, and stick-slip

effects between the tire and road surface. Air pumping is the mechanism which generates air resonances, but a horn effect can also occur when multiple reflections arise between the tire and the roadway. They make fairly extensive analysis of the theoretical benefits of changes to material parameters (layer depth, porosity, etc.), in an effort to develop an ideal asphalt microstructure that can withstand the reductions of porosity that can occur with aging due to compacted debris. A thickness was found for the acoustically-absorptive, wearing-course layer, beyond which further increases of layer depth bring no benefit. The effects of humidity, grading, and binder content are also considered. Wet pavement was found to be less acoustically absorptive — largely due to a decrease in porosity.

Miki [60] noted that, when the Delany & Bazley model is used to predict the characteristic impedance of a layer that lies on a rigid backing, the surface impedance of this layer can have a negative real part at low frequencies (e.g. dimensional ratios of $f/\sigma < 10$). This is not physically plausible. By modelling the ground as a linear, passive, one-port network of cylindrical tubes, a positive-real property is obtained. A new characteristic-impedance model was derived that has this property when a layered surface is described; predictions were also made for the propagation coefficient of the surface. It was concluded that a single-parameter model is not able to provide perfect predictions over the entire frequency range of interest, but that the model should at least give well-behaved, physically-realizable predictions even outside the range specified by Delany & Bazley. Future work would involve further developments for both the porosity and shape factor, since the model developed in this paper is only useful for materials that have porosities near unity.

Miki [61] generalized his empirical models for both the characteristic impedance and the propagation constant of porous materials by introducing parameters for porosity, tortuosity and pore-shape-factor ratio. The model assumes cylinders that are inclined at an angle with respect to the surface's normal vector, as described by a structure factor q . The new models still restrict the material's porosity to values near unity. It was concluded that the model agreed well with Attenborough's four-parameter model for ground surfaces [62, 56]. The characteristic

impedance and the propagation constant could each be evaluated, respectively, by only two parameters: the effective flow resistivity and the ratio of tortuosity to porosity; and the effective flow resistivity and tortuosity.

Moore *et al.* [63] conducted experiments over snow to determine the acoustical parameters of snow and develop methods for non-intrusively characterizing snow. Level-difference tests were used to evaluate the certainty with which snow can be assumed to be an external-reaction, homogeneous, rigid-framed, porous material. The level-difference technique is a variant of the *EA* since it employs two microphones, but they are aligned vertically with respect to the ground at some distance from a noise source. The level difference is calculated by taking the base-ten logarithm of the ratio of the total field at the upper microphone divided to that of the lower microphone. The snow was thought to be deep enough to be treated as being a semi-infinite medium. If the measured ground-effect dip falls below 1 kHz, due to either the ground's properties or the test geometry, then low-frequency/high-flow-resistivity approximation models can be employed. The Delany & Bazley model was originally derived using fibreglass materials with porosities near unity, so dry snow, with porosities near 0.9, can be adequately modelled using their impedance model; however, wet snow has porosities in the range 0.15–0.30. The authors proposed that it was questionable to persist in the use of the Delany & Bazley model given that different snow surfaces with the same density can have different directly-measured flow resistivities. The ground-surface model used was a three-parameter approximation (porosity, effective flow resistivity, and tortuosity) to a four-parameter model. This was thought to be adequate for snow-covered surfaces at frequencies below 2 kHz. The three-parameter model can give non-unique solutions, since for a given geometry there will be two different parametric solutions. The level-difference technique was used to determine porosities, monitor surface crusts and locate subsurface layering in snow. On the basis of the good agreement between theory and measurement, they claimed that the non-intrusive, acoustically-determined porosities were more accurate than the intrusively measured values; the acoustically-determined porosities were 15% lower than measured. Probe-microphone measurements indicated that more sound

penetrated into the snow than was expected, indicating that future modelling of snow surfaces may require a ground model that assumes both external reaction, and multiple layers.

Van Wyk, Bolton and Sherman [64] employed the single-parameter Delany & Bazley model to generate estimates of the effective flow resistivity for tests conducted at grazing incidence. The objective was to develop a single-number characterization of asphalt surfaces — before and after the application of a sealant. Measurements were made over asphalt, with the source and receiver placed on the pavement at distances from 0.1–12.8 m. The least-squares errors between theoretical and measured squared-rms pressures were normalized with respect to the theoretical values. These errors were calculated for differing ranges of frequency and distance, and plotted over a range of effective flow resistivities. Minima were observed in the plotted least-squares surfaces, suggesting a best-fit value of σ_e . It was possible to distinguish between asphalt surfaces that were with and without a sealant, when monitoring the repeatability of tests at different locations, and when evaluating the long-term stability of different asphalts. However, the authors observed that the parametric estimates varied significantly with the horizontal source/receiver separation distance and the frequency ranges for which the estimates were made. Thus, meaningful comparisons could be made only if best-fit effective flow resistivities were generated for a common set of frequencies and distance. The authors concluded that a multi-parameter model would be more useful in correlating the microstructural properties of ground with the observed normal-incidence surface impedance.

Attenborough [65, 66] introduced a two-parameter approximation for the normal surface impedance of a non-hard-backed layer. Previous measurement data for outdoor ground surfaces were used to calculate the best-fit parameters of the new model (σ_e and α_e). It was noted that a single-parameter model is at a disadvantage since the frequency dependence is fixed, as are the relative magnitudes of the real and imaginary parts of the impedance. The Delany & Bazley single-parameter model, though capable in restricted instances of giving good results, was shown to overpredict, below 300 Hz, the real and imaginary components of impedance. Other low-frequency measurement artifacts include apparent resonances, perhaps

due to quarter-wavelength seismic resonances. The new model was derived by assuming that the near-surface structure consists of one or more layers terminated by a non-rigidly backed, semi-infinite, porous layer, or the porosity gradually decreases with depth at an exponential rate. When dealing with soils that have a significantly layered structure, the two-parameter model for a porous soil outperformed the Delany & Bazley model when used in conjunction with mathematical corrections for the impedance transformation of layers. The use of Delany & Bazley to predict the low-frequency EA over an extended-reaction surface, like snow, was not found to be satisfactory even when employing a velocity-potential model that accounts for extended-reaction surface. For both a compacted earth and a grass surface, the two-parameter model was plotted with the best-fit values of its parameters versus the best-fit Delany & Bazley model; significant differences were observed between the two models for each of the two ground types.

Sabatier, Raspet and Frederickson [67] evaluated Attenborough's four-parameter model for homogeneous, rigidly-framed, porous media. Experimental results for soil surfaces — measured using the level-difference technique — were evaluated to see if the parameters are independent of one another. These four parameters were reduced to a three-parameter model including the tortuosity T , porosity and an effective flow resistivity $\sigma_e = s_p^2 \sigma \Omega$ (where s_p is the pore-shape factor). They concluded that there are, in fact, only two independent parameters: the reduced flow resistivity $s' = \sigma_e / \Omega^2$ and reduced tortuosity $t' = T / \Omega^2$. It was suggested that the three-parameter model can be utilized if one of the three parameters is physically measured — allowing the remaining two to be defined uniquely. When estimating the ground surface's parameters, the level-difference technique was also shown to produce geometry-dependent differences.

Hutchinson-Howorth, Attenborough and Heap [68] evaluated the level-difference method to see how robust it was at generating estimates of the resistance or reactance of an impedance model or the parameters thereof. The spectral-magnitude differences between the two microphone signals are evaluated to assess the impedance. The technique proved useful since it is relatively immune to changes in the position of the ground surface. Turbulence, refraction,

and a non-plane surface can compromise surface impedance measurements. Errors due to meteorological conditions were minimized by keeping the source/receiver distance less than 3 m; microphone heights were more variable, though the lowest microphone was kept high enough to minimize the effects of microclimatic variations. The sensitivity of the technique was evaluated in terms of different minimization functions, and its robustness in the presence of added systematic and/or random errors. Minimization-function surfaces were plotted over the R , X axes to help visualize the best-fit locations of the interference dips; the smaller the error the better the fit. Phase was not employed since measurements of phase are easily contaminated by extraneous noise and are thus unreliable. Four types of material were tested, using combinations of locally or externally reacting, and semi-infinite or rigidly-backed media. The parameter-fitting method, with its imposed frequency dependence, reduced the number of necessary spectra, and allowed for impedance estimates for both local- and external-reaction surfaces. A determination of R and X was found to be possible for locally-reacting surfaces, but for external-reaction surfaces this was not possible due to the additional unknowns.

Numerous techniques have been used to obtain estimates of the impedance properties of ground. Sprague, Raspet and Bass [69] evaluated four techniques for measuring ground impedance at frequencies below 150 Hz. Power-law approximations such as the Delany & Bazley model tended to overestimate the low-frequency impedance of ground surfaces. The authors attempted to discern how this discrepancy relates to the measurement technique employed. They used an impedance meter, the probe-microphone method, modified Biot-Stoll calculations, and the phase-gradient method. A ground-impedance metre is analogous to a Helmholtz resonator, with a single piston supplying a constant volume velocity and a single microphone measuring the pressure. The other approaches each utilized a pair of microphones. The probe-microphone method involved placing a single microphone on the ground surface, and comparing the measurement to that of a single microphone buried a distance below the surface.

Attenborough [70] examined theoretically the influence of turbulence and short-range geometry on estimates of the effective flow resistivity of a one-parameter, normalized impedance

model: $Z = 0.436 (1 + i) (\sigma_e/f)^{0.5}$. Note that the constant disagrees with that found in [55]. Near-grazing angles of incidence had the greatest sensitivity to changes in effective flow resistivity, at the expense of greater errors at high frequencies due to the effects of turbulence. It was suggested that changing the test geometry so that the ground-effect dip lies between 500 Hz and 1000 Hz results in a good compromise between minimizing the effects of turbulence and maximizing the sensitivity to changes of σ_e — a number of test geometries were proposed. A pair of equations for estimating σ_e were given for application to different regimes of effective flow resistivity.

2.3 Noise Barriers

As will be discussed, a number of studies have been undertaken of the noise attenuation provided by barriers. Studies of noise barriers have been conducted at full scale, model scale, and theoretically using both analytical and numerical techniques. Factors considered for noise-barrier design include the barrier's profile, length and surface impedance, and the presence of ground surfaces with their associated surface impedances. Barrier profiles have included canonical shapes such as walls, wedges, trapezoids and hemispheres. Wall profiles have included vertical, inclined, T-shaped, Y-shaped and arrow-shaped. Increased top widths have been used to increase the effective height of the barrier and to allow for the addition of absorptive material to the barrier top.

For tests at full scale, there are few guidelines available. ANSI S12.8-1987 [71] presented standardized methods for conducting *IL* tests of generic noise barriers. Recommendations included appropriate test procedures, measurement locations and limits on environmental conditions.

Some publications provided authoritative reviews of previous noise-barrier studies. Watts [72, 73] provided a practical and current review, with particular reference to the effects of barrier absorption and profile — results which will be reported herein with reference to the papers cited in [72, 73]. Hayek [74] summarized previous noise-barrier work by categorizing

papers with regard to the boundary conditions (presence/absence of ground, finite/infinite surface impedances) and barrier profiles in question. Keller's geometrical theory of diffraction was compared to scale-model tests of an incoherent line source (a traversing point source) with a satisfactory agreement between prediction and measurement.

Noise attenuation by walls of different profiles has been studied theoretically — the effects of interference due to ground reflections may or may not be included to enhance prediction accuracy. For an incoherent point source, Maekawa [75] addressed the diffraction of a semi-infinite wall in a free-field in terms of its dimensionless Fresnel number, without considering the effects of ground reflection; wall IL was found to increase monotonically with frequency. Kurze and Anderson [76] extended the Kirchoff diffraction theory to allow for an incoherent line source and a barrier of finite length. Finite-length barriers have also been studied by Pirinchievara [77], who reported that a barrier needs to be four to six times longer than its height for it effectively to be infinite in length. Lam [78] developed an extension of Maekawa's energy summation method to allow for predictions of the IL of a three-dimensional barrier of finite length, by considering the interference between each minimum-length diffraction path; it is reported to be reasonably accurate and computationally efficient for octave-band predictions, but not as accurate as integral-equation methods for providing fine details of the sound field. Macdonald's exact solution for a thin screen was adapted to include ground surfaces by Jonasson [79] using the source/receiver image concept; barriers were found to be most effective when ground attenuation was low. Thomasson [80] derived new expressions for predicting barrier diffraction from the integral equation for a diffracting object, so good predictive results were possible for an infinitely-long, thin screen of low height on finite-impedance ground; an excellent collection of figures presented the effects on barrier attenuation of variable ground surfaces, receiver height, screen height, screen length, side-edge position and angle-of-incidence. Hothersall, Crombie and Chandler-Wilde [81] used the boundary-element-method (BEM) solutions of the Helmholtz equation to study walls of varying profile; they found that: the addition of absorption to an upper surface will increase IL progressively with increasing absorption; Y

and arrow profiles were generally inferior to a T-shaped barrier; when controlling for effective height, width increases to a top had little effect; and arrow and T-profiled barriers outperformed their wedge and flat-topped mound counterparts by 1–2 dB. This last result suggests that the presence of slopes towards the crest of the barrier are detrimental to IL . In [82] walls were given vertical, T-shaped, arrow-shaped and Y-shaped profiles, and a line source was simulated using scale-model vehicles to scatter noise from a stationary spark source. The results found in [81] were shown to compare favourably to the A-weighted total IL s May and Osman [82] measured using 1:16 scale modelling.

Wide barriers like trapezoids and circular barriers have been the object of theoretical research. Among the most commonly cited papers on wide-barrier noise attenuation is Pierce's [83] work on the diffraction of a reflective semi-infinite wedge or trapezoid in a free-field. For diffraction predictions, both amplitude and phase-change effects are accounted for. Predictions show that walls outperform three-sided trapezoids by 1–3 dBA. The theory has been used recently as an analytical benchmark by Salomons [84] and Cremers, Fyfe and Cremers [85], to evaluate their numerical studies of diffraction using PEs and the BEM, respectively; they found good agreement between analytical and numerical results. Thick barriers of infinite and finite impedance over finite-impedance ground have been studied by Jonasson [86], using the source/receiver image method; at large receiver distances depressed roads were found to be more effective than barriers of equal height, with the reverse conclusion at short receiver distances. In de Jong, Moerkerken and van der Toorn [87], Jonasson's work was updated and the Delany & Bazley model applied to the study of field tests of outdoor ground surfaces; improved agreement between field tests and theory was obtained for earth-berm measurements, when the impedance discontinuity between asphalt and grass was accounted for; they noted that meteorological effects and the ground effect have their greatest effect on barrier attenuation in different frequency bands. A round-robin comparison was made by Saunders and Ford [88] of five analytical methods for predicting attenuation due to diffraction by thick barriers with

two diffracting edges; they concluded that predictions using the theories of Medwin [89], Hadden and Pierce [90] and Medwin, Childs and Jebsen [91] were similar and gave fairly accurate predictions in the shadow zone. Interestingly, all of these methods were unable to accurately predict levels in the illuminated zones and the transition zone (penumbra). The penumbra problem has recently been addressed by Berthelot *et al.* [92] using matched-asymptotic expansions to predict *ILs* for a hemispherical barrier; they measured levels along the line-of-sight in the penumbra that were within 1 dB of predicted levels. Deep in the shadow zone along the barrier surface, theory systematically overestimated measurements by 0.5 dB. Rasmussen [93] studied theoretically the noise attenuation of wedges and three-sided trapezoids (to represent earth berms) in the presence of an impedance discontinuity on the ground surface; good correlations between measurement and theory were obtained by employing the geometrical theory of diffraction for a wedge and accounting for finite surface impedances. Hasebe and Kaneyasu [94] employed Green's functions to generalize the problem of noise attenuation by a wedge to allow for varying impedances on each wedge surface; the authors claimed excellent agreement with scale-model tests. The noise attenuation provided by a thin wall placed atop a wedge has been studied theoretically by Matsui *et al.* [95]. Results agreed well with scale-model tests; it was observed that an absorptive-faced barrier had an *IL* with smaller amplitude variations with frequency than the *IL* for a reflective-faced barrier.

A series of separate barriers can be used to increase noise attenuation by creating multiple-diffractive edges. A review of parallel-barrier studies — carried out by Bowlby, Cohn and Harris [96] — clearly demonstrated that reflections between parallel barriers degrade the *ILs* of each wall, but that adding surface absorption to the barrier offsets this. Panneton *et al.* [97] have employed the theoretical model of Nicolas, Embleton and Piercy [98] to study parallel vertical walls, with or without surface absorption, in the presence of finite-impedance ground that was described using effective flow resistivity; scale-model tests compared favourably to prediction. Crombie and Hothersall [99] employed the BEM and scale modelling to study multiple diffraction by a series of parallel walls, wedges or earth mounds; the BEM was found

to be an effective predictive approach, especially when the receiver was in the shadow zone formed by each individual barrier. Comparisons between the noise-attenuation performance of different barrier profiles can be found in Watts [100], in which controlled full-scale tests of 2 m high T-shaped, multiple-edge and double barriers are compared; these modified barriers were noted to be 1.4–3.6 dBA better than a reflective vertical wall. Theoretical studies using the BEM have been undertaken by Cremers, Fyfe and Cremers [85], who compared the performance of T-shaped, semi-circular and wedge-shaped barriers on reflective ground to that of a vertical wall, finding them to be, respectively, 1.9 dBA more effective, 1.4 dBA less effective and 2.6 dBA less effective. Hothersall, Chandler-Wilde and Hajmirzae [101] used the BEM to study the total IL of barriers in the presence of reflective ground. It was found that progressively shallower wedges of constant 3 m height had progressively lower IL s; walls were 1 dB better than a flat-topped grass mound, 3 dB better than a 127° internal angled wedge, and approximately as effective as a semi-circular barrier topped by a wall.

Vegetation has been studied as a noise barrier. Harris [102] found that when a thin band of vegetation blocked the line-of-sight it provided attenuations of 0.4 dBA/ft, but that as the band thickness increased the average rate dropped towards 0.1 dBA/ft. Fricke [103] measured high-frequency (4 and 8 kHz third-octave) attenuations of 0.1 dB/m in a pine-tree plantation. Huisman *et al.* [104] observed overall attenuations of 0.1 dBA/m over a 100 m distance through a pine forest; an interesting observation was that a temperature inversion persisted beneath the tree canopy throughout the day. These latter two papers elucidated the three most important attenuation mechanisms: low-frequency interference due to ground reflections; mid-range scattering due to turbulence, ground and trees; high-frequency absorption by air, ground and trees.

Current frontiers for noise-barrier-attenuation studies involve assessments of the effects of atmospheric refraction and impedance discontinuities on barrier IL . Salomons [84], Scholes, Salvidge and Sargent [105], and DeJong and Stusnick [106] have used the PE method, full-scale tests, and scale modelling, respectively, to study the compromising effects of a downwardly

refracting atmosphere on the noise attenuation of a barrier. The collective conclusion was that higher frequencies (e.g. 1000 Hz) are more susceptible to downward refraction than are lower frequencies (e.g. 100 Hz); furthermore, the effects are more significant as a receiver moves away from the barrier.

Hutchins, Jones and Russell [107] presented the results of extensive 1:80 scale-modelling tests of noise barriers in the presence of scale-model grounds described in terms of their effective flow resistivities. Thin, perfectly-reflecting, semi-infinite barriers were tested in the presence of both model asphalt- and grass-covered surfaces; the IL was strongly dependent on the ground surface — being significantly reduced when the open-ground tests were made over model grass surfaces. A uniform surface impedance was introduced for some tests, with model asphalt on both the source and receiver side of the barrier. An impedance discontinuity was introduced for some tests by using asphalt on the source side and grass on the receiver side. The full-scale dimensions were source height = 0.3 m, receiver height = 1.2 m, barrier height = 3 m, source-barrier distance = 5 m and receiver-barrier distance = 30 m. A pronounced IL minima appeared near 500 Hz when soft ground was on the receiver side. The effect of changes in barrier height on IL was studied in the presence of the different ground types mentioned — uniform asphalt or an asphalt/grass discontinuity. With asphalt on both sides of the barrier, the noise barrier increased the attenuation over and above the ground attenuation, but mostly at lower frequencies below about 800 Hz. With an impedance discontinuity due to mixed ground there was little change in the minimum value of IL near 500 Hz, but ILs increased elsewhere — particularly at higher frequencies. Interestingly, with grass on the source and receiver sides it was clearly shown that a barrier could increase sound-pressure levels at frequencies where pre-barrier attenuation occurred due to destructive interference, by blocking the path of reflection from the ground. The effect increased with increases in the source/receiver distance.

Subsequently, Hutchins, Jones and Russell [108] used a point source to study how different barrier profiles affect the frequency-dependent behaviour of barrier IL . Barrier test configurations included thin barriers, earth berms, earth berms with a vertical crest wall, and earth

berms with a T-shaped crest wall. Interference effects were an important feature of noise-barrier performance. Since ground reflections can attenuate sound via destructive interference, and a barrier blocks these paths of reflection, the barrier's IL will exhibit a minima at these frequencies. Changes in barrier profile over asphalt ground produced greater variations in IL than tests over model-grass ground, since interference phenomena were more evident when a barrier was placed on model-asphalt ground. This was true when model asphalt ground was used on either one side or two sides of a berm. Increases in barrier top width were beneficial in all cases. Over model-grass ground, an earth berm with a wall reintroduced destructive interference, increasing the IL in frequency bands where the barrier had blocked the pre-barrier paths of ground reflection. A T-shaped wall on a berm was among the most effective profiles.

Hajek [109] conducted scale-model tests, using the equipment outlined in [82] and a point source, to compare walls to earth berms. An extensive review was made of previous work comparing earth berms to thin walls, along with discussion of contradictory reports of barrier effectiveness. The conclusions were: thin walls of 3 m height outperformed earth berms by about 1 dBA; the addition of a thin wall to the top of a berm increased its IL in proportion to the wall height; if the berm top was made highly absorptive, such that it outperformed the grass berm by 3 dBA, the addition of a wall reduced the IL , such that a wall height of at least 1.2 m was necessary to restore the lost IL . More recently, Rasmussen [110] studied the noise performance of scale-model earth berms, to test the utility of the uniform theory of diffraction in predicting the diffraction over a curved surface — good agreement was reported between measurement and theory.

Few researchers have had success comparing the results of full-scale tests to theory; two such efforts are: Jonasson [79]; and de Jong *et al.* [87]. Preferential barrier geometries, shapes, and sizes have been the focus of research by academics and highways practitioners of all stripes; although these realms of inquiry are largely separated from each other to the detriment of both. Highway noise-control practitioners continue to assume (based on statements made to the author by such practitioners) that earth berms are more effective than a wall of the same

height. The widely-used manual [2] refers to [111] as a literature source which justifies the 3 dBA soft-top-correction assumption. No evidence in [111] substantiates the soft-top-correction assumption.

2.4 Acoustical Scale Modelling

The principles of acoustical scale modelling were first presented comprehensively by Spandöck [112]. Since then, scale-modelling techniques have been applied to study concert halls, factories and outdoor sound propagation. Independent of the application, the development of an acoustical scale model requires the consideration of numerous factors. Model scales have ranged from from 1:8 to 1:100. Ultrasonic air absorption has proven to be problematic since it causes non-linear increases in sound attenuation. A variety of sound sources such as air-jet and electro-acoustic sources have been used, depending on the scale-modelling application. Scale-model material selection has depended on the scale-model application, and scale factor. An anechoic chamber can be used to isolate the model from extraneous noise and prevent reflections from interfering with the test results. Receiver characteristics have been accounted for by Xiang and Blauert [113] who used a scale-model dummy head for binaural measurements. Hodgson and Orłowski [114] give a comprehensive discussion of the principles of acoustical scale modelling with a historical perspective.

The application of scale modelling to outdoor sound propagation has often focussed on noise-barrier design, by making measurements of the barrier's IL . Previously noted and described examples of this include May and Osman [82], Hajek [109] (both of which employed the facility and materials developed by Osman [115]), Hutchins, Jones and Stredulinsky [107, 108], Pirinchievara [77], and DeJong and Stusnick [106]. Scale modelling has been employed by Hutchins, Jones and Russell [116] to study the effects of ground contour on both interference phenomena and dispersive effects. EAs were measured for: sinusoidally shaped ground; a sinusoidal bump (earth mound); single changes of slope; and highway cut-like changes in ground height. Sinusoidal bumps discouraged interference, leading to increased levels. Single changes

of slope created interference effects even when the source and receiver were both on the ground. Almgren [117] used scale models to study the effects of sound-speed gradients by curving the ground surface, in place of a refracting atmosphere. A lapse/upwind condition was simulated by curving the ground downwards; an inversion/downwind condition was studied by curving the ground upwards. As will be described, Delany, Rennie and Collins [118, 119] discussed the scale modelling of traffic noise, validation criteria and the results of scale-modelling tests of highway cuts and buildings at 1:30 scale. Some of the previously mentioned works employed scale modelling to validate theoretical techniques for predicting noise-barrier attenuation; among these are: Thomasson [80]; Nicolas, Embleton and Piercy [98]; Hayek [74]; Matsui *et al.* [95]; Panneton *et al.* [97]; and Rasmussen [110]. Attempts to simultaneously compare theory, scale-model and full-scale tests include: Jonasson [86]; Hasebe and Kaneyasu [94]; and Rasmussen [93]. Jones *et al.* [120] and Jones, Stredulinsky and Vermeulen [121] employed 1:80 scale in their comprehensive development of a scale-model facility — as will be noted later, they developed an air-jet source and selected scale-model materials. The tradeoffs involved when using different compositions of gaseous media are discussed. The factors to be considered when scaling are geometric, temporal and air-absorption effects. They point out that in a free-field it is virtually impossible to choose both a reasonable scaling factor and to overcome air-absorption effects even by using gas mixtures other than air. Tables are presented to enable the reader to consider the merits of other gases. The possible implications of using different test gases, in regards to the selection of scale-modelling materials, was not discussed. Osman [115] reviewed previous scale-model studies with reference to the materials used to simulate hard or soft ground, building surfaces, barriers, trees and intervening vehicles. Rasmussen [110] noted that, “Scale-model acoustical experiments can introduce a number of errors in comparison with full-scale measurements, since not all physical phenomena involved are transformed according to a linear scale factor. The influence of atmospheric absorption as well as boundary layer effects are two such examples of phenomena which are not transformed according to scale.” Horoshenkov, Hothersall and Attenborough [122] reviewed work on the empirical and theoretical selection of

scale-model materials; they noted that few researchers have studied the relationship between the microstructural parameters — i.e. layer depth, tortuosity and porosity — of a material and its impedance at scaled frequencies.

Scale-Model Sound Source — Different types of scale-model noise source have been used, including electro-acoustic, electro-discharge, and air-jet sources. Xiang and Blauert [113] have used an electro-acoustic source that combines both dodecahedral and cylindrical components to radiate sound. Kuttruff [123] studied concert halls using an electro-acoustic source — a dodecahedron of 4 cm diameter. Electric sparks have good directivity and good signal-to-noise ratios, but they suffer from poor reproducibility and the lack of control over their emitted spectra, necessitating some corrections. A candidate for a future electro-acoustic source might be that described by Schindel *et al.* [124], since the air-coupled capacitance transducer has some flexibility with regards to its shape and output. Almgren [125] developed an electro-discharge source which generated adequate sound power levels beyond 200 kHz. For studies of factory- and traffic-noise propagation, pressurized air is often used as the energy source for generating sound at high frequencies. If a steady-state source signal is used there is no means by which to isolate the contributions due to direct sound from other paths. The properties of crossing air-jet noise sources have been investigated [114]. Researchers [118, 119] have employed a mono-jet air-jet source to study traffic-noise, at frequencies from 2–80 kHz. Ultrasonic noise was generated due to the turbulence induced by air flow when it passed across the edges of metal vanes. Hutchins, Jones and Vermeulen [126] discussed in detail the development of air-jet sources as used in [120, 121]. They developed a compound modulated-whistle source of the modified Hartmann type, for use at 1:80 scale, that is capable of generating sound from 16–160 kHz. A jet of air is over-expanded using a nozzle before entering an opposing cavity containing an oscillating pin. The final design incorporated three such jets (hence the description “compound source”), located closely together to allow for coverage across the desired frequencies. The air pressure (typically 500 kPa), nozzle/cavity separation and nozzle/cavity dimensions could be adjusted for each jet, so the spectra could be adjusted to make allowances for high-frequency

air absorption. Hodgson and Orłowski [114] developed a crossing air-jet source for factory-noise work. A tetrahedral four-jet design, with the jets focussed at a common point, was found to be the most useful for their work, since it possessed good omni-directional properties. Myncke, Jans and Cops [127] designed and tested two air-jet designs intended for traffic-noise studies at a scale of 1:50, with sufficient sound-power output from 5–160 kHz. Both designs incorporated eight equally-spaced co-planar jets of 1.2 mm diameter. One design had a total output 5 dB higher due to the placement of resonant cavities, and the inclination of four of the jets out of the common plane. Thirty-seven such sources were built for use in simulating an incoherent line source by controlling air flows to each source by computer control of electromagnetic valves. The third-octave sound-power outputs for all of these sources were studied. The output did not vary in any band by more than 0.8 dB, with the mean standard deviation being 0.5 dB; for the summed output, the standard deviation was 0.4 dB. The airflow reportedly moved the acoustic centre of the sound away from the geometric centre of the jets; a frequency-dependent distance from 1–12 mm was reported. Novak [128] developed a similar co-planar air-jet source. A design with a 6.5 mm diameter cavity was used, with six equally spaced co-planar air-jets of 0.35 mm diameter directed straight inwards towards a common central point. It was reported that the sound-power output increased and the spectral shape smoothed out as air pressures increased to 500 kPa, without changing the directivity appreciably. For the simultaneous operation of forty sources, an air pressure of 200 kPa was employed. Crossing air-jet sources offer some advantages: they can provide omnidirectivity; they have broadband spectra; they have highly reproducible output; they are steady-state; and the signal-to-noise ratio is functionally dependent on air pressure. The spectra can be tailored to resemble scaled traffic noise, and increased to offset the expected attenuation due to air absorption.

Scale-Model Materials — To construct an acoustical scale model to study outdoor sound propagation, the full-scale acoustical properties of ground need to be reproduced using materials which act in an acoustically analogous way at frequencies which are higher by a scale factor n . The material selection process was discussed qualitatively [118, 119], by referring to the

flow resistivity and porosity of a material. It was concluded that materials denser than their full-scale counterparts are necessary to successfully model ground. Insulite (11 mm soft boards) was used to simulate grassland. Materials were selected [120, 121] by assuming local reaction and comparing the normal-incidence surface impedance to the then-existing values associated with outdoor ground. Tissue on polystyrene was deemed to reproduce grass. Hutchins, Jones and Russell [129] further refined the state-of-the-art in selecting scale-model materials by using the Delany & Bazley surface-impedance model in conjunction with *EA* predictions for a local-reaction boundary. The Delany & Bazley model was used to generate a least-squares fit between measurement and predictions of the *EA*. The best-fit flow resistivity was considered to be the effective flow resistivity. Sanded sheets of expanded polystyrene covered with tissue were found to have an effective flow resistivity of approximately 300 c.g.s. Rayls/cm (as for grass); unsanded sheets of expanded polystyrene covered with tissue were found to have an effective flow resistivity of approximately 600 c.g.s. Rayls/cm (as for gravel). Acoustic-boundary-layer effects (first discussed theoretically in [125]) were not contemplated in this article, though they might be responsible for the apparent softness of the scale-model materials. Yamashita and Yamamoto [130] presented scale-modelling techniques at 1:50 scale, using three different noise sources — a simple, co-planar, air-jet design, a prototype pneumatic line source, and a line source consisting of an oscillating channel filled with ball bearings. The ground materials used were vinyl-chloride plate for roads, houses and buildings, and thin felt for grassy areas. A variety of scale-model configurations were studied: spiral interchanges; tunnel openings; and double-deck highways. Most recently, Pirinchievara [131, 45] employed the effective-flow-resistivity concept to select materials for a 1:20 scale model using a point source. Polystirol was found to be good for simulating asphalt, velveteen for grass (200 c.g.s Rayls/cm), and mineral wool for snow-covered ground. Day [132] noted that a scale-model material which is acoustically analogous to a full-scale material may not be physically analogous in terms of its scaled microstructure, due to physical phenomena which do not scale linearly; as a result, a material which works at one scale factor may not work at another. For the scale modelling of fibrous materials, Voronina

[133] discussed the relationship between layer thickness and material density, with reference to some of the non-linear aspects of material scaling. Osman [115] presented separate criteria for the selection of scale-model materials which are either ground surfaces or other-than-ground surfaces, at scales of 1:16, 1:32 and 1:64. Other-than-ground surfaces were chosen by studying their absorption coefficients. Ground surfaces were studied using their *EAs* without reference to any parameters, such as effective flow resistivity. Buildings and barriers were simulated using wall, mounting, crescent or illustration boards; rigid foam was used as an absorptive material; hard ground was simulated at all scales by 10 mil vinyl sheet. Soft ground at 1:16 and 1:32 scales were simulated using fibreboard; at 1:64 scale, a felt layer was used. Materials were also proposed for the scale modelling of trees — wood dowelling, wire and crumpled paper. Almgren [125] discussed the effect of the acoustic boundary layer on the scale-model simulation of sound propagation above a solid surface. He showed that the non-linear aspects of frequency scaling are compounded by this boundary layer, which creates an apparent non-zero admittance at the surface of a material that adds to the pre-existing admittance of the material. He further showed that, unlike for a local-reaction surface, the acoustic boundary layer's admittance depends on the angle-of-incidence of the sound, so the effective impedance of the surface also displays angular dependencies. Its effect is amplified with the proximity of a source and receiver to the surface. Errors from 1–7 dB were observed in studies of *EA* over full-scale frequencies from 100–10000 Hz as compared to predicted *EAs* at a scale of 1:100. The error's magnitude varied with geometry, scale and frequency; the apparent absorption of a solid surface increased with frequency. Almgren [134] verified the theoretically-predicted effects of an acoustic boundary layer on *EA* using a scale model.

To summarize the process of scale-model material selection, the effective-flow-resistivity technique for selecting scale-model materials represents the current state-of-the-art. Some examples of the Delany & Bazley approach being directly applied to noise barrier studies are: Hasebe and Kaneyasu [94]; Hutchins, Jones and Russell [107, 108]; and Pirinchievara [77]. In [110], a canvas layer on a hard surface was reported to have an effective flow resistivity of 500

kNs-m^{-4} (equivalent to c.g.s. Rayls/cm) at a scale of 1:25. Panneton *et al.* [97] employed the Miki [60, 61] model of flow resistivity to generate effective flow resistivities for their scale-model materials. Horoshenkov, Hothersall and Attenborough [122] developed a theory and methodology for predicting the microstructural parameters required for correct surface impedances at scale frequencies; they claim that comparisons are good between measurements of a material's reflection coefficient and its predicted value. They concluded that the first criterion for selecting a material is that the flow resistivity of a scale-model material should be n -times higher than the full-scale material. The second criterion is that the statistical distributions of tortuosity, porosity, and number of pores per unit volume should remain unchanged.

Anechoic Chambers — Anechoic chambers, which act to minimize both the internal reflection and the external transmission of sound, are used to approximate a free-field. The anechoicity of such rooms at ultrasonic frequencies has not been widely considered in the literature. Peppin [135] noted that no accepted standard exists for the design or post-construction assessment of anechoic chambers. Delany & Bazley [136] developed a theory treating each wedge as a small scattering sphere of finite impedance; predicted results agreed qualitatively with measurements. They suggested that the amplitude of the scattered sound should increase directly with frequency — posing a potential problem at ultrasonic frequencies. ANSI S12.35-1990 [137] contained an appendix of guidelines for the design and construction of an anechoic chamber. A chamber's volume should be 200+ times the source's volume. Tests should be made at a distance greater than both 1 m or twice the length of the source's major dimension, with the microphone kept a quarter wavelength or more from the boundaries. The free-field radius is the distance away from a test source, over which the deviation from free-field levels is less than 1 dB. Ballagh [138] presented a method, involving the simultaneous solution of a system of equations, for inferring the sound-power level from a series of sound-pressure levels measured at varying distances. Given small errors in distance, improved estimates are made of the sound-power level and the location of the source's acoustical centre. Measurements were made at distances from 200 mm out to several metres from the source; within this range 10

mm intervals were employed from 40–1000 Hz and 3 mm from 1–15 kHz. At least 0.75λ should be traversed to get satisfactory results. Free-field deviations were assessed by making traverses along the room's major diagonal, a diagonal parallel to the floor, and close to and along the suspended ceiling.

2.5 Human Response to Traffic Noise

Attempts to mitigate traffic-noise exposure are often predicated upon the assumption that the noise itself is the source of annoyance to people; Job [139] suggests that "...18 to 22 percent... of the variation in reaction is attributable to highway noise." Job [140] attempted to identify which causal factors are of the most significance in determining the reaction of people to general noise exposure. Three causal factors were deemed to be of paramount importance: noise loudness and duration, attitude towards the noise, and listener sensitivity; some of the remaining factors include: perceived necessity of the noise, visibility of the source, perceived fear of a health risk, listener demographics, and changes in the noise. Any A-weighting which is to be applied will ideally be used for acoustic sound-pressure levels below 55 dB, B-weightings for the range of 55–85 dB, and the C-weighting for 85 dB and above — the degree of correction reflects changes in the ear's sensitivity to loudness. Watts and Nelson [141] concluded that "... the maximum loudness (measured in phones or sones) and the A-weighted level were significantly more closely related to average ratings of vehicle noise than B- or C-weighted measures". It was also found that the correlation of subjective ratings to the chosen measures was not greatly improved by the simultaneous assessment of more than one indicator. Kuwano, Namba and Miura [142] explored the subjective assessment of loudness, concluding that: A-weighted sound-exposure levels $L_{eq,A}$ are adequate for noises with no specific, dominant component of frequency; and if a specific, dominant frequency component is present, then the psychoacoustical approaches adopted in reference [143] should be employed to calculate the Zwicker loudness level LL_z — thereby considering physiological phenomena frequency masking.

Chapter 3

Theoretical Considerations

In this chapter outdoor ground materials have been studied with the aid of theoretical models that predict the sound-field interference patterns over a flat surface that is described by a complex-valued surface impedance. The surface impedance of full- or model-scale ground can be inferred by comparing measurements to best-fit values of the input parameters — such as the effective flow resistivity — for these theoretical models (see Section 2.2 on page 23). Predicted *EAs* can be used as theoretical benchmarks for identifying the best scale-model material for simulating a full-scale outdoor ground surface (see pages 44–47 of Section 2.4). The principles of acoustical scale modelling were developed with particular reference to a new technique for selecting scale-model materials. By applying these scale-modelling principles, it was possible to develop a technique for selecting scale-model materials which involved comparisons of scale-model *EA* measurements to the analogous full-scale *EA* for a given ground surface.

3.1 Excess Attenuation: Prediction

In this section, a theoretical model for predicting the sound field above a ground surface will be developed, in terms of the velocity potential Φ above the surface. The velocity potential takes into account a specified source and receiver geometry; as well as the surface impedance of the ground plane. The model will be employed to help select appropriate scale-model materials. For the purpose of deriving the theoretical model, it is assumed that the ground-surface impedance is locally reacting. The predicted sound-field accounts for plane-wave propagation along the direct and reflected sound paths, the extra contributions upon reflection of spherical wavefronts, and the contribution of a surface wave which propagates along the surface. The direct and reflected

sound waves both diverge spherically from the source. If plane-wave fronts were assumed a physically-unrealizable prediction would be made when the source approaches the surface; plane-wave reflection coefficient of $R_p = -1$ would result, which implies that no sound field will exist due to the perfect cancellation of the direct and reflected components. A spherical-wave reflection coefficient (see Eq. (3.11)) corrects for this deficiency by predicting a non-zero sound field, and allows for the mathematical existence of a surface wave. The term 'ground wave' refers to the correction introduced by spherical wavefronts — with or without a surface-wave component. A surface wave can exist mathematically when the source and receiver are on the ground if the surface-impedance properties of the ground are such that $X > R$ [52], or when surface roughness is present [48]. Where the direct- and reflected-wave's amplitudes decay with the distance squared, the surface wave decays cylindrically with distance. The resistive impedance component gives rise to exponential attenuation of the surface wave with distance. In the far-field, as the distance from a point source to a point receiver increases, the weaker surface wave becomes the dominant component. The velocity potential, in Cartesian co-ordinates (x, y, z) , is the solution to the Helmholtz equation over an impedance plane of height z_o , where a time-dependence of $\exp(-j\omega t)$ is assumed.

$$(\nabla^2 + k^2) \Phi = \delta(x) \delta(y) \delta(z - z_o), \quad (3.1)$$

in which $\nabla = (\partial/\partial x, \partial/\partial y, \partial/\partial z)$ and $\delta(x)\delta(y)\delta(z - z_o)$ is the Dirac measure at $(0, 0, z_o)$. The boundary condition for a porous, locally-reacting surface with a normalized surface admittance $\beta = \rho c/Z$ is:

$$\frac{\partial \Phi(x, y, 0)}{\partial z} + j k \beta \Phi(x, y, 0) = 0, \quad (3.2)$$

From the velocity-potential solution, the acoustic pressure p can be calculated as follows, where ρ_{air} is the density of air:

$$p = -\rho_{air} \frac{\partial \Phi}{\partial t} \quad (3.3)$$

The EA has been previously defined in Eq. (1.8) in terms of measurements, but it can also be predicted using Eq.(3.4), and the measurement and prediction compared in order to study the

surface impedance of an outdoor ground plane:

$$EA = 10 \log_{10} \left(\frac{\Phi}{\Phi_{free-field}} \right) \quad (3.4)$$

Now the velocity-potential prediction model will be developed. The following derivation, taken from references [43, 44, 42, 46], assumes that the exponential time dependence $exp(-j\omega t)$ has been divided out of the expressions. The source and receiver are taken to be volumeless points in space. It assumes that the universe is divided by a plane, semi-infinite boundary into two semi-infinite media, one of which is a quiescent and homogeneous fluid, the other a solid boundary with an impedance magnitude that is much greater than the fluid's characteristic impedance. Acoustic pressures within each medium match at the boundary, as do the particle velocities normal to the surface. The boundary between the two is locally reacting. Perfect coherence exists between the direct and reflected waves.

The test geometry (see Fig. 1.3 on page 10) is defined by the source height h_1 , receiver height h_2 , the horizontal source/receiver separation distance d , and combined source/receiver height h_{1+2} . For the direct source/receiver path, the radial distance is calculated using Eq. (3.5); for the reflected path, the radial image-source/receiver distance is found using Eq. (3.6):

$$r_1 = \left(d^2 + (h_2 - h_1)^2 \right)^{0.5} \quad (3.5)$$

$$r_2 = \left(d^2 + (h_2 + h_1)^2 \right)^{0.5} \quad (3.6)$$

As calculated in Eq. (3.7), the angle ψ of the path of reflection with respect to the ground is called the grazing angle:

$$\psi = \text{atan} \left(\frac{h_{1+2}}{d} \right) \quad (3.7)$$

Given the wavenumber k of air, source/receiver geometry and surface impedance, the complex-valued plane-wave reflection coefficient R_p for a locally-reacting boundary is calculated using Eq. (3.8). This equation assumes that the magnitude of the wavenumber in the ground is far larger than that in the air above it.

$$R_p = \frac{\sin\psi - \beta}{\sin\psi + \beta} \quad (3.8)$$

The plane-wave reflection coefficient describes changes on reflection of a wave, for a given normalized surface admittance and angle of incidence. The numerical distance, w , for a locally-reacting boundary, is calculated using Eq. (3.9), with the aforementioned assumptions about impedance and wavenumber:

$$w = \left(\frac{1+j}{2} \right) (r_2 k)^{0.5} (\sin\psi + \beta) \quad (3.9)$$

It is particularly important when taking the square-root of this calculated value of w to choose complex roots from the correct quadrant in the complex-number plane [46]. The recommended selection process insures that a spring-like surface is being modelled. Using Eq. (3.10) the spherical-correction (or loss) factor is calculated from:

$$F(w) = 1 + j \sqrt{\pi} w \exp(-w^2) \operatorname{erfc}(-jw) \quad (3.10)$$

This equation makes use of the preceding numerical distance to calculate the additional wave components which arise from the sphericity of the propagating wavefronts. By multiplying the terms $\exp(-w^2)$ and $\operatorname{erfc}(-jw)$ together a modified form of the complementary-error function is obtained. Replacing them with $f(w)$, Eq. (3.10) can be rewritten as $F(w) = 1 + j \sqrt{\pi} w f(w)$. Approximations for $f(w)$ can be found in [46], but a more accurate approach is given by [42], with the latter technique employed by [43, 44, 45]. Using Eq. (3.11), the spherical-wave reflection coefficient, Q , is calculated:

$$Q = R_p + (1 - R_p) F(w), \quad (3.11)$$

in which the contributions of the plane-wave reflection coefficient and the ground wave are superimposed. The final step is to calculate the velocity potential Φ :

$$\Phi = \frac{\exp(jkr_1)}{4\pi r_1} + Q \frac{\exp(jkr_2)}{4\pi r_2} \quad (3.12)$$

For $Q = 0$, Eq. (3.12) can be used to calculate the free-field potential $\Phi_{free-field}$. As $|w| \rightarrow \infty$, $|F(w)| \rightarrow 0$ and $\Phi \rightarrow 0$. For calculations of EA using Eq. (3.4), the constant terms in the denominator will simply cancel out. If corrections for air absorption are necessary, the

propagation constant of air, γ , can be substituted for k . One remaining area of complication involves the calculation of the modified form of the complementary-error function:

$$f(w) = H_{yx} + j K_{yx} \quad (3.13)$$

How are the real and imaginary parts of this expression evaluated? For a start, from the numerical distance w , define $x = \text{Re}(w)$, $y = \text{imag}(w)$ (assuming y is positive), along with the new constant $h = 1$. Define four new variables as follows:

$$A_1 = \cos(2xy) \quad (3.14)$$

$$B_1 = \cos(2xy)$$

$$C_1 = \exp(-2\pi y/h) - \cos(2\pi x/h)$$

$$D_1 = \sin(2\pi x/h)$$

Two new terms are then calculated from these:

$$P_2 = 2 \exp(-(x^2 + (2\pi y/h) - y^2)) \frac{A_1 C_1 - B_1 D_1}{C_1^2 + D_1^2} \quad (3.15)$$

$$Q_2 = 2 \exp(-(x^2 + (2\pi y/h) - y^2)) \frac{A_1 C_1 + B_1 D_1}{C_1^2 + D_1^2}$$

An indication of the error involved in calculating $f(w)$ is found by calculating the bound E_h as follows:

$$E_h = 2 \sqrt{\pi} \frac{\exp(-\pi^2/h^2)}{1 - \exp(-\pi^2/h^2)} \quad (3.16)$$

Smaller values of h reduce the value of E_h , leading to more accurate calculations of $f(w)$. The real and imaginary terms in Eq. (3.13) are calculated from Eq. (3.17) and Eq. (3.18):

$$H_{yx} = \frac{hy}{\pi(y^2 + x^2)} + \frac{2yh}{\pi} + \sum_n \frac{\exp(-n^2 h^2) (y^2 + x^2 + n^2 h^2)}{(y^2 - x^2 + n^2 h^2)^2 + 4y^2 x^2} - \frac{yE_h}{\pi} + P_{2,final} \quad (3.17)$$

$$K_{yx} = \frac{hx}{\pi(y^2 + x^2)} + \frac{2xh}{\pi} + \sum_n \frac{\exp(-n^2 h^2) (y^2 + x^2 - n^2 h^2)}{(y^2 - x^2 + n^2 h^2)^2 + 4y^2 x^2} + \frac{xE_h}{\pi} - Q_{2,final} \quad (3.18)$$

The terms $P_{2,final}$ and $Q_{2,final}$ are determined by comparing the value y to the ratio π/h . If $y < \pi/h$ then $P_{2,final} = P_2$ and $Q_{2,final} = Q_2$; if $y = \pi/h$ then $P_{2,final} = P_2/2$ and $Q_{2,final} = Q_2/2$; otherwise $P_{2,final} = 0$ and $Q_{2,final} = 0$.

3.2 Principles of Acoustical Scale Modelling

The objective of acoustical scale modelling of highway noise barriers is to closely reproduce the relative changes in sound-pressure level that occur at full scale due to both the presence of a ground surface and the insertion of a noise barrier. To correctly model the EA of ground and the IL of a noise barrier the factors to be considered are: choosing a scale factor n ; constructing a scale-model noise source; accounting for air absorption; selecting scale-model materials to simulate outdoor ground surfaces; and selecting measurement instrumentation.

An outdoor sound field can be modelled by scaling all model dimensions and surface features by $1/n$, such that the model's wavelength-to-dimension ratios are preserved. For the ensuing discussion, all scale-model quantities are denoted by a prime; the corresponding full-scale lengths are $l = n l'$. When air is used in the scale model, such that $c = c'$, the time it takes for sound to travel a given distance is $t = n t'$. In this case, the constancy of the sound speed between full and model scales requires that the ratio of model- and full-scale wavelengths and frequencies are: $\lambda = n \lambda'$ and $f = f'/n$. Furthermore, since all dimensions have been scaled by $1/n$, the frequency dependence of air absorption β (dB/m) in the model must be scaled by n , meaning that $\beta = \beta'/n$. Ideally, $(\beta r)/(\beta' r') = 1$. The surface impedances at model scales must equal the full-scale values, such that $Z(f) = Z(f')$. The accurate scaling of the model's wavelength-to-dimension ratios and surface impedances means that the effects of interference and diffraction can potentially be reproduced.

Since distances scale by $1/n$, the scale-model sound source produces a certain mean-square pressure at a distance r full scale, but at r/n in the model. The full-scale sound-pressure levels and sound-power levels are related to the model values by multiplying by n , as follows:

$$L_w = L'_w - 20 \log_{10}(n) \quad (3.19)$$

$$L_p = L'_p - 20 \log_{10}(n) \quad (3.20)$$

If a model is constructed in accordance with the above scaling laws, then both L_p and L_w will scale by n .

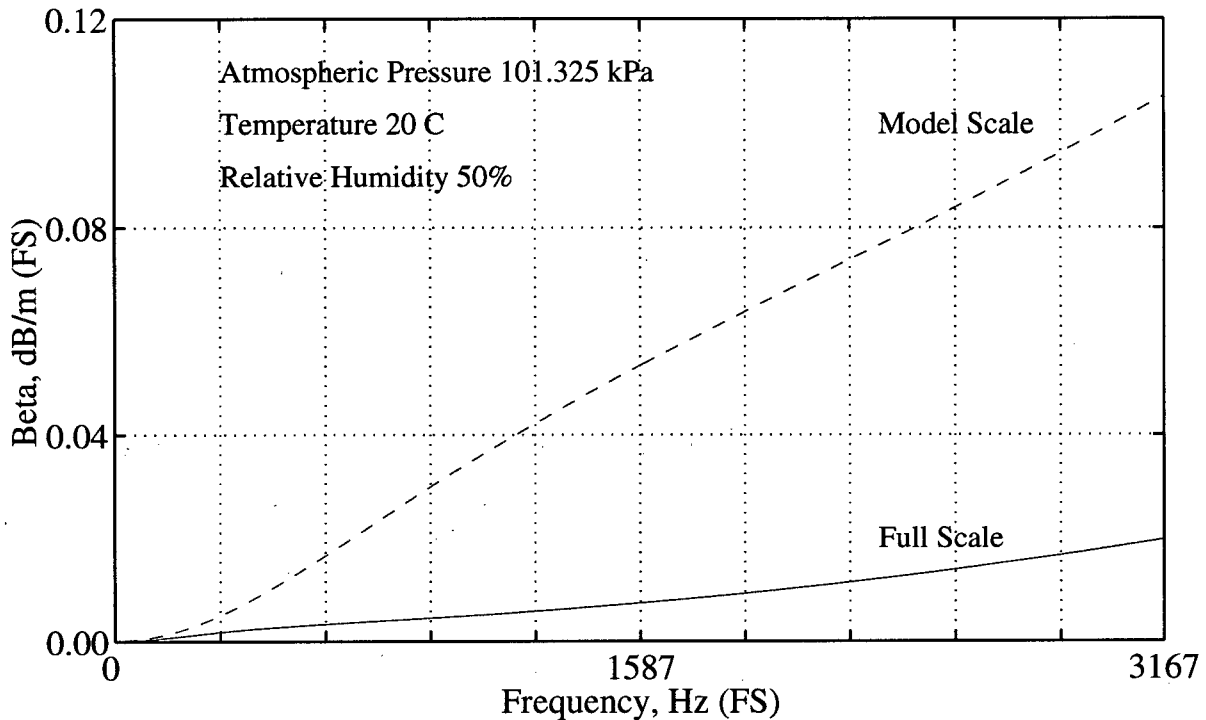


Figure 3.1: Air absorption in decibels per metre at full-scale frequencies for both full-scale calculations and 31.5:1 model-scale calculations translated to full scale. Atmospheric conditions were kept the same for each calculation.

Sound propagation in the scale model suffers excessive air attenuation, the magnitude of which can be found by examining the difference between β'/n and β . The non-linear increase in air absorption is shown in Fig. 3.1. The equivalent full-scale values of absorption and frequency, calculated for standard atmospheric conditions, are used for the plot's axes. The scale-model values of absorption and frequency have both been reduced by a scale of 31.5:1 to illustrate how scale-model testing at higher frequencies leads to higher-than-desired air absorption. The scale-model attenuations translate to full-scale attenuations that are several times higher than desired. This means that free-field tests at model scales cannot accurately reproduce full-scale tests without appropriate correction for air absorption. So it is critical to account for the adverse effect of air absorption except when predicting free-field levels. Fortunately, the adverse effect of excessive air absorption can be minimized for tests of the *EA* of a surface or *IL* of

a barrier. Why? Upon the introduction of a ground surface or a barrier, new source/receiver paths are created. If the path-length differences are small between all source/receiver paths, the significance of air absorption is lessened for coherently-interfering sound waves, since air absorption attenuates all paths in proportion to the distance travelled. Thus, the results of model-tests of EA and IL can accurately represent full-scale tests.

Non-linear increases in air absorption can be mitigated by using scale-model gases other than standard air [121], or conducting tests which involve inherently small path-length differences between the various sound-propagation paths in the model. Air absorption can be reduced by using dry air, which results in a more linear relationship between full- and model-scale air absorption. Other test gases can be used to reduce absorption, but this will lead to changes in the fluid's characteristic impedance, absorption, and speed of sound. As long as the wavelength-to-dimension ratios are preserved the effects of interference and diffraction can potentially be reproduced if the boundary conditions created by the ground surfaces are accurately modelled. When the characteristic impedance of the test gas is altered, the criterion for modelling a locally-reacting ground surface at small angles of incidence changes to $Q(f) = Q(f')$. Furthermore, if this change in characteristic impedance involves a change in the speed of sound, the criterion becomes $Q(\lambda) = Q(\lambda')$.

Another non-linear aspect of scale modelling is associated with the acoustic boundary layer (ABL) which does not scale linearly with frequency [125], [134]. The normalized admittance of the ABL for a given frequency and angle θ with respect to an axis orthogonal to the surface [125] is defined as follows:

$$\beta_{ABL} = 2 \times 10^{-5} (1 - j) \sqrt{f} (\sin^2 \theta + 0.48) \quad (3.21)$$

The effect of this layer on the apparent admittance of the material cannot be accounted for by linear scale-modelling laws. When the non-linear effects of the ABL are considered with or without a consideration air absorption, the requirement for selecting an appropriate scale-model material becomes $EA(f) = EA(f')$. It is proposed that in the presence of a test medium with a different speed of sound that this requirement be defined as $EA(\lambda) = EA(\lambda')$.

3.2.1 Air-Absorption Coefficient Calculation

The air-absorption coefficient, α , can be calculated for a given frequency and atmospheric condition (temperature, relative humidity, atmospheric pressure, molecular composition). Algorithms exist [15, 16] allowing for the prediction of air-absorption coefficients from 50 Hz to 10 MHz with $\pm 5\%$ accuracy. It is applicable for temperatures from 0 to 40° C, relative humidities from 0-100%, and atmospheric pressures down to as low as a few hundredths of an atmosphere. The expression for the ratio of saturation pressure to atmospheric pressure is in error in [15] — a corrected expression is found in [16]. As described in Eq. (3.22), the total air-absorption coefficient is modelled as the sum of contributions by three mechanisms: classical and rotational absorption, α_{cr} ; and vibrational-relaxational absorptions from oxygen, $\alpha_{vib,O}$, and nitrogen, $\alpha_{vib,N}$:

$$\alpha = \alpha_{cr} + \alpha_{vib,O} + \alpha_{vib,N} \quad (3.22)$$

Classical absorption mechanisms include shear viscosity, thermal conductance and mass/thermal diffusion. Classical and rotational losses are combined into one term due to their common dependence on the squared frequency, temperature and atmospheric pressure. Intramolecular modes of rotation and vibration display a relaxation frequency (at which air absorption is maximized) which is different for oxygen and nitrogen. Nitrogen's vibrational-relaxation absorption is the dominant term at low frequencies — below about 2000 Hz. Oxygen's vibrational-relaxation absorption is the dominant loss mechanism up to about 100,000Hz; beyond this, classical and rotational absorption dominate the other two due to their frequency-squared dependence. Vibrational-relaxation absorptions vary with frequency and humidity, along with temperature and atmospheric pressure. Energy is transferred from the translational mode of vibration to other internal modes due to intra-molecular collisions; reductions in translational pressure amplitude result in reductions in sound-pressure level.

3.2.2 Scale-Model Noise Sources

How closely does a scale-model source need to reproduce the properties of either a full-scale vehicular source or a theoretical source? Since both model- and full-scale tests of EA and IL are relative measures of sound-pressure level, and the model- and full-scale sound-pressure levels differ only by a constant, it is not necessary to correctly scale the sound-power output of the scale-model source. An adequate signal-to-noise ratio at all desired full-scale frequencies is necessary. A vehicle is a very complicated noise source and, to date, the directivity, respective source locations, and scaled size have not been accurately reproduced for scale-modelling work. Factors such as vehicle velocity and acceleration are also difficult to account for in a scale model. As such, mathematically-simple sources are often used as the pattern for building a scale-model noise source. A theoretical source that radiates coherently — such as that found in the velocity-potential model — is represented as being a point in space and is assigned an omnidirectional radiation pattern.

It is possible, in both mathematical descriptions and scale models, to effectively recreate a line source by traversing a point source along a path and using decibel addition to superimpose the resulting measurements together. A line of vehicles will produce the same IL as a single vehicle pass, if the sound from each vehicle is incoherent with respect to sound from other vehicular sources. This fact, together with the added complexity of building a larger line source makes point sources a more practical choice.

3.2.3 Method for Determining Optimal Scale-Model Materials and Scale Factor

Different outdoor ground materials have different normal-incidence surface impedances. From measurements of the EA for either full-scale or scale-model surfaces that are locally reacting, the normal-incidence surface impedance of that surface can be determined and described by the effective flow resistivity. Tests at full scale can be compared to scale-model tests to see how real-world ground materials behave in comparison to scale-model materials. Scale-model tests are corrupted by random errors and by bias errors that are introduced due to non-linear

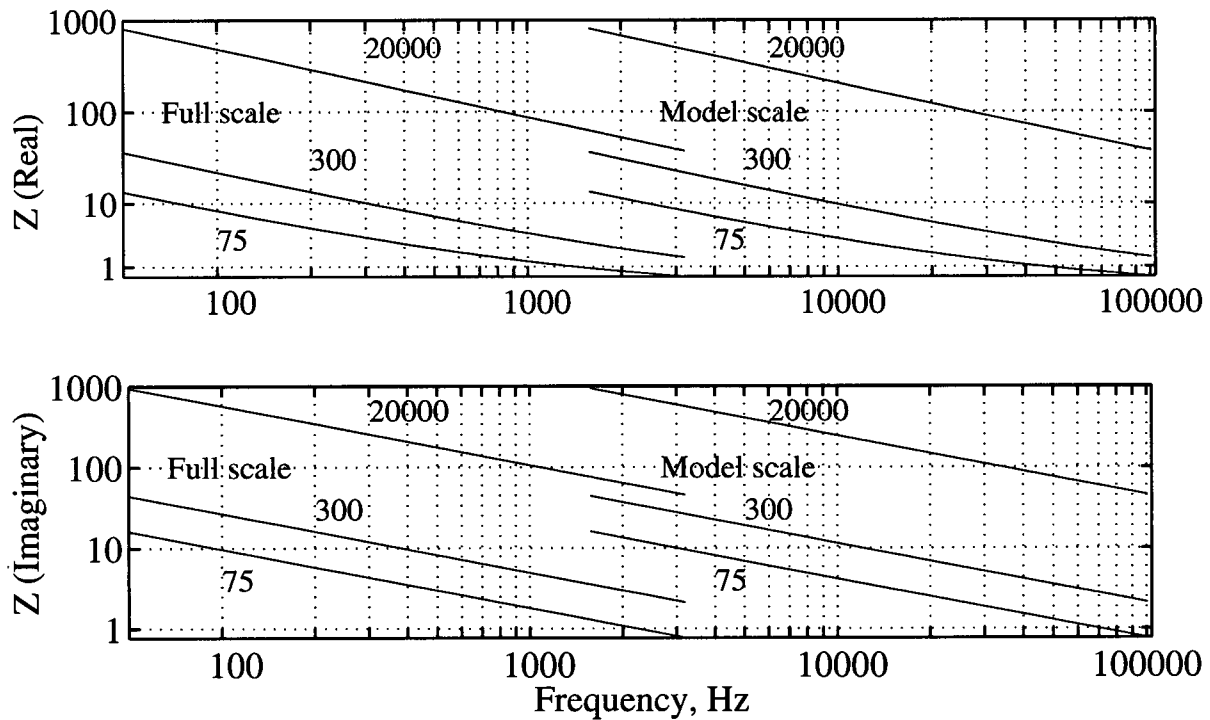


Figure 3.2: Surface impedance at two scale factors ($n = 1$ and 31.5) and three effective flow resistivities (75, 300, 20000 c.g.s. Rayls/cm).

air-absorption and acoustic-boundary-layer phenomena. Full-scale tests are affected by such non-linearities to a lesser degree, so measurements of EA over outdoor ground surfaces are only corrupted by random errors. A modified form of Delany-Bazley [3] impedance model was used:

$$\frac{Z}{\rho c} = 1 + A \left(\frac{f'}{n\sigma} \right)^a + jB \left(\frac{f'}{n\sigma} \right)^b \quad (3.23)$$

The frequency, flow resistivity σ , and scale factor are the only parameters in this equation. The scale-model materials should have effective flow resistivities that are n -times higher than the full-scale materials. Appropriate scale-model materials vary with the scale factor n . Fig. 3.2 compares the calculated impedances over different frequency ranges to illustrate how full-scale and model-scale surface impedances can be equated. The non-linear effects of the acoustic boundary layer are not considered in Fig. 3.2.

A material is thought to be a good scale-model surface when the EA of the scale-model

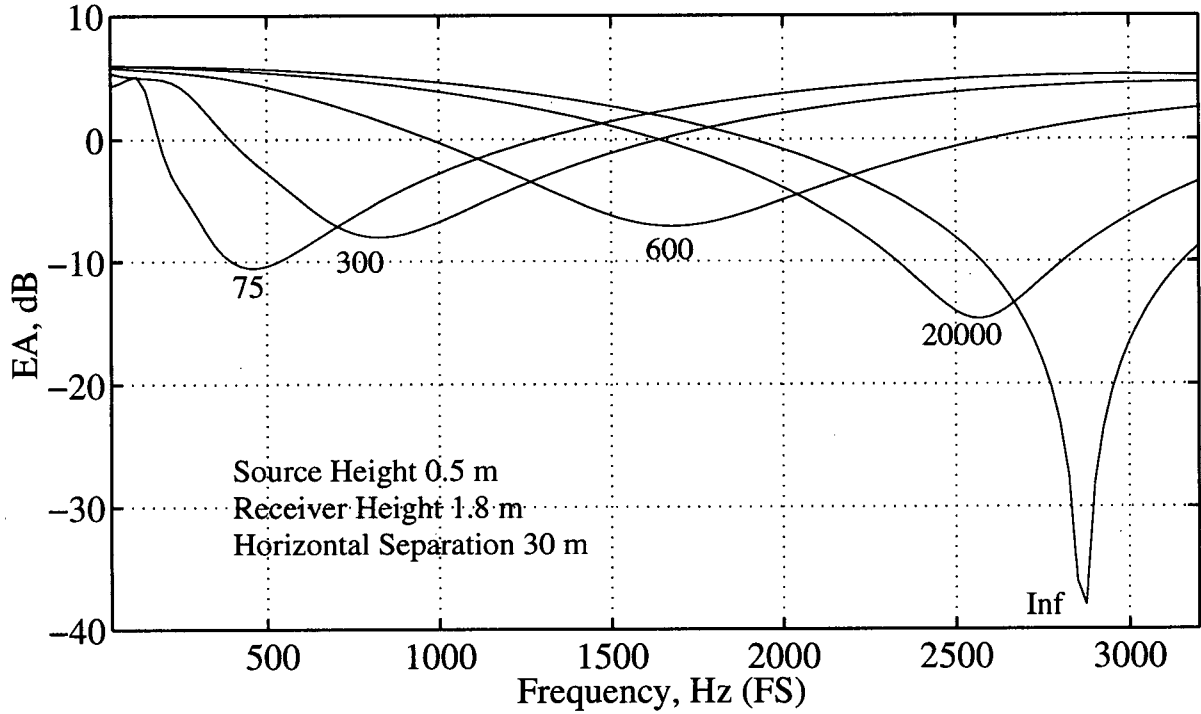


Figure 3.3: Predicted EAs for effective flow resistivities of 75, 300, 600, 20000 and Inf c.g.s. Rayls/cm, for a fixed test geometry: source height 0.5 m, receiver height 1.8 m and horizontal separation 30 m.

surface at ultrasonic test frequencies is equivalent to the EA of the ground surface at full-scale frequencies. EA curves have been generated for a number of effective flow resistivities, and are plotted in Fig. 3.3. An array of scale factor versus effective flow resistivity can be generated for each test material. By studying the values of $F^{n,\sigma}(\vec{f})$ for each cell of this array it should be possible to identify a best-fit value for which the least-squares residuals are minimized:

$$F^{n,\sigma}(\vec{f}) = \left(\frac{\sum_{i=b_1}^{b_2} \left(EA_{measured}^{n,\sigma}(f_i) - EA_{predicted}^{n,\sigma}(f_i) \right)^2}{b_2 - b_1 + 1} \right)^{0.5} \quad (3.24)$$

This being the case, an optimal scale factor and flow resistivity will exist for each material. These best-fit flow resistivities are not necessarily identical to those found using a flow-resistivity apparatus, and are referred to as effective flow resistivities σ_e .

Chapter 4

Field Tests

In preparation for the scale-modelling work, field-tests of barrier attenuation were performed in conjunction with Wakefield Acoustics Ltd. Reference [71] was consulted while preparing for these tests, as a guideline with regard to test conditions and measurement techniques. *EAs* and *ILs* were evaluated, and a representative traffic-noise spectrum was measured. The measuring device was a Larson-Davis Model 2880 portable spectrum analyzer, measuring in unweighted or A-weighted third-octave bands from 0.8–20000 Hz. All field tests conducted using traffic-noise as a source were recorded as 15-minute L_{eqs} .

4.1 Traffic-Noise Spectra

To determine barrier attenuations applicable in typical B.C. traffic configurations from the scale-model *IL* tests, it was necessary to identify an A-weighted traffic-noise spectrum representative of B.C. traffic, since barrier *IL* is not constant with frequency. To evaluate the performance of scale-model barriers, the *ILs* of all third-octave bands can be integrated together to give an overall *IL*. The sound power that is radiated by vehicles is not constant across the audible spectrum, and the sensitivity of human hearing also varies with frequency. To assess the acoustical utility of a noise barrier, it is essential to account for hearing's influence by weighting the *IL* test results. A-weighting is a means of accounting for the sensitivity of human hearing to different frequencies of sound [142]. Weightings are applied before integrating the third-octave results to give a useful attenuation indicator — the A-weighted traffic-noise Insertion Loss (*ILA*). Vehicular spectra also vary from location to location, so the *ILA* could vary somewhat due to changes in the location of the barrier.

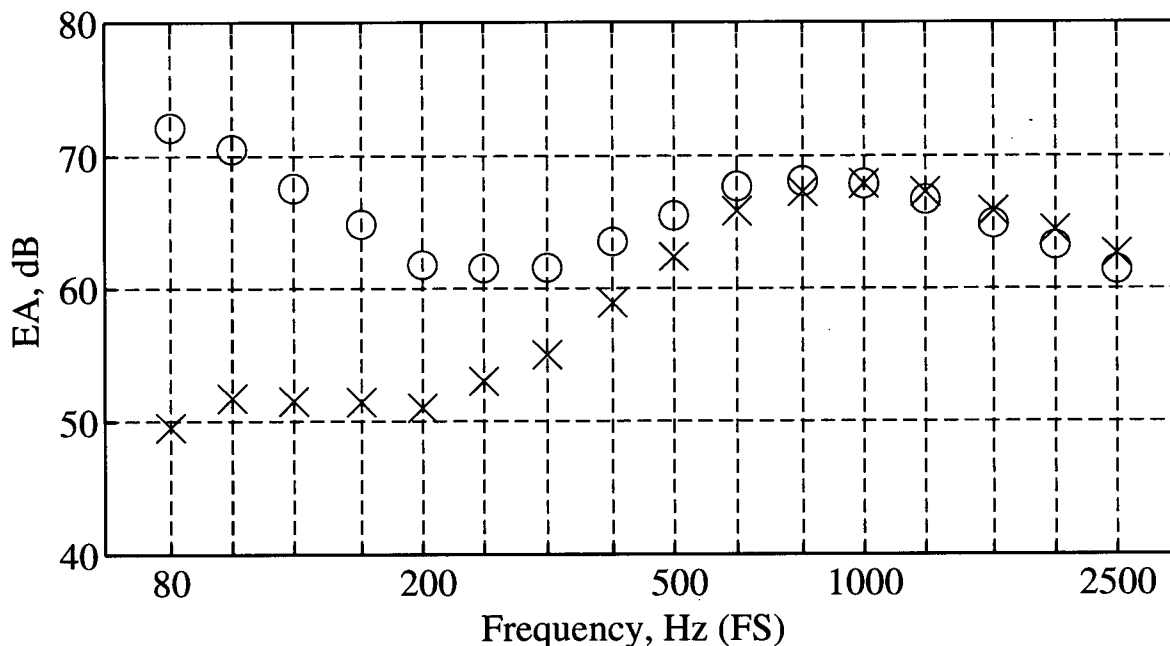


Figure 4.1: Measured unweighted and A-weighted third-octave traffic-noise spectra: Nanaimo, B.C., January 1996: (o) L_{eq} , sum=81.7 dB; (x) $L_{eq,A}$, sum=75.5 dBA.

In early January 1996, Wakefield Acoustics Ltd. measured traffic-noise spectra over grass-land, at positions 15 m from the centreline of the two near lanes of a divided four-lane highway — Highway 19 north of Nanaimo, B.C. Average vehicle speeds over the standard asphalt road were 75–80 km/h with a vehicle mix of 5–7% heavy trucks. The microphone was 1.8 m above the surface for traffic-noise tests.

Both the unweighted and A-weighted traffic-noise spectra are shown in Fig. 4.1. The frequency of the maximum level is clearly different in the two cases, going from 72.3 dB in the 63 Hz third-octave band unweighted to 68 dB in the 1000 Hz third-octave band A-weighted. This shift of the frequency of the maximum level has a significant effect on the attenuation provided by a noise barrier, since the IL varies with frequency. Although it would have been desirable to add the weightings to even narrower frequency bands, so the A-weighted third-octave results could be obtained, this was not strictly possible due to the acquisition of the traffic-noise spectrum in third-octave bands.

Table 4.1: Location of outdoor test co-ordinates relative to the road-shoulder datum: The microphone was 1.5 m higher. (A) Highway shoulder at berm base; (B) Crest of berm; (C) Receiver-side base of berm; (D) Receiver-side of berm at a typical front-yard distance.

Date	Test-type	(A)x/y	(B)x/y	(C)x/y	(D)x/y
August 3	Barrier	13.00/0.66	20.70/3.91	31.50/-0.85	41.40/-0.90
August 3	Open	13.00/1.03	20.70/1.16	31.50/1.50	41.40/1.80
August 16	Barrier	10.06/0.00	21.67/4.00	35.17/0.08	47.50/-0.14
August 16	Open	10.06/0.00	21.67/0.00	35.17/0.00	47.50/0.00
August 24	Barrier	5.64/-0.12	22.09/2.76	41.95/-0.65	
August 24	Open	5.64/0.00	22.09/0.00	41.95/0.00	

4.2 Field-Test Geometries: Earth Berms

To determine both the EA for sound propagation over open ground and the IL of existing noise barriers, three test locations were identified and noise measurements were made at various distances from the roadway. All of the test sites were near to four-lane divided highways. Measurements were made at no more than four test positions for each barrier site and each nearby open-ground site. The microphone height was 1.5 m above the surface for noise-barrier tests of EA and IL . Open-ground tests were conducted at locations as close as possible to the barrier site, to maintain similar traffic-flow conditions at the two locations. Tests were conducted during sunny afternoons and over as short a time period as possible, to reduce variability in L_{eqs} due to traffic-flow changes. Table 4.1 summarizes the test positions. The datum for each berm location was taken to be the far-lane edge of the near two lanes.

On August 3, 1994, along Highway 17 north of Victoria B.C., an earth berm covered with bark mulch was tested with traffic-noise as a source. This location was just north of the McKenzie overpass. On August 16, 1994, further tests were conducted at a highway barrier consisting of mixed sand and earth, near the intersection of Highways 10 and 17, in Delta, B.C. This location had a merging lane of traffic near the berm site which was not present at the open-ground site. Finally, on August 24, 1994, tests were conducted further north of Victoria B.C. at Baxter Park, the site of a large, grass-covered berm.

4.3 Excess Attenuation of Ground

EAs vary with test geometry and frequency. Since the source powers and locations of traffic-noise sources are not well defined, the free-field sound-pressure level is taken to be the that measured at location A, and more distant tests are referenced to this position. As seen in Eq. (4.1), the x-coordinate is taken as the ratio of the distance d_A to reference position A to each more-distant location d_2 :

$$EA = L_{p,open-ground} - L_{p,position(A)} + D \log_{10}(d_2/d_A) \quad (4.1)$$

Eq. (4.1) neglects air-absorption effects, and considers source divergence via the term D . For an incoherent point source, D would equal 20, while for an incoherent line source, D would equal 10. Intermediate values of D could be assigned to deal with the transition from one source type to another, to improve traffic-noise prediction.

In Fig. 4.2 the *EAs* of all three sites can be seen for three receiver locations, for a line source of traffic. The third-octave *EAs* at three receiver positions are presented at the three test sites, with respect to fixed locations and variable frequency. Lines are used instead of discrete points, so that trends in the graphs are more discernible. Generally, the data show positive gain at low frequencies, and attenuation at middle to high frequencies. However, there are differences between the three open-ground test locations. Location B's *EAs* are lowest in the 200, 315 and 800 Hz bands. The August 3rd berm's *EA* is different from the others due to the increase around the 500 Hz band. Location C's *EAs* are lowest in the 800, 1000 and 2500 Hz bands; while the *EAs* are the most similar among the three sites at this location. Location D's *EAs* are lowest in the 315 and 800 Hz (twice) bands. These *EAs* are the smoothest of the three locations, with a greater range of levels between the three berm sites.

Inconsistencies in the *EAs* can be expected due to differences in test geometry, ground types, ground irregularity and traffic-flow variations. The ground for the August 3rd open-ground location consisted of rocky soil with newly-planted grass. The berm itself — with a total height of 3.91 m relative to the berm datum — was covered in bark mulch, with roadways

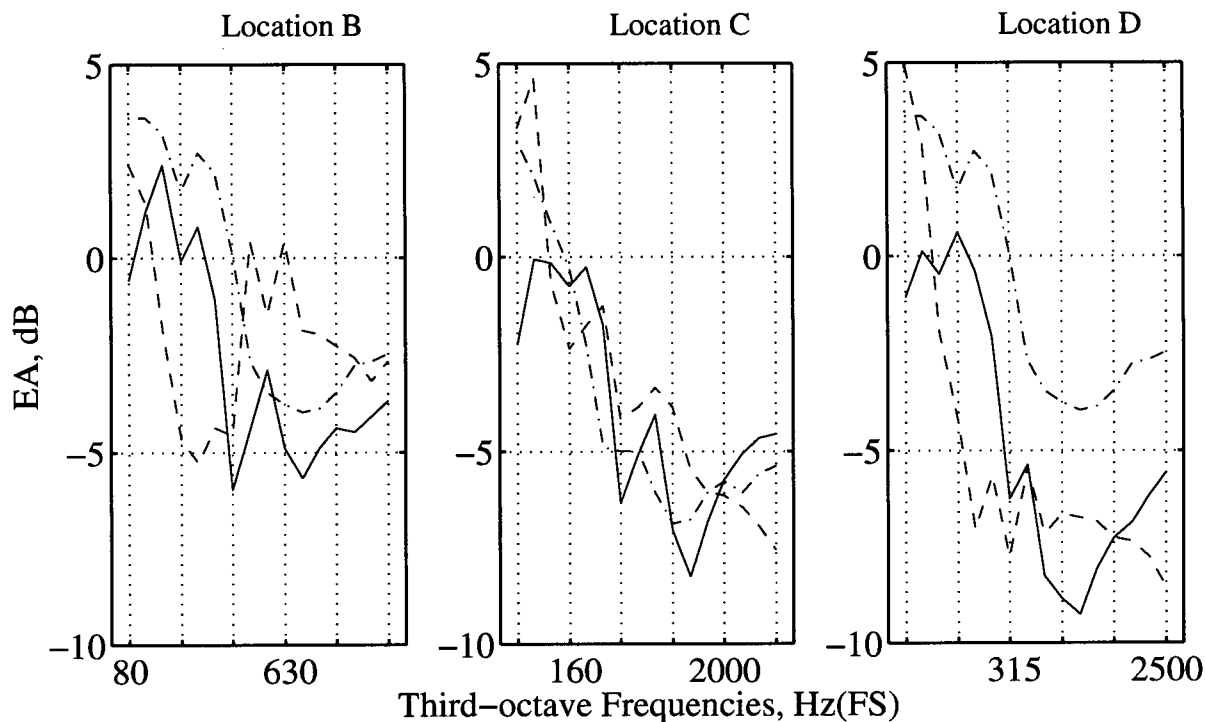


Figure 4.2: Measured EA s in third-octaves for three test geometries with traffic-noise at three outdoor test locations: (-) August 3, 1994, Victoria B.C., Hwy 17; (- -) August 16, 1994, Delta B.C., Hwy10/17; (-.) August 24, 1994, Victoria B.C., Baxter Park, Hwy 17

on both sides — one a highway, the other a residential side street. Testing was not conducted at this site when vehicles were present on the residential street. At the August 16th location, the soil was a ploughed potato field with rows of sprouting plants aligned parallel to the highway — the tests were conducted along a packed-dirt access road that was perpendicular the highway. At Baxter Park, the soil consisted of maintained parkland grass. Trends in the variation of EA spectra with distance are not clear for any of the three test sites. The only trend is a general decrease in EA with distance for a given test frequency — this was the case for the 400 Hz and higher third-octaves for all three barrier sites. For the 80–315 Hz third-octaves, the McKenzie and Delta berms displayed more erratic variations with distance. For the Delta berm, in the 80 Hz third-octave, progressive increases in level were observed with distance.

4.4 Barrier Insertion Loss

Fig. 4.3 compares *ILs* for the three barrier sites at the four test positions. For roadside location A, the *ILs* varied with test site across the entire frequency range. Since location A was earlier used as the reference position for predictions of *EA*, the *ILs* should be 0 dB across the entire frequency range for each of the three sites. That they are not suggests that the reference-position levels deviate from the free-field levels that they are meant to supplant. The 800 Hz third-octave *ILs* have values close to 0 dB for all three test sites. For location B, there was more variability among the *ILs*. The *IL* results for this location were not expected to be 0 dB for all sites across the entire frequency range. For location C, the *IL* is highest for the McKenzie berm, which is the tallest and steepest. The lowest *ILs* were obtained for the Delta berm of August 16th, it being the shortest and shallowest. Furthermore, the Delta berm was only about 200 m long, so a notable amount of traffic noise could have been diffracted around the ends, compounding its poor performance. Intermediate *ILs* are seen for the Baxter Park berm — though it is as tall as the McKenzie berm, it is of shallower slope. The berm at Baxter Park was similarly limited in length — a disadvantage not found with the McKenzie berm — even though this berm did not fully block the line of sight to more distant portions of its adjoining highway. At location D, further from the berm, the *ILs* for the two measured cases are reduced, with the taller, steeper berm outperforming the shorter, shallower one. The exact parameters that differentiate the *ILs* of the three berms at the various test location cannot be isolated with this test data. This illustrates the difficulties associated with studying barrier performance using existing test sites.

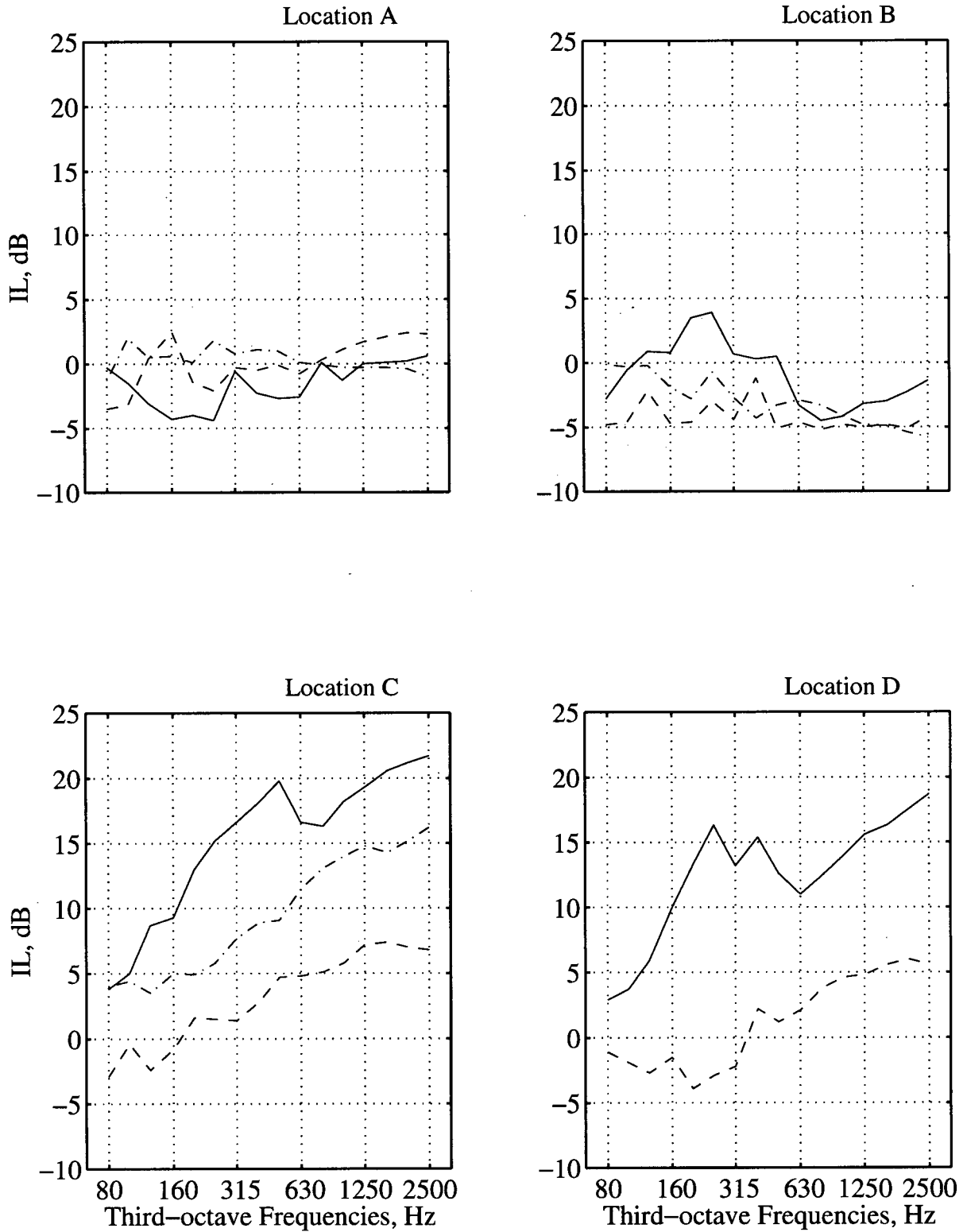


Figure 4.3: Measured *ILs* in third-octaves with traffic-noise for three outdoor test locations: (-) August 3, 1994, Victoria B.C., Hwy 17; (- -) August 16, 1994, Delta B.C., Hwy 10/17; (-·-) August 24, 1994, Victoria B.C., Baxter Park, Hwy 17.

Chapter 5

Experiment

5.1 Experimental Introduction

This chapter presents details of the development of an experimental scale-modelling facility. The scale modelling was undertaken within an anechoic chamber located at the University of British Columbia's Department of Mechanical Engineering. During the development of the test facility, accuracy and reproducibility were considered to be highly important considerations. Test frequencies were to extend well into the ultrasonic range; test equipment was chosen which could sample and record up to 100 kHz. To generate the necessary ultrasonic frequencies, a crossing air-jet source was constructed and its characteristics studied after equipment for the regulation of air pressure was installed. The anechoic chamber's properties were examined using the air-jet source, since it was unlikely that ultrasonic frequencies were considered during the design of the anechoic chamber. A platform on which the scale-model configurations were tested was constructed in the anechoic chamber. Materials were evaluated in terms of their suitability as scale-model materials. A procedure was developed for the time- and cost-effective assembly of acoustically suitable scale-model noise barriers. Measurements of the IL of scale-model noise barriers were conducted at 1:31.5 scale. Numerical data-analysis procedures were developed to permit for error analysis, data reduction, visualization, and plot preparation.

5.2 Test Equipment

Compressed air was needed to operate the scale-model noise source. Fig. 5.1 shows the plan-view layout of the anechoic chamber, air-jet-source apparatus, and test platform. An on-site air supply was available at supply pressures that were always kept between 90 psi (612 kPa)

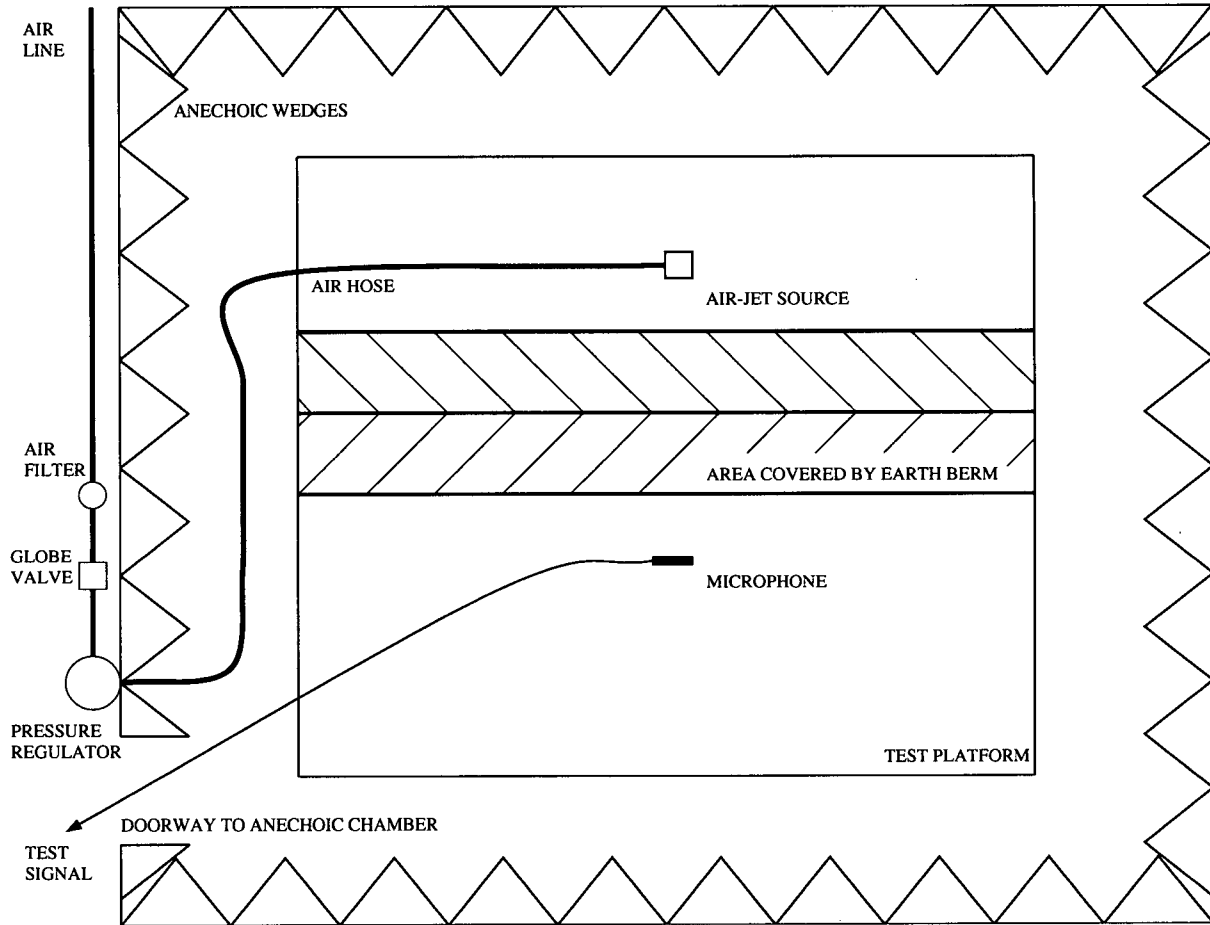


Figure 5.1: Plan view of the anechoic chamber, air-jet-source apparatus and test platform.

and 110 psi (748 kPa). A 1/4" brass air line was installed; this supplied air to the air-jet source through a Wilkerson Model F20-02-000 moisture and particulate filter, a globe valve, a Fairchild Model 10 pressure regulator, and a flexible air-hose of 1/4" inner diameter. A Weksler Model GR2-D101 pressure gauge, capable of monitoring air-line pressures from 0-700 kPa (± 5 kPa), was attached to the pressure regulator to allow for accurate monitoring and adjustment. This was of particular importance during periods when the air compressor was in operation.

Sound-pressure-level measurements were made using test equipment to sequentially receive, amplify, sample, and record the test signals; Fig. 5.2 is a picture of part of the test apparatus. A 1/8" Brüel & Kjær Type 4138 condenser microphone was used for all measurements. A Brüel

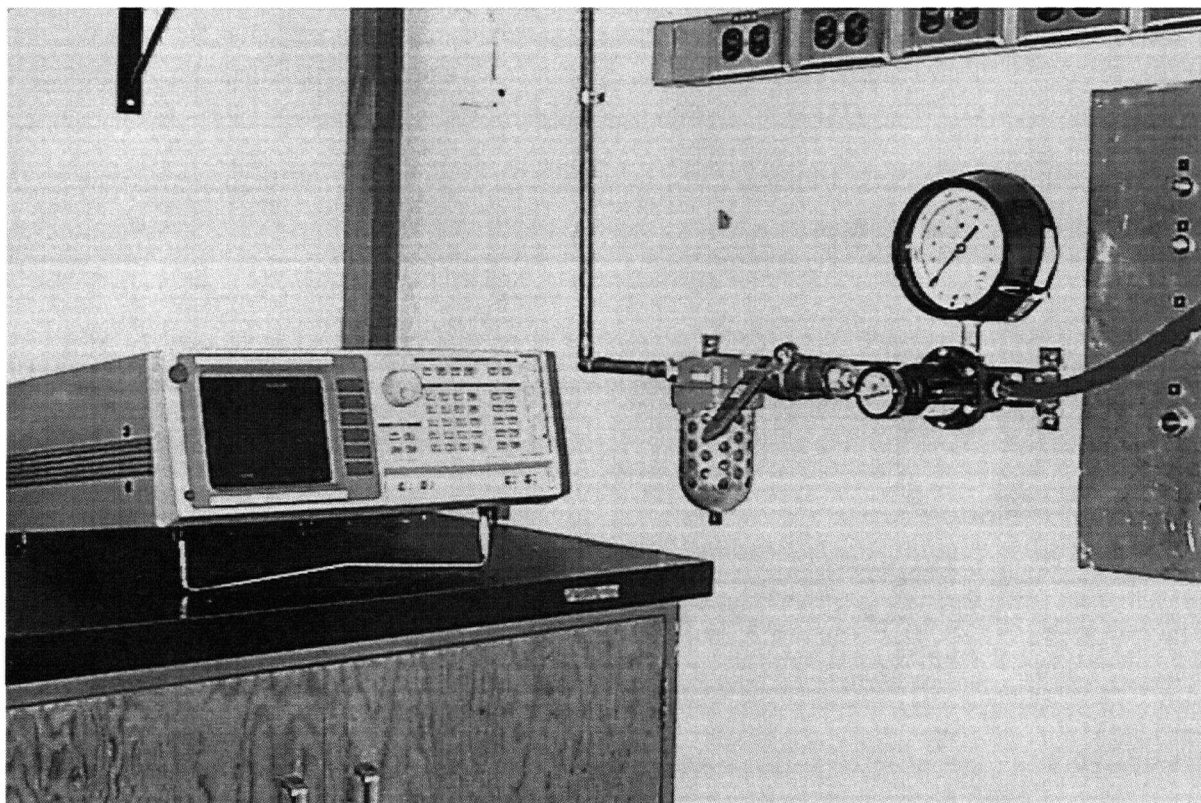


Figure 5.2: Photograph of Stanford Research Systems SR-770 and air-line.

& Kjær Type 2619 pre-amplifier carried the signal to a Brüel & Kjær Type 2804 Microphone Power Supply. To preclude problems with electrical grounding, the metallic surfaces of the pre-amplifiers were insulated from the metallic mesh forming the floor of the anechoic chamber using small wooden blocks. From the power supply, a cable fed the signal into the direct input of a Brüel & Kjær Type 2607 Measuring Amplifier — with the ‘meter’ function set to RMS, and the averaging time set to fast, since all signal averaging was performed by the network analyzer. Additionally, the signal was high-pass filtered by the measuring amplifier above a cut-off frequency of 22.5 Hz, since frequencies this low were not of significance to the scale-model tests. The input section attenuator was set at 30 mV and the output section attenuator to ‘x1’ — this allowed for pistonphone calibrations without voltage overload indications by the

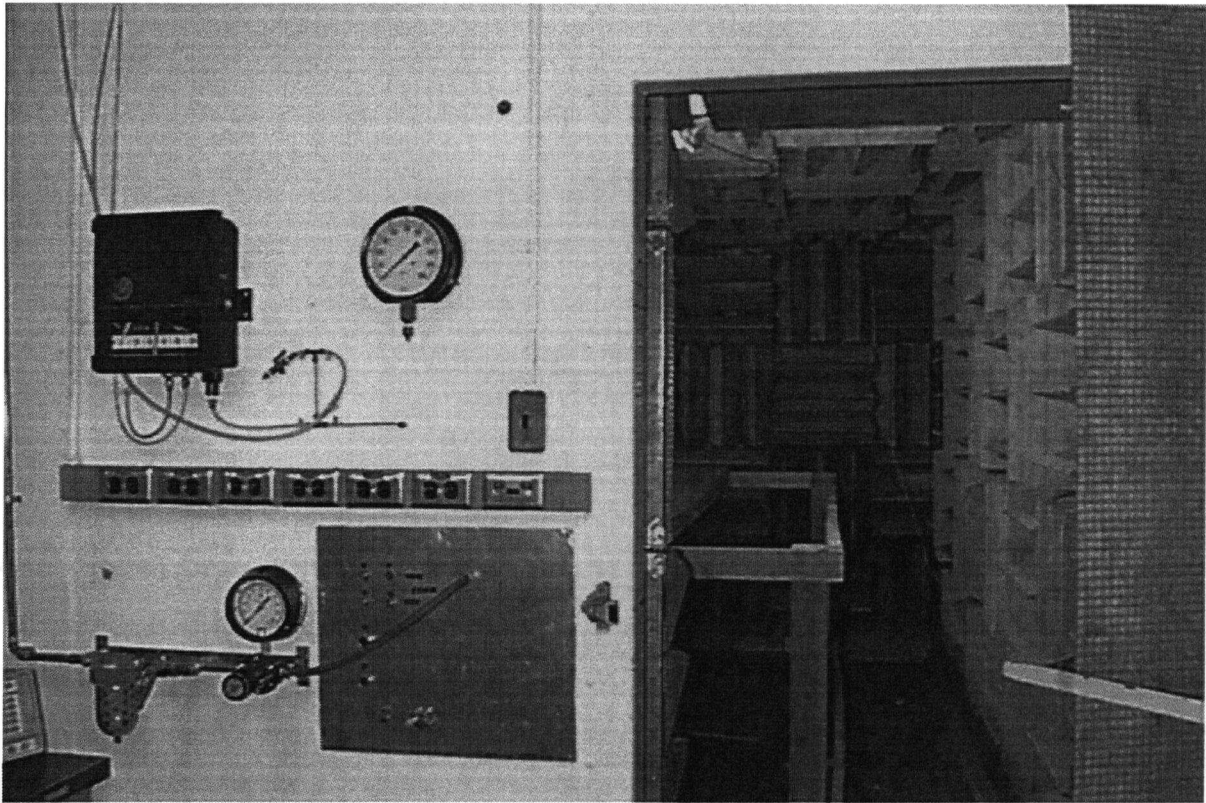


Figure 5.3: Photograph taken outside of the anechoic-chamber, with the test platform visible.

measuring amplifier, while minimizing the introduction of noise to the signal. A Stanford Research Systems SR-770 FFT Network Analyzer was used to sample the acoustic signal, compile spectral averages, and record the results onto 3.5" diskettes. Spectral data were recorded in four-hundred frequency bins, extending from the 0–250 Hz DC bin up to the 99750–100000 Hz bin. Each test employed at least fifteen-hundred non-overlapping spectral averages, requiring a sample time of 6 s per test.

A Brüel & Kjær Type 4220 Pistonphone (with a calibration frequency of 250 Hz) was used to calibrate the analyzer's 250–500 Hz band to 124.0 dB. Narrower bandwidths were not employed when calibrating the analyzer, since different input sensitivities would be required. Data analysis was performed almost exclusively using a UNIX-based implementation of MATLAB.

In Figs. 5.3 and 5.4 the entrance to the anechoic chamber can be seen, along with the test

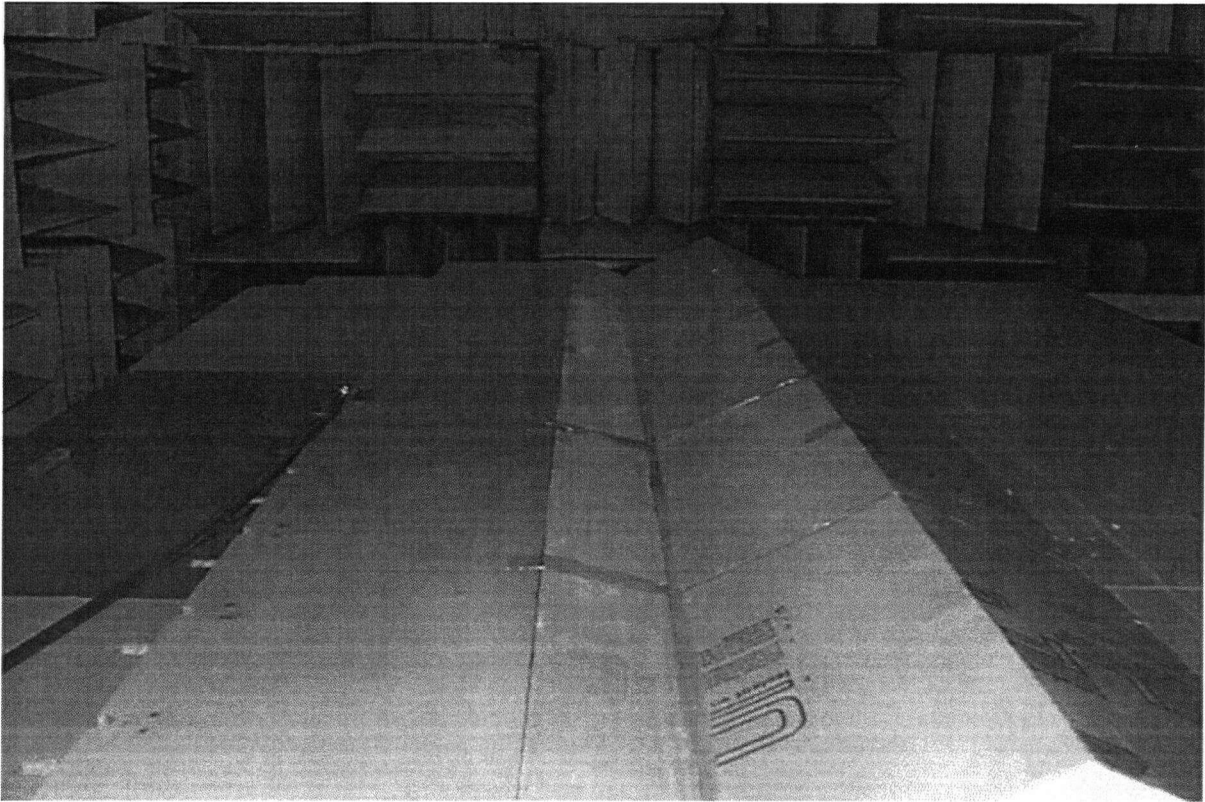


Figure 5.4: Photograph taken inside of the anechoic chamber, with the test platform visible.

platform that was assembled in the chamber. The anechoic chamber has fibreglass wedges (33 cm tip length and 19.5 cm per square-base side) mounted with alternating wedge orientations on all interior surfaces. The available work space provides a 4.0 m \times 4.7 m floor space and a 2.6 m height. The slanted surfaces of each wedge are protected by a 1.2 cm square mesh of 1 mm wire. To allow room users access to the anechoic chamber, 2 mm steel wire is used to form a taught floor with a 5 cm square mesh. This work surface lies 18 cm above the floor wedges, which are further covered by a 0.5 cm square mesh to catch debris. After the free-field testing was completed, a platform was constructed on which to mount material samples for *EA* testing and for testing the *ILs* of scale-model noise barriers.

5.3 Air-Jet Source Design

An optimal scale-model traffic-noise source reproduces the acoustical characteristics of a full-scale prototype vehicle. It should bear a resemblance to the full-scale prototype (e.g. point or line) in terms of its scaled dimensions, relative location of the noise sources, scaled sound power, directivity patterns, and transient or steady-state nature. If the source locations and directivity patterns of full-scale vehicles cannot be reproduced correctly then an omnidirectional point source is a suitable prototype. The sound-power output should provide an adequate signal-to-noise ratio, and should allow for reproducible test results.

The air-jet source was patterned after that described by Novak [128]. Its acoustic properties included omnidirectivity, sufficient power output, and broadband spectra. The source is comprised of six co-planar jets, of 0.3 mm diameter, spaced at 60° intervals around a cylinder of 6.5 mm diameter. It generates broadband noise up to, and possibly beyond, 100 kHz. The airflow from each jet travels directly inward towards a common geometric centre, where the turbulent interaction of the air generates sound. The source has an acoustic centre which is transported, by the air flow, away from the geometric centre of the jets — the distance was reported to be small. While some modifications were made to Novak's design to facilitate fabrication, the essential features of the source were retained. Fig. 5.5 shows the outer housing and core piece, both of which were machined out of brass, and the o-ring which was used to seal the gap between the two pieces. Air flowing into the left-hand end passed through six holes (drilled at 60° intervals into the base of the core-piece) along to a further set of six jets (also at 60°) through which the air exits to atmospheric pressure. The core-piece has six holes drilled into the base, maximizing the area for air flow from the 1/4" diameter air-supply hose, while providing a point of support between the core-piece and outer housing. The volume between the core-piece and outer housing provides a transition between the six air-flow holes and the six air jets located just below the top cap of the core-piece. The core-piece contains resonant cavities which, according to Novak [128], amplify the source power at lower frequencies.

Because the air-jet is a steady-state source, the measurements could not be used to identify

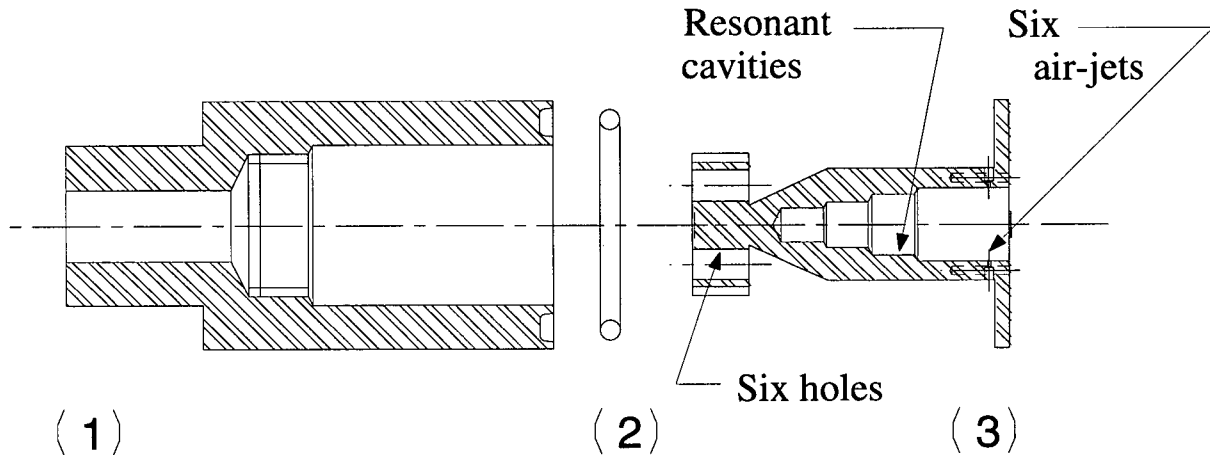


Figure 5.5: Air-jet source: assembly drawing where (1) is the outer housing, (2) is an o-ring of size no.15 and (3) is the core-piece.

the phase of the incoming diffracted/reflected sound waves. However, if the objective were to study concert hall acoustics, it definitely would be, given that a time-domain signal would be needed. Impulsive sources generate a time record from which reflections can be removed and excessive air absorption can be corrected for. In the context of traffic-noise testing a steady-state source will suffice. The size of the source in comparison to a full-scale vehicle is of importance. For a scale of about 1:30, the source at full scale would be roughly 20 cm in size. Considering the size of a full-scale-vehicle, and the much larger spatial region from which sound emanates, it should be apparent that the coherence for a given source/receiver position in the scale model is higher than would be seen from a vehicle in the real world. The source is thought, but not proven, to produce broadband spectra on a continuous basis, thereby insuring that sound radiated along all paths can interact coherently — for instance, at the crest of a barrier.

5.4 Air-Jet-Source Testing

Tests were conducted to characterize the properties of the air-jet source. These tests were conducted with the source mounted vertically at the room centre; measurements were recorded over the frequency range 0–100 kHz. The microphone was oriented vertically for all tests.

Four parameters were varied, namely air-line pressure, source-microphone distance, inclination angle of the source relative to the microphone, and the source's rotational angle relative to the microphone. The objective was to quantify the errors related to the variation of each parameter, along with those associated with room reflections, calibration error, and fluctuations of air absorption. The temperature, air pressure, and relative humidity were recorded during all test runs, in order to calculate and correct when necessary for the significant free-field losses associated with air absorption. The following sub-sections describe the results of these parametric tests.

5.4.1 Variation of Noise Spectrum with Air-Line Pressure

To maintain adequate signal-to-noise ratios in the presence of excessive air absorption at ultrasonic frequencies, it is advantageous to maximize the sound-power output at all operating frequencies. Air-line pressure is a determinant of the power and frequency distribution of sound radiated by the air-jet source. Fig. 5.6 shows the sound-power level measured at 1 m from the source for various air-line pressures, based on the average of seven tests. It can be seen that the sound-pressure output at all frequencies increases with air-line pressure, but that the magnitude of the fluctuations in sound-pressure level decrease. The total decibel output at 1 m is shown in Fig. 5.7; the exponential shape of the curves suggests that a limiting value is being approached. In any event, the maximum air-line supply pressure is restricted to about 90 psi (612 kPa); it is prudent to operate below this threshold to lengthen the intervals between periods of the air-compressor operation.

Reproducibility is a necessary source property. An optimum operating pressure was sought which resulted in the smallest standard deviation of output sound-pressure level averaged over the measured frequency range. Variance data were calculated by averaging measurements at seven different rotational orientations: two made at 0° , two at 30° , and three at random angles of rotation. It was assumed that variances arising from pressure changes were not severely affected by air-absorption fluctuations over the duration of the test schedule. How does the

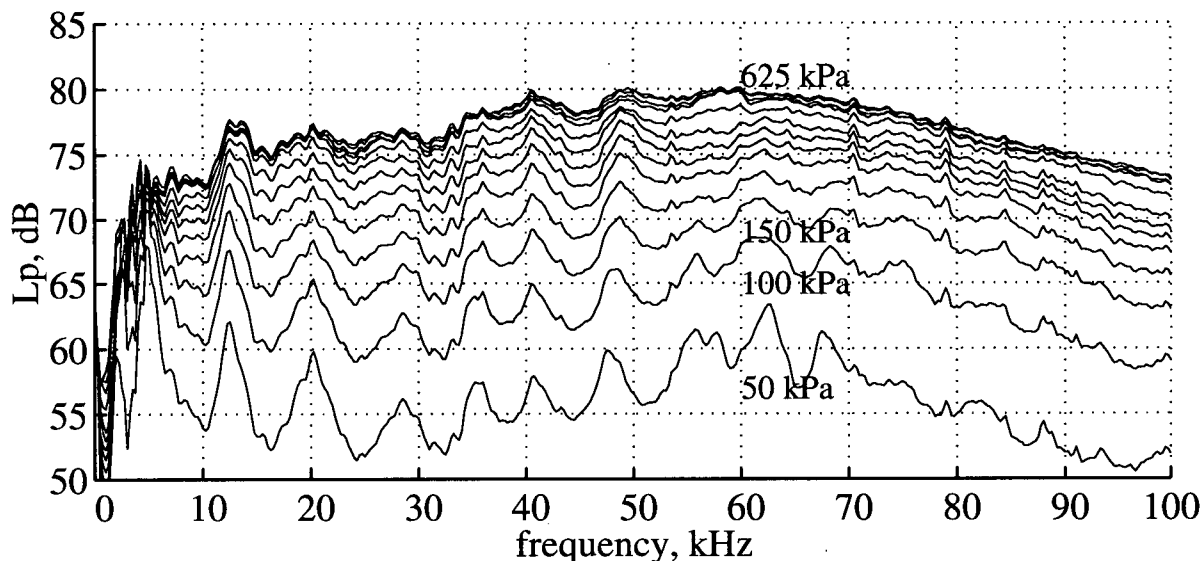


Figure 5.6: Variation of air-jet source spectra with air-line pressure (50, 100, 150, 200, 250, 300, 350, 400, 450, 500, 550, 600, and 625 kPa). Distance is 1 m.

variance for a given frequency change as frequency increases? Fig. 5.8 contains the cumulative variance versus frequency for various air-line pressures. The variance data for each air-line pressure were based on the results of three tests at each of thirteen air-line pressures. If the variance was identical in all frequency bins for a given air-line pressure, the variance would increase linearly with frequency. It can be seen that lower frequencies contribute significantly to the variance, with a progressive decrease in the relative amount of variance being added at higher frequencies. The variability can be quite significant, despite the similarity of atmospheric conditions and efforts to reproduce the same experimental set-up. The accumulated variances were used to calculate the average standard deviation over the entire frequency range; as seen in Fig. 5.9, it is apparent that the overall standard deviation is minimized at 450 kPa, and is only slightly larger at 500 kPa. The errors would likely be further reduced by the addition of an air buffer into the system, or by omitting low-frequency data.

An assessment of the results, with regard to maximizing signal-to-noise ratios and minimizing measurement error, suggests that 500 kPa is the preferred operating pressure for the

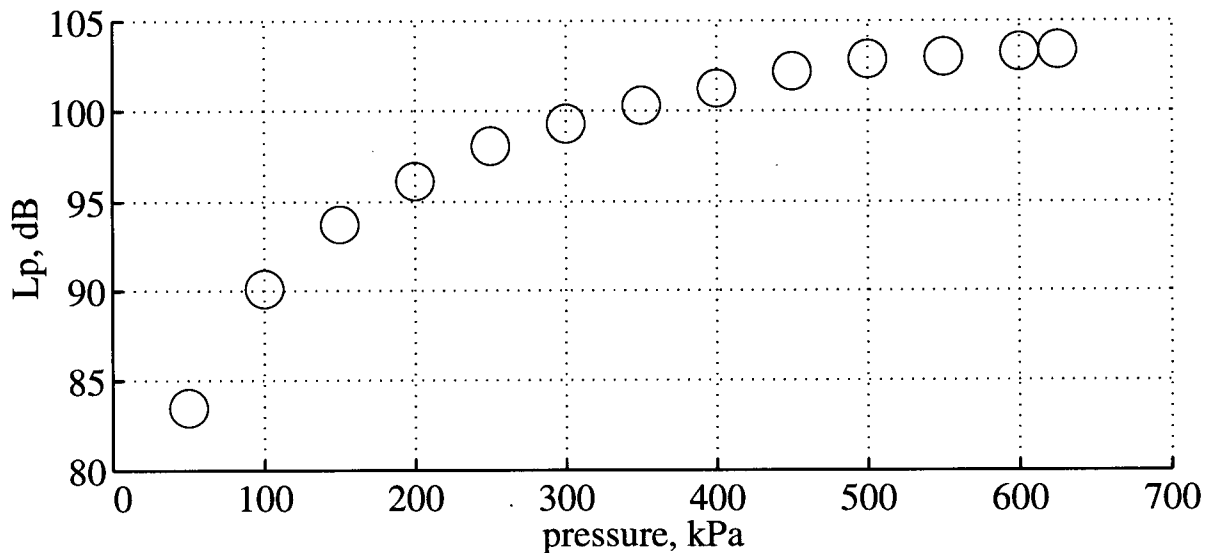


Figure 5.7: Source-pressure study: measured variation of total sound-pressure level generated by the air-jet source with air-line pressure.

air-jet source. Air-line-pressure fluctuations will always contribute to the source's variability. For instance, if source rotation produces similar standard deviations at one or more air-line pressures, then it would be reasonable to conclude that source rotation produces a uniform radiation pattern in a plane about the source's axis, with the observed variation being, in fact, due to the inherent fluctuations of air-line pressure.

5.4.2 Variation of Noise Spectrum with Source Rotation

The ultrasonic source generates noise via the turbulent interaction of six co-planar air-jets that are spaced at 60° intervals. It is desirable to know the angular variation of the source's sound power, when the rotational orientation of these air-jets relative to the measurement microphone is varied while the distance is kept fixed at 1 m. If changes to the rotational alignment of the air jets produce significant variations in measured sound-pressure levels, the repeatability of tests would be compromised. Fig. 5.10 contains the standard deviation of the test results for seven tests. It reveals clearly that the errors resulting from rotation of the source

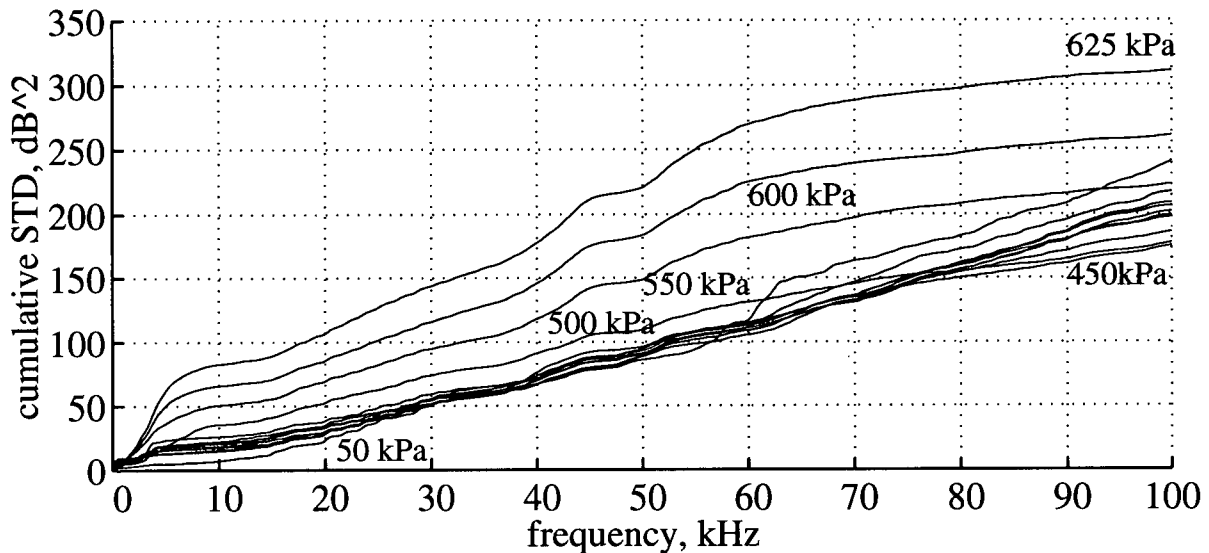


Figure 5.8: Source-pressure study: the accumulation of variance with frequency for thirteen air-line pressures.

are greatest below 10 kHz, with up to 2 dB of standard deviation; at higher frequencies the highest standard deviation is approximately 0.9 dB. The noise radiation in the plane of the jets was fairly omnidirectional, with a standard deviation of about 0.5 dB if low-frequency errors are neglected. It was concluded that rotation of the source about its axis does not lead to a significant variation in sound-pressure level. Thus, the exact orientation of the rotational axis need not be considered while conducting scale-model tests.

5.4.3 Variation of Noise Spectrum with Distance

The output sound-power level of the source can be inferred from measurements of sound-pressure level. Measurements of sound-pressure level were conducted at increasing horizontal distances from the source, so that the source's sound-power level could be determined. The decrease in sound-pressure level should approach the point-source rate of 6 dB per doubling of distance. Frequency-dependent corrections for both air absorption and microphone response are required to obtain the correct values of sound-power level. After these corrections are made,

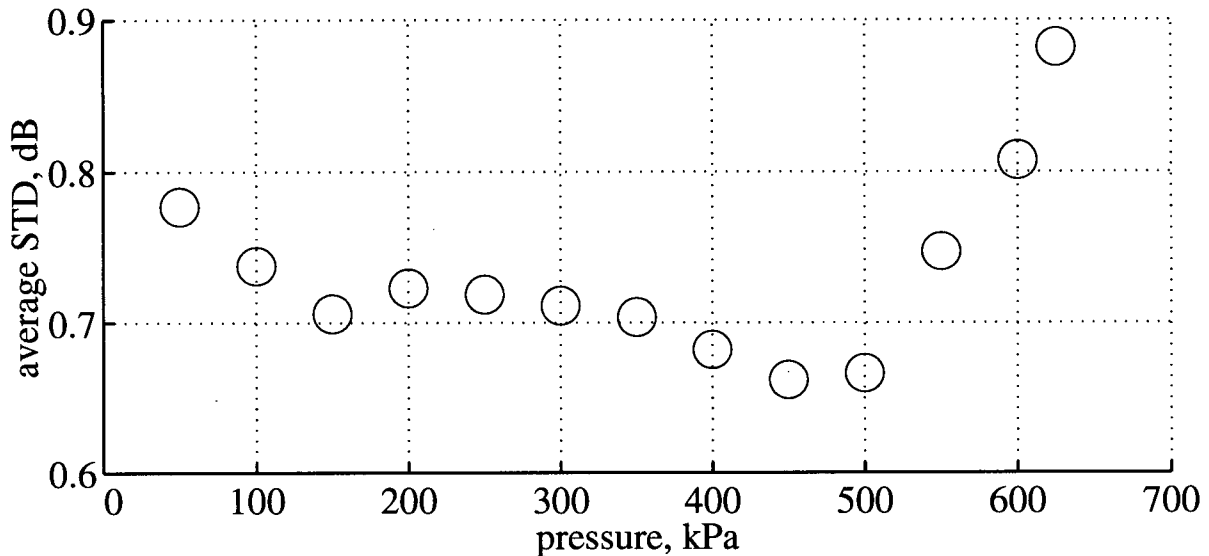


Figure 5.9: Source-pressure study: the average standard deviation, from 0–100 kHz, at thirteen air-line pressures.

any remaining deviations from the point-source rate can be attributed to either the source's near-field or to the free-field performance of the anechoic chamber. Fig. 5.11 demonstrates how correcting for air absorption can affect the total sound-pressure-level decrease with distance. Microphone response is also accounted for, but its significance is negligible compared to that of air absorption, and microphone response was not a factor since the same microphone was used for all tests. Fig. 5.12 presents the sound-power levels of the source inferred from the tests of sound decay with distance. A least-squares fit generated the sound-pressure-level data from measurements at twelve distances from the source, normalized to the usual 1 m distance:

$$L_p = L_w - 20\log_{10}(r) - 10\log_{10}(4\pi) - \Delta L_{p,air} + \Delta L_{p,microphone} \quad (5.1)$$

5.4.4 Variation of Noise Spectrum with Source and Microphone Inclination Angle

The metal body of the source restricts the radiation of sound, and the air stream from the source moves the acoustic centre of the sound out from the geometric centre of the air jets. The high-velocity air refracts sound away from the source's cylindrical axis, and turbulence from the

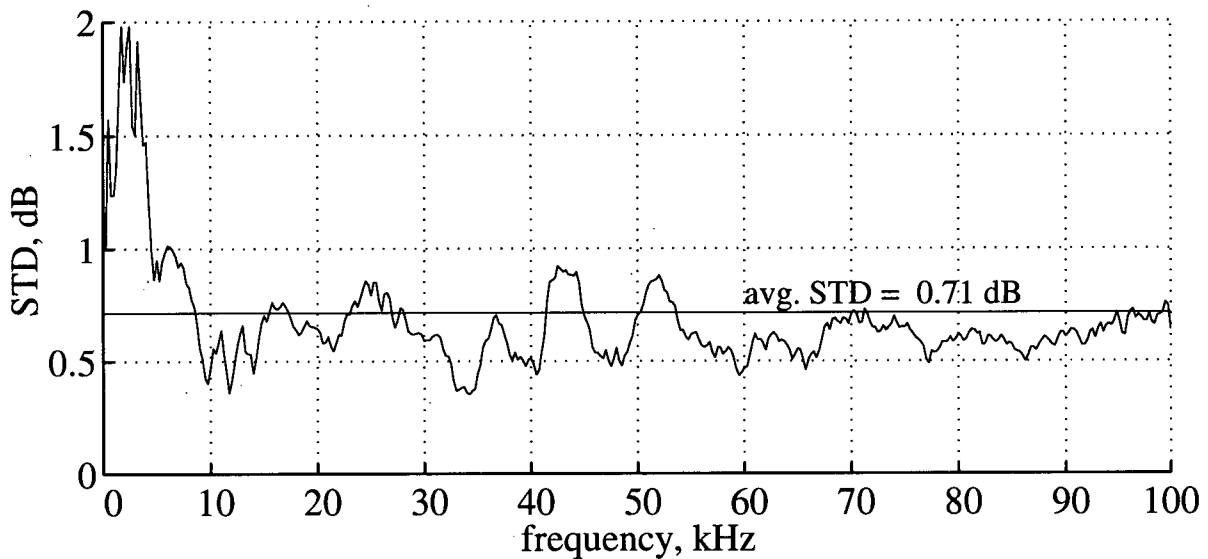


Figure 5.10: Source-rotation study: standard deviation from thirty-six tests over the frequency range of 0–100 kHz.

air stream also produces short-term fluctuations in measured levels — particularly when the air stream strikes the microphone. These effects would be expected to result in significant source directivity, which is a potential source of error when making measurements of barrier IL. Source directivity was evaluated to see if constraints should be placed on the source's inclination angle.

In Fig. 5.13, the sound pressure of the source at a 1 m distance is seen to be dependent upon both the frequency and the angle of source inclination. The source was inclined, at various angles with respect to the geometric centre of the air jets, towards the measurement microphone. 0° is taken to be the plane perpendicular to the air-jet axis; 90° is taken to be directly in line with the air stream from the source. The source's maximum output can be seen to decrease in frequency as the angle of inclination decreases. The air-stream leaving the source has a pronounced affect on levels when inclination angles of 70° , 80° , and 90° are used.

The total source output, seen in Fig. 5.14, reveals that the air-jet-source's output reaches a maximum near 40° . The total output at 40° is about 5 dB greater than at 0° ; this is an increase of roughly 0.1 dB per degree. Narrow-band results are also shown, with the maximum values

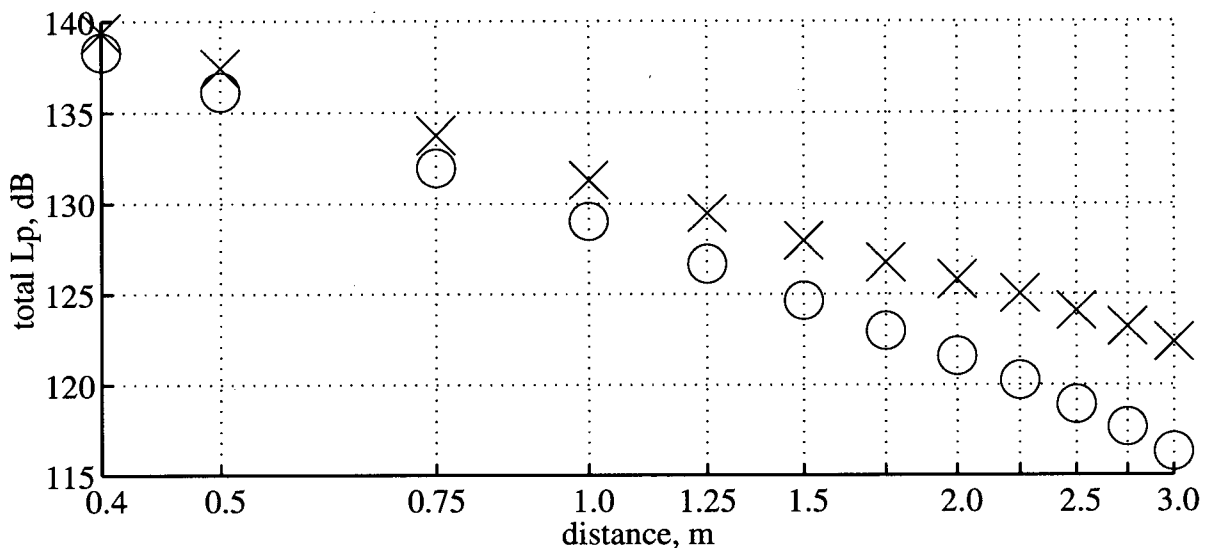


Figure 5.11: Source sound-power-level study: (x) uncorrected L_p data; (o) L_p corrected for air absorption and microphone response.

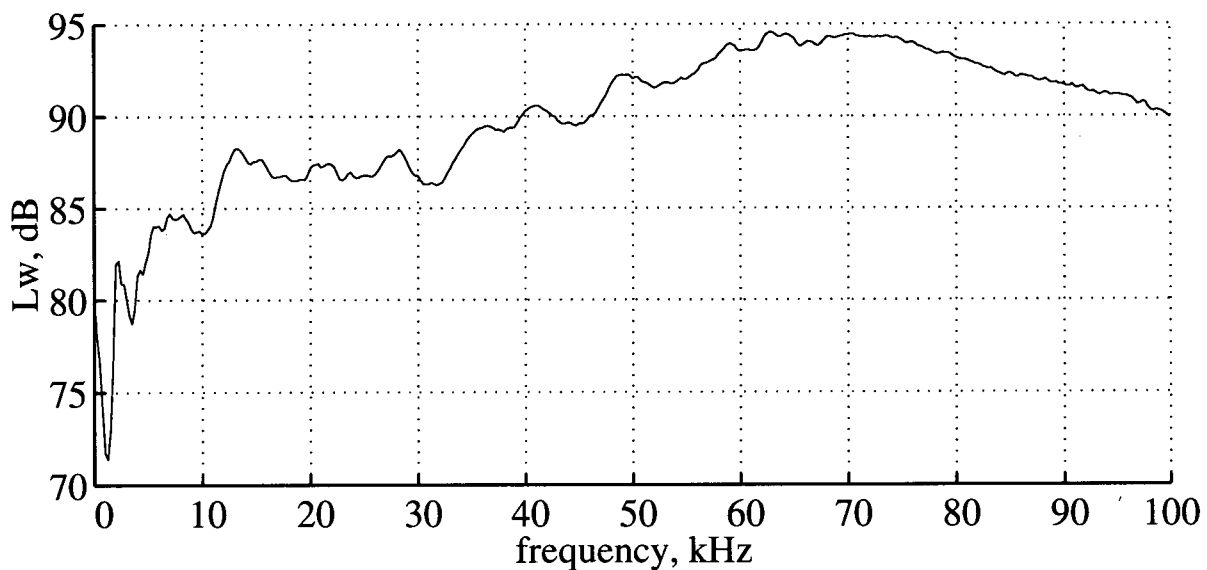


Figure 5.12: Source sound-power-level study: best-fit sound power levels.

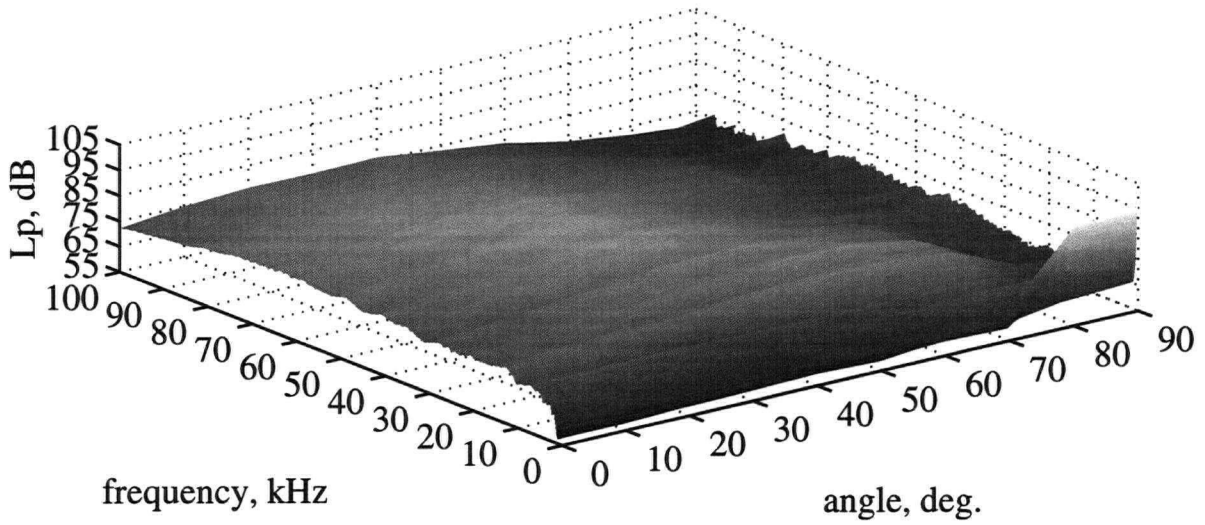


Figure 5.13: Source-inclination study: a 3-D plot of sound pressure 1 m from the air-jet source over angles from 0° to 90°.

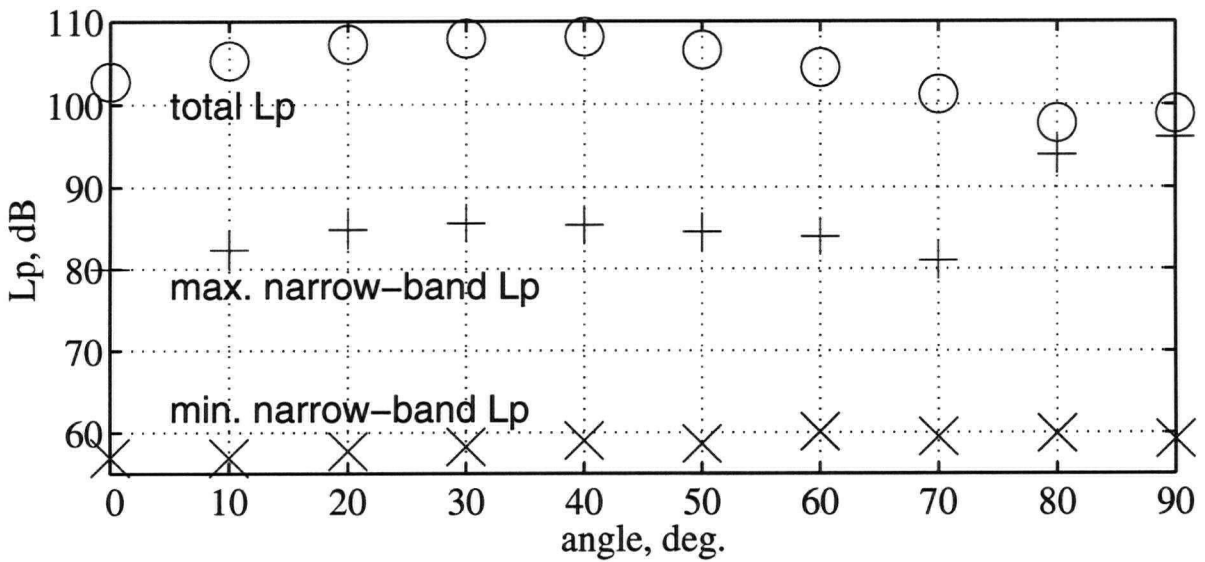


Figure 5.14: Source-inclination study: total source output over the 0° to 90° interval.

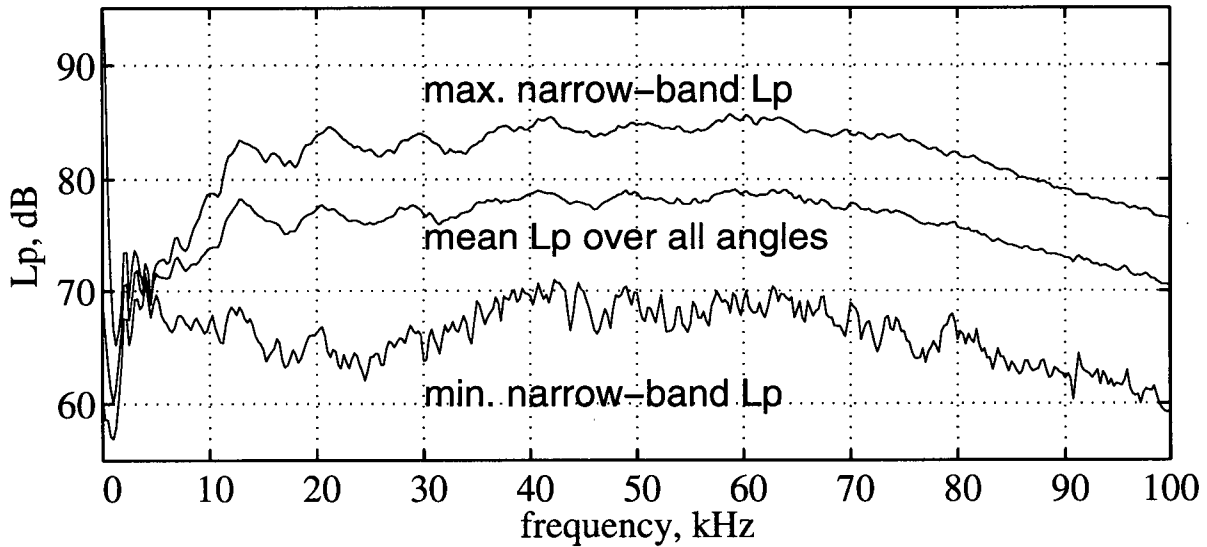


Figure 5.15: Source-inclination study: the frequency dependency of sound-pressure levels averaged over ten inclination-angle measurements.

occurring at 80° and 90° — despite the expectation that refraction directs sound away from the air-stream's axis.

After numerical averaging over all measured angles, Fig. 5.15 displays the maximum, mean, and minimum levels measured at a 1 m distance with varying source inclination angle. The output over the entire frequency range displays significant variability.

5.5 Anechoic-Chamber Testing

Tests were conducted using the air-jet source in order to characterize the free-field performance of the anechoic chamber. The objective of these tests was to study how source proximity to the chamber's inner surfaces affected the free-field levels — the extent to which the decrease of L_p with distance deviates from 6 dB/dd. These deviations can be attributed to unwanted reflections from interior surfaces, or to sound from noise sources external to the chamber. Referring to Fig. 5.11, the corrected total sound-pressure-level decrease with distance reveals the slight effects of the walls of the chamber at and beyond a 2 m distance from the source —

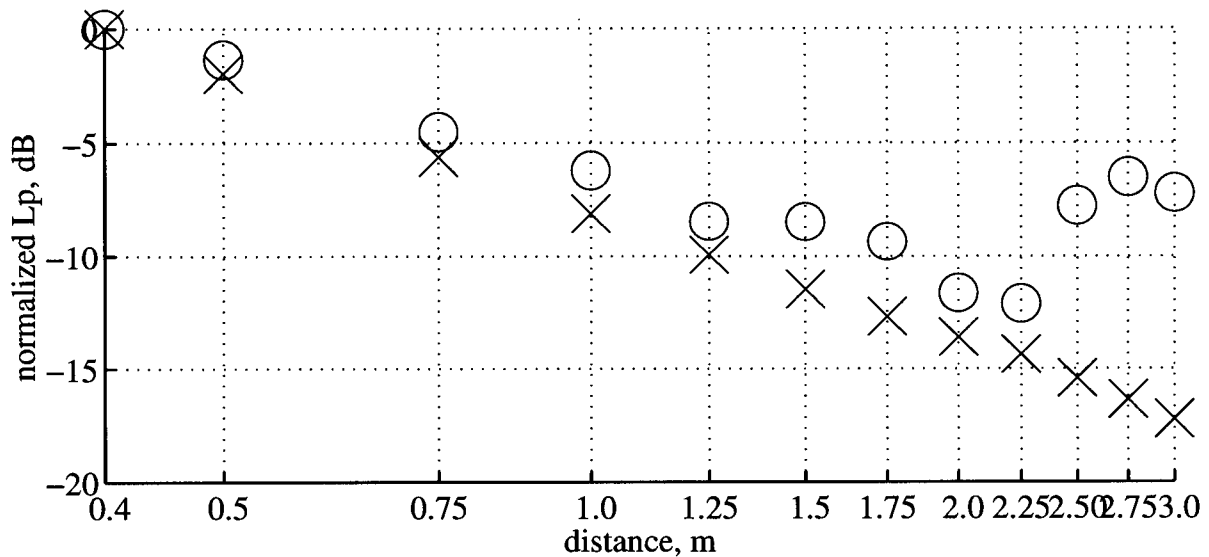


Figure 5.16: Anechoic-chamber study: (o) low-frequency data include the 0 to 4750 Hz bins; (x) high-frequency data is the total level from the 5000 to 99750 Hz bins.

this corresponds to a distance of slightly greater than 1 m from a chamber wall. Reflections from the inner surfaces of the anechoic chamber will affect the accuracy of measurements. However, if the reflected energy is 20 dB or more below the direct sound at a point of measurement, the error in the measured value will be less than 0.1 dB. Most barrier testing was therefore conducted at distances of 1 m or more from chamber surfaces.

Examining the rate of decrease with distance in 250 Hz bands, a deviation from 6 dB/dd (after correction for air and microphone effects) was observed at frequencies below 5 kHz. After calculating the total level for twelve low-frequency bands from 0–4750 Hz, and for the remaining high-frequency bands from 5000–99750 Hz, Fig. 5.16 reveals quite clearly that the low-frequency bins do not decay with distance as in the free field. This further substantiates arguments in favour of neglecting low-frequency information when conducting scale-model tests. Reflections from the wall apparently increase levels over a wide range of frequencies at distances of about 1 m from the wall and closer.

The free-field deviation is characterized as being the difference in decibels between the

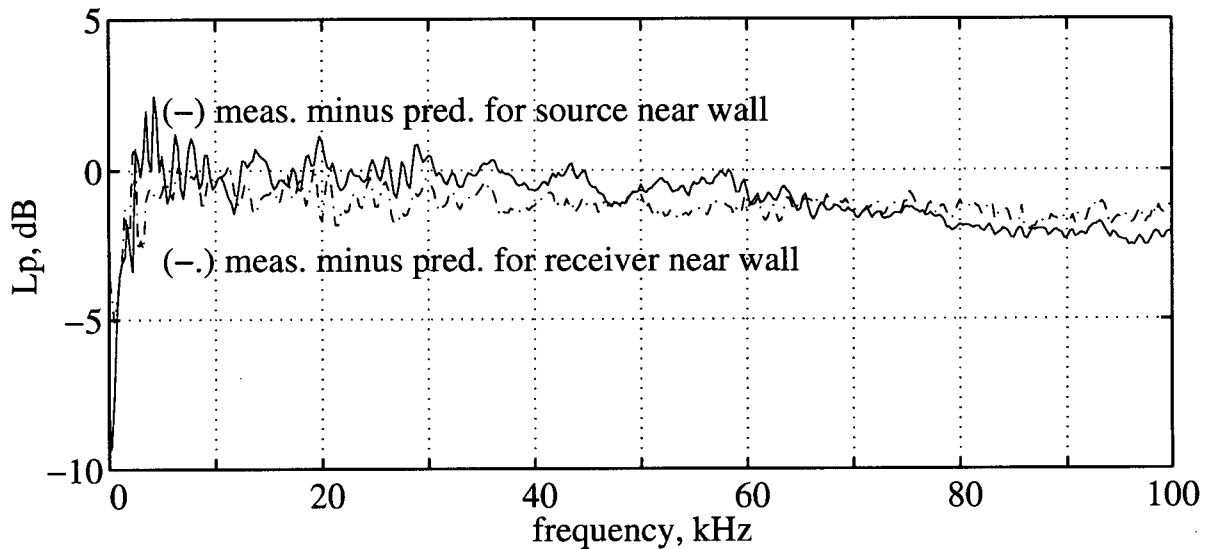


Figure 5.17: Anechoic-chamber study: the plot shows the difference between the near-wall and room-centre measurements and the predicted level.

sound-pressure level expected in a free field at a given source-receiver distance and the levels in the presence of wall reflections. To characterize the deviation from free-field levels at ultrasonic frequencies, the source and receiver were kept at a fixed distance from each other, but their respective locations were varied relative to the chamber's walls. The tests with the closest proximity to the wall were run with the microphone 0.25 m from the wedge tips; the source was 1 m further from the wall. Five such tests were run at arbitrary positions along one wall, and then the source and microphone positions were reversed for five further tests. The difference between these measurements and the predicted levels were examined to assess the room's anechoicity.

Free-field deviations are displayed in Fig. 5.17. The plot shows the difference between the two near-wall measurements and the predicted level; it can be seen that levels near the wall are lower than expected. Predictions were made using Eq. (5.1) for the spectrum shown in Fig. 5.12. The near-wall tests were made with the source held at a virtually constant rotational orientation with respect to a room wall, but at different positions with respect to the surface of

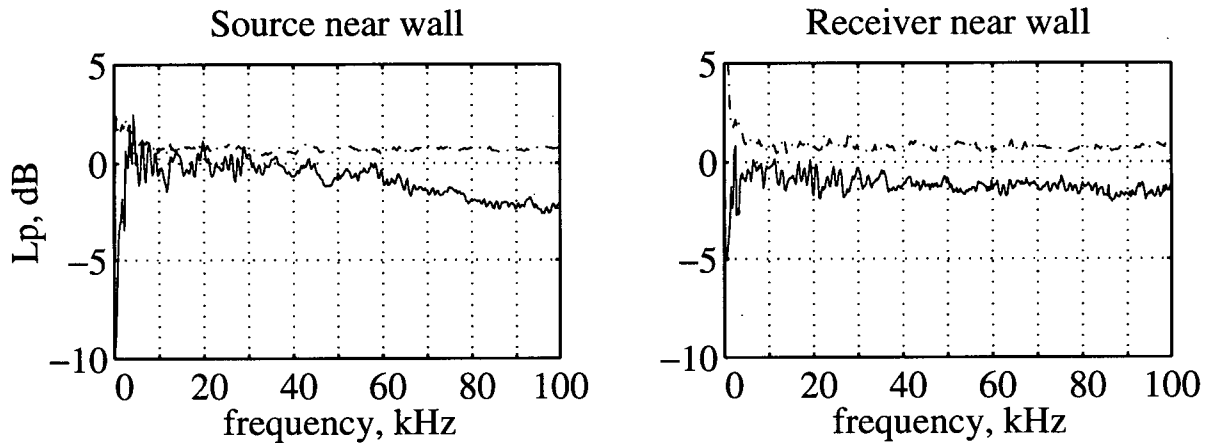


Figure 5.18: Anechoic-chamber study: near-wall reflection-induced error: (-) measured minus predicted; (-.-) standard deviations of this difference.

this wall. the trend at higher frequencies is for measured levels to decrease by up to 2 dB. This result is unlike the earlier tests of decay versus distance, where low frequencies were found to be amplified by surface reflections. This could be due to an overprediction of air absorption, or perhaps to power fluctuations arising from changes in the rotational angle of the source. However, assuming the results are valid, destructive interference appears to occur at distances of 25 cm from the wall over a wide-frequency range.

The variances of the separate measurements made at the near-wall positions and in the predicted level contribute to errors in the predicted difference in levels due to wall reflections. Fig. 5.18 introduces the standard deviation of the difference due to measurements, while neglecting the error in the predicted level. Comparing the magnitude of the error to the magnitude of the differences, it can be seen that large coefficients of variation exist across the frequency range. Fluctuations of air-line pressure contribute to this uncertainty.

Tests of scale-model material EA would not benefit from wall reflections, so keeping an adequate distance from the chamber wall was essential. Measurements were conducted with scale-model noise barriers in place to study the severity of the reflections when the direct sound path to the microphone was blocked by the noise barrier.

5.6 Scale-Model Material Testing

In an acoustical scale model it is necessary to conduct tests at frequencies that are higher than full scale by the scale factor n . At these higher frequencies, the materials have different surface impedances, so it is necessary to find scale-model materials to act as analogues of the real-world ground surfaces. A material is a good scale-model surface when the normal impedance of the scale-model surface at ultrasonic frequencies is equivalent to the normal impedance of the ground surface at full-scale frequencies. As well, limitations imposed by the available test space and measuring equipment imposed a minimum and a maximum scale factor. From a geometric perspective, the floor area available in which to build a scale model, and the overall area of the outdoor region under consideration, contribute to the selection of a scaling factor. The test space available is a 4.0 m \times 4.7 m floor area (and 2.6 m height); for tests of traffic noise and noise barrier IL it is desirable to measure a square area with 100 m sides. Based on this consideration, a minimum scaling factor is $n = 25$. From a frequency perspective, the properties of available measurement equipment limit, to 100 kHz, the upper frequency that can be measured in the scale model. Traffic-noise frequencies of interest are determined from the location of the peak in the A-weighted spectrum which, depending on the traffic mix and locale, will exhibit a maximum between 500 Hz and 1500 Hz. It is desirable to have information about traffic noise up to the 2000 Hz third-octave band; this band has an upper frequency of 2245 Hz. Frequency considerations thus establish a maximum scaling factor of $n = 44.5$. The optimal scale factor should fall within the range $25 \leq n \leq 44.5$.

5.6.1 Measurement of Excess Attenuation

Ground materials found in the proximity of highways — such as grass, gravel, soil, and asphalt — cannot be used in a scale-model since they do not have the same acoustical properties at scaled frequencies. Effective flow resistivities for different outdoor ground materials are seen in Table 2.1 on page 25. Theoretical EAs were calculated using full-scale frequencies and a sound-propagation model that describes the normal impedance using the Delany & Bazley [3] model,

and using effective flow resistivities ranging from 2–20000 c.g.s. Rayls/cm. Source height, receiver height, source-receiver separation, and frequency can be varied when studying the EA of a ground surface. The following full-scale geometry was used: source height = 0.5 m; receiver height = 1.8 m; and horizontal distance = 30 m. Free-field reference levels were calculated from the inferred sound-power levels using the measured atmospheric conditions and distances, using Eq. (5.1) on page 79. Scale-model materials were evaluated by measuring the material's EA at scale-factors of 1:20, 25, 31.5, 40, and 50. Theoretical predictions were made of the EA for a given scale factor and flow resistivity for comparison to the measured of a material at each scale factor. An array of EAs for each combination of scale-factor and effective flow resistivity was generated for each test material, and the residuals between the measured and theoretical curves were calculated for each cell of the array using Eq. 3.24 on page 60. Scale-model materials will have different surface impedances at each frequency, so the scale factor selected will vary the range of scale-model frequencies to be compared with full-scale frequencies. When conducting tests over candidate scale-model materials the objective is to select materials for which the effective flow resistivities match that of the full-scale material. For scale-model materials, acoustically hard materials include aluminum, acrylic, vinyl, polystyrene, and painted boards. Acoustically soft materials include tissue paper, cloth, felt, and tissue on expanded polystyrene.

For each of five scale factors and nine test materials, three tests were performed to assess the reproducibility of the measured EAs . The raw data were examined in their narrow-band form to see if their standard deviations were excessive for any one of the scale factors examined. The standard deviations of the measurements of EA for these forty-five combinations of scale factor and test material are seen in Table 5.1. The errors were calculated using the range of frequencies subsequently used for the scale-modelling of noise barriers (see Table 5.2 on page 115). In some cases, it was decided that a measurement would be discarded when it was seen to differ significantly from the others, in terms of its sound-pressure levels and/or shifts in the location of minima. The mean values and standard deviations were then calculated using the remaining measurement pair for that material and scale factor. The source data were

Table 5.1: Average standard deviations based on three and (best two of three) tests of EA for each scale factor and test material.

	$n = 20$	$n = 25$	$n = 31.5$	$n = 40$	$n = 50$	Avg - All n
Aluminum	1.6(1.3)	2.3(1.9)	2.0(1.1)	1.8(1.4)	1.3	1.8(1.4)
Cloth-Single Layer	0.8	1.0	0.7	0.5	2.1(1.5)	1.2(1.0)
Cloth-Double Layer	1.2	1.1	0.7	0.7	0.6	0.9
Felt	0.3	0.6	2.5(1.7)	1.4	0.9	1.4(1.1)
Celfort 200/300	1.1	1.1	1.1	1.1	0.9	1.0
Dense Polystyrene	0.6	1.0	1.1	0.6	0.7	0.8
Masonite Panel - Rough	1.0	0.9	0.8	1.6(1.2)	1.8(1.0)	1.3(1.0)
Masonite Panel - Smooth	1.1	1.0	0.7	0.8	0.7	0.9
Varnished Particle Board	1.2	0.8	1.2	2.0(1.0)	1.3	1.3(1.1)
Average - All Materials	1.0(1.0)	1.2(1.1)	1.3(1.0)	1.3(1.0)	1.2(1.0)	1.2(1.0)

re-examined in an effort to reduce the error by discarding a data set from the nine worst of the forty-five average standard deviations. These points lie above the threshold of 1.5 dB that is arbitrarily $\sqrt{1.5}$ times higher than the mean standard deviation from all forty-five tests. It should also be noted that four of these nine poor results were measured over the Aluminum sheet. The marginal values in Table 5.1 are based on a further averaging of the values across either all scale factors (in the last column), or across all materials (in the bottom row). The average standard deviation for all materials and scale factors was 1.0 dB (bottom right corner). The average value of the remaining measurements of EA was used for the curve-fitting process.

5.6.2 Effective Flow Resistivity of Scale-Model Materials

For each material a figure is presented in which the residuals are plotted against scale factor and flow resistivity. *A priori*, it was believed that such a surface would display one of two trends: a progressive increase in the magnitude of the residuals would be seen as scale factors increased; or a minimum would exist somewhere on the least-squares surface. Both trends were observed among the materials tested: acoustically soft materials always had a distinctive minimum; acoustically harder materials generally lacked a distinct minimum. This is thought

to be due to the shifting of the interference minima of a material's *EAs* to frequencies that were beyond those tested, thus making it impossible to take advantage of this feature when generating least-squares residuals. To calculate least-squares residuals for the predicted flow resistivities, it was necessary to iterate the process of generating a theoretical *EA* curve for each individual measurement of *EA*. In this way a relationship was found between the magnitude of errors in measurements of the *EA* and the inferred values of effective flow resistivity. For each of the nine materials, a 2-D array of residuals is shown, along with associated plots of *EA*. Ideally these plots of *EA* at different scale factors would display destructive-interference minima at the same full-scale frequency — this was not always the case.

Aluminum

Fig. 5.19 shows the *STD* of flow resistivity and scale factor for aluminum sheet. As indicated, the best fit between measurement and theory was observed at $n = 50$, where an effective flow resistivity of approximately 100 c.g.s. Rayls/cm gave a standard deviation of 1.6 dB. At a 1:31.5 scale, the best fit was at 400 c.g.s. Rayls/cm with a 2.0 dB *STD*. Between these two points a trough exists, where the material's effective flow resistivity decreases with increasing scale factor. Fig. 5.20 shows, on the left-hand side, the best-fit predicted and measured *EAs*, based on the least-squares differences. The grid lines of frequency correspond to third-octave centre frequencies. On the right-hand side, predicted and measured *EAs* are shown for a scale factor of $n = 31.5$, based on the least-squares differences. Surprisingly, the plotted *EA* results differ in that the curves do not display a minimum near the same frequency. This material appears to be surprisingly soft — given that it is a metal sheet. For simulating asphalt — at 20000 c.g.s. Rayls/cm — if one moves upwards in scale factor, a best-fit is reached between $n = 40$ and $n = 50$.

Cloth (One Layer)

Fig. 5.21 shows the variation of standard deviation with flow resistivity and n for a single layer of linen. A minimum value of 1.8 dB occurs in the region enclosing the best-fit point of $n = 40$ and 15 c.g.s. Rayls/cm. This region is fairly small — a characteristic of materials whose measured EAs display a distinct minimum in the EA spectra. The trough suggests that the material appears to get softer with increasing scale factor. Fig. 5.22 plots the overall best-fit EA curve and the best-fit curve for 1:31.5 scale for a single cloth layer. These EA curves are similar to one another, with the effective flow resistivity for the overall best-fit curve (15 c.g.s. Rayls/cm) being slightly less than the $n = 31.5$ value of 20 c.g.s. Rayls/cm.

Cloth (Two Layers)

Fig. 5.23 shows the variation of standard deviation with flow resistivity and n for two layers of the linen. The material appears to get softer with increasing scale factor, and there is no region with an STD better than 2 dB. The 3 dB contour line is separated into two regions with $STDs$ better than 3 dB. Fig. 5.24 plots the overall best-fit EA curve and the 1:31.5 scale best fit of flow resistivity for two layers of cloth. As expected, the second layer of cloth made the material acoustically softer than the single cloth layer. The overall best-fit is 2 c.g.s. Rayls/cm, slightly softer than the $n = 31.5$ value of 5 c.g.s. Rayls/cm. The frequency location of the minimum EA shifts slightly higher for the $n = 31.5$ test.

Felt

Fig. 5.25 shows the least-squares surface for a layer of felt. An STD contour of 2 dB can be seen in the lower left-hand corner. Fig. 5.26 plots out the overall best-fit curve of EA and the best fit for $n = 31.5$ for the layer of felt. The overall best-fit value of effective flow resistivity is 3 c.g.s. Rayls/cm, and the $n = 31.5$ best-fit is 2 c.g.s. Rayls/cm. Although the minima are fairly close to one another, the most-negative value of EA appears at a lower frequency than for the 3 c.g.s. Rayls/cm curve. This material was the acoustically softest material tested. It

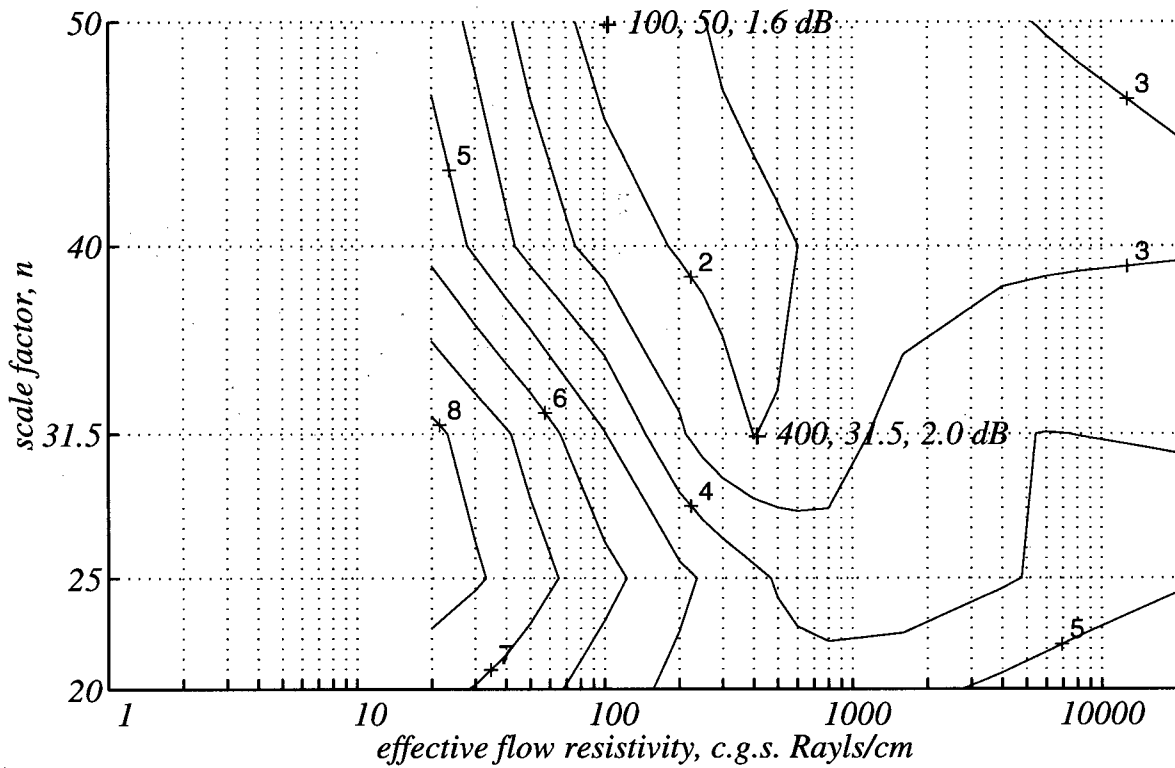


Figure 5.19: Aluminum — array of effective flow resistivity versus scale factor with contours denoting regions where the average standard deviation, over all test frequencies, between best-fit curves and measurements, falls below the labelled value.

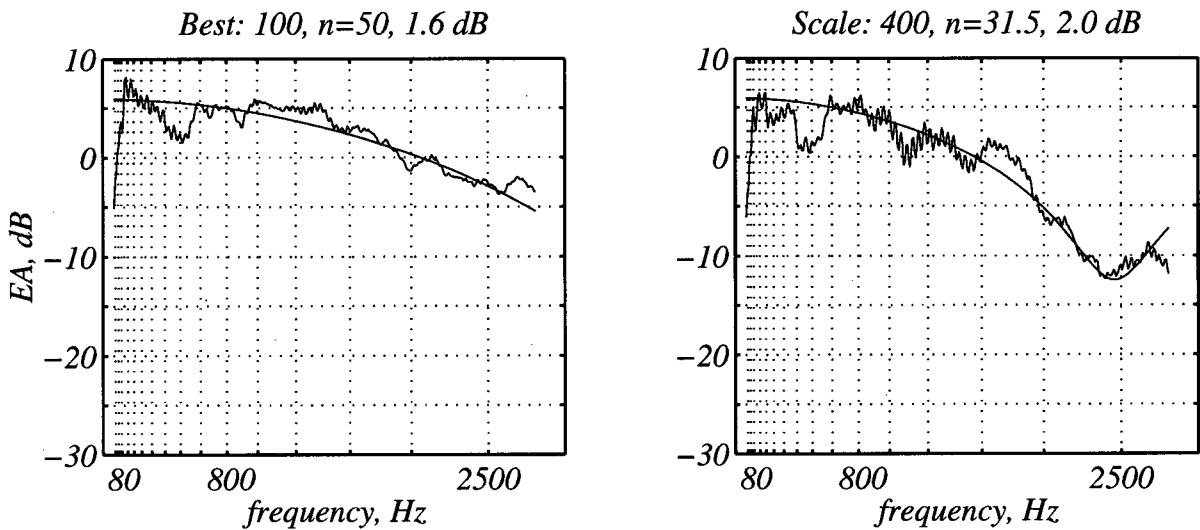


Figure 5.20: Measured EA of aluminum compared to theoretical best-fit curves.

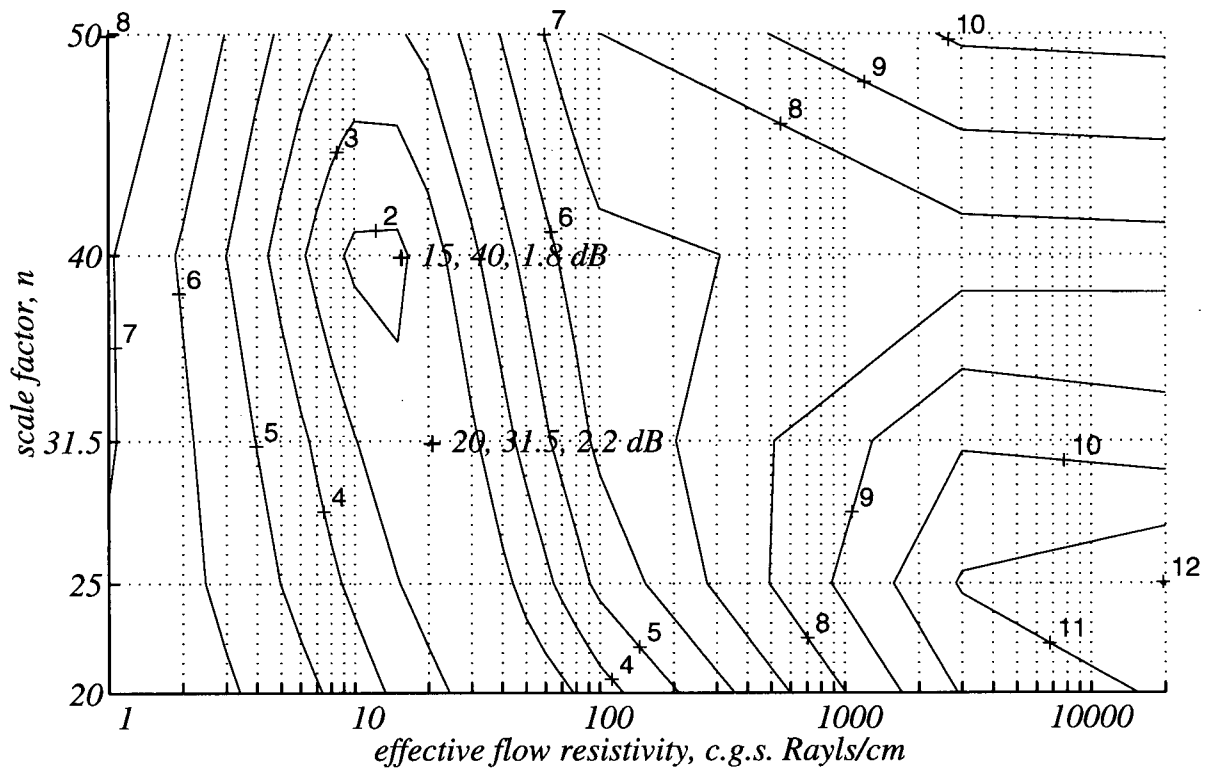


Figure 5.21: Cloth (one layer) — array of effective flow resistivity versus scale factor with contours denoting regions where the average standard deviation, over all test frequencies, between best-fit curves and measurements, falls below the labelled value.

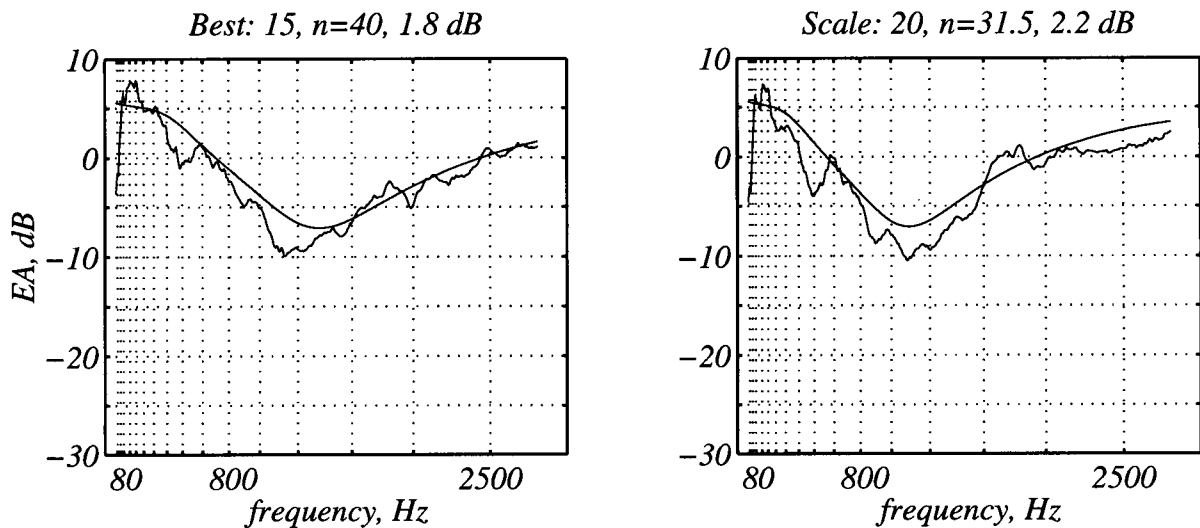


Figure 5.22: Measured EA of cloth (one layer) compared to theoretical best-fit curves.

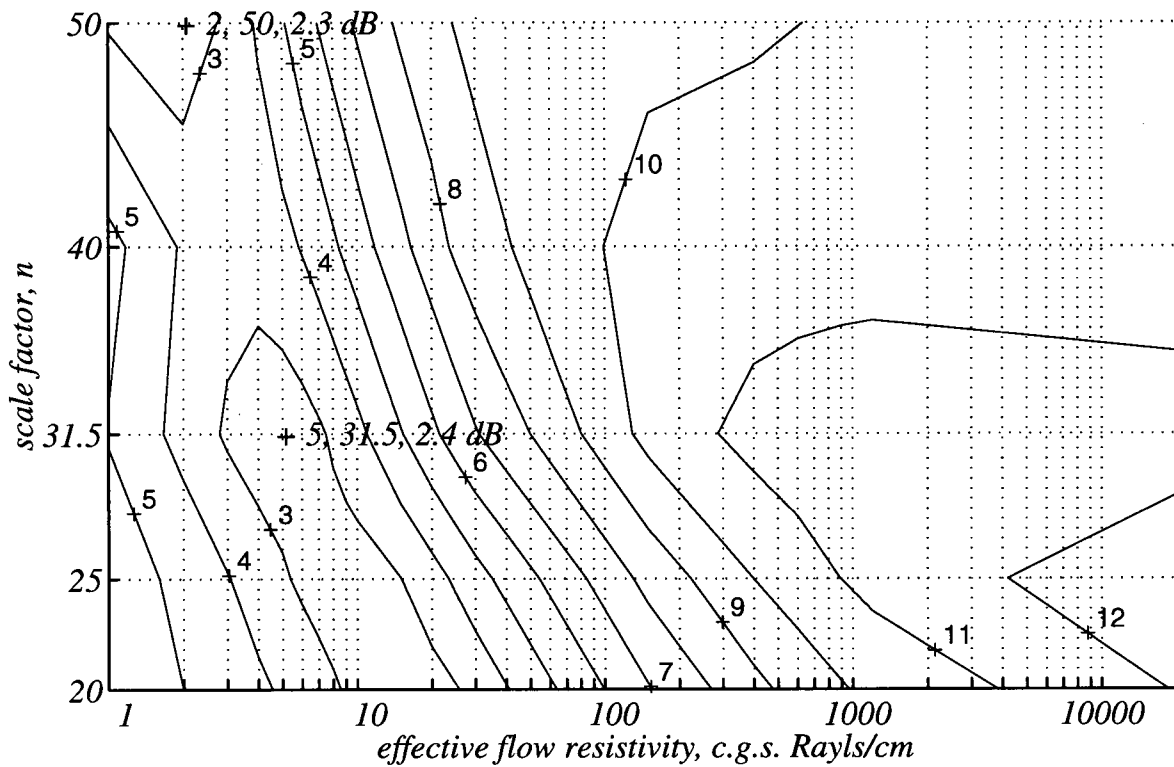


Figure 5.23: Cloth (two layer) — array of effective flow resistivity versus scale factor with contours denoting regions where the average standard deviation, over all test frequencies, between best-fit curves and measurements, falls below the labelled value.

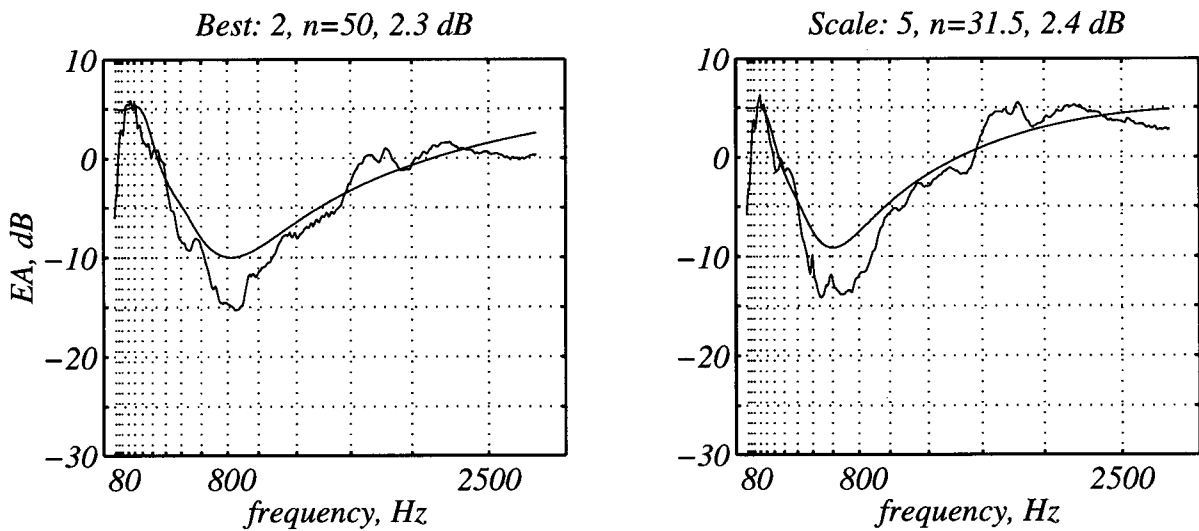


Figure 5.24: Measured EA of cloth (two layers) compared to theoretical best-fit curves.

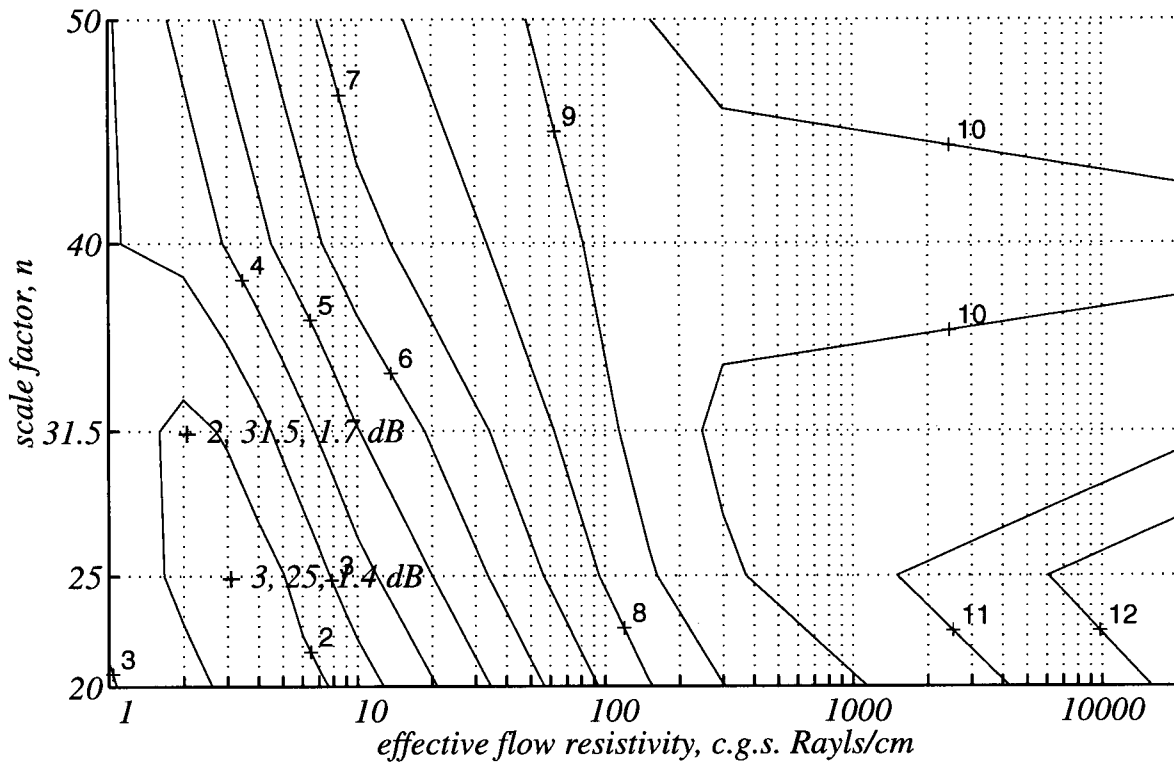


Figure 5.25: Felt — array of effective flow resistivity versus scale factor with contours denoting regions where the average standard deviation, over all test frequencies, between best-fit curves and measurements, falls below the labelled value.

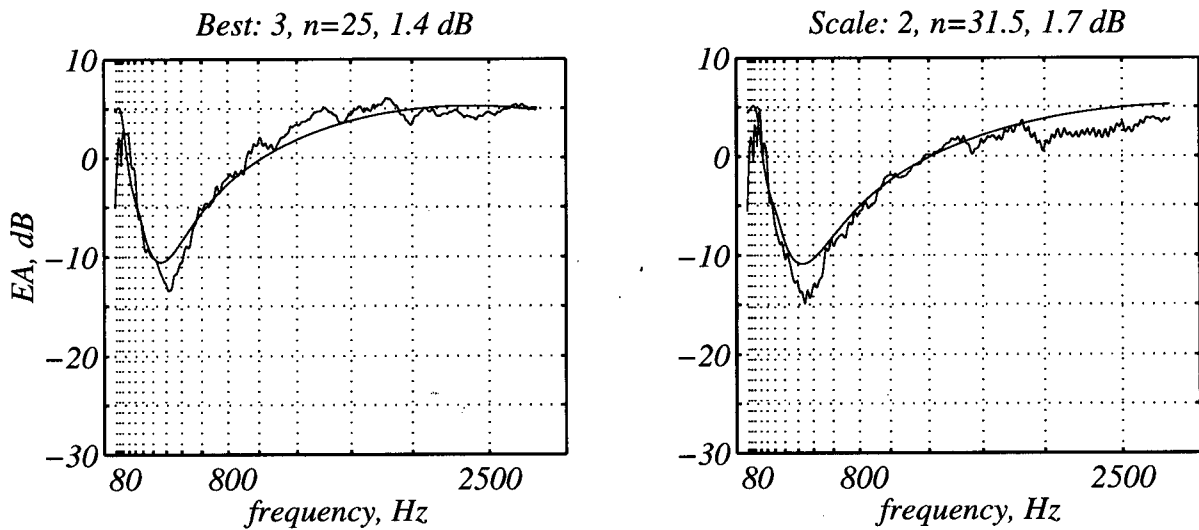


Figure 5.26: Measured *EA* of felt compared to theoretical best-fit curves.

was the only material for which a best-fit EA curve was at a scale factor lower than $n = 31.5$.

Expanded Polystyrene Insulation

Fig. 5.27 shows the variation of standard deviation with flow resistivity and scale factor for expanded polystyrene (Celfort insulation). A long trough is formed by the 2 dB contour, with the material generally becoming softer with increasing scale factor — particularly beyond the $n = 31.5$ scale factor. Fig. 5.28 shows the overall best-fit EA curve (150 c.g.s. Rayls/cm) and the $n = 31.5$ best-fit EA curve (300 c.g.s. Rayls/cm) for the Celfort insulation. The frequency location of the most-negative value of EA is not the same for the two plots of measured and predicted EA . The overall best-fit material in this case is acoustically softer than the 1:31.5 scale case, but the frequency location of the most negative EA actually appears at higher full-scale frequencies.

Dense Polystyrene

Fig. 5.29 shows the variation of standard deviation with σ and n for a sheet of dense polystyrene. The material appears to get softer as scale factor increases, with a broad region enclosed by a 2 dB contour. Within this region the best-fit of 200 c.g.s. Rayls/cm occurs at a 1:50 scale, increasing to 400 c.g.s. Rayls/cm at 1:31.5 scale. Fig. 5.30 shows the overall best-fit EA curve (200 c.g.s. Rayls/cm) and the 1:31.5 scale best-fit EA curve (400 c.g.s. Rayls/cm) for dense polystyrene. The location of the most-negative EA minima is not preserved in the two plots of EA best-fit curves, so the magnitude of the differences is not maintained.

Masonite Panel (Rough Face)

Fig. 5.31 shows the variation of standard deviation with flow resistivity and scale factor for the rough side of masonite panels. A trough is evident with a decrease of flow resistivity with increasing scale factor. Fig. 5.32 shows the overall best-fit curve of EA (5 c.g.s. Rayls/cm) and the 1:31.5 scale best-fit EA curve (15 c.g.s. Rayls/cm) for the rough-sided masonite. The

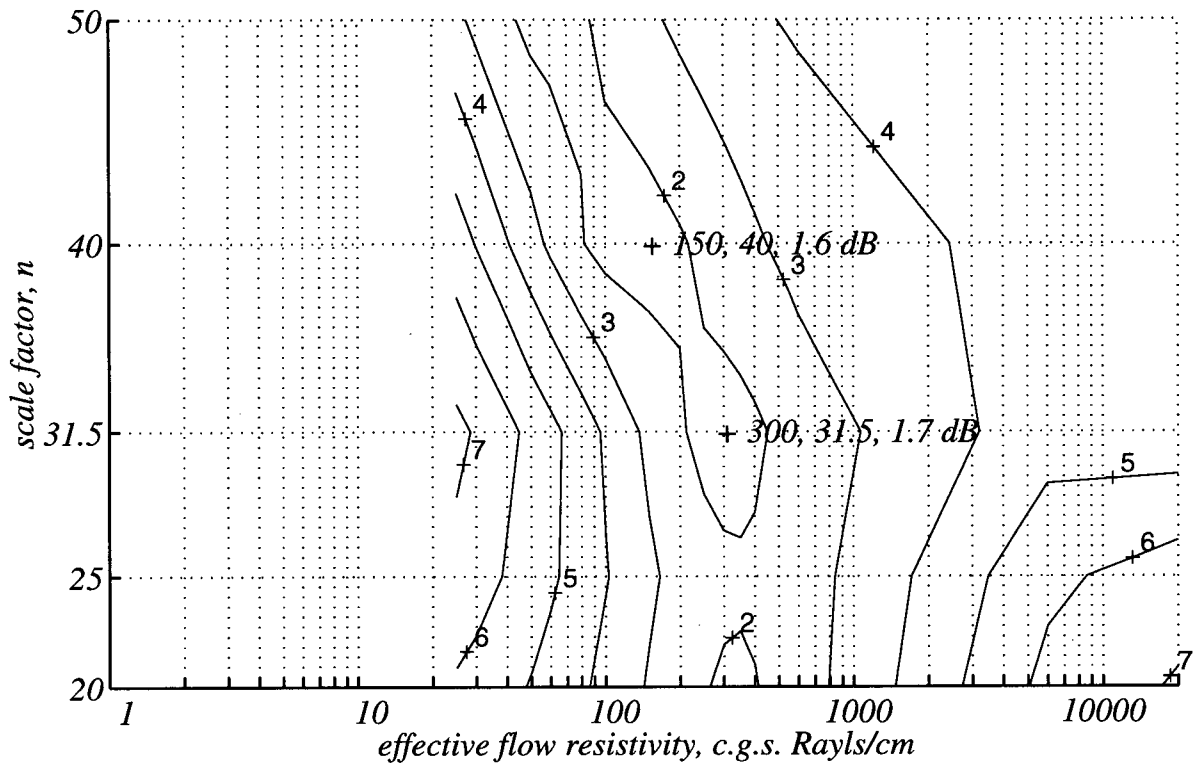


Figure 5.27: Expanded Polystyrene — array of effective flow resistivity versus scale factor with contours denoting regions where the average standard deviation, over all test frequencies, between best-fit curves and measurements, falls below the labelled value.

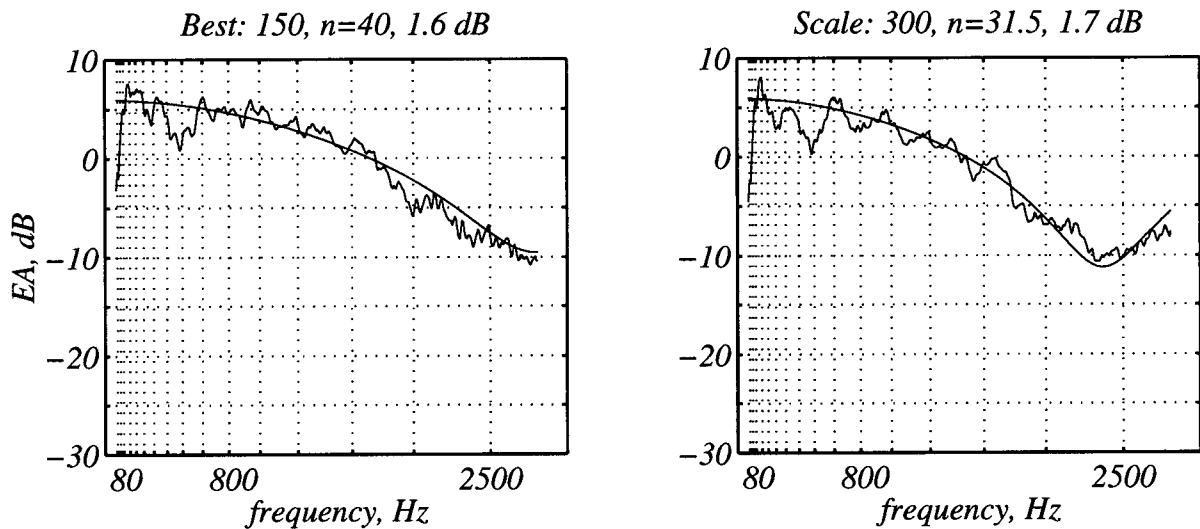


Figure 5.28: Measured EA of expanded polystyrene compared to theoretical best-fit curves.

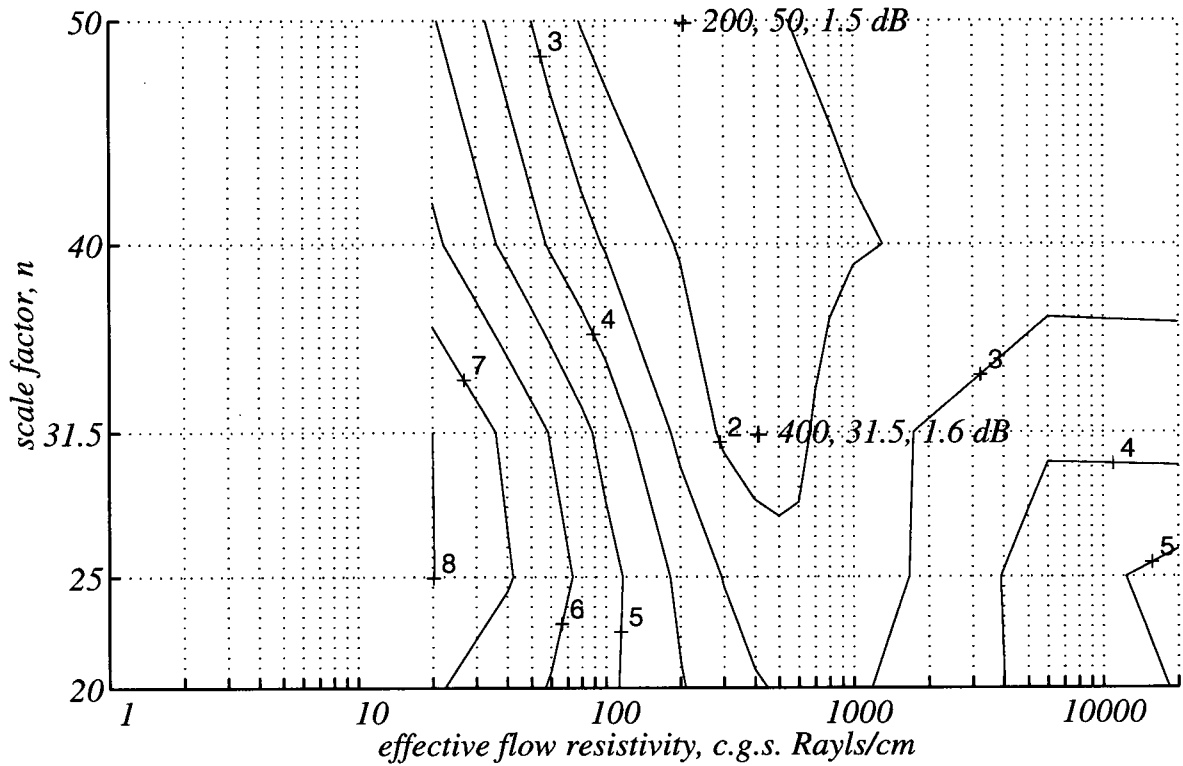


Figure 5.29: Dense Polystyrene — array of effective flow resistivity versus scale factor with contours denoting regions where the average standard deviation, over all test frequencies, between best-fit curves and measurements, falls below the labelled value.

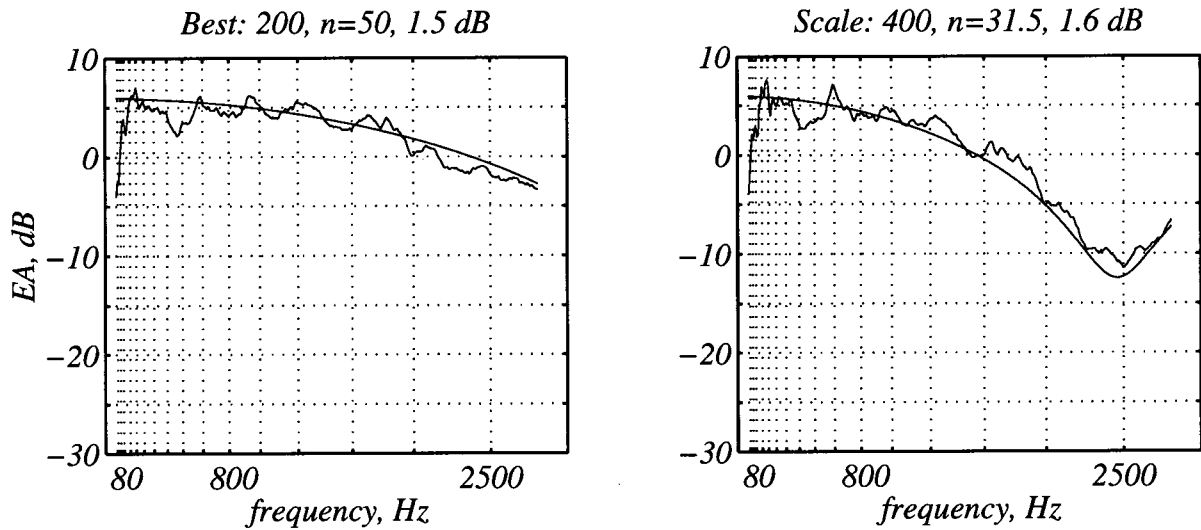


Figure 5.30: Measured *EA* of dense polystyrene compared to theoretical best-fit curves.

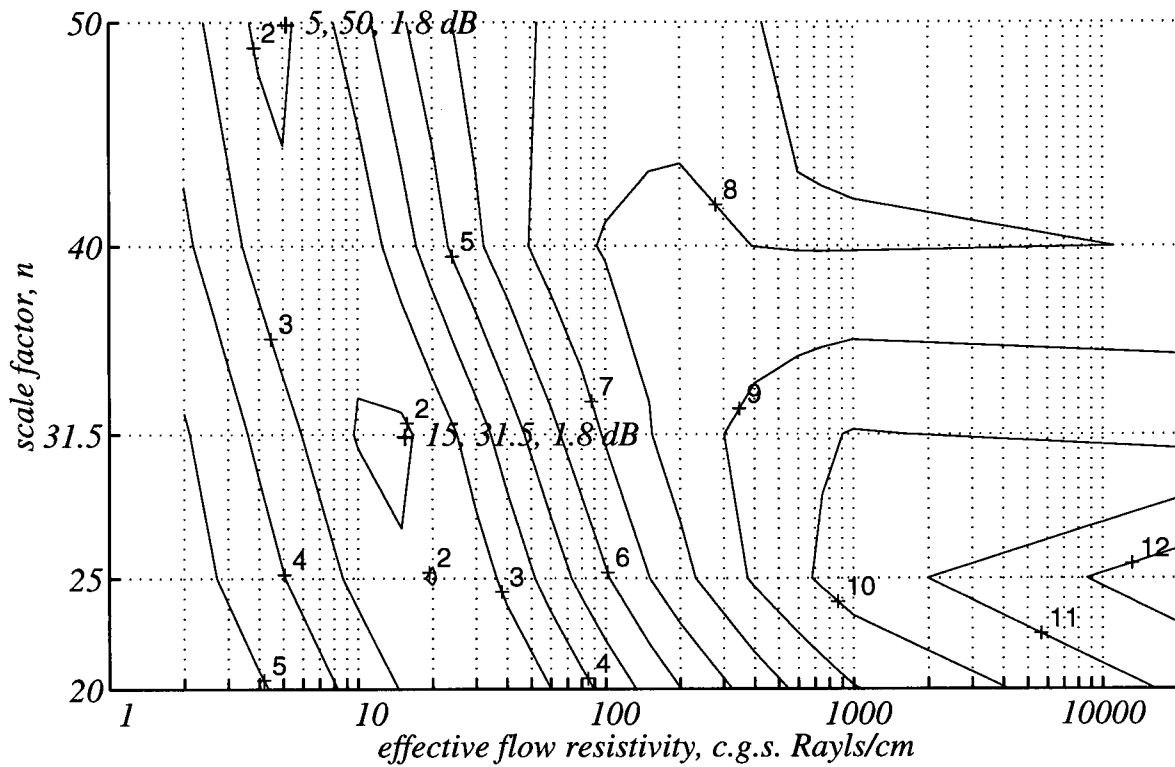


Figure 5.31: Rough Masonite — array of effective flow resistivity versus scale factor with contours denoting regions where the average standard deviation, over all test frequencies, between best-fit curves and measurements, falls below the labelled value.

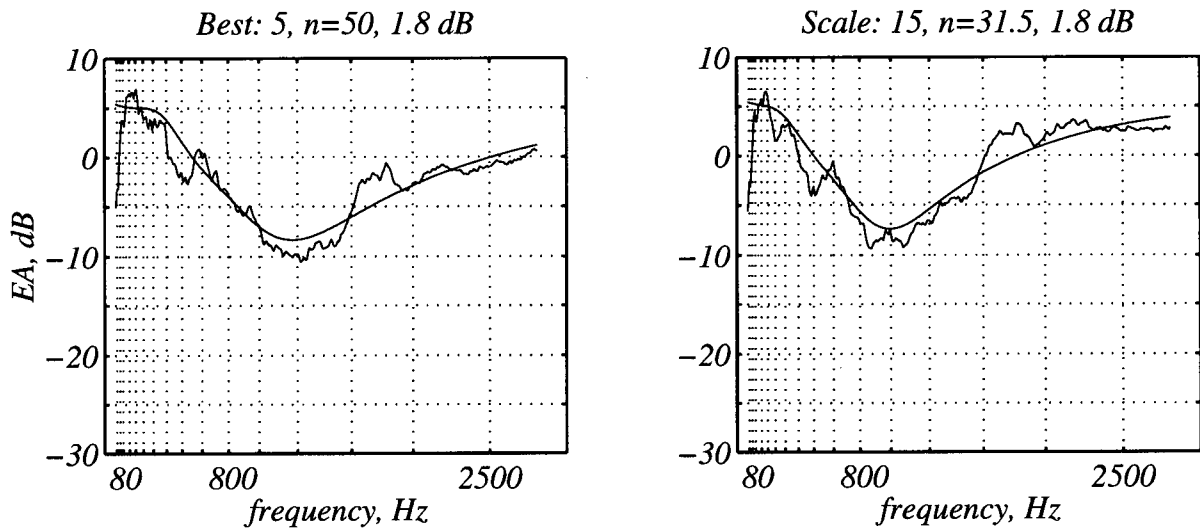


Figure 5.32: Measured EA of rough masonite compared to theoretical best-fit curves.

most-negative EA appears at a frequency of approximately 1250 Hz for the overall best-fit plot at a 1:50 scale; while the $n = 31.5$ plot of best-fit EA displays a minimum at approximately 1000 Hz.

Masonite Panel (Smooth Face)

Fig. 5.33 shows the variation of standard deviation with scale factor and flow resistivity for the smooth side of masonite panels. Contours of 2 dB can be seen at scale factors of $n = 40$ and $n = 50$. Fig. 5.34 shows the overall best-fit EA curve (250 c.g.s. Rayls/cm) and the 1:31.5 scale best-fit EA curve (300 c.g.s. Rayls/cm) for smooth-sided masonite. The minima of the two EA curves are not at the same frequency. The 1:31.5 scale best-fit EA curve isn't really satisfactory since the locations of the minima of the measurement and prediction are noticeably displaced from one another.

Varnished Particle Board

Fig. 5.35 shows the variation of standard deviation with σ and n for varnished particle board. A 2 dB contour is seen at 1:50 scale, for which the material's best-fit EA curve has an effective flow resistivity of 100 c.g.s. Rayls/cm. Fig. 5.36 shows the best-fit EA curve (100 c.g.s. Rayls/cm) and the 1:31.5 scale best-fit EA curve (20000 c.g.s. Rayls/cm) for varnished particle board. The EA plots are similar in that neither displays a distinct negative value of EA — unlike the other candidate asphalt materials — aluminum, dense polystyrene and smooth masonite. For the $n = 31.5$ case, there is an obvious discrepancy due to the large negative values of the predicted EA curve; an EA curve based on a flow resistivity of 600 c.g.s. Rayls/cm might be more realistic.

Comments on the Measured Excess Attenuation Curves

All of the plots of best-fit EA curves and measurements contain some irregularities in the measurement data. First, below about 250 Hz the measured EA always decreases to negative

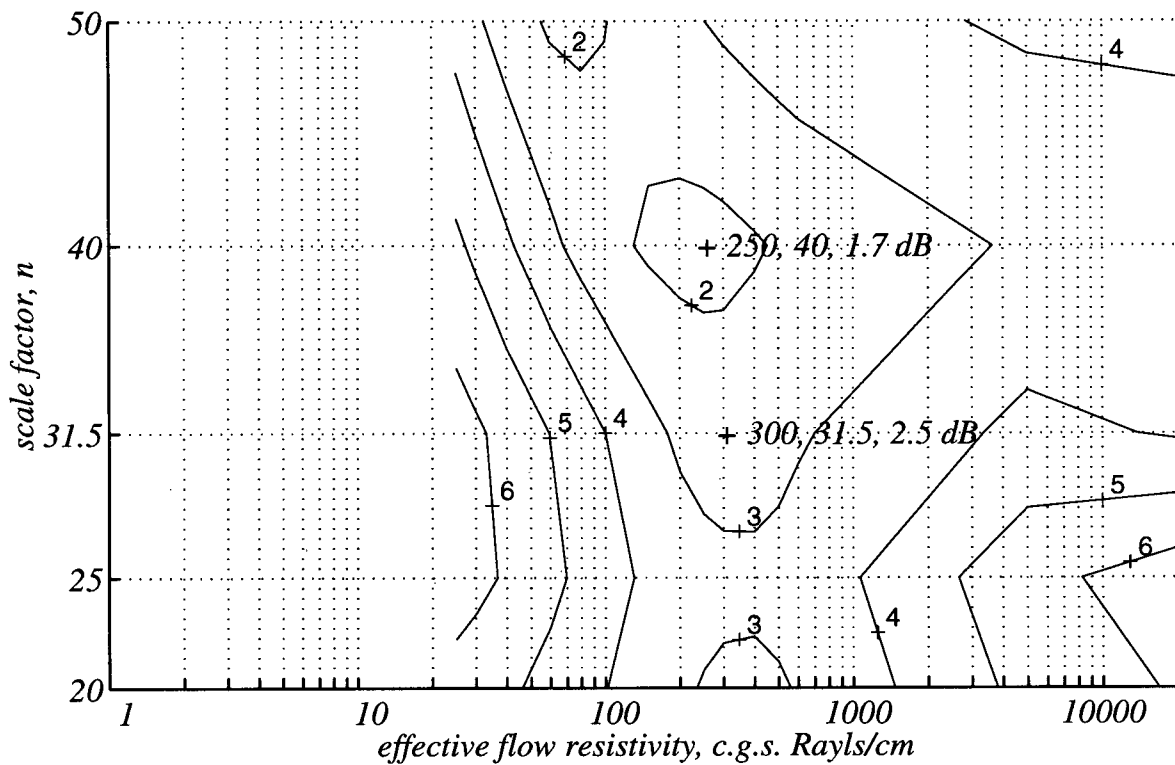


Figure 5.33: Smooth Masonite — array of effective flow resistivity versus scale factor with contours denoting regions where the average standard deviation, over all test frequencies, between best-fit curves and measurements, falls below the labelled value.

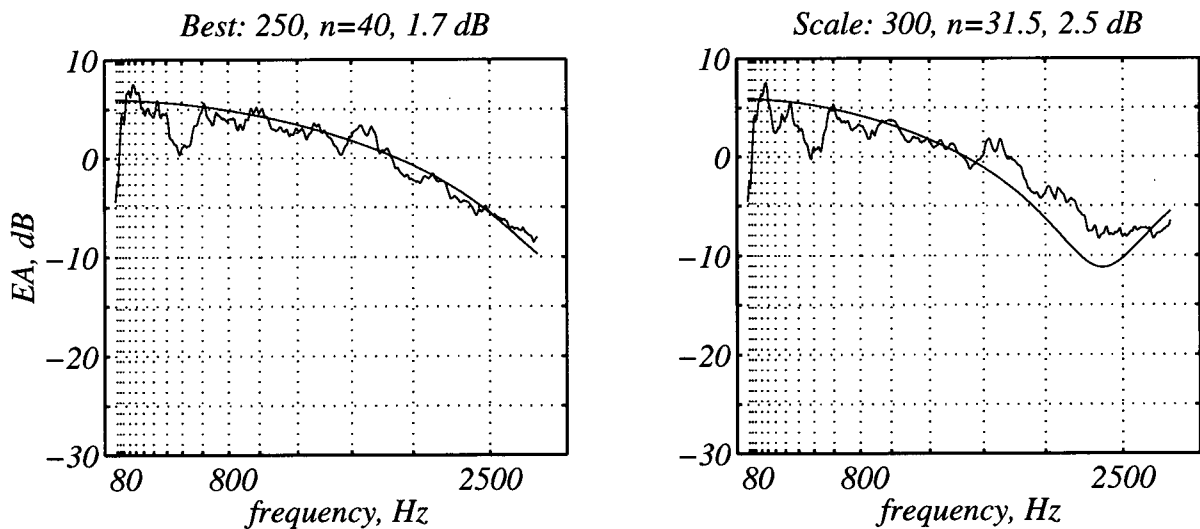


Figure 5.34: Measured EA of smooth masonite compared to theoretical best-fit curves.

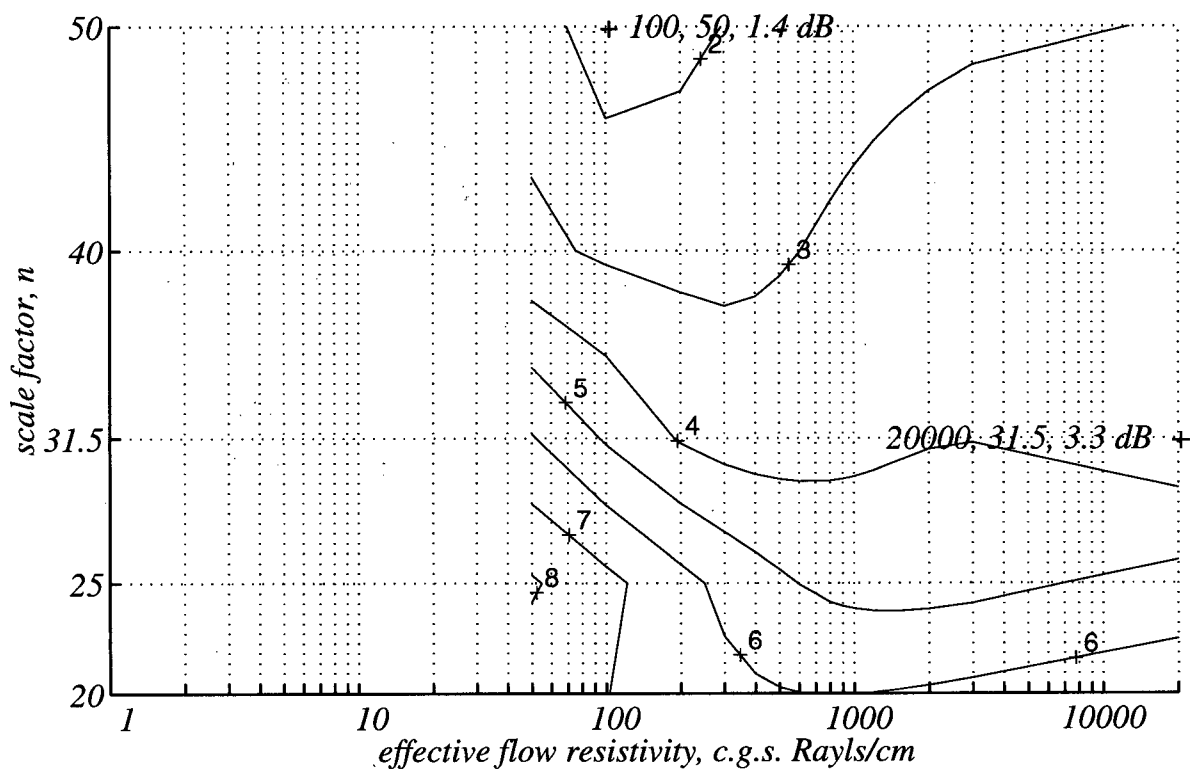


Figure 5.35: Varnished Particle Board — array of effective flow resistivity versus scale factor with contours denoting regions where the average standard deviation, over all test frequencies, between best-fit curves and measurements, falls below the labelled value.

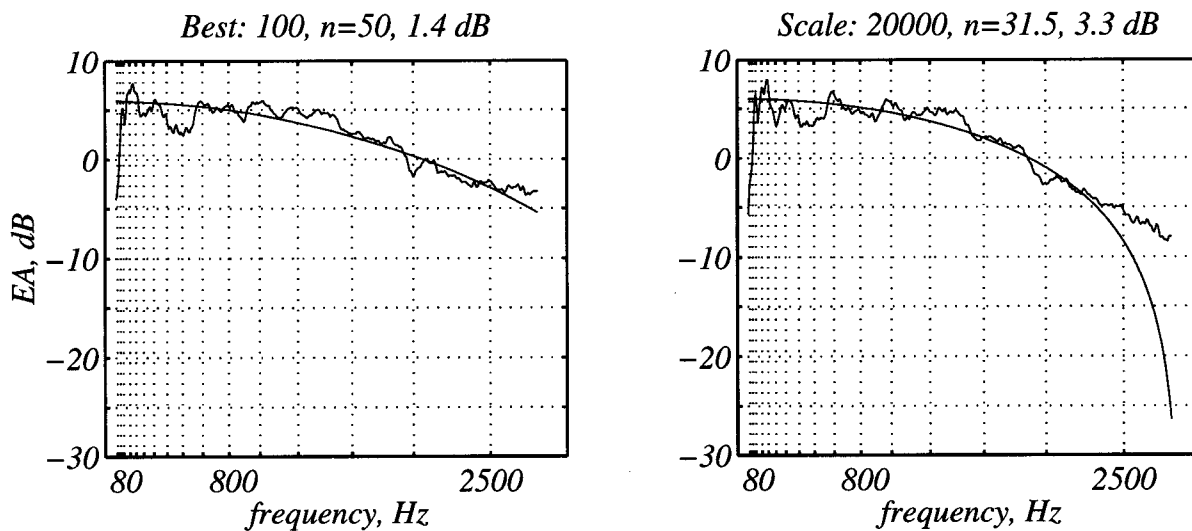


Figure 5.36: Measured EA of varnished particle board compared to theoretical best-fit curves.

values. Second, in the vicinity of 630 Hz the measured EA typically drops to 0 dB, or even lower. Both of these discrepancies could be due to source directivity, since the free-field sound-pressure levels were calculated and then predicted from average values of source power.

How do the overall best-fit EA curves compare to the best-fit EA curve at 1:31.5 scale? When the overall best-fit EA curve is at a higher than 1:31.5 scale (1:40 or 50), the frequency-location of the most-negative predicted EA shifts to higher frequencies. In the one case (felt) for which the overall best-fit EA curve is at a lower than 1:31.5 scale (1:25), the frequency location of the most-negative predicted EA shifts to a lower frequency. Acoustically softer materials tended to exhibit a distinct minimum value of EA in their accompanying plots of best-fit EA . Acoustically-harder materials often exhibited a distinct minimum for only the 1:31.5 scale plot of best-fit EA , with the accompanying plot at 1:40 or 50 scale lacking such a distinct minimum. The absence of a distinct trough in the EA inhibits the ability of the approach to differentiate between materials, particularly for acoustically harder materials. It also reinforces the fact that there are acoustically significant phenomena that do not scale linearly with frequency. The relative magnitude of errors due to surface roughness or the location of the source's acoustic centre will increase as scale factor increases.

5.6.3 Selecting Scale-Model Materials

Considering an effective flow resistivity of 20000 c.g.s. Rayls/cm to be the benchmark for asphalt, no material was found to be suitable. The most suitable materials all seemed to have been detrimentally affected by the acoustic boundary layer. For previous discussion refer to Sections 2.4 (on page 41) and 3.2 (on page 54). Candidates to simulate acoustically-hard materials such as asphalt include: aluminum at a scale factor of $n = 40$ with an STD less than 3 dB; dense polystyrene ($n = 40, 50; < 3$ dB); smooth masonite ($n = 40; < 4$ dB); and varnished particle board ($n = 31.5, 40, 50; < 4$ dB).

Considering an effective flow resistivity of 300 c.g.s. Rayls/cm to be the benchmark for grass, several materials might be adequate. Candidates for acoustically soft materials, such as

grass, include aluminum ($n = 40$; < 2 dB), expanded polystyrene ($n = 20, 31.5$; < 2 dB), dense polystyrene ($n = 31.5, 40, 50$; < 2 dB), smooth masonite ($n = 40$; < 2 dB) and varnished particle board ($n = 50$; < 3 dB). Note that expanded polystyrene is the only material which did not appear in the first list of acoustically hard materials. It is not reasonable to assume that the other four materials were equally good representations of both asphalt and grass. Examining the expanded polystyrene results more closely, it would appear that, at $n = 31.5$, the material shows a very good correlation with the predicted curve for grass. The curve for smooth masonite suggests that the material might be suitable for simulating materials with effective flow resistivities below 300 c.g.s. Rayls/cm. At $n = 31.5$, the varnished particle board does not display a distinct minimum in its best-fit EA curve, which results in its similar curve fit for a wide range of flow resistivities below approximately 2000 Hz — up to and including an effective flow resistivity of 20000 c.g.s. Rayls/cm. Varnished particle board is thus the most suitable choice for asphalt. For simulating scale-model obstacles such as walls and/or structures, varnished particle board would be difficult to work with. Comparing dense polystyrene to aluminum at $n = 31.5$, both have best fits of 400 c.g.s. Rayls/cm, but the dense polystyrene is a less expensive and more workable choice for thin walls or perhaps even to represent gravel surfaces (600 c.g.s. Rayls/cm).

Four of the materials were not considered for either asphalt, walls, gravel, or grass. The cloth of one or two layers, felt, and rough masonite were too acoustically soft to represent any of these full-scale surfaces. At a scale factor of 1:31.5 the felt was the most acoustically soft, with 2 c.g.s. Rayls/cm; it was also the most suitable for laying over other surfaces to simulate an unnaturally soft ground material.

Based on these predictions an optimal scale of 1:31.5 was selected, in conjunction with the selection of three model materials to simulate earth berms and soft ground (150–300 c.g.s. Rayls/cm), and vertical walls or roadways (20000 c.g.s. Rayls/cm). These materials represented the optimal choices based on the best-fit results, and the associated objective of choosing three distinct materials. Roadways were simulated using varnished particle board, walls using dense

polystyrene, and both earth berms and soft ground were simulated using expanded polystyrene. The impedance of berm surfaces was made harder or softer using dense polystyrene and felt, respectively. The scale-model material with the best correspondance to full-scale was the expanded polystyrene material — at 1:31.5 scale it has an effective flow resistivity very close to 300 c.g.s. Rayls/cm. Other scale-model materials were less-optimal representatives of their full-scale counterparts, with the expanded polystyrene being a closer representative of grass and earth berms than harder surfaces were of concrete walls or asphalt. This is thought to be due to the ABL (see Almgren [125, 134]) which exists at the surface of a material; it absorbs sound energy incident on any scale-model surface, making it appear to be softer than expected. An ABL makes it impossible at ultrasonic frequencies to obtain a material which is acoustically hard enough to act as a scale-model asphalt. This effect becomes progressively worse with increasing frequency, so there is an upper limit on scale factors beyond which no material, no matter how dense or rigid, can reproduce the impedances seen for common outdoor ground surfaces like asphalt and concrete. For this reason, even though the hard-surface analogues were not optimal, they at least differ from one another, in terms of their surface impedances. It would be useful to measure the broadband EA over a set of distances and perform a broadband least-squares minimization at all receiver distances simultaneously. The EA of the scale-model materials, as represented by the effective flow resistivity, would be even more accurately revealed by this approach.

5.7 Insertion-Loss Experiments

A 1:31.5 scale-model highway was designed and constructed to study the noise attenuation of a barrier. Earth berms and soft ground were modelled by expanded polystyrene, walls by dense polystyrene, and roadways by varnished particle board. Hot-wiring equipment was used to cut the scale-model barriers to the desired slope. An extensive number of berm sections were cut from the expanded-polystyrene sheets to allow for subsequent assembly into a barrier of sufficient length.

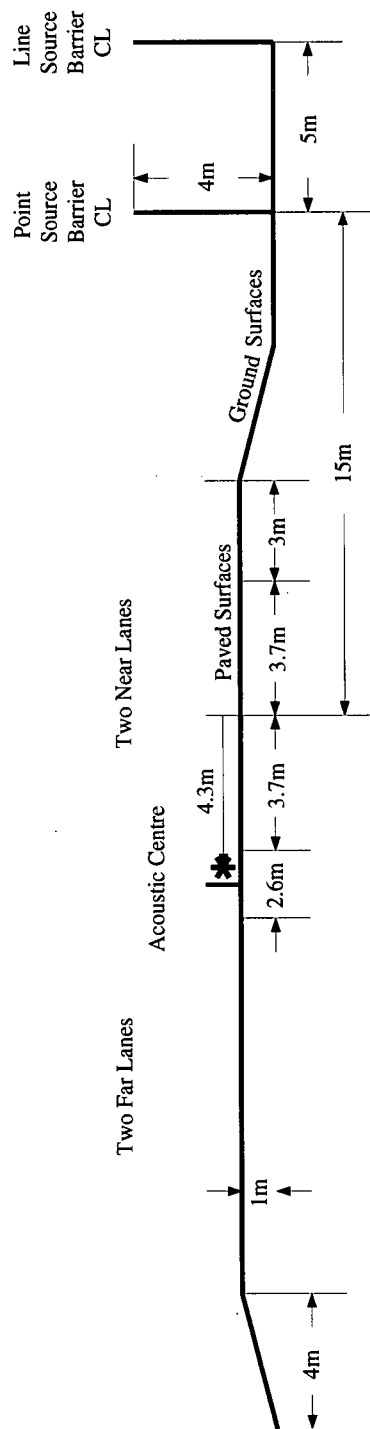


Figure 5.37: Profile view of the highway configuration.

The *IL* results are grouped into two major test classes — fixed source/receiver line perpendicular to the barrier, and fixed receiver position with the source traversed along a fixed line parallel to the barrier. The distances to the barrier crest, and from the crest to the receiver, were varied depending on the barrier class being tested. Barrier configurations were selected in order to study the effects of changes in barrier profile and surface impedance. As seen in Fig. 5.37, the scale-model highway configuration modelled a four-lane divided highway. The dimensions of the roadway were as follows: highway elevation 1 m, median width 2.6 m, lane widths 3.7 m, shoulder width 3 m, and a 4:1 sloped shoulder. The acoustic centre of the noise from the highway was calculated as the geometric mean of the distance to the lane centres from the point-source-test barrier centreline — effectively 4.3 m from the centreline of the two near lanes. It was assumed that the effective source height was 0.5 m; the receiver height was 1.8 m. Barriers were constructed to a 4 m height, which equates to 3 m above the surface of the elevated highway.

5.7.1 Point-Source Insertion-Loss Tests

For the first class of tests the source and receiver were positioned along a line perpendicular to the barrier, as seen in Fig. 5.38. Two barrier profiles were used: a wall of 10 cm thickness, and a 2:1 sloped grass berm; the barrier's crest position was always the same, with the line separating the two near lanes being 15 m from the barrier crest. Relative to the barrier centreline, the source distances were 8.3, 14.9 and 19.3 m, and the receiver distances were 5, 10, 15, 20, 25, 30 and 40 m. Tests were conducted as far from the ends of the berms as possible; in Fig. 5.39 this position is the (S8-R8) source/receiver line. The variations of total dB or dBA with source and receiver distance were studied to see how shifts in the position of the source and/or receiver affect the total *IL* and total *ILA*.

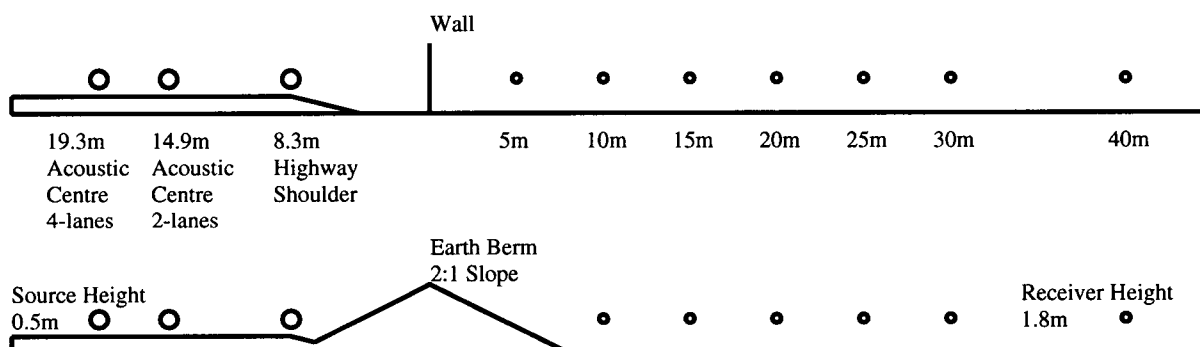


Figure 5.38: Profile view of the point-source test configurations.

5.7.2 Line-Source Insertion-Loss Tests

For the second class of tests, the receiver was kept in one position while the source was traversed along a series of points. Fig. 5.39 is a plan view of the roadway, barrier and source positions. The dividing line between the two near lanes of traffic was chosen to be 20 m from the barrier crest, so there would be sufficient space for the shallow 3:1 berms. The acoustic centre was 4.3 m beyond this, giving a total source-to-crest distance of 24.3 m. The microphone was located at a 15 m distance beyond the berm crest — a representative distance from a noise barrier for a receiver at full scale. The source and receiver rows consisted of points spaced 7.88 m apart — a linear spacing appropriate for closely-spaced vehicles travelling along a highway at a constant speed. Assuming the noise between vehicles is incoherent, the measurements along the series of points can be integrated together to simulate an incoherent line source.

The minimum distance from the barrier ends was identified by making sound-pressure-level measurements, with a barrier in place, at all perpendicular source/receiver positions (S1-R1, ..., S15-R15), and examining the results to see at what positions diffraction around the barrier ends became problematic. Pirinchievara [77] reported that a barrier needs to be four to six times longer than its height for it effectively to be infinite in length. Diffraction around the ends of the scale-model barriers had a fairly small, but measurable effect on the *ILs* measured when the source and/or receiver were too close to the ends.

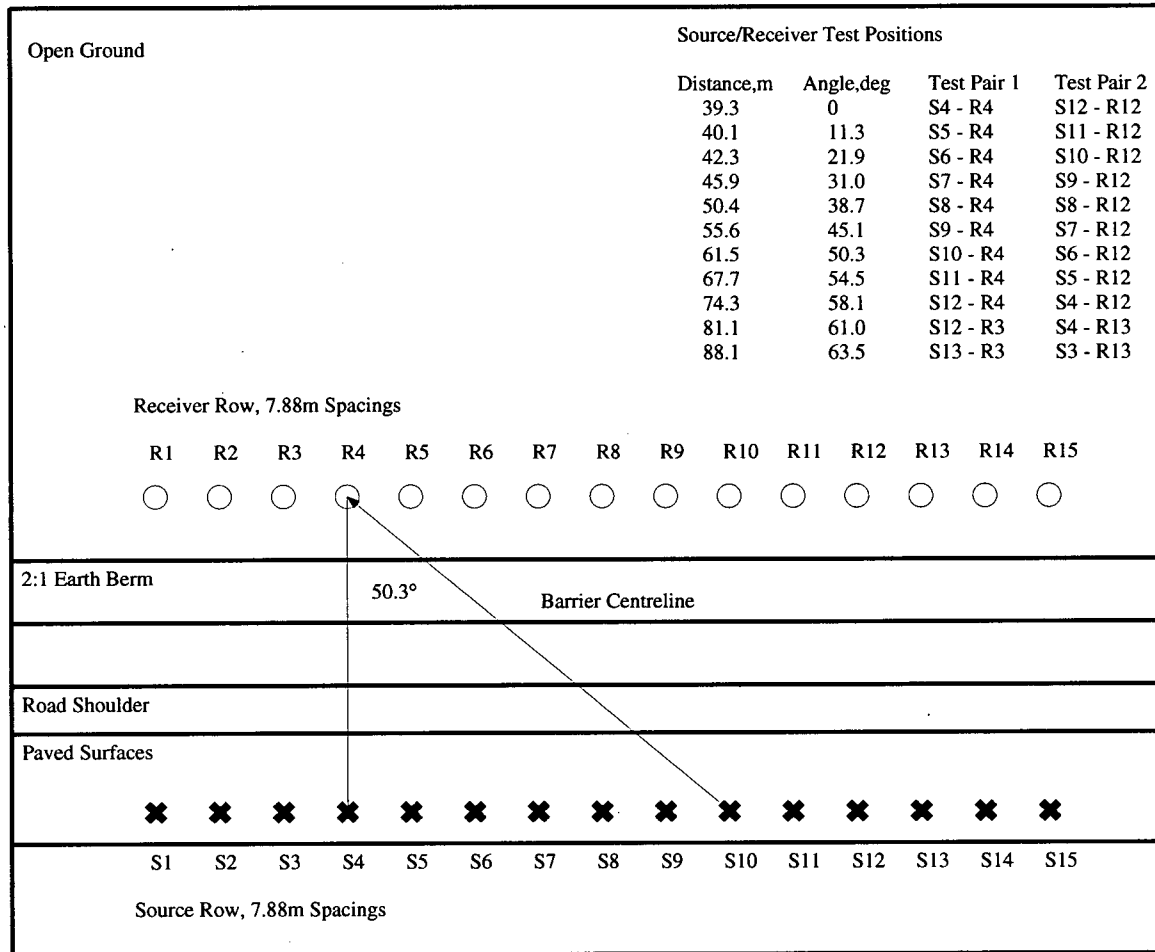


Figure 5.39: Plan view of the line-source test configuration.

The sound-pressure levels at eleven positions were measured along a scale-model highway, with and without a noise barrier, then the entire process was repeated by using an equivalent set of points but with the source traversed in the opposite direction.

Being a physical model, with (ideally) small amounts of turbulence along the sound paths, the pressure signal for a given source/receiver location resulted from coherently interfering sound waves. The average and standard deviations were calculated for each equivalent source/receiver location (e.g. S9-R4 and S7-R12), for both the with-barrier and without-barrier measurements. The resulting average sound-pressure levels were used to reconstruct the sound-pressure levels

for a source length equivalent to twenty-one such source/receiver positions which, when viewed from the receiver position, spanned a 127° angle of highway. This coverage was considered sufficient to generate stable line-source sound-pressure levels for both the open-ground and with-barrier tests. Tests of barriers using a line source were repeated using both grass and non-grass surface impedances for a berm — scale-model berms were constructed of expanded polystyrene to simulate grass surfaces, dense polystyrene to simulate gravel, and felt to simulate unusually soft ground.

The ability to use point-source measurements to generate line-source IL is a highly-important consideration. For vehicles on a highway, it is important to consider to what degree the sound waves from a single vehicle interact coherently, for sound paths that are direct, reflected and/or diffracted; here it is assumed that, from a single vehicle, sound waves interact coherently. If it is assumed that the integration represents a single vehicle passby, at a constant speed and with constant noise radiation, the results could be integrated together in terms of energy (rms pressure squared) to produce an energy sum or an average. Changing from a sum to an average simply requires subtracting $10 \log_{10} N$ (N being the number of test positions) from the integrated result. This would be true for both the open ground and noise barrier configurations, so if IL (the difference between the two) is desired, this subtraction becomes redundant. To justify using point-source measurement to calculate incoherent line-source IL , it is necessary to assume that the noise from a line of simultaneously radiating sources (vehicles) is not coherent. This allows for a strict addition of energy in terms of the rms-pressure squared for each contributing source/receiver position, without considering the correlation/coherence between different source/receiver positions. So to get the IL , all the open ground tests were integrated energetically, and the energetically integrated with-barrier tests were subtracted from this. If the assumption of incoherence between vehicles is correct, the IL s for a single vehicle or line source will be equal. Why should this be so? One reason would be the vehicles themselves: separate vehicles display differing speeds, accelerations and orientations as they move along a roadway, so the sound radiation will fluctuate accordingly. Denser flows of traffic would be

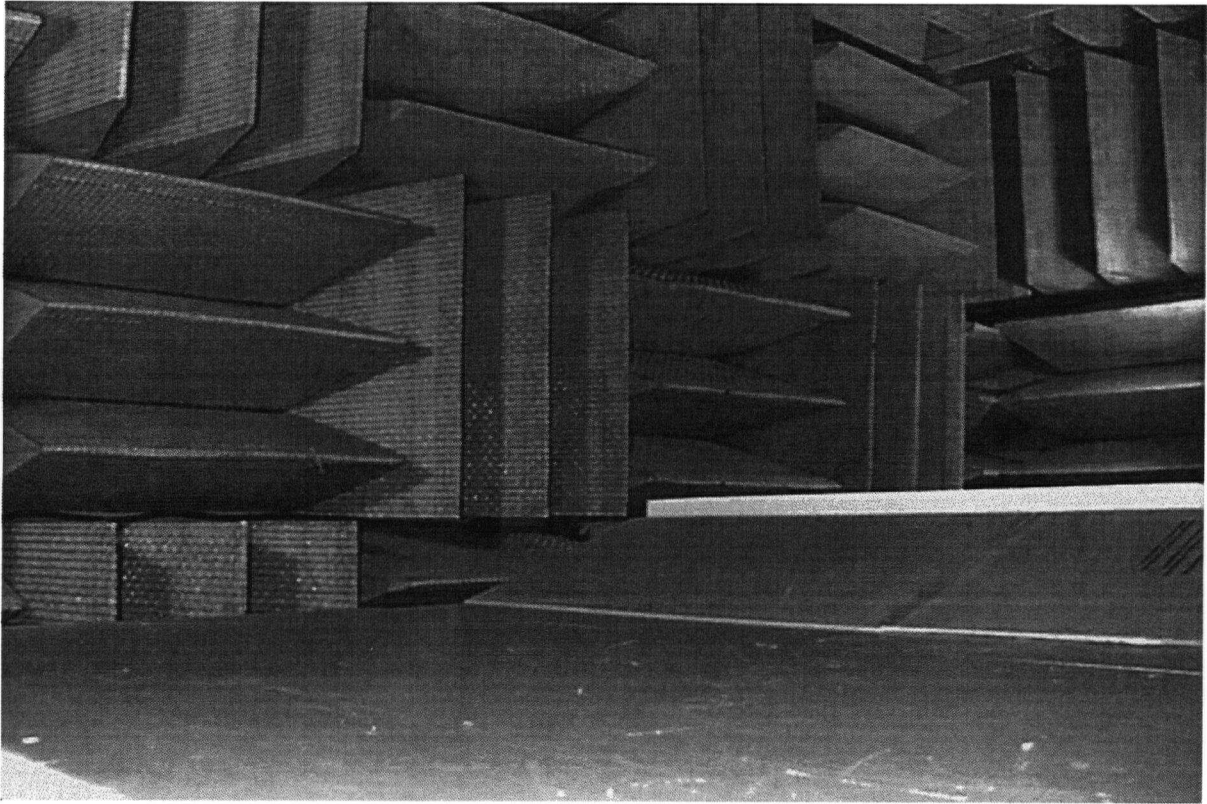


Figure 5.40: Picture of a scale-model earth berm of 3 m height, 2:1 sloped, 2 m top width, with a crest wall of 1 m height.

more apt to exhibit coherent interference between sound waves from separate vehicles. Another reason would be the ground itself, with irregularities in its impedance and topography contributing to the potential randomness of the phase relationships between different sound paths. Additionally, atmospheric turbulence is a constant factor in outdoor sound propagation, so this would also contribute to the incoherence of sound waves from separate vehicles (and between direct and reflected sound from a single vehicle).

5.7.3 Barrier Configurations for Line-Source Insertion-Loss Tests

Fig. 5.40 shows a scale-model earth berm. The line-source results have been grouped into categories based on single-variable changes to surface impedance or geometry. Barriers typically

had a constant total height of 4 m above the surrounding ground surface. The test results are broadly divided into two classifications: tests using the best-choice material to simulate a wall or berm surface, and tests using alternate surfaces for berms. First, the best-choice surface material for walls was dense polystyrene (to simulate wood/concrete/etc), while for barriers the best-choice material was expanded polystyrene (to simulate grass). Second, dense polystyrene was used to simulate acoustically harder surfaces, while felt was used to simulate acoustically softer surfaces. Within these material classifications, there are sub-classes based on barrier profiles — walls, sloped berms, or wall/berm combinations. Within each sub-class, geometric features were varied in a systematic way. Vertical walls were given different thicknesses. Sloped barriers were altered with respect to their profile (wedge, flat-top(2 widths) and radius (2 radii)). Combined wall/berms were always flat-topped berms which were given several heights (1, 2, 3 m) and slopes (1.5, 2, and 3:1). Fig. 5.41 depicts the barrier profiles that were tested; the following list itemizes the research question being tested, in terms of single-variable changes.

1. Best-Choice Surface Impedances:

- (a) For a vertical wall profile, how does variable wall thickness affect barrier *IL*?
- (b) For five different berm profiles, how does variable berm slope affect barrier *IL*?
- (c) For three berm slopes, how does a change in top profile affect barrier *IL*? This question ties in with the next three questions.
- (d) For three berm slopes, how does variable top width affect barrier *IL*?
- (e) For three berm slopes, how does top radius affect barrier *IL*?
- (f) For three berm slopes, how do changes from a flat top to a round top affect barrier *IL*?
- (g) For three berm/wall slopes, how does berm height affect barrier *IL*?
- (h) For three berm/wall heights, how does berm slope affect barrier *IL*?
- (i) For a pair of 3:1 sloped flat-top berms of 2 m top width with/without a wall, how does a height increase of 1 m achieved by adding a wall affect barrier *IL*, as compared

Wall 4m H	5 5cmT 6 10cmT 7 15cmT	Round-top 4m H, 1.5K, 2m R	20 EP
Wedge 4m H, 1.5K	8 EP 37 F 38 P	Round-top 4m H, 2K, 2m R	21 EP
Wedge 4m H, 2K	9 EP 36 F 39 P	Round-top 4m H, 3K, 2m R	22 EP
Wedge 4m H, 3K	10 EP 32 F 40 P	Flat-top 3m H, 1.5K, 2m W Wall 1m H	23 EP
Flat-top 4m H, 1.5K, 1m W	11 EP	Flat-top 2m H, 1.5K, 2m W Wall 2m H	24 EP
Flat-top 4m H, 2K, 1m W	12 EP	Flat-top 1m H, 1.5K, 2m W Wall 3m H	25 EP
Flat-top 4m H, 3K, 1m W	13 EP	Flat-top 3m H, 2K, 2m W Wall 1m H	26 EP
Flat-top 4m H, 1.5K, 2m W	14 EP	Flat-top 2m H, 2K, 2m W Wall 2m H	27 EP
Flat-top 4m H, 2K, 2m W	15 EP	Flat-top 1m H, 2K, 2m W Wall 3m H	28 EP
Flat-top 4m H, 3K, 2m W	16 EP	Flat-top 3m H, 3K, 2m W Wall 1m H	29 EP 34 F 42 P
Round-top 4m H, 1.5K, 1m R	17 EP	Flat-top 2m H, 3K, 2m W Wall 2m H	30 EP
Round-top 4m H, 2K, 1m R	18 EP	Flat-top 1m H, 3K, 2m W Wall 3m H	31 EP
Round-top 4m H, 3K, 1m R	19 EP	Flat-top 3m H, 3K, 2m W	35 EP 33 F 41 P

Figure 5.41: Profile view of barrier configurations. File numbers are listed alongside the right hand side of each figure, with multiple files listed if different surface impedances were tested. Abbreviations for geometry: *T* for thickness, *W* for width, *R* for radius of curvature, *H* for height, and *K* for slope. Abbreviations for surface impedance: *EP* for expanded polystyrene, *F* for felt, and *P* for polystyrene.

to a height increase of 1 m gained by increasing flat-top height to 4 m?

2. Alternate Surface Materials:

- (a) For three wedge slopes, how does surface impedance affect barrier IL ?
- (b) For three berm surfaces, how does slope affect barrier IL ?
- (c) For two flat-top berms of 3:1 slope, how does surface impedance affect barrier IL ?
- (d) For three surfaces, how does the presence of a 1m vertical wall affect barrier IL ?

5.7.4 Insertion-Loss Test-Result Reporting

The line-source tests are reported in third-octaves; as well, both the point-source and line-source tests are reported as both unweighted total levels and weighted total levels. For the line source, the open-ground and with-barrier sound-pressure levels were integrated separately for all twenty-one line-source test positions. For both the point-source and line-source tests, Eq. (5.2) was employed to convert the fixed-bandwidth measurement bins into the appropriate variable-bandwidth third-octaves. The model-scale bandwidth was 250 Hz, which reduces at full-scale to 7.94 Hz. The upper-frequency bin for a given third-octave band is denoted m_2 , and the lower-frequency bin by m_1 :

$$L_{p,band} = 10 \log_{10} \left(\sum_{i=m_1}^{m_2} 10^{L_{p,i}/10} \right) - 10 \log_{10} (m_2 - m_1 + 1) \quad (5.2)$$

At full-scale frequencies, the 80 Hz third-octave band was the lowest frequency band for which three scale-model frequency bins (10, 11, 12) could be integrated together; this was thought to be the minimum number of bins necessary for accurate third-octave results. At higher full-scale frequencies, the 2500 Hz band required that scale-model bins 283–355 be integrated together. Above this frequency the number of bins was insufficient to form an entire 3150 Hz third-octave. The resulting bin numbers are listed in Table 5.2. The resulting line-source ILs are presented in third-octaves from 80–2500 Hz which corresponds to model-scale frequencies from 2250–88500 Hz. Total ILs are found by energetically averaging the third-octave ILs across the entire

Table 5.2: Bins integrated together to produce third-octaves of a given centre frequency at full-scale: scale-model tests extended from 0–100 kHz in four-hundred bins of 250 Hz bandwidths, at a scale of 1:31.5.

third-octave	80	100	125	160	200	250	315	400
bins	10:12	13:15	16:18	19:23	24:29	30:36	37:45	46:57
third-octave	500	630	800	1000	1250	1600	2000	2500
bins	58:71	72:90	91:113	114:141	142:179	180:226	227:282	283:355

frequency range for bands from 80–2500 Hz. Total *ILAs* are found by applying the A-weighted traffic noise spectra (see Fig. 4.1 on page 62) to the unweighted spectra before integrating energetically to get line-source levels. The weighted line-source levels for the open-ground and with-barrier configurations are then subtracted energetically to get the total line-source *ILA*.

The errors in the total sound-pressure levels were calculated separately for the open-ground and with-barrier tests using the same approach. To calculate the standard deviations for the total *IL* or *ILA* the following steps were taken. The variances were calculated for each frequency bin of the open-ground and with-barrier arrays, and the arrays of variance were added together to produce a single array. This final *IL*-error array was summed over the three-hundred and forty-six frequency bins to calculate the average error at each the twenty-one model-line-source positions. From these position-dependent errors the line-source error was calculated. Lastly, the square root was taken yielding a standard deviation for total line-source *IL* or *ILA*.

5.8 Experimental Conclusion

The properties of the air-jet source have been evaluated, in conjunction with tests of the free-field deviations of the anechoic chamber. Its limitations — especially in terms of reproducibility and directivity — were known when proceeding with the evaluation of model materials and barrier *IL*. A test platform was constructed to allow for ready placement of the scale-model barriers, and allow for easy access to them while traversing the air-jet source. The scale-model-material selection process identified three appropriate model materials.

Chapter 6

Scale-Model Results: Line-Source Third-Octave Insertion Losses

6.1 Introduction to Results

The line-source test results presented in this chapter are divided into two categories: results from tests using the optimum material to simulate a barrier surface, and those tests using alternative surfaces. The highway configuration is described in Section 5.7; the noise-barrier configurations can be seen in Fig. 5.41 on page 113. All *IL*-result graphs have frequency plotted on a logarithmic scale and the vertical axis is *IL* in dB. Each graph plots the variation in third-octave *ILs* resulting from changes to a barrier's geometry or surface.

There were various sources of error to consider in the tests of barrier *IL*. Some sources of error have already been discussed — namely, the air-jet source, microphone, anechoic chamber, and scale-model materials. The shift of the acoustic centre of the air-jet source away from the geometric centre due to the continual air flow was not considered to be a problem due to the source's orientation relative to the microphone. Additionally, experimental error can arise when a barrier test configuration is realigned. The results were inspected visually to see if they were consistent, and the average sound-pressure level of each test pair was calculated, along with its standard deviation. The open-ground tests routinely had larger standard deviations due to their greater sensitivity to the location of destructive-interference minima. Since the scale-model ground surface is unrealistically flat, the open-ground errors observed for these tests were considered to be excessive, and the with-barrier variances were used in their place. As such, the standard deviation of the test procedure is considered *a posteriori* to be approximately 2 dB for the scale-model tests of total *IL*.

The *ILs* of every barrier configuration typically increase with frequency [75]. However, due

to ground reflections, there are frequency-dependent fluctuations in the IL which are common to all scale-model results. At low frequencies (80–125 Hz), the IL is typically below 5 dB; diffraction is more significant at low frequencies so the barrier will be less effective. From the 160–630 Hz third-octaves, the IL increases gradually in some cases, but in most cases a barrier has an IL which peaks in the 200, 250 or 315 Hz bands, sometimes exceeding 15 dB. For the barriers with peaks in their IL , as frequency increases towards the 800 Hz band, the IL generally decreases, typically to below 5 dB — this is largely due to the contribution of the ground effect to the open-ground test results. For every barrier tested, the IL then increases with frequency, peaking to 10 dB or more in the 1600 Hz band, with the IL decreasing in the 2000 and 2500 Hz bands — this decrease can be attributed to excessive air absorption. Referring back to the IL results of the field tests seen in Fig. 4.3 — particularly locations C and D — the ground-effect dip is evident for the steepest and most effective berm — the bark-mulch berm. Considering the field-test results, a general increase of IL with frequency is also evident; however, air absorption is not a factor in the full-scale field tests.

6.2 Optimum Surface Impedance

6.2.1 Variable Wall Thickness

Fig. 6.1 shows the IL for three wall thicknesses — equivalent to full-scale values of 5, 10, and 15 cm. It can be seen that the range of wall thicknesses tested did not significantly affect IL . The largest third-octave difference between the three configurations is 1.8 dB in the 250 Hz band. Increased wall thickness may have been related to a suppression of transmitted sound energy in the 250 Hz band, but the results are not statistically significant.

6.2.2 Variable Berm Slope

Figs. 6.2, 6.3, 6.4, 6.5 and 6.6 show the variation of IL with berm slope. Fig. 6.2 shows results for wedge-shaped berms; it is apparent that the only significant effect is that, as the slope becomes shallower, the IL is decreased in the vicinity of the 250 Hz third-octave band. This

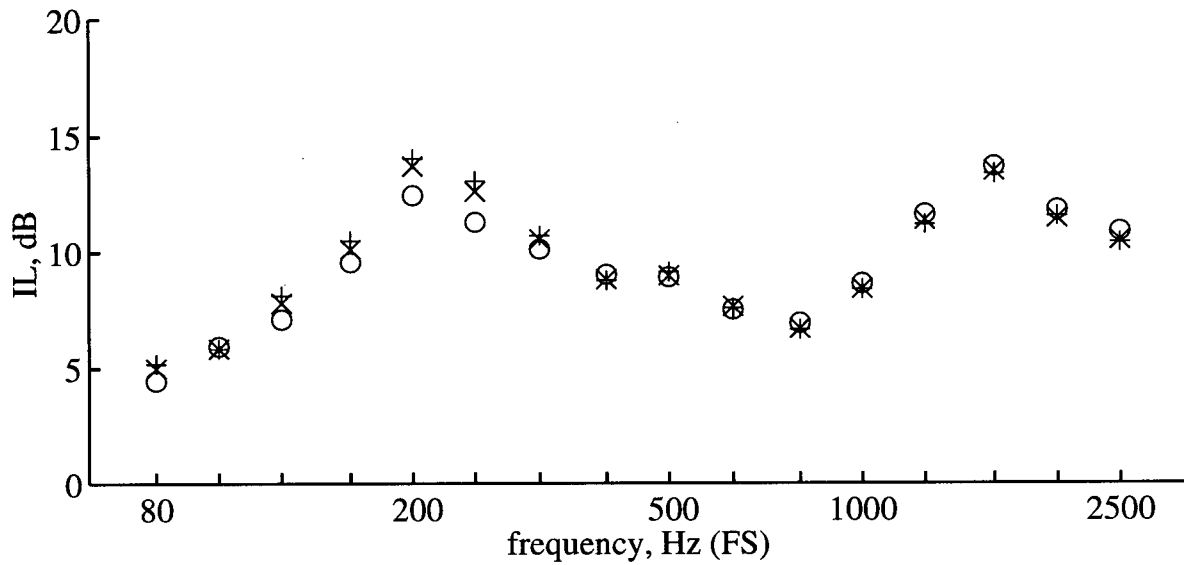


Figure 6.1: Measured third-octave IL s for 4 m high walls with full-scale thicknesses of 5, 10 and 15 cm: (o) 5 cm thick wall(#5), $IL=10.0$, $ILA=9.2$; (x) 10 cm thick wall(#6), $IL=10.3$, $ILA=9.1$; (+) 15 cm thick wall(#7), $IL=10.4$, $ILA=9.0$.

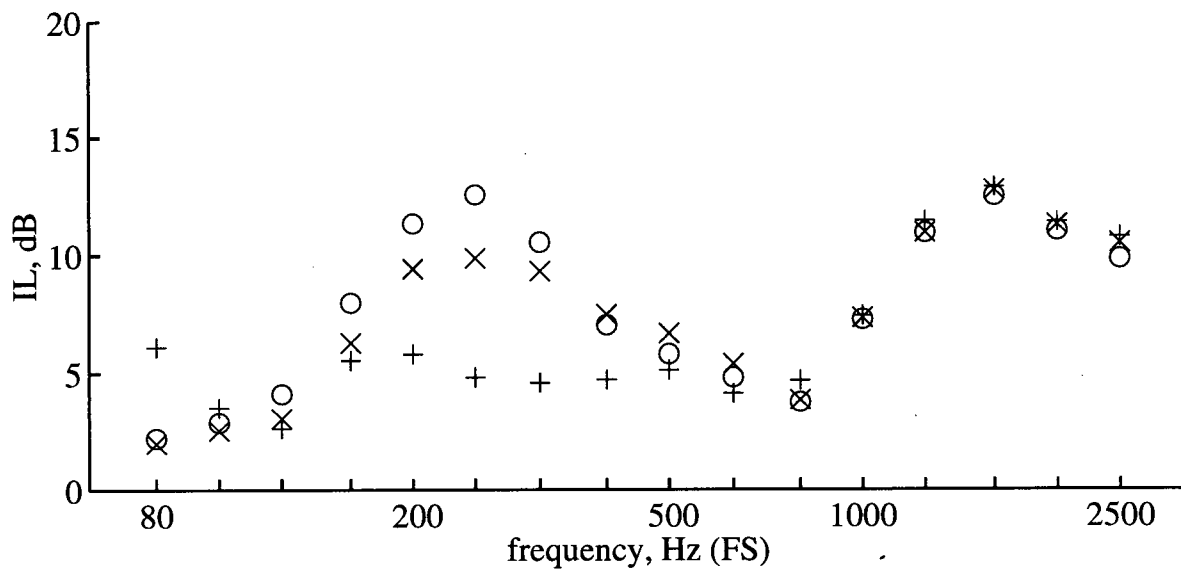


Figure 6.2: Measured third-octave IL s for wedge-shaped grass berms of 4 m height, and with 1.5, 2 and 3:1 slopes: (o) 1.5:1 wedge(#8), $IL=9.0$, $ILA=7.0$; (x) 2:1 wedge(#9), $IL=8.5$, $ILA=7.2$; (+) 3:1 wedge(#10), $IL=7.9$, $ILA=7.0$.

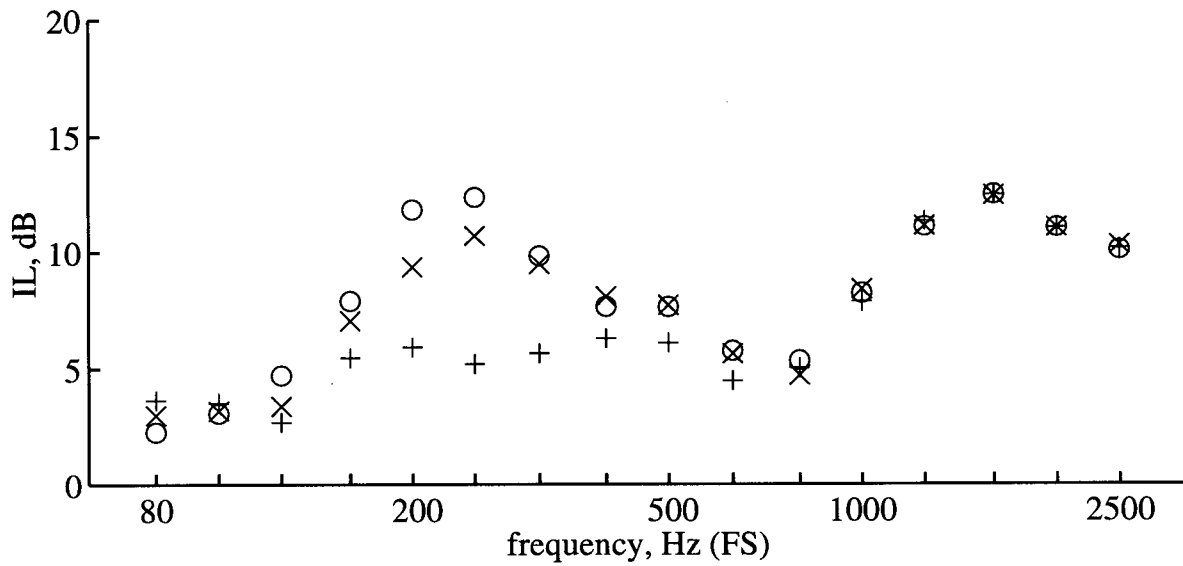


Figure 6.3: Measured third-octave IL s for flat-topped grass berms of 4 m height, with a 1 m wide flat-top, and with 1.5, 2 and 3:1 slopes: (o) 1.5:1 flat-top(#11), $IL=9.2$, $ILA=8.0$; (x) 2:1 flat-top(#12), $IL=8.8$, $ILA=7.8$; (+) 3:1 flat-top(#13), $IL=7.8$, $ILA=7.3$.

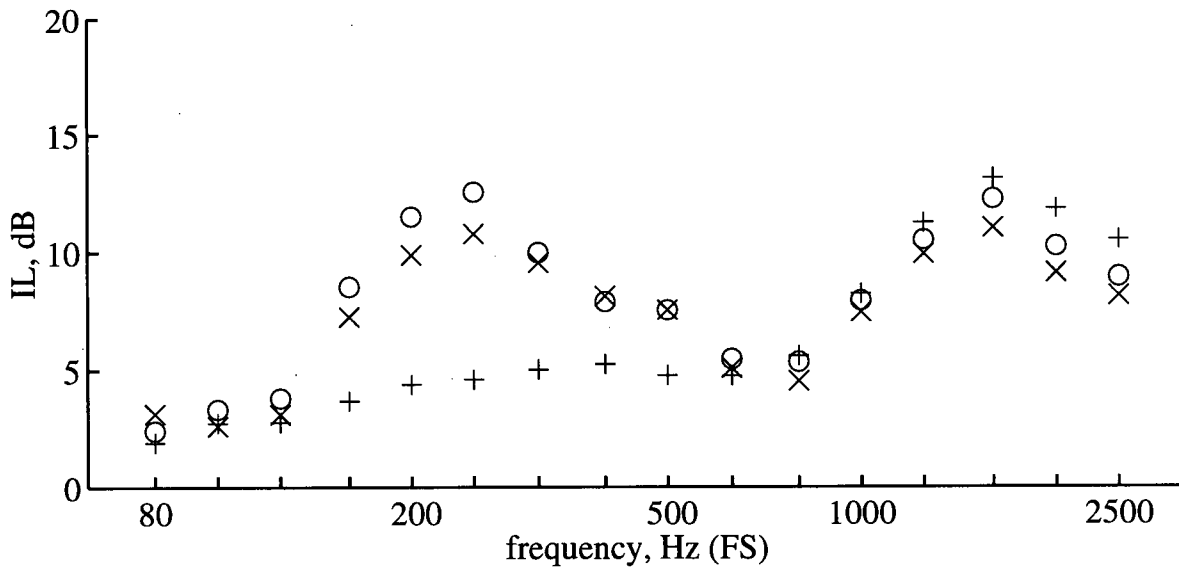


Figure 6.4: Measured third-octave IL s for flat-topped grass berms of 4 m height, with a 2 m wide flat-top, and with 1.5, 2 and 3:1 slopes: (o) 1.5:1 flat-top(#14), $IL=9.0$, $ILA=7.7$; (x) 2:1 flat-top(#15), $IL=8.1$, $ILA=7.1$; (+) 3:1 flat-top(#16), $IL=7.8$, $ILA=7.4$.

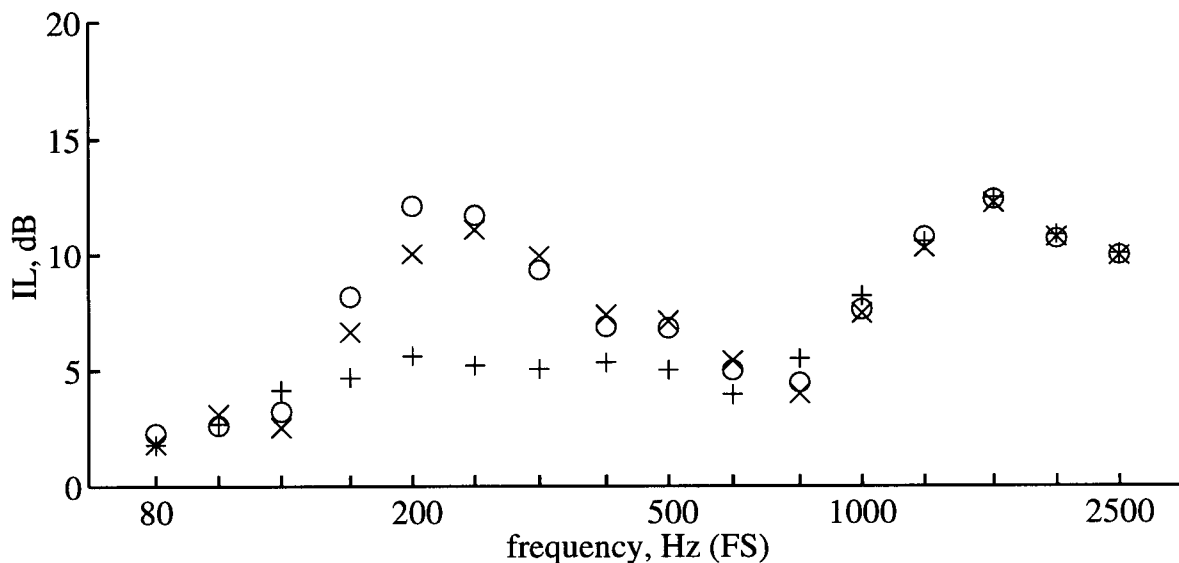


Figure 6.5: Measured third-octave IL s for round-topped grass berms of 4 m height, with a 1 m radius round-top, and with 1.5, 2 and 3:1 slopes: (o) 1.5:1 round-top(#17), $IL=8.9$, $ILA=7.3$; (x) 2:1 round-top(#18), $IL=8.5$, $ILA=7.2$; (+) 3:1 round-top(#19), $IL=7.5$, $ILA=7.2$.

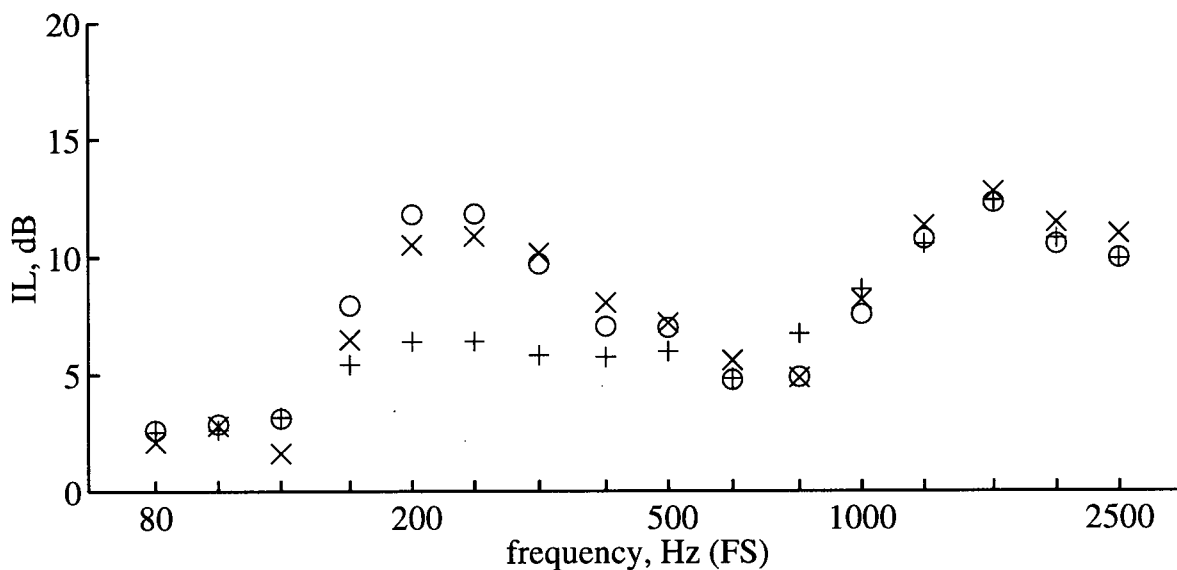


Figure 6.6: Measured third-octave IL s for round-topped grass berms of 4 m height, with a 2 m radius round-top, and with 1.5, 2 and 3:1 slopes: (o) 1.5:1 round-top(#20), $IL=8.9$, $ILA=7.4$; (x) 2:1 round-top(#21), $IL=9.0$, $ILA=7.8$; (+) 3:1 round-top(#22), $IL=7.7$, $ILA=7.8$.

effect also occurred for other top profiles, as seen in Figs. 6.3 (1 m flat top), 6.4 (2 m flat top), 6.5 (1 m round top), and 6.6 (2 m round top). It was expected that a wider berm top would have an increased IL , but the effects of increased width and radius were not of practical interest. However, comparisons show that walls (barriers of infinite slope) consistently outperform earth berms. For all berm slopes and profiles the 80, 100 and 125 Hz bands have lower IL s than for the walls seen in Fig. 6.1. The effect of berm slope is most evident in the 250 Hz band, around which other bands exhibit decreases in IL with shallower slope.

Using the same information, consider the following question: given three berm slopes, how does variable top profile affect barrier IL ? In Figs. 6.4 and 6.6 the only real difference in trends appears in the 250 Hz band, where a range of IL is evident. This question is answered in the following two subsections by considering cases involving either flat- or round-topped berms.

6.2.3 Variable Berm Top Width

Figs. 6.7, 6.8 and 6.9 show the variation of IL with top width. For the steeper 1.5:1 berm (Fig. 6.7) the largest effects can be seen in the 500 and 800 Hz bands. For the 2:1 sloped berm (Fig. 6.8) the most obvious effect is a trend in the higher frequency bands for the wider-berms IL to decrease; small increases in IL with top width are observed around the 250 Hz band. For the shallower 3:1 sloped berm (Fig. 6.9) there is more variation in IL in the low-frequency bands. It can be concluded that the effect of widening the top from 0 m to 2 m is not as significant as variations of slope.

6.2.4 Variable Berm Top Radius

Figs. 6.10, 6.11 and 6.12 show that changes in the slope have a greater effect on IL s than the top-radius changes. For the steeper 1.5:1 berm (Fig. 6.7) variations in IL were small across all bands. For the 2:1 sloped berm (Fig. 6.8) the high-frequency bands exhibited more variation in IL ; around the 250 Hz band the increase in top width increased IL . For the shallower 3:1 sloped berm (Fig. 6.9) there is inconsistent variation of IL with top radius in all frequency

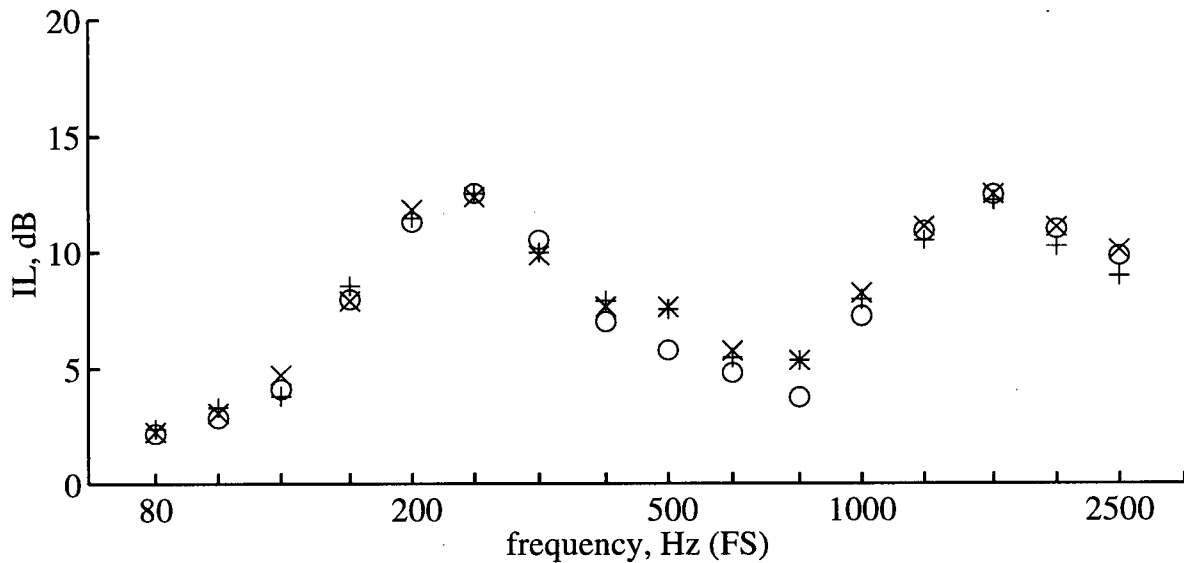


Figure 6.7: Measured third-octave IL s for grass berms of 4 m height with a fixed slope of 1.5:1, and with top widths of 0, 1 and 2 m: (o) 0 m top width wedge(#8), $IL=9.0$, $ILA=7.0$; (x) 1 m wide flat-top(#11), $IL=9.2$, $ILA=8.0$; (+) 2 m wide flat-top(#14), $IL=9.0$, $ILA=7.7$.

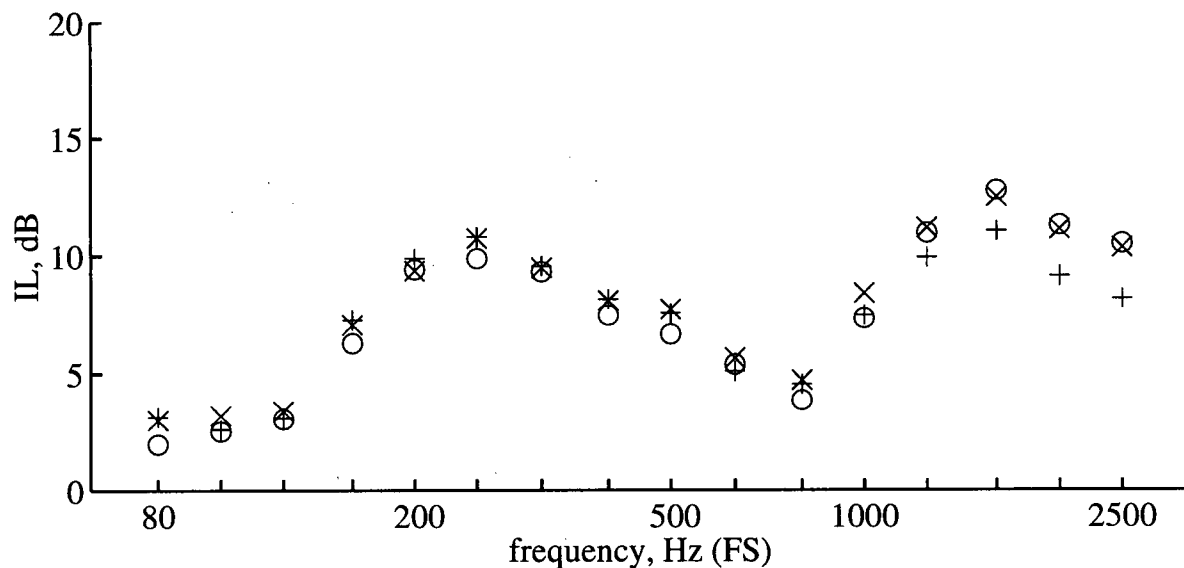


Figure 6.8: Measured third-octave IL s for grass berms of 4 m height with a fixed slope of 2:1, and with top widths of 0, 1 and 2 m: (o) 0 m top width wedge(#9), $IL=8.5$, $ILA=7.2$; (x) 1 m wide flat-top(#12), $IL=8.8$, $ILA=7.8$; (+) 2 m wide flat-top(#15), $IL=8.1$, $ILA=7.1$.

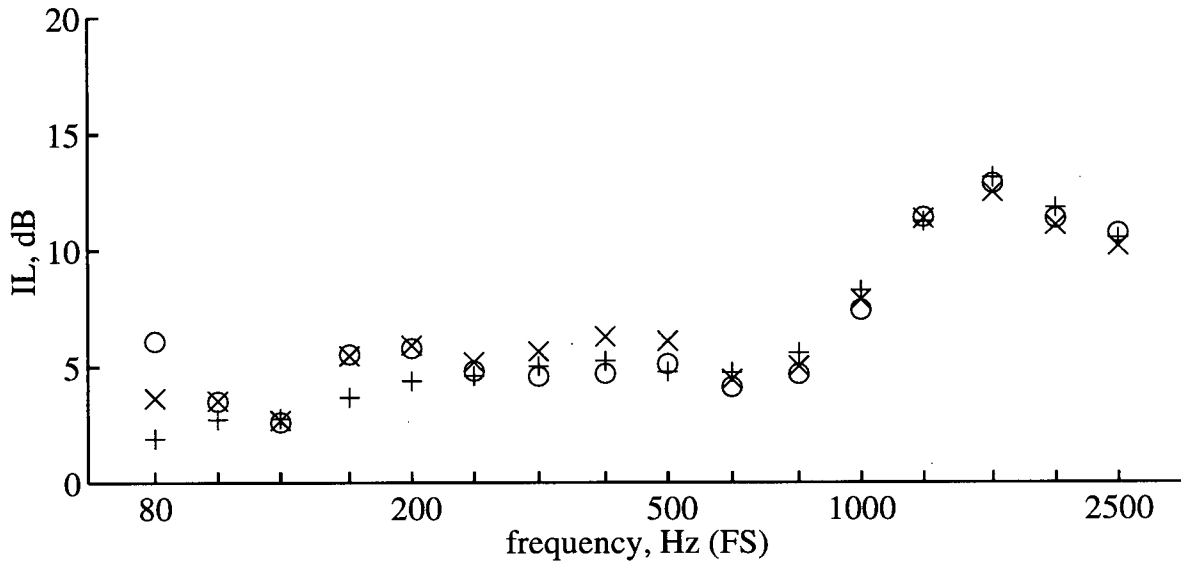
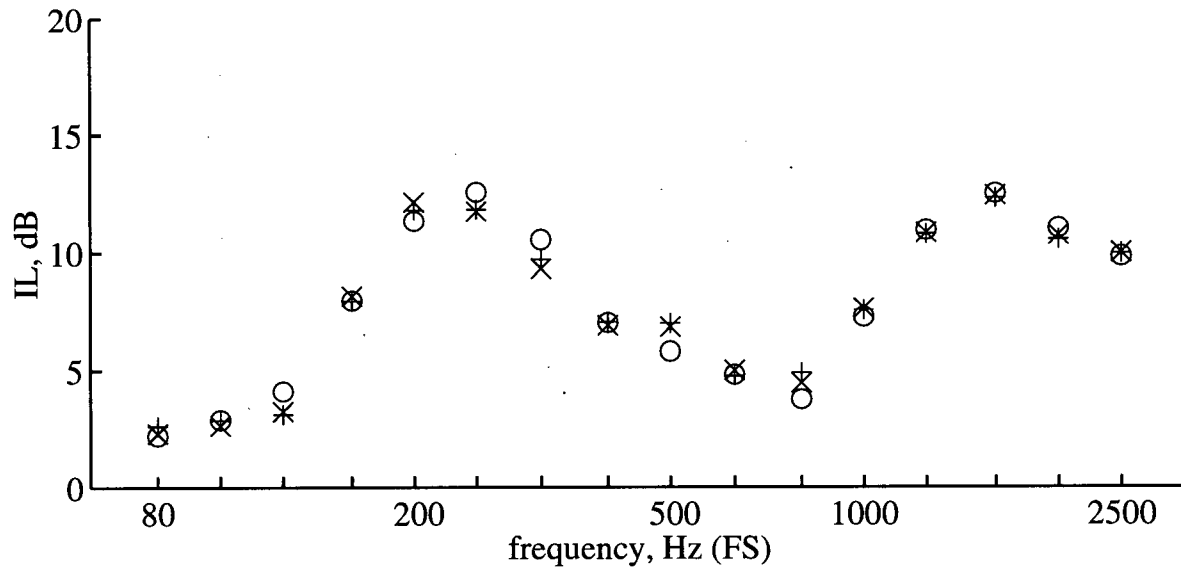


Figure 6.9: Measured third-octave IL s for grass berms of 4 m height with a fixed slope of 3:1, and with top widths of 0, 1 and 2 m: (o) 0 m top width wedge(#10), $IL=7.9$, $ILA=7.0$; (x) 1 m width flat-top(#13), $IL=7.8$, $ILA=7.3$; (+) 2 m width flat-top(#16), $IL=7.8$, $ILA=7.4$.



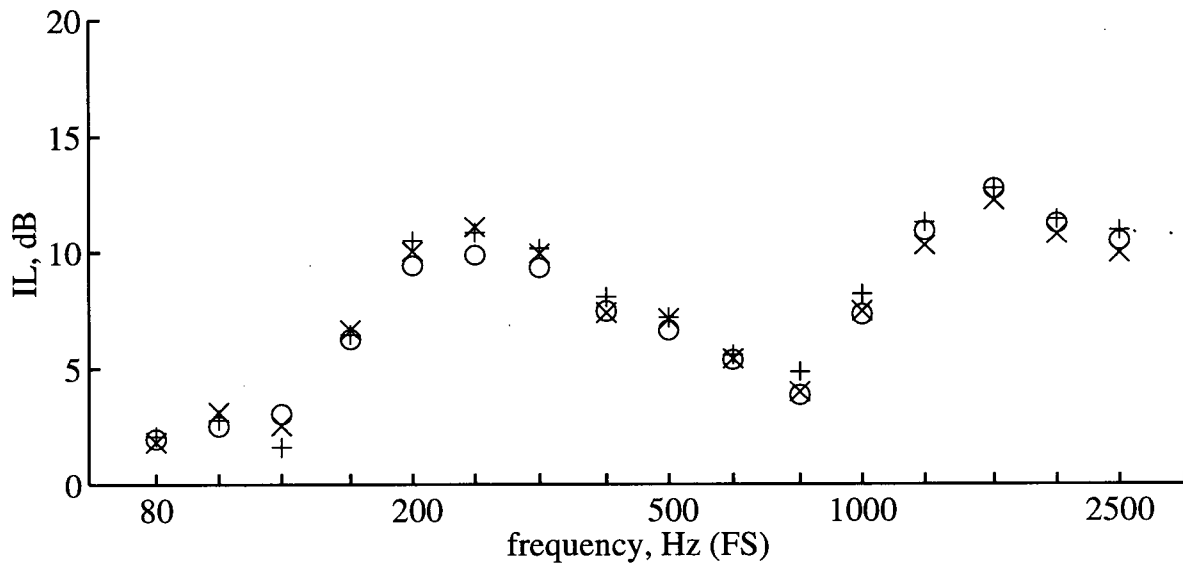


Figure 6.11: Measured third-octave IL s for grass berms of 4 m height with a fixed slope of 2:1, and with top radii of 0, 1 and 2 m: (o) 0 m radius wedge(#9), $IL=8.5$, $ILA=7.2$; (x) 1 m radius round-top(#18), $IL=8.5$, $ILA=7.2$; (+) 2 m radius round-top(#21), $IL=9.0$, $ILA=7.8$.

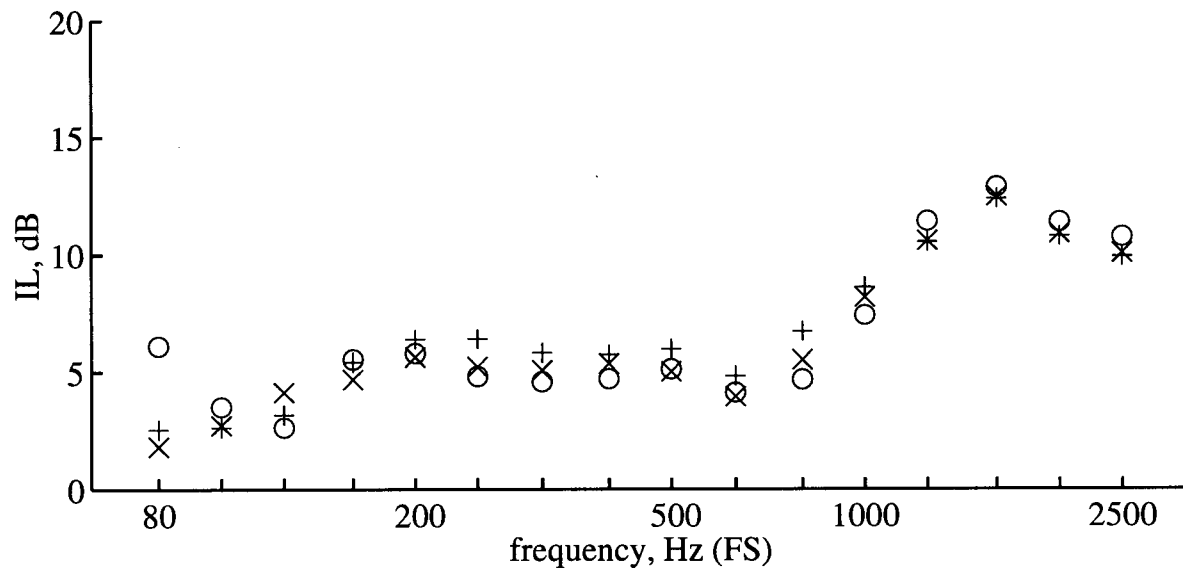


Figure 6.12: Measured third-octave IL s for grass berms of 4 m height with a fixed slope of 3:1, and with top radii of 0, 1 and 2 m: (o) 0 m radius wedge(#10), $IL=7.9$, $ILA=7.0$; (x) 1 m radius round-top(#19), $IL=7.5$, $ILA=7.2$; (+) 2 m radius round-top(#22), $IL=7.7$, $ILA=7.8$.

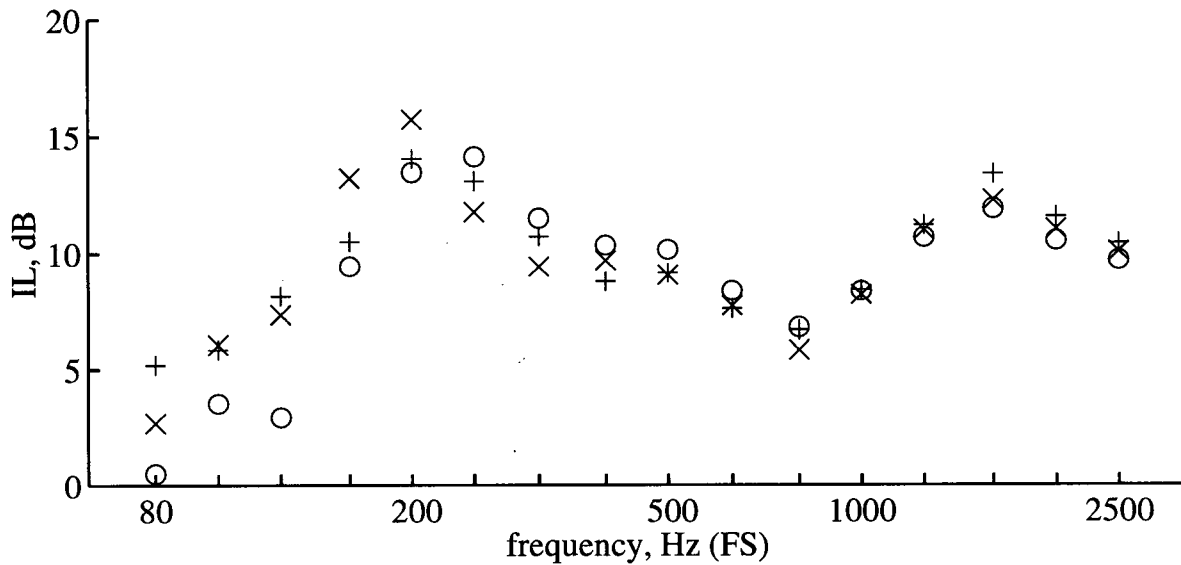


Figure 6.13: Measured third-octave *IL*s for flat-topped grass berms of 1.5:1 slope, with 2 m top width, and with 1/3, 2/2 and 3/1 m berm/wall heights: (o) 3 m high flat-top with 1 m wall (#23), $IL=10.1$, $ILA=8.9$; (x) 2 m high flat-top with 2 m wall (#24), $IL=10.5$, $ILA=8.6$; (+) 1 m high flat-top with 3 m wall (#25), $IL=10.4$, $ILA=9.0$.

bands, but more so at lower frequencies.

6.2.5 Variable Flat-Top-Berm/Wall Height

Figs. 6.13, 6.14 and 6.15 show how, for a fixed total height of 4 m, variations in the relative berm and wall height affect *IL*. For the steeper 1.5:1 berm (Fig. 6.13) the effect of varying the wall height occurs around the 200 Hz band, with more erratic variations at lower frequencies. Very little effect is seen in the mid- to high-frequency bands. For the 2:1 berm (Fig. 6.14) the effect of varying the wall height occurs around the 200 Hz band, with more erratic behaviour at lower frequencies. There is a benefit at mid-frequencies in having a 3 m berm topped by a 1 m wall. For the shallower 3:1 berm (Fig. 6.15) the effect of varying the wall height occurs in the 250 Hz band and below. There is a noticeable increase in *IL* across the mid-band frequencies, suggesting that a shallower and higher berm is the best choice when a wall is present. When a berm's height was a smaller proportion of the total 4 m barrier height, the effect of slope on

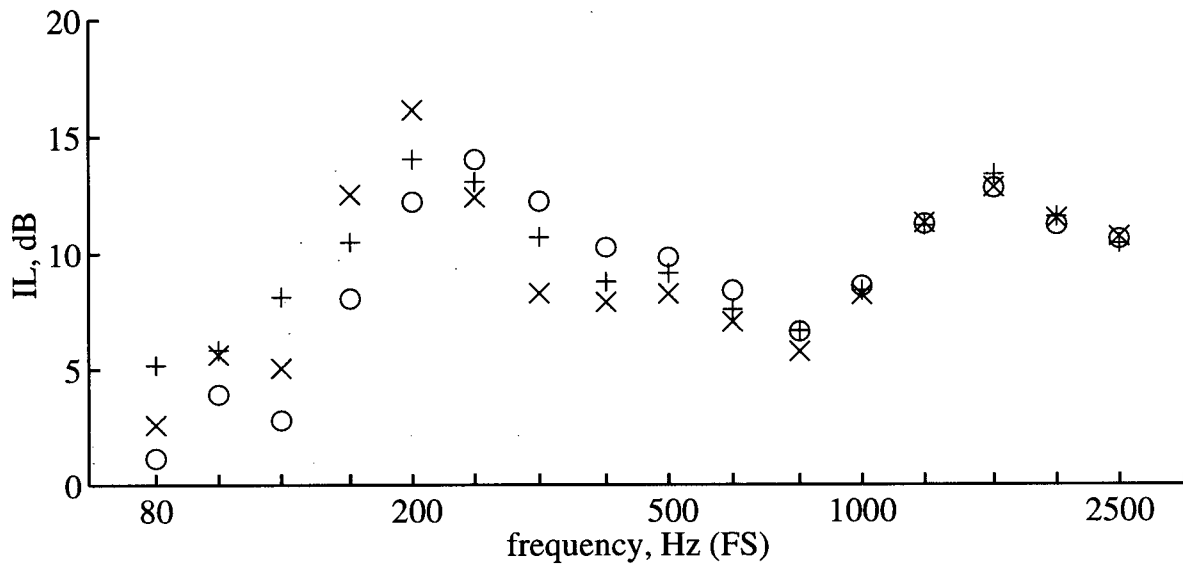


Figure 6.14: Measured third-octave IL s for flat-topped grass berms of 2:1 slope, with 2 m top width, and with 1/3, 2/2 and 3/1 m berm/wall heights: (o) 3 m high flat-top with 1 m wall (#26), $IL=10.2$, $ILA=9.1$; (x) 2 m high flat-top with 2 m wall (#27), $IL=10.5$, $ILA=8.5$; (+) 1 m high flat-top with 3 m wall (#28), $IL=10.4$, $ILA=9.0$.

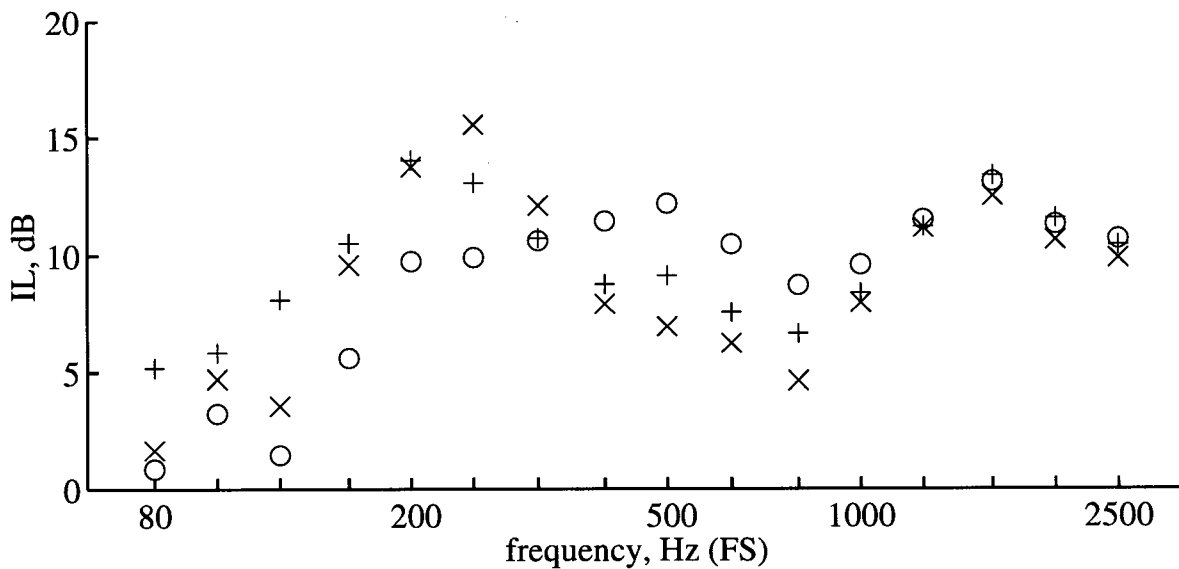


Figure 6.15: Measured third-octave IL s for flat-topped grass berms of 3:1 slope, with 2 m top width, and with 1/3, 2/2 and 3/1 m berm/wall heights: (o) 3 m high flat-top with 1 m wall (#29), $IL=9.9$, $ILA=10.2$; (x) 2 m high flat-top with 2 m wall (#30), $IL=10.2$, $ILA=7.8$; (+) 1 m high flat-top with 3 m wall (#31), $IL=10.4$, $ILA=9.0$.

attenuation was reduced. For a 1 m earth berm topped by a 3 m vertical wall, the results were indistinguishable from those of a vertical wall. A possible explanation is that the additional reflections from the earth berm reach the berm crest, interfering destructively at that point — thereby reducing sound levels in the noise-barrier's shadow zone. Importantly, the results indicate that a berm/wall combination can be as effective as, or even more effective than, a vertical wall. When an earth berm is combined with a crest wall, it might be possible to tune the slope of the earth berm to maximize the *IL* of the noise barrier.

6.2.6 Variable Flat-Top-Berm/Wall Slope

Figs. 6.1, 6.16 and 6.17 show how, for a barrier of a fixed 4 m height, changes in berm slope affect berm/wall *IL*. In Fig. 6.16 the *ILs* are similar above the 800 Hz band; below that the barrier performance is more erratic. In Fig. 6.17 it is clear that the effect of shallower slope is not the same as it is for a berm (consider Fig. 6.2). In the case of a berm/wall combination the opposite trend was observed for berm slope — shallower earth berms resulted in increased *ILs*. The slight decrease with slope of the effectiveness of the earth berm around the 250 Hz third-octave band is clearly offset by an increase in effectiveness across the mid-band frequencies.

6.2.7 Variable Barrier Height

Fig. 6.18 shows that the effect of increasing the height of a 3 m berm of 3:1 slope, by making the berm 4 m high, differs from the effect of adding a 1 m wall. The added berm height increases *IL* consistently in the 630 Hz band and above. A 1 m wall increases the *IL* in the same frequency bands, but also increases *IL* over and above those for the berm from 160 to 1000 Hz. This advantage may not extend to steeper berms of 1.5 or 2:1 slope.

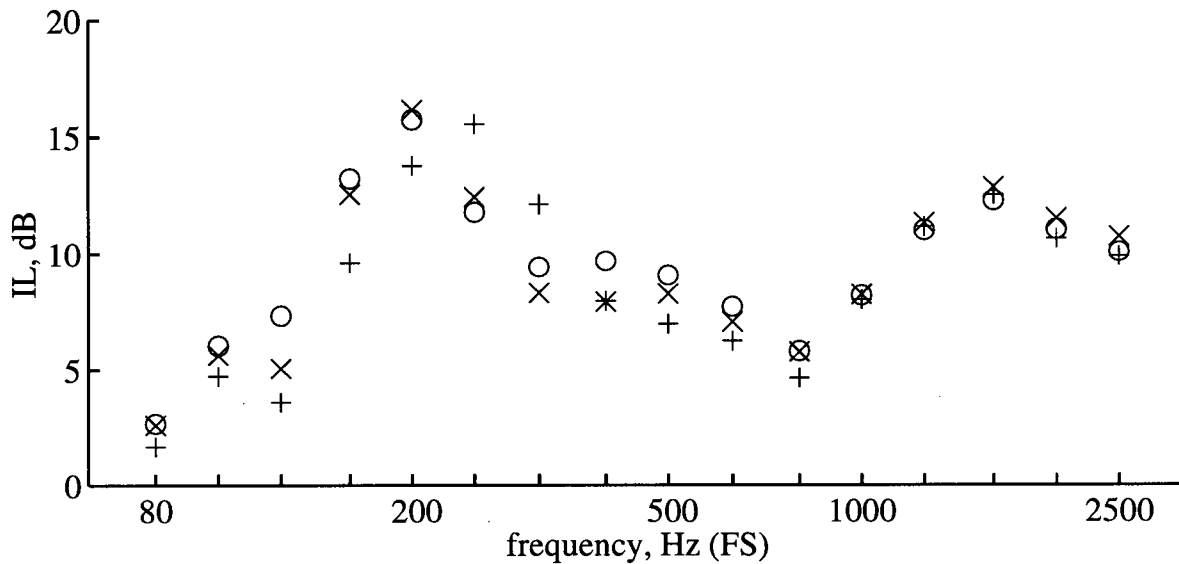


Figure 6.16: Measured third-octave IL s for flat-topped grass berms of 2 m height, with 2 m top width, and with slopes of 1.5:1, 2:1 and 3:1, topped by a 2 m high crest wall: (o) 1.5:1 flat-top with wall(#24), $IL=10.5$, $ILA=8.6$; (x) 2:1 flat-top with wall(#27), $IL=10.5$, $ILA=8.5$; (+) 3:1 flat-top with wall(#30), $IL=10.2$, $ILA=7.8$.

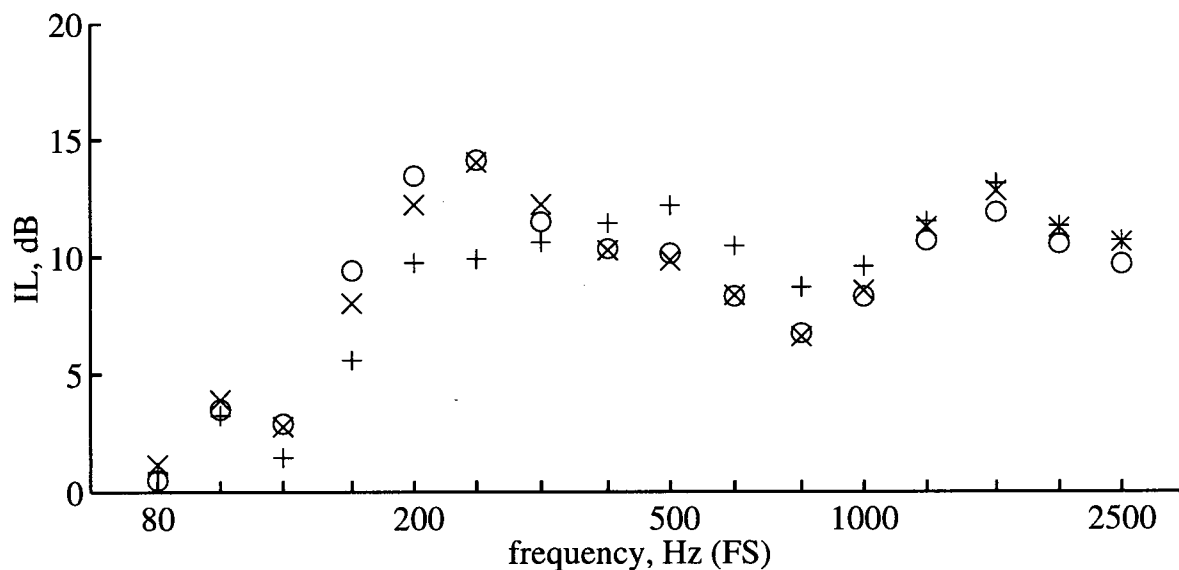


Figure 6.17: Measured third-octave IL s for flat-topped grass berms of 3 m height, with 2 m top width, and with slopes of 1.5:1, 2:1 and 3:1, topped by a 1 m high crest wall: (o) 1.5:1 flat-top with wall(#23), $IL=10.1$, $ILA=8.9$; (x) 2:1 flat-top with wall(#26), $IL=10.2$, $ILA=9.1$; (+) 3:1 flat-top with wall(#29), $IL=9.9$, $ILA=10.2$.

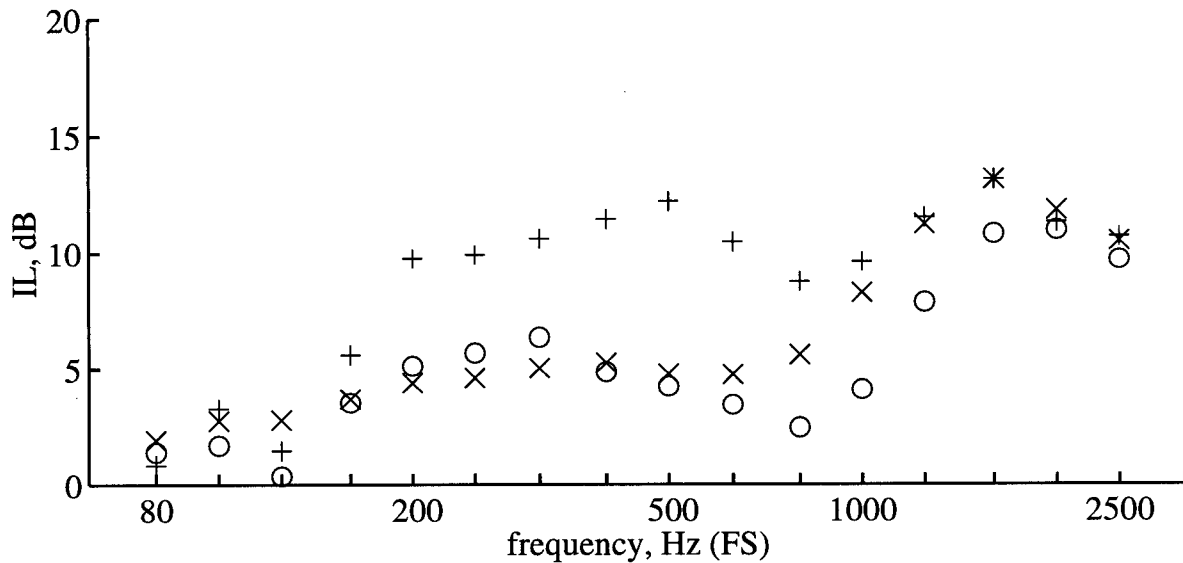


Figure 6.18: Measured third-octave IL s for flat-topped grass berms of both 3 m and 4 m heights, with 2 m top width, and with a fixed slope of 3:1; also considered is a 3 m berms with a 1 m crest wall: (o) 3 m high flat-top of 2 m width (#35), $IL=6.4$, $ILA=5.1$; (x) 4 m high flat-top of 2 m width (#16), $IL=7.8$, $ILA=7.4$; (+) 3 m high flat-top of 2 m width topped by a 1 m wall(#29), $IL=9.9$, $ILA=10.2$.

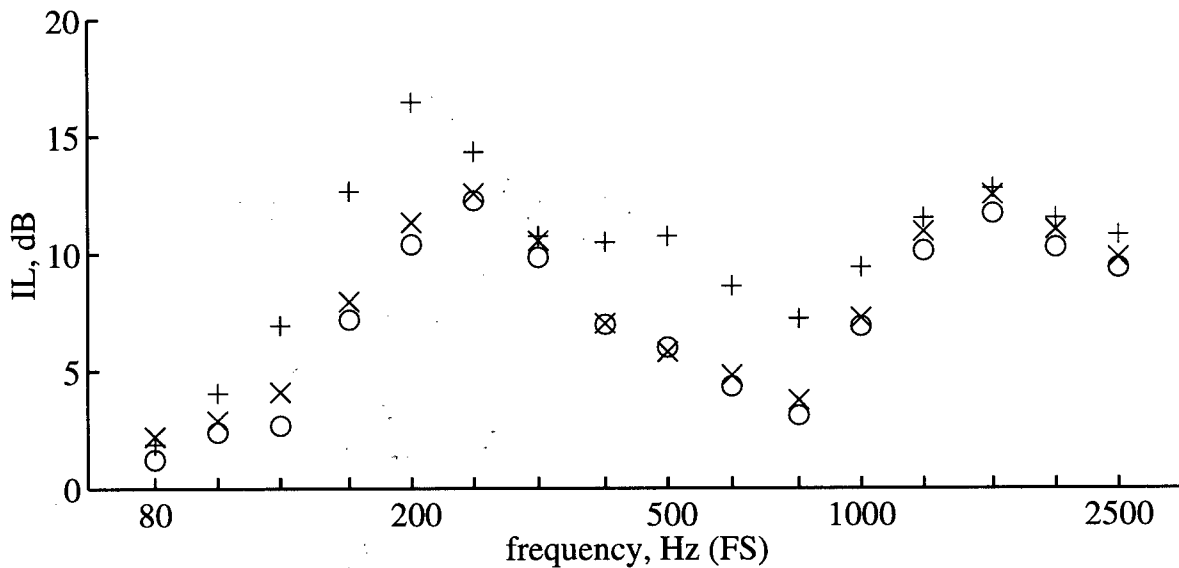


Figure 6.19: Measured third-octave IL s for wedge-shaped berms of 4 m height, with 1.5:1 slope, covered by dense polystyrene, expanded polystyrene and felt: (o) dense polystyrene wedge(#38), $IL=8.4$, $ILA=6.4$; (x) grass wedge(#8), $IL=9.0$, $ILA=7.0$; (+) felt wedge(#37), $IL=11.3$, $ILA=9.6$.

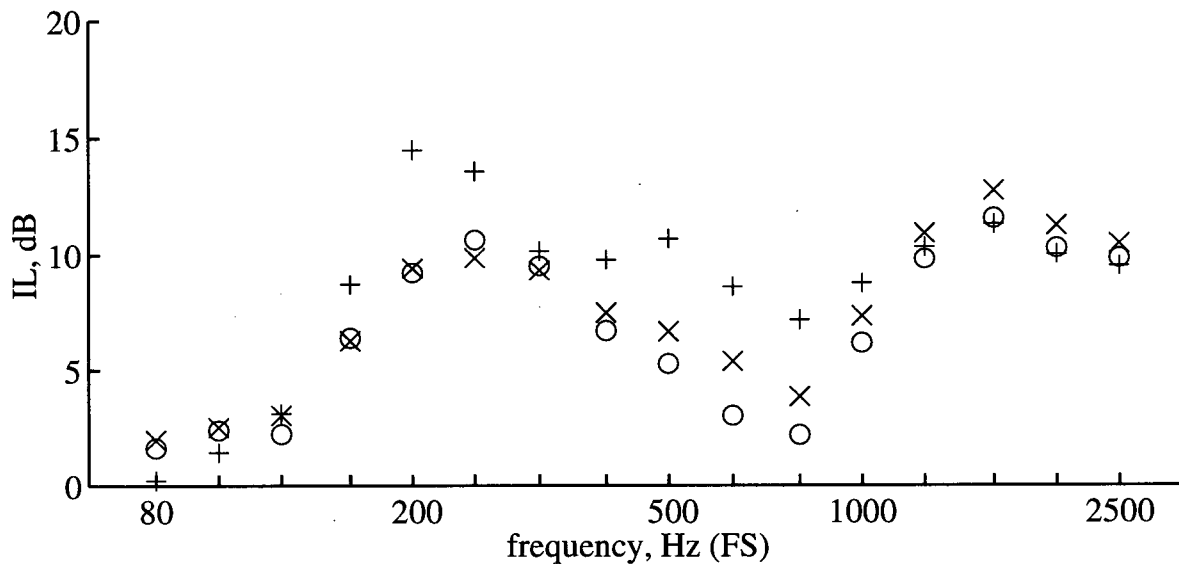


Figure 6.20: Measured third-octave IL s for wedge-shaped berms of 4 m height, with 2:1 slope, covered by dense polystyrene, expanded polystyrene and felt: (o) dense polystyrene wedge(#39), $IL=7.9$, $ILA=5.7$; (x) grass wedge(#9), $IL=8.5$, $ILA=7.2$; (+) felt wedge(#36), $IL=9.9$, $ILA=8.9$.

6.3 Alternative Surface Impedances

6.3.1 Variable Berm Surface Impedance

Figs. 6.19, 6.20 and 6.21 show, for wedge-shaped berms, the variation of IL due to changes in berm surface. For the steeper 1.5:1 berm (Fig. 6.19) the hardening of the berm makes it slightly less effective in most third-octave bands; softening of the berm leads to increased IL s in all but the 80 Hz band. For the 2:1 berm (Fig. 6.20) the hardening of the berm creates small, but noticeable, decreases in IL , particularly across the mid-bands; for the soft felt material the IL s increase strongly at some frequencies, though in the extreme frequency bands they decrease. For the shallower 3:1 berm (Fig. 6.21) the polystyrene "hard ground" produced small decreases in the IL at middle frequencies; however, the felt surface showed substantial increases in IL in the 160–1000 Hz third-octaves. The benefit of softening a berm is more significant for the 3:1 berm.

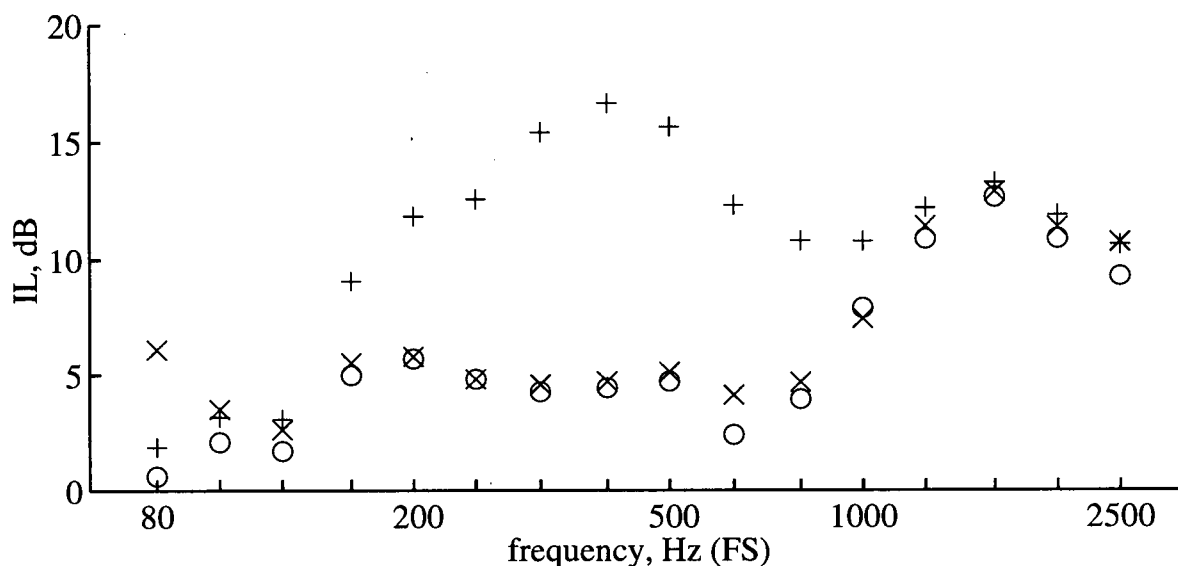


Figure 6.21: Measured third-octave IL s for wedge-shaped berms of 4 m height, with 3:1 slope, covered by dense polystyrene, expanded polystyrene and felt: (o) dense polystyrene wedge(#40), $IL=7.2$, $ILA=6.2$; (x) grass wedge(#10), $IL=7.9$, $ILA=7.0$; (+) felt wedge(#32), $IL=12.3$, $ILA=11.5$.

6.3.2 Variable Berm Slope

Figs. 6.22, 6.2 and 6.23 show how, for 3 different surfaces, variable slope affects barrier IL . For the hard-surfaced berm (Fig. 6.22), the steepest berm outperforms the shallower berms over the 125 to 630 Hz bands. For the grass berm (Fig. 6.2) there is still a general decrease in IL with slope, with the benefit of a steeper berm most clearly seen in the 125 to 315 Hz bands. For the soft-surfaced berm (Fig. 6.23) the 1.5:1 berm matches or outperforms the 2:1 berm in all third-octave bands, while the 3:1 berm has much higher IL s at mid frequencies. This suggests that for extremely soft berms there may be some benefit to making the berm shallower than a 3:1 run-to-rise.

6.3.3 Variable Flat-Top-Berm Surface Impedance with/without a Wall

Figs. 6.24 and 6.25 show how varying a berm's surface has different effects when a crest wall is, or is not, present. IL s of hard-surfaced and felt-surfaced berms were slightly higher than

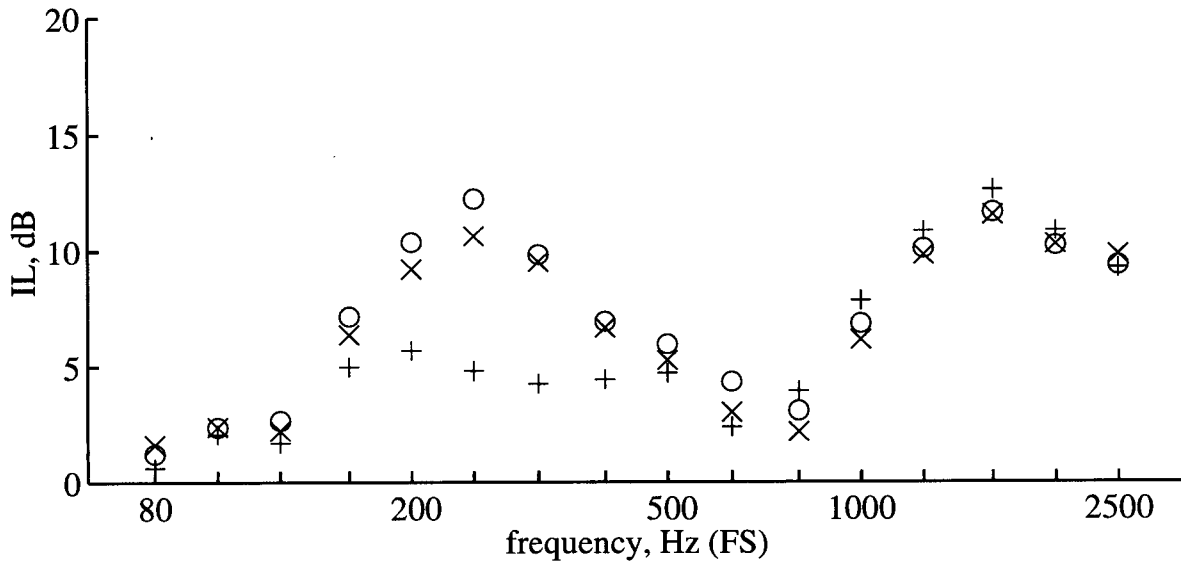


Figure 6.22: Measured third-octave IL s for wedge-shaped berms of 4 m height, covered by dense polystyrene, and with 1.5, 2 and 3:1 slopes: (o) 1.5:1 wedge(#38), $IL=8.4$, $ILA=6.4$; (x) 2:1 wedge(#39), $IL=7.9$, $ILA=5.7$; (+) 3:1 wedge(#40), $IL=7.2$, $ILA=6.2$.

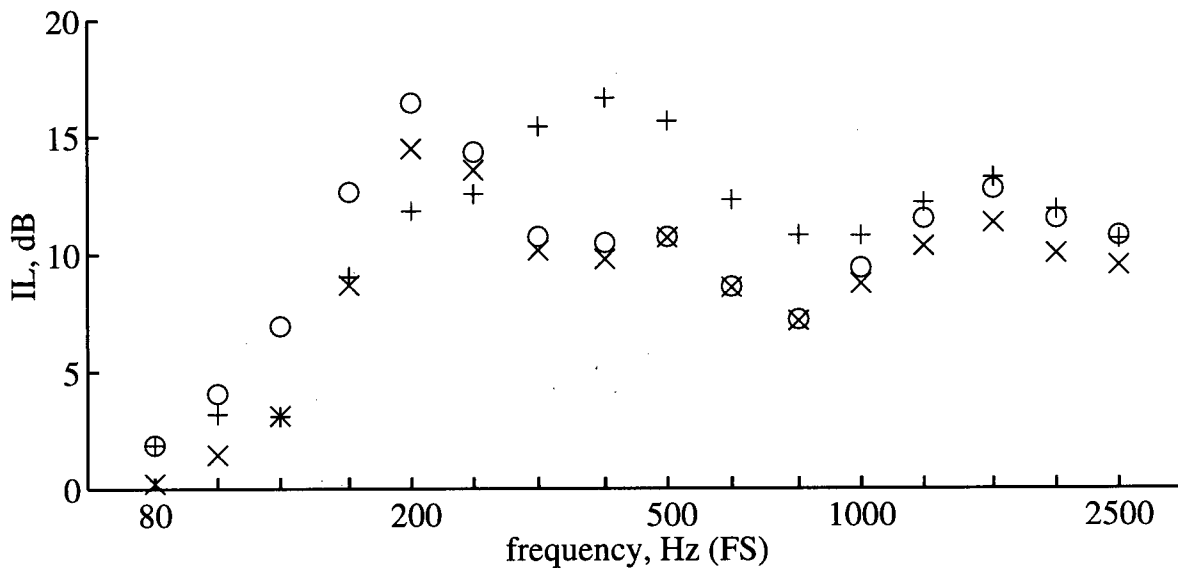


Figure 6.23: Measured third-octave IL s for wedge-shaped berms of 4 m height, covered by felt, and with 1.5, 2 and 3:1 slopes: (o) 1.5:1 wedge(#37), $IL=11.3$, $ILA=9.6$; (x) 2:1 wedge(#36), $IL=9.9$, $ILA=8.9$; (+) 3:1 wedge(#32), $IL=12.3$, $ILA=11.5$.

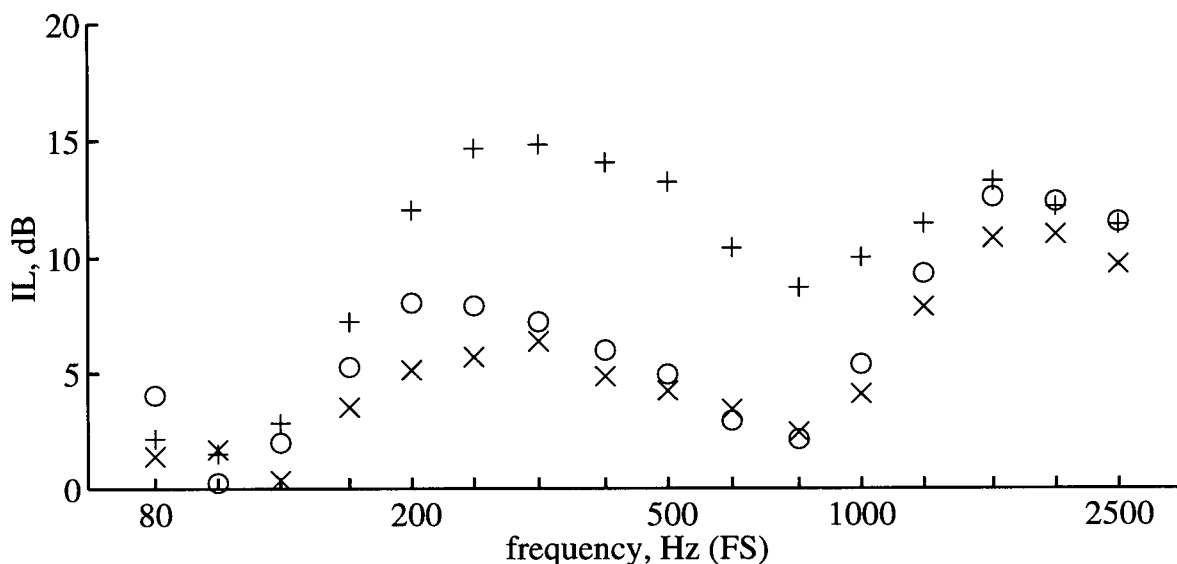


Figure 6.24: Measured third-octave IL s for flat-topped berms of 2 m top width, 3 m height, a fixed 3:1 berm slope, and with surfaces of dense polystyrene, expanded polystyrene and felt: (o) dense polystyrene flat-top(#41), $IL=7.9$, $ILA=5.5$; (x) grass flat-top(#35), $IL=6.4$, $ILA=5.1$; (+) felt flat-top(#33), $IL=11.5$, $ILA=10.4$.

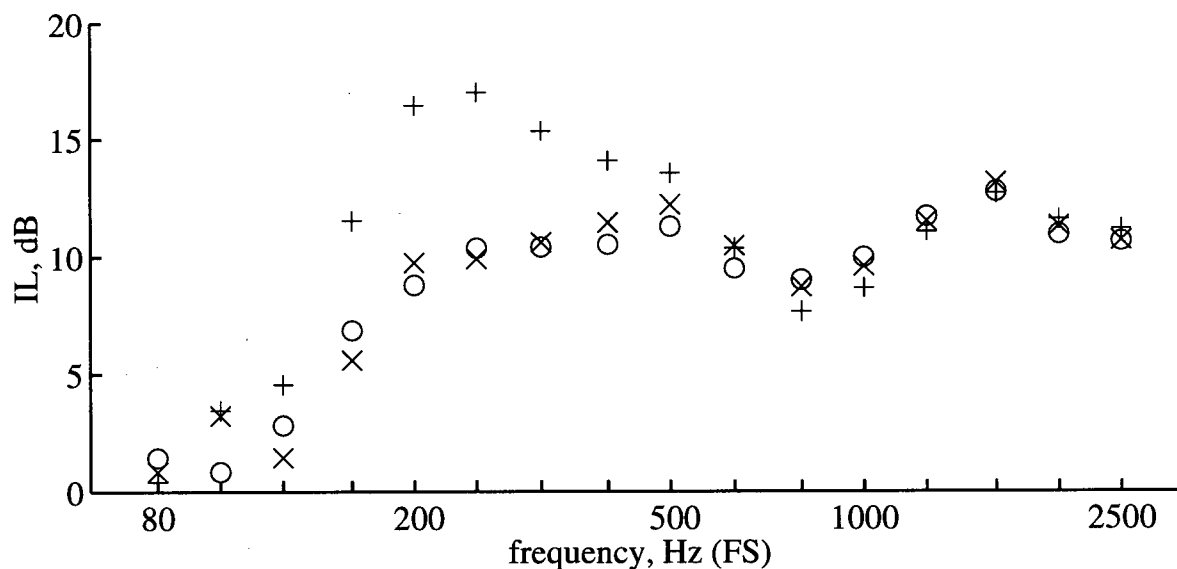


Figure 6.25: Measured third-octave IL s for flat-topped berms of 2 m top width, 3 m height, topped by a 1 m high crest wall, and with surfaces of dense polystyrene, expanded polystyrene and felt: (o) dense polystyrene flat-top with wall(#42), $IL=9.7$, $ILA=10.1$; (x) grass flat-top with wall(#29), $IL=9.9$, $ILA=10.2$; (+) felt flat-top with wall(#34), $IL=12.4$, $ILA=9.9$.

those of the grass-surfaced berm, due perhaps to a small height increase when the materials covered the berm. When the flat-top berm is of 3 m height (Fig. 6.24) the hard-surfaced berm outperforms the grass-surfaced berm; the soft-surfaced berm has much higher IL s at mid frequencies. In Fig. 6.25, with a 1 m wall present, the hard- and grass-surfaced berms perform almost identically; for the felt berm there is still an increase in IL , noticeable in the 160–500 Hz bands. Above this frequency the effect of varying the berm surface in the presence of a wall is lost. For a berm with a soft crest, the addition of a wall may prove to be ineffective; conversely, if a berm has a crest wall, softening the berm's crest will not significantly improve the IL . Examining the third-octave IL s closely, it can be seen that the felt-surfaced berm/wall outperforms the other two surfaces, and actually had the highest IL (17.0 dB) observed for any third-octave.

6.3.4 Variable Berm-Crest-Wall Height

Figs. 6.26, 6.27 and 6.28 show the effect of adding a wall to a 3 m berm with different surfaces. Fig. 6.26, for a hard-surfaced berm, shows significant increases in IL from 250–1250 Hz with the addition of a crest wall. In Fig. 6.27, the results for a grass surface show significant increases in IL from 160–1600 Hz. Finally, in Fig. 6.28, the felt surface shows significant increases in IL from 160–250 Hz, with the IL s in other bands either increasing or decreasing. When a wall was placed on top of the berm, the beneficial effects of adding a wall or altering the berm's surface impedance were not independent of one another.

6.4 Conclusion to Results

Scale-model results generally agree with field tests. A decrease in IL at mid frequencies was observed at both full and model scale due to the pre-berm ground effect. Increased wall thickness was not significant. Increased berm-top width or radius was not significant. As berms became shallower, the IL decreased near the 250 Hz band. As a berm became steeper, the IL increased, becoming more like that of a wall. Walls consistently outperformed earth berms — especially

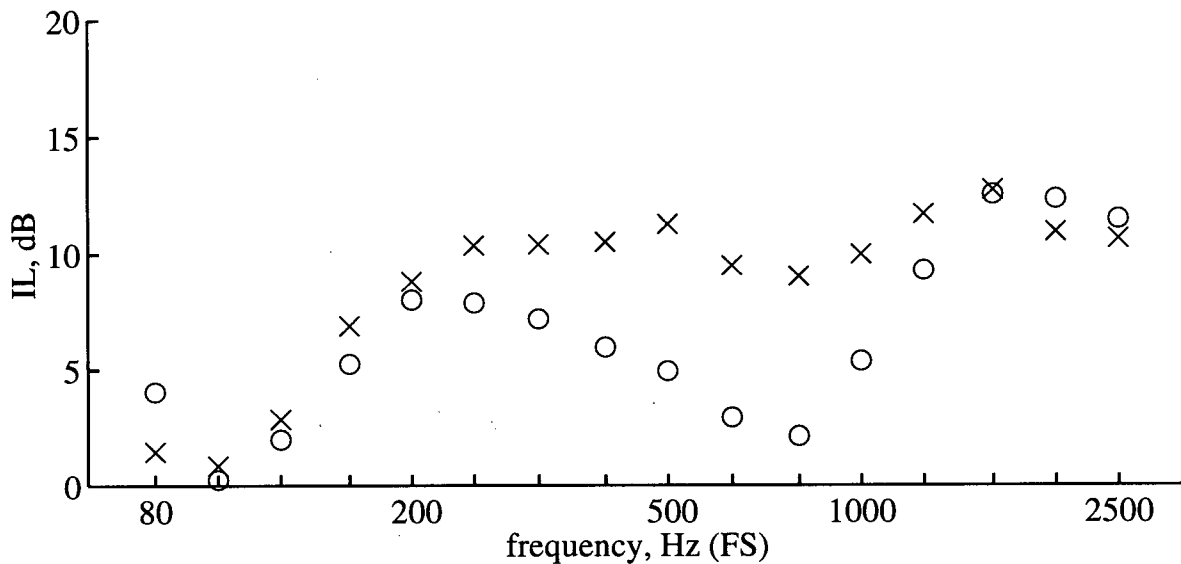


Figure 6.26: Measured third-octave IL s for flat-topped berms of 2 m top width, 3 m height, fixed 3:1 slope, a berm surface of dense polystyrene, and topped with or without a 1 m crest wall: (o) flat-top(#41), $IL=7.9$, $ILA=5.5$; (x) flat-top with wall(#42), $IL=9.7$, $ILA=10.1$.

at low frequencies. For a 1 m berm with a 3 m crest wall, the results were indistinguishable from those for a vertical wall. As a berm's height increased, representing a larger proportion of the total 4 m barrier height, the effect of slope on attenuation was increased. When an berm is combined with a crest wall, the opposite trend was observed for berm slope — shallower berms resulted in increased IL s. The results indicate that a berm/wall combination can be as effective as, or even more effective than, a vertical wall. For a 3 m berm of 3:1 slope, an increase in berm height of 1 m increased the IL in the 630 Hz band and above; if a wall was used to increase the height by 1 m the increases IL over and above that of the berm from 160–1000 Hz. The benefit of softening a berm was more significant for the 3:1 berm than for the steeper berms. When barrier height was increased by placing a wall on top of the berm, the beneficial effects of adding a wall or altering the berm's surface impedance were not independent of one another. For a berm with a soft crest, the addition of a wall may prove to be ineffective; conversely, if a berm has a crest wall, softening the berm's crest will not significantly improve the IL .

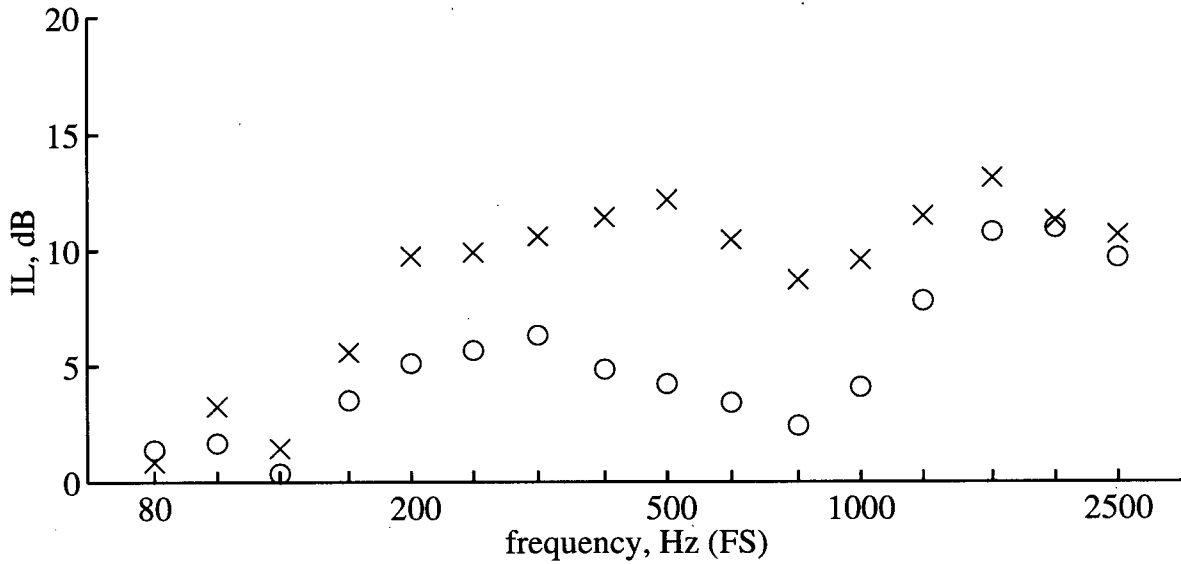


Figure 6.27: Measured third-octave IL s for flat-topped berms of 2 m top width, 3 m height, fixed 3:1 slope, a berm surface of expanded polystyrene, and topped with or without a 1 m crest wall: (o) flat-top(#35), $IL=6.4$, $ILA=5.1$; (x) flat-top with wall(#29), $IL=9.9$, $ILA=10.2$.

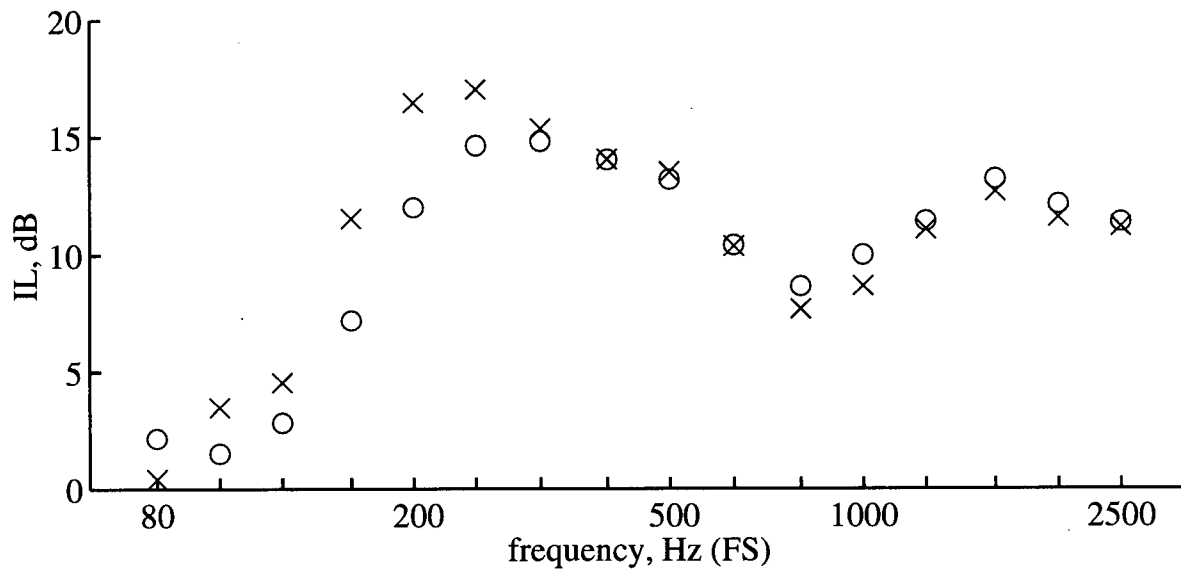


Figure 6.28: Measured third-octave IL s for flat-topped berms of 2 m top width, 3 m height, fixed 3:1 slope, a berm surface of felt, and topped with or without a 1 m crest wall: (o) flat-top(#33), $IL=11.5$, $ILA=10.4$; (x) flat-top with wall(#34), $IL=12.4$, $ILA=9.9$.

Chapter 7

Applications

7.1 Introduction to Applications

To understand how barrier design affects noise-attenuation performance, it is necessary to consider how the traffic-noise spectra and the sensitivity of human hearing affect a barrier's total effective *IL* as perceived by a human listener. When the *IL* of a barrier is energetically averaged over the measured full-scale spectrum, a total *IL* will result; by weighting the sound-pressure levels with an A-weighted traffic-noise spectrum, a weighted *IL* will result, which is referred to as an *ILA*. In this chapter the results of both point-source tests and the line-source barrier tests presented in Chapter 6 are discussed. The literature presented in Chapter 2 is used to support the discussion, reinforce the conclusions and provide guidance for future work.

We begin by summarizing the test results in more practical terms. The results are grouped into two test classes: point-source tests with a source/receiver that was perpendicular to the barrier; and line-source tests with the source traversed along a line parallel to the barrier. For the point-source tests the results have been subdivided in terms of their unweighted and weighted total *ILs*. For the line-source tests the results have been subdivided in terms of their unweighted and weighted total *ILs*. The consequences of applying an A-weighted traffic-noise spectrum were different for the point-source tests than they were for the line-source tests.

For the first, point-source test class the source and receiver were always positioned along a line perpendicular to the barrier. Tests in this category explore how much the unweighted and weighted point-source total *ILs* varied with the horizontal distance between the source and the receiver, using two types of noise barrier. For this class, the differences between total *ILs* at a series of receiver positions were greater for the total *ILA* than for the unweighted total *IL*

Table 7.1: Unweighted Total Insertion Losses versus Distance

Barrier	Source Distance	Receiver Distance							Δ dB
		5 m	10 m	15 m	20 m	25 m	30 m	40 m	
Wall	8.3 m	18.7	17.7	16.6	16.9	17.6	17.1	15.9	2.8
	14.9 m	16.0	14.2	12.2	12.2	13.2	13.4	12.4	3.8
	19.3 m	14.2	13.6	11.5	11.5	11.9	12.3	11.6	2.7
Wedge	8.3 m	-	14.9	13.8	14.9	16.4	15.8	14.4	2.6
	14.9 m	-	10.8	9.6	9.6	11.5	12.0	11.0	2.4
	19.3 m	-	10.0	9.3	9.2	10.2	10.8	9.9	1.6

— the A-weighted traffic-noise spectrum increased the observed changes with distance in the total *ILA*. For the second, line-source test class the source was traversed along line at a fixed distance from the barrier's crest. Tests in this category determined the unweighted and weighted line-source total *ILs* for different types of barrier. For this class, the effect of a single-variable change on the total *IL* was greater for the unweighted total than for the weighted total — the A-weighted traffic-noise spectrum reduced the differences in total *ILA* among noise barriers.

7.2 Scale-Model Results: Point-Source Total *IL* and Total *ILA*

Table 7.1 shows the unweighted total *IL* results at various source and receiver distances (see Fig. 5.38 on page 108). For a given source distance, the total *ILs* of both the wall and the wedge do not decrease monotonically with receiver distance. For the wall, it can be seen that the maximum total *IL* is at the 5 m receiver position, and that the total *IL* typically decreases as receiver distance increases. For the wedge-shaped berm, tests at the 5 m position were precluded by the berm's width; the maximum total *IL* is at the 25 m or 30 m positions. For a given receiver distance, both the wall and the wedge have total *ILs* that decrease as the source distance increases. As can be seen in the right-most column of Table 7.1, for a given source distance, the wall has a greater range of total *IL* than does the wedge. For each source/receiver position the wall produced higher total *ILs* than the berm, with the least increase being 1.2 dB.

Table 7.2 shows the weighted total *ILA* results at various distances. For a given source

Table 7.2: Weighted Total Insertion Losses versus Distance

Barrier	Source Distance	Receiver Distance							Δ dB
		5 m	10 m	15 m	20 m	25 m	30 m	40 m	
Wall	8.3 m	19.1	16.5	14.6	14.2	12.1	10.7	9.0	10.1
	14.9 m	14.9	12.5	11.1	9.5	10.0	10.6	8.6	6.3
	19.3 m	14.1	12.2	10.7	9.8	8.3	9.5	8.3	5.8
Wedge	8.3 m	-	13.3	12.2	11.5	9.4	7.2	5.7	7.6
	14.9 m	-	8.9	9.3	7.4	7.1	7.3	5.8	3.1
	19.3 m	-	8.3	8.6	6.9	6.0	5.9	5.3	3.3

distance, the total *ILAs* of both the wall and the wedge do not decrease monotonically with distance. For the wall, it can be seen that the maximum total *ILA* is at the 5 m receiver position, and the total *ILA* typically decreases as receiver distance increases. For the wedge, the slope again precluded making tests at 5 m, and the maximum total *ILA* is at the 10 m or 15 m positions. For a given receiver distance, the total *ILAs* of both the wall and the wedge do not decrease monotonically as the source distance increases. As can be seen in the right-most column of Table 7.2, for a given source distance, the wall has a greater range of total *ILA* than does the wedge. For each source/receiver position the wall produced higher total *ILAs* than the berm, with the smallest advantage being 1.8 dBA.

The total *ILA* is typically less than the total *IL* — this applies to both the wall and the earth-berm barrier. As an example, for the wall, at a source distance of 8.3 m and a receiver distance of 30 m, the total *IL* (Table 7.1) is 17.1 dB, while the total *ILA* is 10.7 dBA (Table 7.2). Considering the right-most column (denoted Δ dB) of each table, the total *ILAs* decrease much more with increasing receiver distance than do the total *ILs*.

7.3 Scale-Model Results: Line-Source Total *IL* and Total *ILA*

The total unweighted and weighted *ILs* of the barriers (walls and earth berms) as compared in Figs. 6.1 through 6.12, are seen in Table 7.3. The columns are described by their file number, barrier geometry, height (berm/wall) *H*, top width *W*, top radius *R*, wall thickness *T* and berm

Table 7.3: Total *ILs/ILAs* of Scale-Model Barriers: Walls and Earth Berms

File #	Description	H	W	R	T	K	Z	IL	ILA	STD
5	Wall	0/4 m			5 cm			10.0	9.2	2.1
6	Wall	0/4 m			10 cm			10.3	9.1	1.9
7	Wall	0/4 m			15 cm			10.4	9.0	2.0
8	Wedge	4/0 m				1.5	EP	9.0	7.0	1.9
9	Wedge	4/0 m				2	EP	8.5	7.2	1.9
10	Wedge	4/0 m				3	EP	7.9	7.0	2.1
11	Flat	4/0 m	1 m			1.5	EP	9.2	8.0	1.9
12	Flat	4/0 m	1 m			2	EP	8.8	7.8	1.8
13	Flat	4/0 m	1 m			3	EP	7.8	7.3	1.9
14	Flat	4/0 m	2 m			1.5	EP	9.0	7.7	1.7
15	Flat	4/0 m	2 m			2	EP	8.1	7.1	1.7
16	Flat	4/0 m	2 m			3	EP	7.8	7.4	1.9
17	Round	4/0 m		1 m		1.5	EP	8.9	7.3	2.1
18	Round	4/0 m		1 m		2	EP	8.5	7.2	1.9
19	Round	4/0 m		1 m		3	EP	7.5	7.2	1.9
20	Round	4/0 m		2 m		1.5	EP	8.9	7.4	2.0
21	Round	4/0 m		2 m		2	EP	9.0	7.8	2.0
22	Round	4/0 m		2 m		3	EP	7.7	7.8	1.8
8	Wedge	4/0 m				1.5	EP	9.0	7.0	1.9
11	Flat	4/0 m	1 m			1.5	EP	9.2	8.0	1.9
14	Flat	4/0 m	2 m			1.5	EP	9.0	7.7	1.7
9	Wedge	4/0 m				2	EP	8.5	7.2	1.9
12	Flat	4/0 m	1 m			2	EP	8.8	7.8	1.8
15	Flat	4/0 m	2 m			2	EP	8.1	7.1	1.7
10	Wedge	4/0 m				3	EP	7.9	7.0	2.1
13	Flat	4/0 m	1 m			3	EP	7.8	7.3	1.9
16	Flat	4/0 m	2 m			3	EP	7.8	7.4	1.9
8	Wedge	4/0 m				1.5	EP	9.0	7.0	1.9
17	Round	4/0 m		1 m		1.5	EP	8.9	7.3	2.1
20	Round	4/0 m		2 m		1.5	EP	8.9	7.4	2.0
9	Wedge	4/0 m				2	EP	8.5	7.2	1.9
18	Round	4/0 m		1 m		2	EP	8.5	7.2	1.9
21	Round	4/0 m		2 m		2	EP	9.0	7.8	2.0
10	Wedge	4/0 m				3	EP	7.9	7.0	2.1
19	Round	4/0 m		1 m		3	EP	7.5	7.2	1.9
22	Round	4/0 m		2 m		3	EP	7.7	7.8	1.8

surface Z . As well, the total IL and ILA are listed for each barrier, along with the STD of the measurement. The total ILA of a barrier was typically less than its total IL . It was observed, when calculating the STD of a noise barrier that it was typical for approximately 60% of the variance to come from the open-ground tests of sound-pressure level, with 40% coming from the with-barrier tests. Referring to Fig. 4.1 on page 62 it should be noted that no error was reported for the tests of traffic-noise spectra, and that the calculated A-weighting values are essentially error free. The rows of Tables 7.3, 7.4 and 7.5 are grouped in clusters of three (and sometimes two) barriers, based on the sequence of appearance of the figures in Chapter 6. The total unweighted and weighted ILs of the barriers (earth berms crested by walls) compared in Figs. 6.13 through 6.18, can be seen in Table 7.4. The total unweighted and weighted ILs of the barriers with alternative surface impedances as previously compared in Figs. 6.19 through 6.28, can be seen in Table 7.5.

The results of scale-model measurements of total IL/ILA for scale-model walls and earth berms (Table 7.3) will now be discussed. Increased wall thickness was not found to be significant. Walls were found to outperform earth berms, with the total ILA improved by about 2 dBA. The total IL decreased as berm slope became shallower — though the total ILA was not strongly affected, since the weighting procedure reduced the importance of the low-frequency, third-octave differences between barriers. The range of total $ILAs$ with decreasing berm slope are 0.4, 0.6, and 2.4 dBA. As a berm became steeper, the total IL increased, becoming more like that of a wall. The average difference between the total $ILAs$ of wedge-tops of a given slope and all other total $ILAs$ of a given slope is 0.6 dBA for 1.5:1 berms, 0.3 dBA for 2:1 berms, and 0.4 dBA for 3:1 berms. Increased berm-top width or radius was not significant: increases in top width, from a wedge to a flat-top of 1 m or 2 m width, produced at most a 1 dBA change in berm performance; increases in top radius lead to a maximum increase in total ILA of 0.6 dBA.

What about the effect of adding a crest wall to a berm, and the further effect of varying berm parameters in the presence of a crest wall (Table 7.4)? For a 1 m berm crested with a

Table 7.4: Total *ILs/ILAs* of Scale-Model Barriers: Berms with Crest Walls

File #	Description	<i>H</i>	<i>W</i>	<i>R</i>	<i>T</i>	<i>K</i>	<i>Z</i>	<i>IL</i>	<i>ILA</i>	<i>STD</i>
23	Flat/Wall	3/1 m	2 m		10 cm	1.5	EP	10.1	8.9	2.1
24	Flat/Wall	2/2 m	2 m		10 cm	1.5	EP	10.5	8.6	2.1
25(6)	Flat/Wall	1/3 m	2 m		10 cm	1.5	EP	(10.3)	(9.1)	(1.9)
26	Flat/Wall	3/1 m	2 m		10 cm	2	EP	10.2	9.1	2.1
27	Flat/Wall	2/2 m	2 m		10 cm	2	EP	10.5	8.5	2.1
28(6)	Flat/Wall	1/3 m	2 m		10 cm	2	EP	(10.3)	(9.1)	(1.9)
29	Flat/Wall	3/1 m	2 m		10 cm	3	EP	9.9	10.2	2.0
30	Flat/Wall	2/2 m	2 m		10 cm	3	EP	10.2	7.8	2.3
31(6)	Flat/Wall	1/3 m	2 m		10 cm	3	EP	(10.3)	(9.1)	(1.9)
24	Flat/Wall	2/2 m	2 m		10 cm	1.5	EP	10.5	8.6	2.1
27	Flat/Wall	2/2 m	2 m		10 cm	2	EP	10.5	8.5	2.1
30	Flat/Wall	2/2 m	2 m		10 cm	3	EP	10.2	7.8	2.3
23	Flat/Wall	3/1 m	2 m		10 cm	1.5	EP	10.1	8.9	2.1
26	Flat/Wall	3/1 m	2 m		10 cm	2	EP	10.2	9.1	2.1
29	Flat/Wall	3/1 m	2 m		10 cm	3	EP	9.9	10.2	2.0
35	Flat	3/0 m	2 m			3	EP	6.4	5.1	1.9
16	Flat	4/0 m	2 m			3	EP	7.8	7.4	1.9
29	Flat/Wall	3/1 m	2 m		10 cm	3	EP	9.9	10.2	2.0

3 m wall, the results were indistinguishable from those for a vertical wall. As a berm's height increased, representing a larger proportion of the total 4 m barrier height, the effect of slope on attenuation was more evident. As well, as the berm becomes shallower the impact of varying the crest-wall height becomes more significant. Shallow 3:1 earth berms (with a crest wall) increased the total *ILAs* so that they are as high as, or higher than, those for a pure wall — this advantage may not extend to the 1.5 or 2:1 sloped berms. It might be possible to tune the slope of the earth berm, when a crest wall is present, in order to take improve the total *ILA* — consider as evidence the 3 m height earth berm topped by a 1 m wall, where total *ILAs* increased from 8.9 to 9.1 and finally to 10.2 dBA. Considering the total *ILA*, the results indicate that a berm/wall combination can be as effective, or even up to 1 dBA more effective, than a vertical wall. The maximum total *ILA* among grass-covered berm/walls is 10.2 dBA —

for the 3:1 berm of 3 m height with a 1 m crest wall — while the highest total *ILA* of the walls tested was 9.2 dBA. It was more beneficial to increase barrier height by adding a 1 m wall to the top of a 3 m berm (total *ILA* increased by 5.1 dBA), than it was to increase the barrier height using a 4 m berm (total *ILA* increased by 2.3 dBA).

How did changes to the surface impedance of a barrier (Table 7.5) affect its noise-attenuating performance? The softening of an earth berm's surface produced substantial improvements in the earth berm's total *ILA* — the softer the berm the higher the *ILA*, with the benefit being more dramatic for the shallowest (3:1) berm slope. The increase in total *ILA* due to felt as compared to dense polystyrene for berm slopes of 1.5, 2, and 3:1 was, respectively, 3.2, 3.2, and 5.3 dBA. However, the influence of slope was not clear for the barriers with alternative surface impedances — for earth berms of 1.5 and 2:1 slope, a softer surface increases the total *ILA* over that of a hard-surface berm by about 3 dBA; for berms of 3:1 slope the advantage is about 5 dBA. However, when a wall was present the benefits of softer berm slope were not as substantial. With a wall in place, the three surfaces give similar total *ILAs* of about 10 dBA. When adding 1 m of height to a 3 m flat-top berm, it was observed that the effects of adding a wall or softening the earth berm's surfaces were not independent of one another. In this case, for hard ground and grass, a wall is beneficial and increases *ILAs* by 4.6 and 5.1 dBA, respectively; the addition of a wall to a 3 m high soft flat-top berm actually decreased the *ILA* by 0.5 dBA. For a berm with a soft crest, the addition of a wall may prove to be ineffective; conversely, if a berm has a crest wall, softening the berm's crest will not significantly improve the *ILA*. As an observation, it should be noted that if the scale-model grass material needed to be softer to correctly represent an earth berm surface, then the 2 dBA advantage of a wall over a berm has been exaggerated. This is not to say that the soft-top assumption is correct, only that the differences in total *ILAs* would be reduced for the results reported in this work.

The contents of Tables 7.3, 7.4 and 7.5 can be summarized in terms of the ranges of total *IL* (ΔIL) and *ILA* (ΔILA) that were observed for each variable (e.g. wall thickness). In Table 7.6 each row contains the file numbers that were compared, the parameter in question,

Table 7.5: Total *ILs/ILAs* of Scale-Model Barriers: Alternative Surface *Z*

File #	Description	<i>H</i>	<i>W</i>	<i>R</i>	<i>T</i>	<i>K</i>	<i>Z</i>	<i>IL</i>	<i>ILA</i>	<i>STD</i>
38	Wedge	4/0 m				1.5	P	8.4	6.4	2.0
8	Berm	4/0 m				1.5	EP	9.0	7.0	1.9
37	Wedge	4/0 m				1.5	F	11.3	9.6	1.7
39	Wedge	4/0 m				2	P	7.9	5.7	1.9
9	Berm	4/0 m				2	EP	8.5	7.2	1.9
36	Wedge	4/0 m				2	F	9.9	8.9	1.8
40	Wedge	4/0 m				3	P	7.2	6.2	2.0
10	Berm	4/0 m				3	EP	7.9	7.0	2.1
32	Wedge	4/0 m				3	F	12.3	11.5	2.2
38	Wedge	4/0 m				1.5	P	8.4	6.4	2.0
39	Wedge	4/0 m				2	P	7.9	5.7	1.9
40	Wedge	4/0 m				3	P	7.2	6.2	2.0
37	Wedge	4/0 m				1.5	F	11.3	9.6	1.7
36	Wedge	4/0 m				2	F	9.9	8.9	1.8
32	Wedge	4/0 m				3	F	12.3	11.5	2.2
41	Flat	3/0 m	2 m			3	P	7.9	5.5	1.9
35	Flat	3/0 m	2 m			3	EP	6.4	5.1	1.9
33	Flat	3/0 m	2 m			3	F	11.5	10.4	1.8
42	Flat/Wall	3/1 m	2 m		10 cm	3	P	9.7	10.1	2.0
29	Flat/Wall	3/1 m	2 m		10 cm	3	EP	9.9	10.2	2.0
34	Flat/Wall	3/1 m	2 m		10 cm	3	F	12.4	9.9	1.8
41	Flat	3/0 m	2 m			3	P	7.9	5.5	1.9
42	Flat/Wall	3/1 m	2 m		10 cm	3	P	9.7	10.1	2.0
35	Flat	3/0 m	2 m			3	EP	6.4	5.1	1.9
29	Flat/Wall	3/1 m	2 m		10 cm	3	EP	9.9	10.2	2.0
33	Flat	3/0 m	2 m			3	F	11.5	10.4	1.8
34	Flat/Wall	3/1 m	2 m		10 cm	3	F	12.4	9.9	1.8

Table 7.6: Range of Scale-Model Barrier Total *ILs/ILAs*

File #s	Barrier Type(s)	Parameter	Values	ΔIL	ΔILA
050607	Wall	<i>T</i>	5, 10, 15 cm	0.4	0.2
080910	Wedge	<i>K</i>	1.5, 2, 3	1.1	0.2
111213	Flat-Top (1m)	<i>K</i>	1.5, 2, 3	1.4	0.7
141516	Flat-Top (2m)	<i>K</i>	1.5, 2, 3	1.2	0.6
171819	Round-Top (1m)	<i>K</i>	1.5, 2, 3	1.4	0.1
202122	Round-Top (2m)	<i>K</i>	1.5, 2, 3	1.3	0.4
081114	1.5:1 Berm-Top	<i>W</i>	0, 1, 2 m	0.2	1.0
091215	2:1 Berm-Top	<i>W</i>	0, 1, 2 m	0.7	0.7
101316	3:1 Berm-Top	<i>W</i>	0, 1, 2 m	0.1	0.4
081720	1.5:1 Berm-Top	<i>R</i>	0, 1, 2 m	0.1	0.4
091821	2:1 Berm-Top	<i>R</i>	0, 1, 2 m	0.5	0.6
101922	3:1 Berm-Top	<i>R</i>	0, 1, 2 m	0.4	0.8
232425	1.5:1 Flat-Top Berm/Wall	<i>H</i>	1/3, 2/2, 3/1 m	0.4	0.5
262728	2:1 Flat-Top Berm/Wall	<i>H</i>	1/3, 2/2, 3/1 m	0.3	0.6
293031	3:1 Flat-Top Berm/Wall	<i>H</i>	1/3, 2/2, 3/1 m	0.4	2.4
252831(050607)	1/3 m Flat-Top Berm/Wall	<i>K</i>	1.5, 2, 3	0.4	0.2
242730	2/2 m Flat-Top Berm/Wall	<i>K</i>	1.5, 2, 3	0.3	0.8
232629	3/1 m Flat-Top Berm/Wall	<i>K</i>	1.5, 2, 3	0.3	1.3
351629	Berm and/or Wall	<i>H</i>	3/0 4/0 3/1 m	3.5	5.1
380837	1.5:1 Wedge	<i>Z</i>	P, EP, F	2.9	3.2
390936	2:1 Wedge	<i>Z</i>	P, EP, F	2.0	3.2
401032	3:1 Wedge	<i>Z</i>	P, EP, F	5.1	5.3
383940	P Wedge	<i>K</i>	1.5, 2, 3	1.2	0.7
see 080910	EP Wedge	<i>K</i>	1.5, 2, 3	1.1	0.2
373632	F Wedge	<i>K</i>	1.5, 2, 3	2.4	2.6
413533	3:1 3m high Flat-Top	<i>Z</i>	P, EP, F	5.1	5.3
422934	3:1 3/1 m Flat-Top/Wall	<i>Z</i>	P, EP, F	2.7	0.3
4142	3 m P Berm Crest-Wall	<i>H</i>	0, 1 m	1.8	4.6
3529	3 m EP Berm Crest-Wall	<i>H</i>	0, 1 m	3.5	5.1
3334	3 m F Berm Crest-Wall	<i>H</i>	0, 1 m	0.9	0.5

the values assigned to that parameter, and the ranges of total IL and total ILA . From this information the significance to barrier attenuation of changing the value of a barrier parameter can be assessed.

By referring to Table 7.6 the significance can be established of varying wall thickness T , berm slope K , berm-top width W , berm-top radius R , barrier height H , and surface impedance Z . What constitutes a significant variable? For the following discussion of total ILA (and to a lesser extent the total IL), a four-tier hierarchy will be used to rate the significance. Listed from most significant to least significant, the tiers are defined by changes in the total ILA such that: $\Delta ILA \geq 4$; $\Delta ILA \geq 2$; and $\Delta ILA \geq 1$. Barriers for which $\Delta ILA < 1$ will not be discussed except in contrast to values of ΔIL for the same barrier. In application, this information will enhance the ability of the noise-barrier designer to specify, for a given barrier configuration, reliable recommendations for steps to improve the barrier's attenuation.

Changes to the surface impedance of a barrier produced the most significant variations in total ILA . The 3:1 wedge of 4 m height has a ΔILA range of 5.3 dBA. The 3:1 flat-top berm of 3 m height has a range of $\Delta ILA = 5.3$ dBA. The 1.5 and 2:1 sloped wedges of 4 m height have a range of $\Delta ILA = 3.2$ dBA. Thus, berms experienced large changes in ILA when different surface impedances were used — the acoustically softer the berm, the more effective it is. Softening an earth berm's surface produces substantial improvements in the noise-attenuation performance. The softer the berm, the higher the ILA , with the benefit being greatest for the shallowest (3:1) berm slope.

Height changes were significant. A 3 m grass-covered flat-top, with the height increased either by increasing berm height to 4 m or by adding a 1 m crest wall, had a range of $\Delta ILA = 5.1$ dBA. For a polystyrene-surfaced flat-top of 3 m height, the addition of a 1 m wall produced a $\Delta ILA = 5.1$ dBA range. The benefit of adding a 1 m wall was greater than increasing flat-top height by 1 m. The grass-covered 2 m wide flat-top berm of 3:1 slope had a range of $\Delta ILA = 2.4$ dBA when the proportion of total barrier height due to the berm was varied. Based on the scale-model results increases in height have a more broadband benefit than did

changes to slope.

Changes to a berm's slope proved to be significant for two of the sets of compared parameters. A felt-covered wedge of 4 m height had a $\Delta ILA = 2.6$ dBA range when the slope was varied. The 2 m wide flat-top berm of 3 m height when crested with a 1 m wall, had a $\Delta ILA = 1.3$ dBA range when the berm's slope was varied. None of the other barrier types was affected as significantly by variations in slope.

The last parameter of significance was top width. Variations in the top profile of the earth berm, from a wedge to a flat-top of 1 or 2 m width, produced at most a 1 dBA change in berm performance. When a 1.5:1 flat-top berm was assigned different top widths it had a $\Delta ILA = 1.0$. Increased top-width is typically used to increase the effective height of the barrier and to allow for the addition of absorptive material on the barrier's top.

What then is the significance of ΔIL ? Some barriers had significant levels of change in their ΔILA , but with insignificant ΔILs , or visa versa. When the surface impedance of the 3:1 sloped, 2 m wide, flat-top berm of 3 m height, with a 1 m crest wall, was varied, it had a range of $\Delta IL = 2.7$ dB, but an insignificant ΔILA . A number of the cases involving changes of slope had significant ΔILs , but insignificant $\Delta ILAs$. This was the case for all the grass-covered berms, as well as for the hard-surfaced berms.

7.3.1 Comparison to Field Tests

Referring back to Fig. 4.3 on page 67, showing the results for the field tests, it can be seen that the ILs at locations C and D were measured in the shadow zone of a noise barrier. The effect of changing the receiver's proximity to the noise barrier can be found by comparing the IL results at locations C and D for a given barrier. For two of the barriers, it can generally be seen that the closer a receiver is to a barrier, the higher is the IL. Only one of the barrier configurations — the August 3 McKenzie berm — exhibits a distinctive dip in its third-octave-band IL spectrum. At location C this was measured and found to be in the 800 Hz band; at location D it was in the 630 Hz band. The McKenzie bark-mulch-covered berm, which was

the tallest and steepest of the three field-tested berms, had the highest ILs at locations C and D. The Baxter Park grass-covered berm, which is almost as high as the McKenzie berm, had third-octave ILs that were anywhere from 0–10 dB lower at location C. The Delta sand-covered berm, which was lower and shallower than either of the other berms, had third-octave-band ILs at location C that were generally 5 dB less than for the Baxter Park berm, and up to 15 dB less than for the McKenzie berm. At location D, the third-octave ILs were anywhere from 4–20 dB lower. Berm profile had a substantial impact on measured third-octave ILs, but it was not possible to control the tests strictly to allow for an assessment of the impact of single-variable changes in barrier height, slope or surface. Effective flow resistivities are not known for either the three field-tested berms or for their open-ground reference locations. As such, it can only be said that the results of the full-scale tests do not contradict the conclusions reached from the scale-model tests. A decrease in third-octave *IL* at mid frequencies was observed at both full and model scale due, presumably, to the pre-berm ground effect.

7.4 Discussion of Total *IL* and Total *ILA* Results

For each of the open-ground, source-receiver locations along the scale-model highway, the *EAs* displayed their highest attenuation near the same frequency. As such, even after integrating the point-source results together to get a line-source *IL*, a characteristic minimum remained in the 800 Hz band. For the full-scale tests, factors like irregular ground, variable traffic flow, and atmospheric inhomogeneities were present, hindering the existence of destructive interference, so that this dip was not evident for two of the three outdoor-test configurations. These bands are not close to the peak 1000 Hz band found in the A-weighted traffic-noise spectrum. Thus, the effect of weighting the total *IL* is to reduce the significance of low-frequency differences in barrier *IL*. The closeness of this “ground effect” to the dominant 1000 Hz third-octave band in the A-weighted traffic-noise spectrum, suggests that the benefits of noise barriers could be substantially affected by future changes in the traffic-noise spectrum found at a noise-barrier site. Electric vehicles could conceivably effect such a change; but, in terms of highways, this

would not obviate the need to consider vehicle noise, since tire noise is the dominant noise component at highway speeds.

The literature review revealed that successful comparisons of full-scale measurements to theory and/or scale modelling are rare [79], [87], [100]. What the literature did tell us is how the features of a barrier affect its noise attenuation. One area of concern is the surface impedance of the ground before a barrier is put into place. A barrier is most effective when ground attenuation is low [79] — the effectiveness of a barrier would be overestimated if a highly-reflective ground surface was to be employed. The *IL* of a barrier is significantly reduced when open-ground tests are made over model grass surfaces — with asphalt on both sides of the barrier, a noise barrier increased the attenuation over and above the ground attenuation, but mostly at lower frequencies below about 800 Hz [107]. Interference phenomena were more evident when a barrier is placed on model-asphalt ground [108]. When a barrier blocks paths of reflection that allowed for destructive interference at certain frequencies, the barrier's *IL* can exhibit minima at these same frequencies [108]. The topography of the pre-barrier ground can also be significant. Single changes of slope created interference effects even when the source and receiver were both on the ground [116]. Sinusoidally-shaped bumps discouraged interference, thus leading to increased sound-pressure levels [116]. Over model-grass ground, an earth berm with a wall reintroduced destructive interference, increasing the *IL* in frequency bands where the barrier had blocked the pre-barrier paths of ground reflection [108].

How do atmospheric phenomena affect the *IL*? Traffic noise levels have not been shown to be immune to the effects of atmospheric phenomena even at a distance of only 38.1 metres [10]. Next to air absorption, temperature and wind variations provide the most significant atmospheric inhomogeneities due to their refractive effects [17]. Higher frequencies (e.g. 1000Hz) are more susceptible to downward refraction than are lower frequencies (e.g. 100Hz); furthermore, the effects are more significant as a receiver moves away from the barrier [84], [105], [106]. Meteorological and ground effects have their greatest effect on barrier attenuation in different frequency bands [87].

Are there many examples of noise-barrier studies that employed line sources? A line source was simulated using scale-model vehicles to scatter noise from a stationary spark source [82]. Keller's geometrical theory of diffraction was compared to scale-model tests using a traversing point source, with satisfactory agreement between prediction and measurement [74].

How does slope affect berm performance? Shallower wedges of a constant 3 m height had progressively lower *ILs*; walls were 1 dB better than a flat-topped grass mound, 3 dB better than a 127° internal-angled wedge, and were approximately as effective as a semi-circular barrier topped by a wall [101].

Have many authors compared walls to berms? Predictions show that, in a free-field, walls outperform three-sided trapezoids by 1–3 dBA [83]. Thin walls of 3 m height outperformed earth berms by about 1 dBA; the addition of a thin wall to the top of a berm increased its *IL* in proportion to the wall height; if the berm top was made highly absorptive, such that it outperformed the grass berm by 3 dBA, the addition of a wall reduced the *IL*, such that a wall height of at least 1.2 m was necessary to restore the lost *IL* [109]. The presence of slopes towards the crest of the barrier are detrimental to *IL*; Y and arrow profiles are generally inferior to a T-shaped barrier; when controlling for effective height, width increases to a top had little effect, and arrow and T-profiled barriers outperformed their wedge and flat-topped mound counterparts by 1–2 dB [81]. The performance of T-shaped, semi-circular, and wedge-shaped barriers on reflective ground were compared with that of a vertical wall and found to be, respectively, 1.9 dBA more effective, 1.4 dBA less effective and 2.6 dBA less effective [85].

Are surface waves important to consider? Perhaps. Experience with the scale-model reveals that the effect of steeper slopes on *IL* is confined to lower frequencies. For shallower berms additional low-frequency wave components were thought to reach the receiver side of the berm, thus compromising the *IL*. This may be due to surface waves. For the scale-model berm experiments, it is thought that a surface-wave component propagated over the shallow berms, at frequencies where the radius of curvature is much larger than the wavelength. Currently, [41] provides the most lucid discussion of surface waves. If surface waves meet an impedance

discontinuity along a surface they will be partly reflected and partly transmitted, depending on the nature of the discontinuity. Surface waves are partly reflected by surface obstacles, and they can be contained by proper design of surface structures. Other factors can predominate over curved terrain, such as creeping waves and shedding.

Do changes in the source/receiver geometry affect the magnitude of noise-barrier attenuation? Yes. If the only waves reaching a receiver point are spherically diverging waves, the pressure measured at a receiver will display interference effects, which are strongly dependent upon the source/receiver geometry and surface impedance. Do the relative rankings of barrier attenuation vary significantly when the locations of the source, receiver, and/or barrier are changed? Not necessarily. There is no direct way of predicting the acoustic pressure at more distant receiver positions since the interference-field over the surface will change. At larger setback distances, low-frequency traffic-noise components gradually become more prevalent, since an associated aspect of the ground effect is to low-pass filter the spectra, such that the cut-off frequency decreases with increasing distance. For a point source, surface waves attenuate at 3 dB/dd rather than at the 6 dB/dd rate of decrease experienced by spherical waves. This means that, in principle, surface waves can contribute a progressively greater fraction of the sound energy at greater distances than do waves that diverge spherically. Can the results of the tests at one receiver distance be extrapolated to justify reductions in sound-pressure level at greater receiver distances? In particular, is there a benefit to having a steeper berm that is effective in the 250 Hz third-octave band, and as such, is there superior low-frequency performance for a steeper berm? The benefit of steeper slopes is to reduce the transmission of source-side surface waves to the receiver side of the barrier. A barrier without approach slopes, like a wall or T-shaped barrier, would be expected to transmit very little surface-wave energy; while a barrier with approach slopes, like a wedge, might allow surface waves to reach the barrier crest, at which point they could themselves be diffracted. By extension, over a smooth-topped barrier, one would expect even more surface-wave energy to reach the receiver side via diffraction or by ducting along the surface. Thus, it might be correct to assert that the performance of a

barrier in the 250 Hz band can become progressively more important as distance increases. Creeping waves are waves that are generated by spherical waves at a discontinuity like a berm crest; in some sense they could be argued to be the diffracted component that travels along the receiver-side surface. A question then arises, can surface waves generate creeping waves?

What about vegetation? Vegetation that blocks the line-of-sight will provide attenuations of 0.4 dBA/ft if the band of foliage is sufficiently thin, but as the band thickness increases the average rate drops towards 0.1 dBA/ft [102]. High-frequency (4 and 8 kHz third-octave) attenuations of 0.1 dB/m in a pine-tree plantation were reported [103]. 0.1 dBA/m over a 100 m distance through a pine forest was reported [104].

How can the attenuation of a barrier be improved upon? At large receiver distances, depressed roads were more effective than barriers of equal height, with the reverse conclusion at short receiver distances [86]. Increases in barrier top width were beneficial in all cases; a T-shaped wall on a berm was among the most effective profiles [108]. Reflections between parallel barriers degrade the *ILs* of each wall, but adding surface absorption to the barrier offsets this [96]. Controlled full-scale tests of T-shaped, multiple-edge and double barriers of 2 m height were compared; these modified barriers were noted to be 1.4–3.6 dBA better than a reflective vertical wall [100]. The addition of absorption to an upper surface will increase *IL* progressively with increasing absorption. If a wall is crested with a circular absorber, multiple-diffractive edges, or resonant cavities, then the *IL* can be increased.

7.5 Conclusion to Applications

Scale-model tests with a line source showed that, for 4 m high barriers, the *ILA* varied with the class of barrier being tested. Walls (Table 7.3) have an *ILA* of 9 dBA (truncated to the nearest decibel). Earth berms of various top profiles (Table 7.3) have *ILAs* ranging from 7–8 dBA. Earth berms with crest walls (Table 7.4) have *ILAs* ranging from 8–10 dBA. Barriers with non-grass surfaces (Table 7.5) had *ILAs* ranging from 5–11 dBA. Improvements to earth-berm attenuation due to height increases were best achieved using a crest wall (Table 7.4).

After analyzing the effects of A-weighted traffic-noise spectra, the following points are made with respect to the design of traffic-noise barriers for noise-attenuation performance:

- Some highway-noise-control practitioners continue to assume, based on [2], that earth berms are more effective than a wall of the same height — and apply a soft-top correction of 3 dBA to the total *ILA* of a berm;
- This practice is not supported by the measurements reported in this work for both a point source (see Tables 7.1 and 7.2) and a line source (see Table 7.3);
- All of the evidence found in the noise-barrier literature (see Section 2.3 on page 34) supports the assertion that walls outperform earth berms.

Based on the evidence at hand it is fair to claim that walls outperform earth berms by 1–2 dBA when the centrelines of the barriers are offset from the highway by the same distance. The difference in attenuation, between assigning a berm a +3 dBA benefit with respect to a wall and penalizing a berm by –2 dBA, amounts to 5 dBA. Of course, since the ground area taken up by a wall is less than for a berm, it can be moved closer to the highway noise sources, further increasing the *ILA* of a wall. The point-source results (see Tables 7.1 and 7.2) show that by moving the wall closer to the source, further improvements in barrier attenuation can be achieved.

Chapter 8

Conclusion

The objective of this research was to evaluate the relative effectiveness of different types of highway noise barriers, with the aim of reducing traffic-noise levels in communities. A secondary objective was to develop scale-modelling techniques with an improved method for selecting scale-modelling materials in terms of an optimum scale factor and effective flow resistivity.

The scale-modelling principles and experimental techniques were reviewed and developed in Chapters 3 and 5. It was found that scale-modelling is useful as a tool to study complex sound-propagation phenomena — for example, diffraction over a barrier. The Insertion Loss (*IL*) of a barrier is used to evaluate the barrier's noise attenuation. Since measurements at full scale are inherently more difficult, time consuming and error prone, scale modelling is a preferred alternative. In Chapter 2 the literature was reviewed in five topic areas: outdoor sound propagation; acoustical properties of ground surfaces; noise barriers; acoustical scale modelling; and human perception of traffic noise. In Chapter 3, a simple formula was given for calculating the least-squares residuals between measured and predicted Excess Attenuation (*EA*) — an important indicator of a ground surface's alteration of a sound field. From the published literature an algorithm was found for predicting ultrasonic air-absorption coefficients. One prediction model was employed — the velocity-potential model for predicting the *EA* of a locally-reacting ground surface. In Chapter 4 the results of field measurements of traffic-noise spectra and barrier *IL* were reported. Chapter 5 describes how a scale-model sound source was developed and tested, scale-model materials were assessed, and how a procedure was developed for building noise barriers and testing their *IL*. A new approach to scale-model material selection was successfully developed, and used to find materials with appropriate

effective flow resistivities. Scale-model barriers were constructed, and their *ILs* were measured. In Chapter 6 it was shown that the third-octave *IL* of a noise barrier can vary with source and receiver locations, surface impedance and barrier profile. Interference effects between sound waves were found to be a critical aspect of outdoor sound propagation and barrier *IL*. Noise barriers block sound paths from source to receiver, but their attenuation is limited by the diffraction of sound waves over their crests or around their ends. Barrier shape, size, and surface composition contribute to the resulting barrier mitigation. In Chapter 7 the critical importance of considering source-radiation characteristics and human hearing are discussed in terms of the total *ILA* of a noise barrier. The results of point-source and line-source tests are considered, and the literature is referenced to support the conclusions of this work.

Scale-model tests with a line source showed that, for 4 m high barriers, the *ILA* varied with the class of barrier being tested:

- Walls (Table 7.3) have an *ILA* of 9 dBA;
- Earth berms of various top profiles (Table 7.3) have *ILAs* ranging from 7–8 dBA;
- Earth berms with crest walls (Table 7.4) have *ILAs* ranging from 8–10 dBA;
- Barriers with non-grass surfaces (Table 7.5) had *ILAs* ranging from 5–11 dBA;
- Improvements to earth-berm attenuation due to height increases were best achieved using a crest wall (Table 7.4).

In summary, this research has made a number of major contributions to the field of acoustical scale modelling of highway noise barriers:

- A new method for assessing/choosing scale-model materials was developed;
- Extensive line-source measurements of barrier *IL* were made;
- Demonstrated the relative effectiveness of 4 m high walls, earth berms, and berm/walls;
- The importance to attenuation of crest walls and surface impedance was explored;

- An extensive documentation of the inaccuracy of the soft-top correction assumption was done.

Further work can be done to improve the utility and accuracy of acoustical scale-modelling techniques for predicting highway noise levels, and aid in evaluations of the effectiveness of noise-control measures such as highway noise barriers:

- use a more sophisticated ground-impedance model — preferably a single-parameter model, and account for extended-reaction ground surfaces;
- test a greater number of materials — consider fabricating scale-model materials to have the correct acoustic properties;
- consider how the acoustic boundary layer could be used to some advantage when selecting materials;
- use the empirical least-squares-residuals procedure to assess scale-model materials over a range of both measurement positions and frequencies;
- employ an impulsive source to allow for removal of air-absorption effects (even for cases when the path-length differences are small);
- consider the detrimental effects of scattering objects such as trees and buildings;
- employ analytical methods for predicting barrier attenuation; use numerical techniques such as FEM, BEM, PE, etc.;
- consider how changes in source spectra (noise from railways and electric-powered vehicles) will affect barrier attenuation — tire noise is the dominant noise-generation mechanism at highway speeds;
- understand that environmental phenomena are difficult to reproduce in a scale model; when receivers are downwind of a source a barrier's noise-attenuation performance will be compromised.

Bibliography

- [1] British Columbia Ministry of Transportation and Highways — Highway Engineering Branch, Victoria, British Columbia, Canada. “*Policy for Mitigating the Effects of Highway Traffic Noise from Freeways and Expressways*”, February 1991.
- [2] Federal Highway Administration, Washington, D.C. “*F.H.W.A. Highway Noise Prediction Model*”, December 1978. Model frequently updated.
- [3] M.E. Delany and E.N. Bazley. “Acoustical Properties of Fibrous Absorbent Materials”. *Applied Acoustics*, 3(2):105–116, 1970.
- [4] M.E. Delany. “Sound Propagation in the Atmosphere: A Historical Review”. *Acustica*, 38(4):201–223, 1977.
- [5] J.E. Piercy, T.F.W. Embleton, and L.C. Sutherland. “Review of Noise Propagation in the Atmosphere”. *Journal of the Acoustical Society of America*, 61(6):1403–1418, June 1977.
- [6] T.F.W. Embleton. “Sound Propagation Outdoors — Improved Prediction Schemes for the 80’s”. *Noise Control Engineering*, 18(1):30–39, January–February 1982.
- [7] Tony F.W. Embleton. “Tutorial on Sound Propagation Outdoors”. *Journal of the Acoustical Society of America*, 100(1):31–48, July 1996.
- [8] J.E. Piercy and T.F.W. Embleton. “Noise Testing of Vehicles — Acoustic Propagation Phenomena”. *Canadian Acoustics*, 8(4):29–35, October 1980.
- [9] G.S. Anderson and U.J. Kurze. *Noise Control and Vibration Engineering*, chapter 5, Outdoor Sound Propagation, pages 113–144. John Wiley and Sons, 1992.
- [10] R.L. Wayson and W. Bowlby. “Atmospheric Effects on Traffic Noise Propagation”. *Transportation Research Record*, 1255:59–72, 1990.
- [11] Z. Maekawa. “Noise Reduction by Distance from Sources of Various Shapes”. *Applied Acoustics*, 3(3):225–238, 1970.
- [12] E.J. Rathe. “Note on Two Common Problems of Sound Propagation”. *Journal of Sound and Vibration*, 10(3):472–479, 1969.
- [13] D.K. Wilson and D.W. Thomson. “Natural Temporal Variability of Atmospheric Absorption Coefficients”. *Applied Acoustics*, 34(2):111–121, 1991.

- [14] American National Standards Institute. "American National Standard Method for the Calculation of the Absorption of Sound by the Atmosphere". Technical Report American National Standard ANSI S1.26-1978, American National Standards Institute, New York, 1978. Reapproved in 1990?
- [15] H.E. Bass, L.C. Sutherland, J.E. Piercy, and L. Evans. Absorption of sound by the atmosphere. In *Physical Acoustics*, volume XVII, pages 145–232. Academic Press, New York, 1984.
- [16] H.E. Bass, L.C. Sutherland, A.J. Zuckerwar, D.T. Blackstock, and D.M. Hester. "Atmospheric Absorption of Sound: Further Developments". *Journal of the Acoustical Society of America*, 97(1):680–683, January 1995.
- [17] F.M. Wiener and D.N. Keast. "Experimental Study of the Propagation of Sound over the Ground". *Journal of the Acoustical Society of America*, 31(6):724–733, June 1959.
- [18] T.F.W. Embleton, G.J. Thiessen, and J.E. Piercy. "Propagation in an Inversion and Reflections at the Ground". *Journal of the Acoustical Society of America*, 59(2):278–282, February 1976.
- [19] K.B. Rasmussen. "Sound Propagation over Ground under the Influence of a Sound Speed Profile in the Atmosphere". *Journal of Sound and Vibration*, 139(1):71–81, 1990.
- [20] C.I. Chessell. "Observations of the effects of Atmospheric Turbulence on Low-frequency Sound Propagation". *Journal of the Acoustical Society of America*, 60(1):29–33, July 1976.
- [21] G.A. Daigle, J.E. Piercy, and T.F.W. Embleton. "Effects of Atmospheric Turbulence on the Interference of Sound Waves near a Hard Boundary". *Journal of the Acoustical Society of America*, 64(2):622–630, August 1978.
- [22] P.H. Parkin and W.E. Scholes. "The Horizontal Propagation of Sound from a Jet Engine close to the Ground, at Radlett". *Journal of Sound and Vibration*, 1(1):1–13, 1964.
- [23] P.H. Parkin and W.E. Scholes. "The Horizontal Propagation of Sound from a Jet Engine close to the Ground, at Hatfield". *Journal of Sound and Vibration*, 2(4):353–374, 1965.
- [24] W.E. Scholes and P.H. Parkin. "The Effect of Small Changes in Source Height on the Propagation of Sound over Grassland". *Journal of Sound and Vibration*, 6(3):424–442, 1967.
- [25] J.B. Moreland. "Effect of Directivity on the Sound Field produced by a Source above a Reflecting Plane". *Journal of the Acoustical Society of America*, 78(2):590–597, August 1985.
- [26] I. Rudnick. "The Propagation of an Acoustic Wave along a Boundary". *Journal of the Acoustical Society of America*, 19(2):348–356, March 1947.

- [27] R.B. Lawhead and I. Rudnick. "Measurements on an Acoustic Wave Propagated along a Boundary". *Journal of the Acoustical Society of America*, 23(5):541-545, September 1951.
- [28] R.B. Lawhead and I. Rudnick. "Acoustic Wave Propagation along a Constant Normal Impedance Boundary". *Journal of the Acoustical Society of America*, 23(5):546-549, September 1951.
- [29] U. Ingård. "On the Reflection of a Spherical Wave from an Infinite Plane". *Journal of the Acoustical Society of America*, 23(3):329-335, May 1951.
- [30] G.A. Daigle, T.F.W. Embleton, and J.E. Piercy. "Some Comments on the Literature of Propagation near Boundaries of Finite Acoustical Impedance". *Journal of the Acoustical Society of America*, 66(3):918-919, September 1979.
- [31] K. Attenborough, S.I. Hayek, and J.M. Lawther. "Propagation of Sound above a Porous Half-space". *Journal of the Acoustical Society of America*, 68(5):1493-1501, November 1980.
- [32] C.I. Chessell. "Propagation of Noise along a Finite Impedance Boundary". *Journal of the Acoustical Society of America*, 62(4):825-834, October 1977.
- [33] K.B. Rasmussen. "Technical Note: Approximate Formulae for Short-distance Outdoor Sound Propagation". *Applied Acoustics*, 29:313-324, 1990.
- [34] A.R. Wenzel. "Propagation of Waves along an Impedance Boundary". *Journal of the Acoustical Society of America*, 55(5):956-963, May 1976.
- [35] R.J. Donato. "Propagation of a Spherical Wave near a Boundary with a Complex Impedance". *Journal of the Acoustical Society of America*, 60(1):34-39, July 1976.
- [36] T.F.W. Embleton, J.E. Piercy, and N. Olson. "Outdoor Sound Propagation over Ground of Finite Impedance". *Journal of the Acoustical Society of America*, 61(6):1403-1418, June 1977.
- [37] S.-I. Thomasson. "Reflection of Waves from a Point Source by an Impedance Boundary". *Journal of the Acoustical Society of America*, 59(4):780-785, April 1976.
- [38] S.-I. Thomasson. "Sound Propagation above a Layer with a Large Refraction Index". *Journal of the Acoustical Society of America*, 61(3):659-674, March 1977.
- [39] S.-I. Thomasson. "A Powerful Asymptotic Solution for Sound Propagation above an Impedance Boundary". *Acustica*, 45(2):122-125, June 1980.
- [40] S.-I. Thomasson. "On the Concepts of Hard, Soft, and Surface Wave Boundaries". *Acustica*, 48(4):209-217, 1981.

- [41] Gilles A. Daigle, Michael R. Stinson, and David I. Havelock. "Experiments on Surface Waves over a Model Impedance Plane using Acoustical Pulses". *Journal of the Acoustical Society of America*, 99(4):1993–2005, April 1996.
- [42] F. Matta and A. Reichel. "Uniform Computation of the Error Function and other Related Functions". *Mathematics of Computation*, 25:339–344, 1971.
- [43] C.F. Chien and W.W. Soroka. "Sound Propagation along an Impedance Plane". *Journal of Sound and Vibration*, 43(1):9–20, 1975.
- [44] C.F. Chien and W.W. Soroka. "A Note on the Calculation of Sound Propagation along an Impedance Surface". *Journal of Sound and Vibration*, 69:340–343, 1980.
- [45] R.K. Pirinchievara. "Erratum: 'Model Study of Sound Propagation over Ground of Finite Impedance', [J. Acoust. Soc. Am. 90, 2678–2682 (1991)]". *Journal of the Acoustical Society of America*, 94(3):1722(E), September 1993.
- [46] M.R. Stinson. "Letter to the Editor: A Note on the Use of an Approximate Formula to Predict Sound Fields above an Impedance Plane due to a Point Source". *Journal of the Acoustical Society of America*, 98(3):1810–1812, September 1995.
- [47] M.A. Nobile and S.I. Hayek. "Acoustic Propagation over an Impedance Plane". *Journal of the Acoustical Society of America*, 78(4):1325–1336, October 1985.
- [48] M.S. Howe. "On the Long-Range Propagation of Sound over Irregular Terrain". *Journal of Sound and Vibration*, 98(1):83–94, 1985.
- [49] K.M. Li. "A High-Frequency Approximation of Sound Propagation in a Stratified Moving Atmosphere above a Porous Ground Surface". *Journal of the Acoustical Society of America*, 95(4):1840–1852, April 1994.
- [50] André L'Espérance, P. Herzog, G.A. Daigle, and J.R. Nicolas. "Heuristic Model for Outdoor Sound Propagation based on an Extension of the Geometrical Ray Theory in the Case of a Linear Sound Speed Profile". *Applied Acoustics*, 37:111–139, 1992.
- [51] K. Attenborough, H.E. Bass, X. Di, R. Raspet, G.R. Becker, A. Gudesen, A. Chrestman, G.A. Daigle, A. L'Espérance, Y. Gabillet, K.E. Gilbert, Y.L. Li, M.J. White, P. Naz, J.M. Noble, and H.A.J.M. van Hoof. "Benchmark Cases for Outdoor Sound Propagation Models". *Journal of the Acoustical Society of America*, 97(1):173–191, January 1995.
- [52] K. Attenborough. "Predicted Ground Effect for Highway Noise". *Journal of Sound and Vibration*, 81(3):413–424, 1982.
- [53] T.F.W. Embleton, J.E. Piercy, and G.A. Daigle. "Effective Flow Resistivity of Ground Surfaces determined by Acoustical Measurements". *Journal of the Acoustical Society of America*, 74(4):1239–1244, October 1983.
- [54] B.P. Konstantinov. "On the Absorption of Acoustical Waves due to Reflection at a Hard Boundary". (*in Russian*) *J. Tech. Phys. USSR*, 9(3):226–238, 1939.

- [55] Keith Attenborough. "Near-Grazing Sound Propagation over Open, Flat Continuous Terrain". *Acoustics — Australia*, 13(1):23-30, 1984.
- [56] Keith Attenborough. "Acoustical Impedance Models for Outdoor Ground Surfaces". *Journal of Sound and Vibration*, 99(4):521-544, 1985.
- [57] M.J.M. Martens, L.A.M. van der Heijden, H.H.J. Walthaus, and W.J.J.M. van Rens. "Classification of Soils based on Acoustic Impedance, Air Flow Resistivity and other Physical Soil Parameters". *Journal of the Acoustical Society of America*, 78(3):970-980, September 1985.
- [58] Keith Attenborough. "Review of Ground Effects on Outdoor Sound Propagation from Continuous Broadband Sources". *Applied Acoustics*, 24(4):289-319, 1988.
- [59] M. Berengier, J.F. Hamet, and P. Bar. "Acoustical Properties of Porous Asphalts: Theoretical and Environmental Aspects". *Transportation Research Record*, 1265:9-24, 1990.
- [60] Y. Miki. "Acoustical Properties of Porous Materials — Modification of Delany-Bazley Models". *Journal of the Acoustical Society of Japan(E)*, 11(1):19-24, 1990.
- [61] Yasushi Miki. "Acoustical Properties of Porous Materials — Generalizations of Empirical Models". *Journal of the Acoustical Society of Japan(E)*, 11(1):25-28, 1990.
- [62] Keith Attenborough. "Acoustical Characteristics of Rigid Fibrous Absorbents and Granular Materials". *Journal of the Acoustical Society of America*, 73(3):785-799, March 1983.
- [63] H.M. Moore, K. Attenborough, J. Rogers, and S. Lee. "In-Situ Acoustical Investigations of Deep Snow". *Applied Acoustics*, 33(4):281-301, 1991.
- [64] K.D. Van Wyk, J.S. Bolton, and P.J. Sherman. "The Use of a Single-Parameter Model to Characterize the Condition of Asphalt Surfaces". *Noise Control Engineering Journal*, 38(1):39-50, January-February 1992.
- [65] Keith Attenborough. "Ground Parameter Information for Propagation Modelling". *Journal of the Acoustical Society of America*, 92(1):418-427, July 1992.
- [66] Richard Raspet and Keith Attenborough. "Erratum: Ground Parameter Information for Propagation Modelling, [J.Acoust.Soc.Am. 92(1), 418-427, (1992)]". *Journal of the Acoustical Society of America*, 92(5):3007, November 1992.
- [67] James M. Sabatier, Richard Raspet, and Carl K. Frederickson. "An Improved Procedure for the Determination of Ground Parameters using Level Difference Measurements". *Journal of the Acoustical Society of America*, 94(1):396-399, July 1993.
- [68] Craig Hutchinson-Howorth, Keith Attenborough, and Nicholas W. Heap. "Indirect In-Situ and Free-Field Measurement of Impedance Model Parameters or Surface Impedance of Porous Layers". *Applied Acoustics*, 39(1-2):77-117, 1993.

- [69] Mark W. Sprague, Richard Raspet, and Henry E. Bass. "Low-Frequency Acoustic Ground Impedance Measurement Techniques". *Applied Acoustics*, 39(4):307-325, 1993.
- [70] Keith Attenborough. "A Note on Short-Range Ground Characterization". *Journal of the Acoustical Society of America*, 95(6):3103-3108, June 1994.
- [71] American National Standards Institute. "American National Standard Methods for Determining the Insertion Loss of Outdoor Noise Barriers". Technical Report American National Standard ANSI S12.8-1987, American National Standards Institute, New York, 1987.
- [72] Greg Watts. "Acoustic Performance of Traffic-Noise Barriers — A State of the Art Review Part 1". *Acoustics Bulletin*, 18(3):13-18, May-June 1993.
- [73] Greg Watts. "Acoustic Performance of Traffic-Noise Barriers — A State of the Art Review Part 2". *Acoustics Bulletin*, 18(6):29-39, November-December 1993.
- [74] Sabih I. Hayek. "Mathematical Modelling of Absorbent Highway Noise Barriers". *Applied Acoustics*, 31(1-3):77-100, 1990.
- [75] Z. Maekawa. "Noise Reduction by Screens". *Applied Acoustics*, 1(3):157-173, 1968.
- [76] U.J. Kurze and G.S. Anderson. "Sound Attenuation by Barriers". *Applied Acoustics*, 4(1):35-53, 1971.
- [77] R.K. Pirinchievara. "The Influence of Barrier Size on its Sound Diffraction". *Journal of Sound and Vibration*, 148(2):183-192, 1991.
- [78] Y.W. Lam. "Using Maekawa's Chart to Calculate Finite Length Barrier Insertion Loss". *Applied Acoustics*, 42:29-40, 1994.
- [79] H.G. Jonasson. "Sound Reduction by Barriers on the Ground". *Journal of Sound and Vibration*, 22(1):113-126, 1972.
- [80] Sven-Ingvar Thomasson. "Diffraction by a Screen above an Impedance Boundary". *Journal of the Acoustical Society of America*, 63(6):1768-1781, June 1978.
- [81] D.C. Hothersall, D.H. Crombie, and S.N. Chandler-Wilde. "The Performance of T-Profile and Associated Noise Barriers". *Applied Acoustics*, 32:269-287, 1991.
- [82] D.N. May and M.M. Osman. "Highway Noise Barriers: New Shapes". *Journal of Sound and Vibration*, 71(1):73-101, 1980.
- [83] Allan D. Pierce. "Diffraction of Sound Around Corners and over Wide Barriers". *Journal of the Acoustical Society of America*, 55(5):941-955, May 1974.
- [84] Erik M. Salomons. "Diffraction by a Screen in Downward Sound Propagation: A Parabolic-Equation Approach". *Journal of the Acoustical Society of America*, 95(6):3109-3117, June 1994.

- [85] C.C. Cremers, K.R. Fyfe, and L.J. Cremers. "Insertion Loss Characteristics of Barriers and Berms". *Canadian Acoustics*, 22(3):121-122, 1994.
- [86] H.G. Jonasson. "Diffraction by Wedges of Finite Acoustic Impedance with Applications to Depressed Roads". *Journal of Sound and Vibration*, 25(4):577-585, 1972.
- [87] B.A. de Jong, A. Moerkerken, and J.D. van der Toorn. "Propagation of Sound over an Earth Barrier". *Journal of Sound and Vibration*, 86(1):23-46, 1983.
- [88] David J. Saunders and Roy D. Ford. "A Study of the Reduction of Explosive Impulses by Finite-Sized Barriers". *Journal of the Acoustical Society of America*, 94(5):2859-2875, November 1993.
- [89] H. Medwin. "Shadowing by Finite-Noise Barriers". *Journal of the Acoustical Society of America*, 69:1060-1064, 1981.
- [90] W.J. Hadden and A.D. Pierce. "Sound Diffraction around Screens and Wedges for Arbitrary Point Source Locations". *Journal of the Acoustical Society of America*, 69:1266-1276, 1981.
- [91] H. Medwin, E. Childs, and G.M. Jepsen. "Impulse Studies of Double Diffraction: A Discrete Huygens Interpretation". *Journal of the Acoustical Society of America*, 72:1005-1013, 1982.
- [92] Yves Berthelot and Ji-Xun Zhou. "Scale Model Experiments on the Validity of the Matched Asymptotic Expansions Theory for Sound Diffraction by Curved Surfaces of Finite Impedance". *Journal of the Acoustical Society of America*, 93(2):605-608, February 1993.
- [93] K.B. Rasmussen. "On the Effect of Terrain Profile on Sound Propagation Outdoors". *Journal of Sound and Vibration*, 98:35-44, 1985.
- [94] Masaki Hasebe and Kozo Kaneyasu. "Acoustic Wave Propagation over a Depressed Road having Finite Impedances". *Journal of the Acoustical Society of Japan(E)*, 8(3):77-84, 1987.
- [95] Toshihito Matsui, Koichi Takagi, Kozo Hiramatsu, and Takeo Yamamoto. "Sound Propagation over a Barrier on the Plane or Wedge-Shaped Ground". *Journal of the Acoustical Society of Japan(J)*, 46(3):245-250, 1990.
- [96] William Bowlby, Louis F. Cohn, and R.A. Harris. "A Review of Studies of Insertion Loss Degradation for Parallel Highway Noise Barriers". *Noise Control Engineering Journal*, 28(2):40-53, March-April 1987.
- [97] Raymond Panneton, André L'Espérance, Jean Nicolas, and Gilles A. Daigle. "Development and Validation of a Model Predicting the Performance of Hard or Absorbent Parallel Noise Barriers". *Journal of the Acoustical Society of Japan(E)*, 14(4):251-258, 1993.

- [98] J. Nicolas, T.F.W. Embleton, and J.E. Piercy. "Precise Model Measurements versus Theoretical Prediction of Barrier Insertion Loss in Presence of Ground". *Journal of the Acoustical Society of America*, 73(1):44-54, January 1983.
- [99] D.H. Crombie and D.C. Hothersall. "The Performance of Multiple-Edge Noise Barriers". *Journal of Sound and Vibration*, 176(4):459-473, 1994.
- [100] G.R. Watts, D.H. Crombie, and D.C. Hothersall. "Acoustic Performance of New Designs of Traffic-Noise Barriers: Full-Scale Tests". *Journal of Sound and Vibration*, 177(3):289-305, 1994.
- [101] D.C. Hothersall, S.N. Chandler-Wilde, and M.N. Hajmirzae. "Efficiency of Single Noise Barriers". *Journal of Sound and Vibration*, 146(2):303-322, 1991.
- [102] R.A. Harris. "Vegetative Barriers as an Alternative Noise Abatement Measure". *Noise Control Engineering Journal*, 27(1):4-8, July-August 1984.
- [103] F. Fricke. "Sound Attenuation in Forest". *Journal of Sound and Vibration*, 92(1):149-158, 1984.
- [104] Willibrord H.T. Huisman and Keith Attenborough. "Reverberation and Attenuation in a Pine Forest". *Journal of the Acoustical Society of America*, 90(5):2664-2677, November 1991.
- [105] W.E. Scholes, A.C. Salvidge, and J.W. Sargent. "Field Performance of a Noise Barrier". *Journal of Sound and Vibration*, 16(4):627-642, 1971.
- [106] R. DeJong and E. Stusnick. "Scale-Model Studies of the Effects of Wind on Acoustic Barrier Performance". *Noise Control Engineering Journal*, 6:101-109, 1976.
- [107] D.A. Hutchins, H.W. Jones, and L.T. Russell. "Model Studies of Barrier Performance in the Presence of Ground Surfaces. Part I — Thin, Perfectly Reflecting Barriers". *Journal of the Acoustical Society of America*, 75(6):1807-1816, 1984.
- [108] D.A. Hutchins, H.W. Jones, and L.T. Russell. "Model Studies of Barrier Performance in the Presence of Ground Surfaces. Part II — Different Shapes". *Journal of the Acoustical Society of America*, 75(6):1817-1826, 1984.
- [109] J.J. Hajek. "Are Earth Berms Acoustically Better than Thin-wall Barriers?". *Noise Control Engineering Journal*, 19(2):41-48, 1982.
- [110] Karsten Bo Rasmussen. "Model Experiments Related to Outdoor Propagation over an Earth Berm". *Journal of the Acoustical Society of America*, 96(6):3617-3620, December 1994.
- [111] Federal Highway Administration, Washington, D.C. "Research Report F.H.W.A.-RD-76-58 Noise Barrier Design Handbook", February 1976. Model frequently updated.
- [112] F. Spandock. "Akustische Modellversuche". *Annalen der Physik*, 20:345-360, 1934.

- [113] Ning Xiang and Jens Blauert. "Acoustical Design of the Chiang Kai Shek Cultural Centre in Taipei". *Applied Acoustics*, 27:27-46, 1989.
- [114] M.R. Hodgson and R.J. Orlowski. "Acoustic Scale Modelling of Factories, Part I: Principles, Instrumentation and Techniques". *Journal of Sound and Vibration*, 113(1):29-46, 1987.
- [115] M.M. Osman. "MTC Scale Model Facility for Transportation Noise Problems: Materials Choice and Validation for Scale Modelling". Technical Report 77-AC-4, Ontario Ministry of Transportation and Communications, Downsview, Ontario, Canada, June 1977.
- [116] D.A. Hutchins, H.W. Jones, and L.T. Russell. "Model Studies of Acoustic Propagation over Contoured, Finite Impedance Ground". *Acustica*, 58(4):234-242, 1985.
- [117] M. Almgren. "Simulation by using a Curved Ground Scale Model of Outdoor Sound Propagation under the Influence of a Constant Sound Speed Gradient". *Journal of Sound and Vibration*, 118(2):353-370, 1987.
- [118] M.E. Delany, A.J. Rennie, and K.M. Collins. "Scale Model Investigations of Traffic Noise Propagation". Technical Report Ac58, National Physical Laboratory, September 1972.
- [119] M.E. Delany, A.J. Rennie, and K.M. Collins. "A Scale Model Technique for Investigating Traffic Noise Propagation". *Journal of Sound and Vibration*, 56(3):325-340, 1978.
- [120] H.W. Jones, D.C. Stredulinsky, P.J. Vermeulen, and J. Yu. "An Experimental and Theoretical Study of the Modelling of Urban Noise Problems". Technical report, University of Calgary Physics Department Report for Alberta Surface Transportation Noise and Attenuation Study, July 1977.
- [121] H.W. Jones, D.C. Stredulinsky, and P.J. Vermeulen. "An Experimental and Theoretical Study of the Modelling of Road Traffic Noise and its Transmission in the Urban Environment". *Applied Acoustics*, 13(4):251-265, 1980.
- [122] K.V. Horoshenkov, D.C. Hothersall, and K. Attenborough. "Scale-Model Materials for Simulating Ground". *Journal of Sound and Vibration*, 194(5):685-708, August 1996.
- [123] H. Kuttruff. "Acoustical Design of the Chiang Kai Shek Cultural Centre in Taipei". *Applied Acoustics*, 27(1):27-46, 1989.
- [124] David W. Schindel, David A. Hutchins, Lichun Zou, and Michael Sayer. "The Design and Characterization of Micromachined Air-Coupled Capacitance Transducers". *IEEE Transactions on Ultrasonics, Ferroelectrics and Frequency Control*, 42(1):42-50, January 1995.
- [125] M. Almgren. "Acoustic Boundary Layer Influence on Scale Model Simulation of Sound Propagation: Experimental Verification". *Journal of Sound and Vibration*, 105(2):247-259, 1986.

- [126] D.A. Hutchins, H.W. Jones, and P.J. Vermeulen. "The Modulated Ultrasonic Whistle as an Acoustic Source for Modelling". *Journal of the Acoustical Society of America*, 73(1):110-115, January 1983.
- [127] H. Myncke, A. Jans, and A. Cops. "High Power Ultrasonic Source for Modelling Traffic Noise". In *Proceedings of the 1987 International Conference on Noise Control Engineering*, volume 2, pages 1547-1550, Beijing, September 1987.
- [128] J. Novak. "Technical Note: Sound Source for Scale Model Measurements of Traffic Noise". *Applied Acoustics*, 24(1):63-70, 1988.
- [129] D.A. Hutchins, H.W. Jones, and L.T. Russell. "Model Studies of Acoustic Propagation over Finite Impedance Ground". *Acustica*, 52(3):169-178, 1983.
- [130] Mitsuyasu Yamashita and Kohei Yamamoto. "Scale Model Experiments for the Prediction of Road Traffic Noise and the Design of Noise Control Facilities". *Applied Acoustics*, 31(1-3):185-196, 1990.
- [131] R.K. Pirinchievara. "Model Study of Sound Propagation over Ground of Finite Impedance". *Journal of the Acoustical Society of America*, 90(5):2678-2682, November 1991.
- [132] B. Day. Chapter 6, "acoustic scale modelling materials". In R.K. MacKenzie, editor, *Auditorium Acoustics*, pages 87-99. Applied Science Publishers, 1975.
- [133] N.N. Voronina. "Scale Modelling of the Acoustical Characteristics of Layers of Fibrous Sound-Absorbing Materials". *Soviet Physics — Acoustics*, 31(5):402-404, September-October 1985.
- [134] M. Almgren. "Acoustic Boundary Layer Influence on Scale Model Simulation of Sound Propagation: Theory and Numerical Examples". *Journal of Sound and Vibration*, 105(2):321-337, 1986.
- [135] Richard Peppin. "Anechoic Rooms Evaluation Method under Development". *ASTM Standardization News*, 21(8):14-15, 1992.
- [136] M.E. Delany and E.N. Bazley. "The High Frequency Performance of Wedge Lined Free-field Rooms". *Journal of Sound and Vibration*, 55(2):195-214, 1977.
- [137] American National Standards Institute. "Precision Methods for the Determination of Sound Power Levels of Noise-sources in Anechoic and Hemi-anechoic Rooms". Technical Report American National Standard ANSI S12.35-1990, American National Standards Institute, New York, 1990.
- [138] K.O. Ballagh. "Calibration of an Anechoic Room". *Journal of Sound and Vibration*, 105(2):233-241, March 1986.
- [139] R.F.S. Job. "Internal Consistency and Stability of Measurements of Community Reaction to Noise". *Transportation Research Record*, 1312:101-108, 1991.

- [140] R.F.S. Job. "Impact and Potential Use of Attitude and Other Modifying Variables in Reducing Community Reaction to Noise". *Transportation Research Record*, 1312:109-115, 1991.
- [141] G.R. Watts and P.M. Nelson. "The Relationship between Vehicle Noise Measures and Perceived Noisiness". *Journal of Sound and Vibration*, 164(3):425-444, 1993.
- [142] S. Kuwano, S. Namba, and H. Miura. "Advantages and Disadvantages of A-weighted Sound Pressure Level in Relation to Subjective Impressions of Environmental Noises". *Noise Control Engineering Journal*, 33(3):107-115, May-June 1989.
- [143] International Standards Organization. "Acoustics — Method for Calculating Loudness Level". Technical Report ISO 532 - 1975(E), International Standards Organization, Geneva, 1975.